Title
Underwater Glider System Study
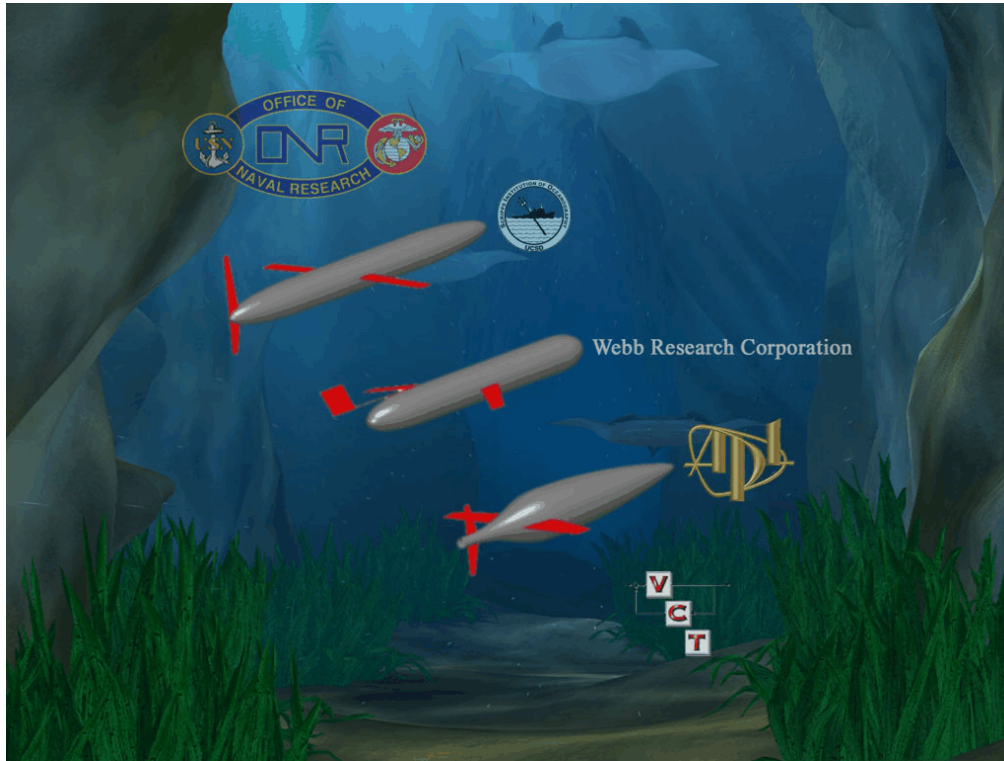
Permalink
https://escholarship.org/uc/item/1c28t6bb

Authors
Jenkins, Scott A
Humphreys, Douglas E
Sherman, Jeff
et al.

Publication Date
2003-05-06

UNDERWATER GLIDER SYSTEM STUDY
Scripps Institution of Oceanography
Technical Report No. 53

Submitted 6 May 2003 by:

Scott A. Jenkins, Scripps Institution of Oceanography
Douglas E. Humphreys, Vehicle Control Technologies, Inc.
Jeff Sherman, Scripps Institution of Oceanography
Jim Osse, University of Washington
Clayton Jones, Webb Research Corporation
Naomi Leonard, Joshua Graver, Ralf Bachmayer, PrincetonUniversity
Ted Clem, Paul Carroll, Philip Davis, Naval Surface Warfare Center
Jon Berry, Paul Worley, Johns Hopkins University
Joseph Wasyl, Scripps Institution of Oceanography

TABLE OF CONTENTS:

EXECUTIVE SUMMARY:

The goals of this study are to determine how to advance from present capabilities of underwater glider (and hybrid motorglider) technology to what could be possible within the next few years; and to identify critical research issues that must be resolved to make such advancements possible. These goals were pursued by merging archival flight data with numerical model results and system spreadsheet analysis to extrapolate from the present state-of-the–art in underwater (UW) gliders to potential future technology levels. Using existing underwater gliders (legacy gliders) as calibration, this merger approach was applied to six basic glider types that were conceived to satisfy the requirements of five functional classes. Functional classes were posed based on an evaluation of the attributes and limitations of underwater gliders in the context of a broad range of potential Navy needs in the littoral and deep-water regimes. Those functional classes included:

Depth- Unlimited Roaming
Depth-Limited Roaming
Virtual Station Keeping
Payload Delivery
Level-Flight Hybrids

The glider types were composites of two basic payload packages (single and bundled), two classes of vehicle shape (body-of-revolution with wings and a flying wing), and three alternative propulsion systems (buoyancy lung, lung with propeller and lung with heat exchanger). Proceeding from the weight, space and power requirements of the payload packages, the analysis worked backward through a series of numerical modeling and spreadsheet computations to map out the viable performance envelope of each glider type. Scaling rules for speed and transport economy were then applied to these performance envelopes to identify the optimal regime of each glider type and to facilitate matching glider type with functional class. Table E.1 provides a summary of the matching of glider types with functional class and the expected dimensions and performance capabilities resulting from those matches. The shaded magenta bands in this table indicate the optimal scale regime for each glider type.

Beneath the surface of Table E.1, a number of interesting findings were made that shed light on critical research issues. Many of these findings come from close examination of the existing technology.

1) The achieved performance of the UW glider is as much dependent on the intrinsic vehicle characteristics as it is on how it is flown.

2) Presently, legacy gliders operate in a scale regime equivalent to that of bats and small birds.

3) The present legacy glider performance does not match the transport economy of its bird and bat counterparts because of the way it is flown, insufficient loading of the wing, excessive wetted surface area and inefficiencies of the buoyancy engine.

4) Legacy gliders are not flown in the most transport efficient manner. They are flown at steep glide angles in order to profile ocean water masses. If they were flown at the flattest glide slopes within present capability (L/D_{max}), their transport economy would improve three fold. To do so would require the controller to trim the glider for nose high attitudes during descending glides and nose low attitudes during ascending glides. Present control systems lack sophistication and supporting flight instrumentation necessary for maintaining such stable high angle of attack flight attitudes.

5) The present glider shapes are analogous to gliding blimps, and have too much wetted surface area for the wing loading at which the gliders are flying. Two remedial approaches were studied: increasing the wing loading by increasing the capacity of the buoyancy engine; and reducing the wetted surface area. Numerous sets of computations based on higher ratios of net buoyancy volume to total vehicle volume found that it is possible to make underwater gliders perform very close to the transport economy of natural flyers when operating in the present scale regime of birds. In larger scale regimes, these computations found that underwater gliders can equal or better the transport economy of some of the most efficient man-made flyers. Numerical modeling was also performed to seek more efficient shapes having less wetted area per unit area of wing, such as flying wings and blended wing-body configurations, wherein nearly all of the wetted area is efficient lift generating area. These new shapes were found to have superior range and speed capability for less energy consumption than more conventional bodies of revolution fitted with wings, (see Table E.1). The remaining alternative for reducing the wetted surface area would be to reduce the volume requirements of the glider body by placing the batteries outside the pressure hull in some free flooding compartment. This concept was not pursued due to uncertainties in the status of pressure compensated battery technology.

6) The buoyancy engines that propel the legacy gliders do not recover the energy on descent that was expended on ascent in order to overcome ocean stratification and hull compressibility. By throwing away that energy, the buoyancy engine is consuming about 30% more than the flight energy required.

7) Flying the UW glider to deeper depths is intrinsically more efficient. Energy consumption increases 30% when the depth excursion of the glide profile is reduced from 1000m to 100m . This is due to 2 factors: 1) the glider must penetrate the thermocline a greater number of times over any given gliding distance when the depth excursion is reduced , and 2) the buoyancy engine pump is less efficient at lower pressures (shallower depths). For Example, the Parker PGP PM5116 high pressure pump has an efficiency of only 23% at a depth of 100m, but increase to an efficiency of 75% at 1000m depth.

8) A certain minimum ratio of net buoyancy volume to total vehicle volume was found ($n_b = V_{buoyancy}/ V_0 \sim 0.4\%$), beyond which, bigger gliders always achieve better transport economy. This improvement is accompanied by higher speed capability, see Table E.1.

9) Maximum along coarse speed in still water is always obtained at a 35 degree glide angle, regardless of vehicle shape or other hydrodynamic properties. Winged bodies of revolution with maximum buoyancy engine capacity (n_b) are the optimal combination for maximum speed.

10) For a given n_b, flying wings of equivalent vehicle volume are slower then winged bodies of revolution, but have superior range and transport economy and require fewer dive cycles (and less near surface exposure time) for a given distance traveled, (see Table E.1)

11) A procedure was defined for sizing and shaping gliders for mission specific functions, although our analysis remains generic in the context of broad functional classes.

12) Communications systems are presently the weak link of the UW glider technology. Near surface exposure time for the purpose of 2-way communications must be minimized. There are a number of attractive communications solutions for the UW-glider missions, including: local geosynchronous phone solutions; high bandwidth satellite solutions; radio frequency solutions in the line of sight (LOS) (UHF/VHF band) to aircraft or UAVs or over the horizon (OTH) (HF groundwave) to ship, shore, gateway node or buoy relay; and UAV data links such as Tactical Common Data Link (TCDL)

Long Term Recommendations:
1) Develop more sophisticated control systems with supporting flight data instrumentation and software for achieving stable, high angle of attack flight and for implementation of speed to fly or avoidance/evasion strategies.

2) Improve the buoyancy engines for energy recovery during descending glides. Explore options for increasing buoyancy engine capacity and for utilizing latest developments in high pressure, high efficiency pumps.

3) Develop and implement pressure compensated battery technology (particularly for the bigger gliders) that will allow the battery package to be placed outside the pressure hull while remaining compatible with safety requirements.

4) Develop vehicle shapes optimized for well posed mission requirements. Exploit computational methodologies that solve for minimum wetted surface area within constraints of volume and position requirements of internal components.

5) Develop optimized wing technologies for bi-directional angle of attack flight. Explore options for articulated wing incidence angle and for variable geometry.

6) Continue development of the thermal glider. Evaluate the potential for extracting and utilizing alternative geophysical energy sources, eg. dynamic soaring in vertical velocity gradients, wave soaring in internal waves, extraction of energy from surface waves via Katzmyr effect, et al.

7) Develop low cost pressure hulls with compressibility that matches seawater. Explore options for maximizing the packing of components and subsystems both inside and outside the pressure hull.

8) Develop an optimal communications solutions for the UW-glider missions from among the list of potential candidates listed above.

Near Term Recommendations:

Develop an Advance Concepts Demonstrator Featuring:
- · At Least 4-Fold Scale (Volume) Increase over Legacy Gliders
- · Configure for ASW Sentry Payload Package
- · New Geometry (alternatives)
  - Flying Wing
  - Legacy Type with Articulated Wing Incidence
  - Apply Surface Area Minimization Codes
- · Code for Maximization of Internal Systems Packing
- · Maximize Buoyancy Engine Capacity Within Packing
- · Off-the Shelf Systems for Glide Cycle Energy Recovery
- · High Pressure Pumps Specific to Patrol Depths
- · Incorporate Inertial Navigation System with Horizon
- · Control Codes Interactive with Navigation/Flight Data
- · TCDL Communication System from Existing AUV

Table E.1. Summary of findings -page 1.

Glider Type	Length Ft	Wing Span Ft	Volume Cu Ft	Loaded Mass (Net Buoyancy) Grams	Cruise Speed Kts	Best L/D Speed Kts	Maximum (Best) *L/D	**Net Transport Economy
Winged-Body-of-Revolution (Depth Unlimited Roaming, Payload Delivery)								
23W-02	6.0	3.6	2.0	150	0.95	0.41	6.9	4.49
23W-12	12.9	7.7	19.6	1,500	1.5	0.76	7.1	1.30
23W-22 Range = 3500 km	27.9	16.6	195.7	15,000	2.3	1.22	7.8	1.04
23W-32 (bundled payloads)	60.0	35.8	1957.0	150,000	3.6	1.58	8.5	0.88
23W-SS	129	77.1	19,569	3,975,000	7.3	3.7	9.2	0.88
Winged-Body-of-Revolution (Depth Unlimited Roaming, Station Keeping)								
23S-03	4.8	2.90	1.1	100	0.62	0.42	6.3	2.22
23S-13	5.1	3.04	1.3	500	1.3	0.62	6.4	0.54
23S-23 Range = 3500 km	5.4	3.24	1.5	1,000	1.7	0.80	6.8	0.47
23S-33 (single payload)	9.2	5.5	7.7	10,000	3.2	1.51	7.1	0.47
23S-43	19.4	11.6	71.5	100,000	4.85	2.32	7.7	0.47
23S-SS	42.7	25.5	698.0	1,000,000	9.75	4.6	7.8	0.79
Flying Wing (Depth Unlimited Roaming, Payload Delivery)								
238-02	2.3	10.5	2.2	400	0.49	0.16	18.1	2.49
238-12	5.0	22.6	22	4,000	1.46	0.44	19.5	0.85
238-22 Range = 3500 km	10.7	48.7	220	40,000	2.78	1.12	23.0	0.79
238-32 (bundled payloads)	22.9	104.9	2198	400,000	4.35	2.03	24.8	0.79
238-42	49.5	226.1	21,980	4,000,000	6.47	3.09	27.0	0.79
Flying Wing (Depth Limited Roaming, Payload Delivery)								
238-04	2.0	9.0	1.3	150	0.14	0.13	17.8	4.85
238-14	2.0	9.0	1.5	1,500	0.46	0.40	18.0	0.27
238-24 Range = 3500 km	3.3	15.0	6.1	15,000	1.09	0.99	19.1	0.13
238-34 (single payload)	6.9	31.5	55.3	150,000	1.91	1.84	22.8	0.12
238-44	15.1	68.9	548.5	1,500,000	3.02	2.91	23.5	0.12

Table E.1. Summary of findings -page 2.

Glider Type	Length Ft	Wing Span Ft	Volume Cu Ft	Loaded Mass (Net Buoyancy) Grams	Cruise Speed Kts	Best L/D Speed Kts	Maximum (Best) *L/D	** Net Transport Economy
Hybrid Glider (Level Flight, Depth limited Roaming)					prop on/ glide			
WRC-H05	5.7	3.2	1.31	110	2.1 / 0.6	0.41	4.4	4.13
WRC-H1	5.9	3.3	1.34	220	2.9 / 0.8	0.76	4.4	2.56
WRC-H2 Range = 500 km	6.1	3.4	1.45	440	4.1 / 1.1	1.22	4.4	1.79
WRC-H5 (single payloads)	6.5	3.6	1.77	1,100	6.0 / 1.7	1.58	4.5	1.36
WRC-H11	7.1	4.0	2.37	2,200	8.2 / 2.3	0.80	4.8	1.26
WRC-H12	13.2	7.4	14.9	22,000	16.7 / 4.7	1.51	5.0	1.39
WRC-H13	30.7	17.2	188.4	220,000	28.9 / 8.1	2.32	5.5	1.94
WRC-H14	74.2	41.5	2,672	2,220,000	43.9 / 12.8	4.6	5.9	2.79
Thermal Glider (Depth Unlimited Roaming, Station Keeping)								
WRC-T05	5.7	3.2	1.1	90	0.33	0.16	5.5	0.61
WRC-T1	5.9	3.3	1.8	180	0.47	0.44	5.5	0.22
WRC-T2 Range = 35,000 km	6.0	3.3	11.1	360	0.64	1.12	5.6	0.08
WRC-T5 (single payloads)	6.2	3.5	105.8	900	0.99	2.03	5.8	0.02
WRC-T11	6.6	3.7	1.5	1,800	1.34	0.40	6.0	0.0075
WRC-T12	10.4	5.8	6.1	18,000	2.84	0.99	6.4	0.0004
WRC-T13	21.2	11.9	55.3	180,000	4.65	1.84	6.9	0.00002
WRC-T14	45.5	25.4	548.5	1,800,000	7.05	2.91	7.5	0.000001

* L/D is the lift to drag ratio and is a measure of glide efficiency, where bigger values represent more efficient gliding. The inverse of L/D gives the glide slope.

** Net transport economy is the energy expended per immersed weight per distance traveled. It is a measure of energy consumption, and smaller values represent more efficient transport.

Optimal Scale Regime

1. Goals:

The goals of this study are to determine how we can advance from present capabilities of underwater glider (and hybrid motorglider) technology to what could be possible within the next few years and to identify R&D requirements that would make such an advancement possible. These broad-based goals require that we:

- Pose Applications (Functional Classes) that are *Obtainable* within Several Years

- Explore Optimization Requirements for each Application

- Identify R&D Requirements to Advance from the Existing State of Technology to Optimized Applications

2. Objectives:

The study objectives are: 1) develop scaling rules for dimensions, performance and cost of underwater gliders and motorglider hybrids, 2) pose functional categories that are well suited to the attributes and limitations of underwater gliders and motorgliders; 3) identify controlling performance variables for each functional category 4) apply scaling rules to controlling variables to establish a theoretical performance envelope for each functional category; 5) identify optimal scale and operational regimes within the performance envelope of each functional category; 6) identify options for adapting vehicle characteristics and design trade-offs to achieve the optimal operational regime of each functional category; 7) identify flight strategies to achieve the optimal operational regime of each functional category; 8) identify "weak links" and potential remedial measures; and 9) provide guidance to ONR on critical pathways of research needed to achieve operational prototypes for each functional category.

3. Approach:

A technical team has been selected by the Office of Naval Research (ONR) to accomplish the study objectives and report to ONR by 1 April 2003. The ONR management team is lead by Dr Thom as F. Swean, Code 321 OE. The technical team consists of the following members and areas of expertise:

Jim Osse: glider system integration, trade-offs spreadsheet analysis

Clayton Jones: glider system integration, motorglider propulsion

Jeff Sherman: sub-system analysis, design rules for payload capability

Douglas Humphreys: vehicle hydrodynamics, dynamics & control

Naomi Leonard: glide control & parametric simulation, lifting bodies

Ted Clem: payload, sensors, navigation systems, deployment strategies

Jon Berry: payload and sensors, integrated undersea surveillance concepts

Scott Jenkins:(team leader), glider aerodynamics & speed-to-fly strategies

The technical team has addressed the study objectives by merging archival flight data with numerical model results to extrapolate from the present state-of-the–art in underwater (UW) gliders to potential future technology levels. Using existing underwater gliders (legacy gliders) as calibration, this merger approach was applied to five functional classes of potential future vehicles to determine the feasible range of performance and optimal characteristics for those classes. The archival flight data was derived from diverse cross-disciplinary sources, including: soaring, low speed aerodynamics, analytic surveys of natural flyers, stability and control theory, naval architecture, propulsion dynamics, thermodynamics, physical oceanography, bio-mechanics, et al. The numerical models employed were a suite of hydrodynamic and dynamic modeling tools provided by Vehicle Control Technologies (VCT), including a fully non-linear 6- degree-of-freedom flight simulator (6-dof model). The lessons learned from existing UW-glider technology were distilled into a spreadsheet methodology developed by Jim Osse, and subsequently modified by Jeff Sherman and Clayton Jones. The spreadsheets were used for vehicle sizing and to digest the archival flight data and numerical model results in order to extrapolate performance and especially energetics over all

viable scale regimes.

The glider system study approach is summarized in Figure 3.1. Functional classes were conceived from an evaluation of the attributes and limitations of underwater gliders in the context of a broad range of potential Navy needs in the littoral and deep water regimes. For each functional class a variety of payloads and sensors were specified based on viable off-the-shelf technology, particularly in the categories of non-acoustic sensors and inertial navigation systems. Proceeding from the weight, space and power requirements of these payloads and sensors, the team worked backward through a series of scaling relations to map out the viable performance envelopes of a variety of glider types that showed promise for satisfying the requirements of the functional classes. These candidate glider types were posed from an amalgam of present experience in underwater gliders and from naval architecture and cutting-edge soaring science. The scale relations applied to these glider types were the by-product of analytic flight survey data and numerical model results and helped to identify leading order variables affecting the performance envelopes. Mapping of the performance envelopes involved two iterations between the spreadsheet analysis and the explicit numerical modeling: an initial sizing of each vehicle by spreadsheet analysis that provided preliminary guidance to the hydrodynamic modeling; followed by updated hydrodynamic inputs to the spreadsheets in order to arrive at final sizing. The final vehicle sizing, in turn produced a final, more refined set of hydrodynamic analyses that were used to evaluate vehicle energetics, optimal scale regimes, optimal flight strategies and control system requirements. These results ultimately produced a matching of glider types with the functional classes based on a criterion of achievable performance within the environmental and operational constraints specific to each functional class. The distillation of existing capabilities and potential capabilities through the system study process identified a series of R&D requirements in both the near and long term.
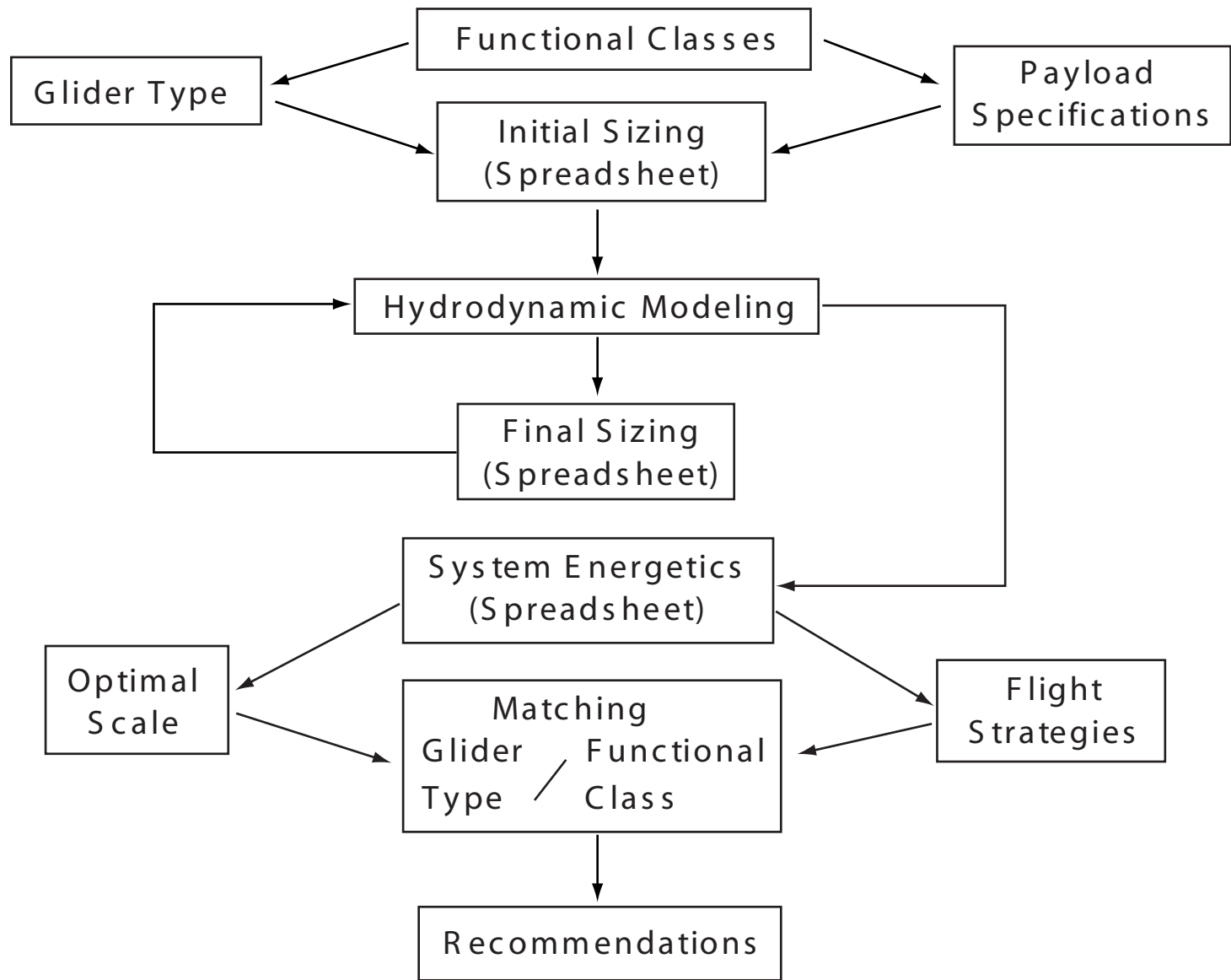
Figure 3.1. Glider Study Approach.

4. Concept, Attributes and Limitations

4.1 Concept: The concept of an underwater glider was first demonstrated by *Concept Whisper*, a prototype 2-man swimmer delivery vehicle (SDV) built by General Dynamics Corporation in the early 1960's (Oversmith and Leadon, 1962, Rains, 1968). In the 1970's, analysis of the energetics of UW gliders and an evaluation of potential naval application was performed at the Naval Electronics Laboratory by Ladd (1977). In the late 1980's, world re-known oceanographer Henry Stommel proposed a fleet of autonomous gliders he referred to as *Slocums* to profile the ocean's water properties, Stommel (1989). However, it wasn't until the 1990's that underwater gliders became more than a vision or a dead-end prototype. After a 7-year effort funded by ONR, 3 operational first generation UW-gliders had been developed and tested primarily for the purpose of profiling ocean water properties, commensurate with the role first envisioned by Henry Stommel.

These first-generation UW gliders are referred to herein as the *legacy gliders*. The legacy gliders include *Seaglider, Spray and Slocum* (Figure 4.1). Because of the often sharp-edged gradient structures of ocean water properties, emphasis was placed on optimizing the performance of the legacy gliders to travel up and down through the water column at rather steep glide angles, rather than optimizing them for cross country performance as in conventional gliders in air. The legacy gliders were also constrained in their physical dimensions by the limited deck space available on small oceanographic vessels, and all are similar in size and weight, typically 2 meters in length, 1 meter in wing span, 50 liters in displaced volume and operating at a net buoyancy of about 1-3 Newtons (about 100 grams loaded mass).   There are subtle differences in the flight control systems and the pumping systems used to vary the net buoyancy of the gliders. The *Seagider* was developed at the University of Washington (Eriksen et al, 2001) of which 11 have been built performing out and return missions as long as 150 days. Three prototypes of *Spray* have been built at Scripps Institution of Oceanography (Sherman, et al 2001) and have demonstrated out and return capabilities of 300 nautical miles in a 17 day period. Seaglider and Spray have been operated primarily in deep water environments off the narrow shelf west coast of the United States. The *Slocum* developed by Webb Research Corporation (Webb et al 2001) is a shallow water specialist that has operated primarily in the broad shelf environments of the east coast of the United States. Slocum has performed 10 day out and return missions in waters as shallow as 4 m and has been built in several

variants including a pure glider, a hybrid glider with auxillary screw propulsion and a thermal glider that utilizes a Carnot cycle energy recovery system to extract energy from the temperature gradient between the surface mixed layer and the bottom water.

The underwater glider concept is directly analogous to gliding in air except that in the underwater environment, ascending glides are also possible. It is a buoyancy driven form of locomotion in which the power needed to overcome the drag (D) on the vehicle as it moves at a speed U through water is supplied by gravity in the form of positive or negative net buoyancy ($+/- B$). Horizontal translation using the vertical force of gravity is made possible by the lift (L) produced by a wing that acts perpendicular to the trajectory of the vehicle. However, horizontal translation is only possible if the trajectory is inclined in the direction of the vertical forces of gravity (upward for a positive net buoyancy and downward for negative net buoyancy). Inclination of the trajectory in this way (glide slope) allows the net hydrodynamic force of lift and drag (F) to balance the net buoyancy, but implies that a net vertical motion will result, (see Figure 4.2). This vertical motion results from a descending glide slope for gliders in air or underwater if the net buoyancy is negative and is referred to as sink rate (w). Unlike gliders in air, underwater gliders can have ascending glide slopes if the net buoyancy is positive, producing a negative sink rate ($-w$). The underwater glider is given a *buoyancy engine* shown schematically in Figure 4.3 that allows it to alternately change its net buoyancy between positive and negative states, thereby imparting it with the ability to string together a succession of descending and ascending glide slopes referred to as a *dolphin glide path*, (Figure 4.2). During each of the descending or ascending slopes of the dolphin glide path, the power needed to overcome drag ($P_e = DU$) is equal to the rate of working by gravity acting down (or up) the glide slope ($P_e = Bw$). Thus

$$P_e = DU = Bw \hspace{4cm} (4.1)$$

Because the force triangle and the speed triangles in Figure 4.2 are proportional, the power expenditure per meter traveled scales in direct proportion to the glide slope ($w/U \sim D/L$), or inversely with the lift-drag ratio (L/D). Therefore by imparting the underwater glider with low drag and high lift properties, its active energy consumption to produced locomotion can be reduced to that consumed by the buoyancy engine in alternately changing the net buoyancy between positive and negative states. Since these engines are small electrically driven pump systems

that force a buoyant fluid in and out of the pressure hull, they are extremely low power systems that are quiet and provide long endurance capability.

4.2 Attributes of Underwater Gliders: The most compelling attribute of an underwater glider from the point of view of Naval sub-surface applications is the very low level of self noise (primarily from buoyancy pump activation) that is only emitted episodically for short intervals. Once the underwater glider re-sets its net buoyancy, it glides silently with no machinery or hydrodynamic noise for many kilometers until reaching the next reversal in the dolphin glide path (Figure 4.2). This mode of intermittent self noise is in sharp contrast to the continuous self noise emissions of prop driven vehicles. A listing of attributes of underwater gliders includes:

　　　　a) Sub-Surface Platform
　　　　b) High Endurance
　　　　　*Long Range Roaming Capability
　　　　　*Long On-Station Time Capability
　　　　　*Round-Trip Patrol Capability
　　　　c) Stealthy
　　　　　*Quiet, Very Low Self-Noise
　　　　　*Small Acoustic Cross Section
　　　　　*Quasi-Wakeless
　　　　d) Scalable (from Small to Large)
　　　　e) Depth Excursion Capability
　　　　f) Energy Recovery Capability
　　　　　*From Ocean Temperature Gradients
　　　　　*From Ocean Currents, Surface Gravity & Internal Waves
　　　　　　(Dynamic Soaring, Katzmayr Effect)
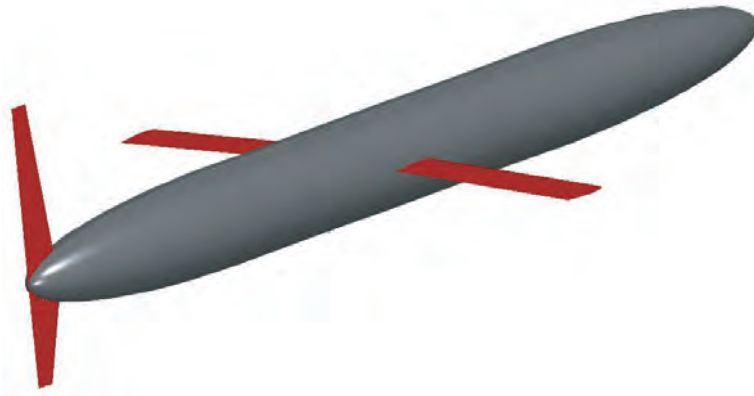
Spray:
Length = 216.28 cm
Diameter = 20.32 cm
Span = 119.38
Wing Area = 502.58 cm^2
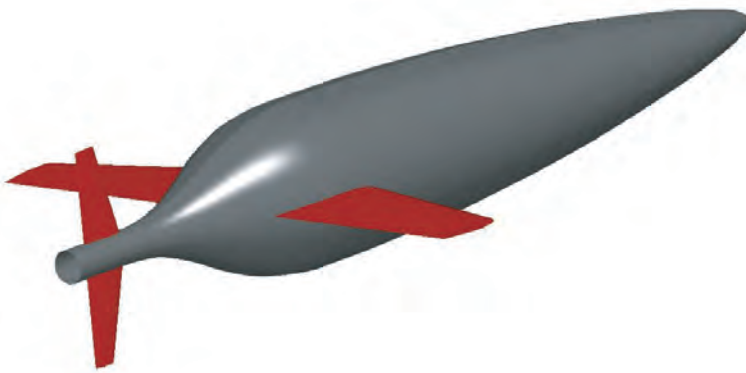
Sea Glider:
Length = 180.01 cm
Diameter = 30.48 cm
Span = 101.27 cm
Wing Area = 668.84 cm^2
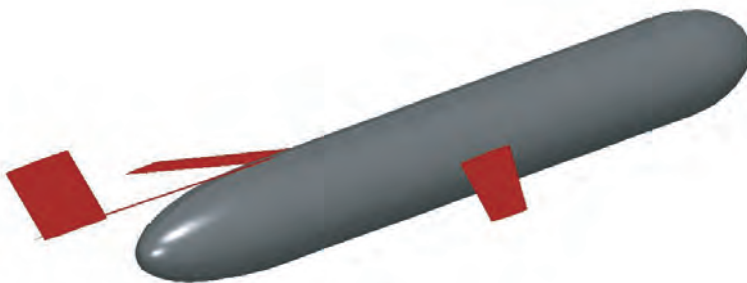
Slocum:
Length = 178.92 cm
Diameter = 21.27 cm
Span = 101.19 cm
Wing Area = 487.35 cm^2

Figure 4.1. Physical characteristics of legacy gliders [after VCT, 2003].

FORCE TRIANGLE

$$\frac{D}{B} = \frac{w}{u}$$

SPEED TRIANGLE

β = Glide Slope
α = Angle of Attack
$\beta - \alpha$ = pitch angle

Γ flow circulation

τ reaction torque (pitching moment)

Dolphin Glide Path

Drag Power, $P_e = DU$

Rate of Working by Gravity, $P_g = Bw$

$DU = Bw$

Specific Energy Consumption, $E_e = \dfrac{DU}{BU} \cong \dfrac{w}{u} \rightarrow \dfrac{D}{L}$
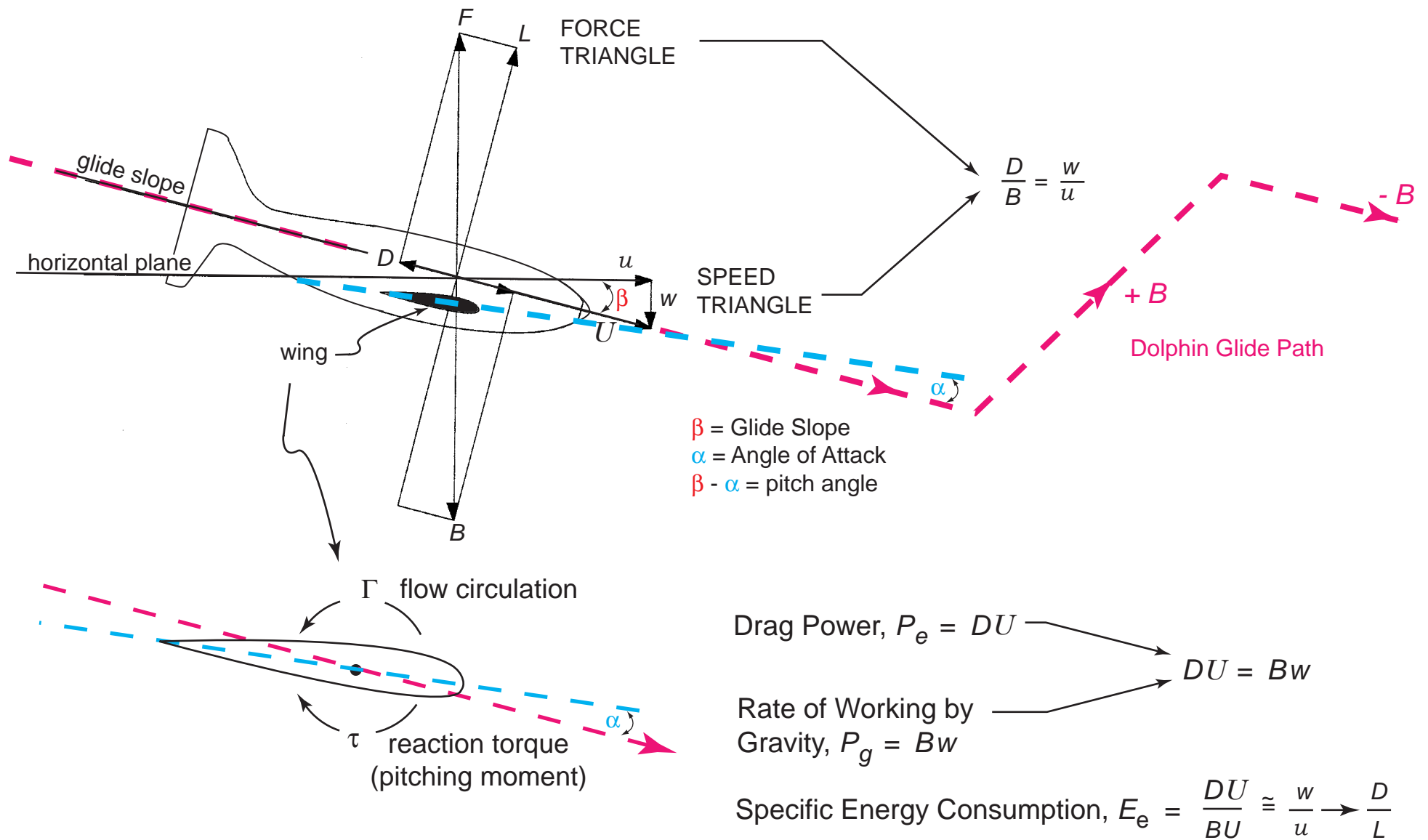
Figure 4.2. Force balance and energetics of gliding flight. B = net buoyancy, L = lift, D = drag, F = resultant of lift and drag, u = horizontal velocity, w = vertical velocity, U = glide velocity = resultant of horizontal and vertical velocity, Γ = flow circulation, τ = pitch moment.

Valve

Internal
Reservoir

EXTERNAL
BLADDER
(The Lung)

Glider Wet Volume Area

High Pressure Pump

Interior of Hull : At 2/3 Atmosphere Pressure
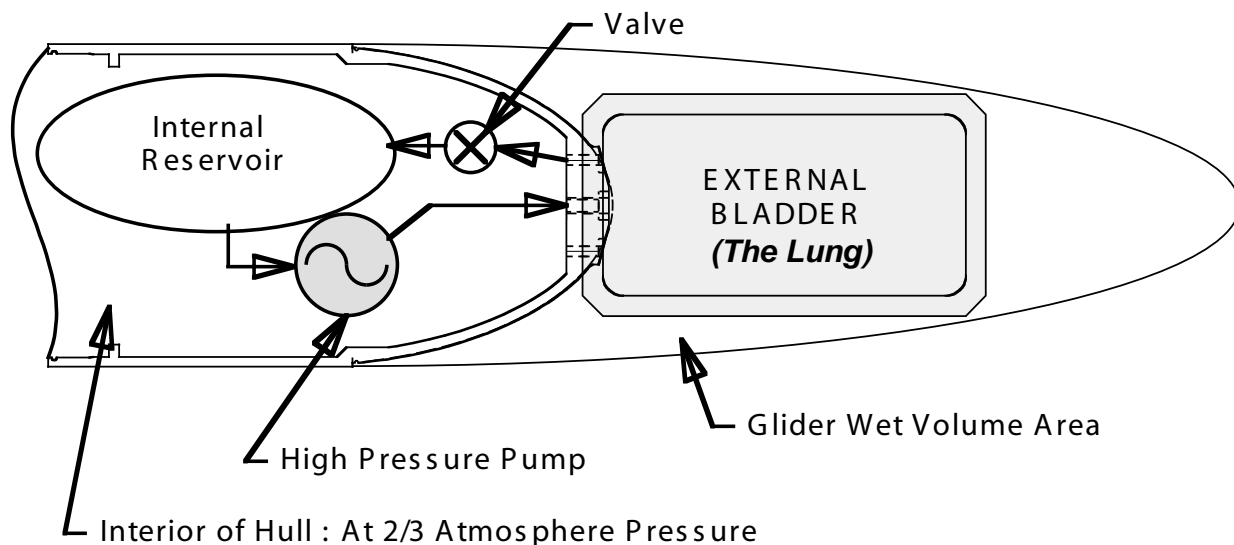
Glider Hydraulic Buoyancy Engine operation:

Beginning of a dive cycle:
1) The valve is opened, and the vacuum inside the pressure case draws in the oil from the external bladder into the internal reservoir, causing the glider to become negatively buoyant, and the descent glide begins. After all of the oil is evacuated from the external bladder, the valve is closed.

Bottom of a dive cycle:
2) The high pressure pump pumps oil from the internal reservoir to the external bladder, increasing the buoyancy until the glider begins to ascend at the desired rise rate. During the ascent the glider loses buoyancy due to having a stiffer hull compressibility than sea water, combined with moving into less dense water. The glider must pump more oil during ascent to maintain the same rise rate.

End of a dive cycle:
3) After reaching the surface the glider pumps more oil to the external bladder, increasing the surface buoyancy and raising the satellite antenna out of the water.

Figure 4.3. Schematic diagram of a buoyancy engine used in underwater gliders to vary net buoyancy, (*B*) from +*B* to -*B.*

4.3 Limitations of Underwater Gliders: The primary weaknesses of the underwater glider arise from its vulnerability to detection and lack of maneuverability while it is at the surface engaging in 2-way communications. All of its stealthy attributes are compromised during those moments. It also suffers from the inability to maintain a constant depth or level flight. As discussed in Section 4.1, the glider must change its depth in order to move from point A to B. A listing of limitations includes:

a) Depth Maintenance
   *Must Change Depth to Translate, Can Not Perform Level Flight
   *Restricted Station Keeping Near Surface
   *Restricted Station Keeping Near Bottom
b) Penetration Against Strong Currents
   *Glide Speed Restricted by Wing Loading & Depth Excursion
c) Control Authority in Surface Gravity Wave Regime
   (Large Waves, Shallow water)
d) Scale Effects:
   *Glide Efficiency (L/D) Degrades With Decreasing Size
   *Control Authority Degrades With Increasing Size
   *Strength to Immersed Weight (Buoyancy) Degrades With
    Increasing Size
e) Bio-Fouling & Fish Bites
   *Degrades Glide Efficiency (L/D)
   *Degrades Control Authority
   *Sensor Damage
   *Total Loss Potential
f) Survivability in Presence of Fishing/Trawling
   *Total Loss Potential
   *Detection/Avoidance
f) Viability of 2-Way Data/Communication Link
   *Performance Issues for ARGOS
   *Service Issues for Iridium & Globalstar

5. Functional Classes

This section defines the generic functions that underwater gliders might perform by exploiting their attributes within their physical limitations. Functional classes are not to be posed as mission specific operations, but rather as broad categories of action. The following items in bold italics is a partial listing of functional categories that underwater gliders might perform, with examples of missions in normal font under each:

5.1 ***Depth Unlimited Roaming:*** In depth unlimited roaming, the glider is not confined to a particular depth regime while translating cross-country, and is free to penetrate across the thermocline and other such water mass density structures within the confines between the surface and bottom of a deep ocean environment. Often such functions will be performed in the mid-ocean basin environment, requiring trans-basin round-trip excursions. The Seaglider and Spray are among this functional class, being designed primarily for the role of gathering ocean soundings of water mass properties. Design adaptations for such depth unlimited roaming require some or all of the following capabilities: long range, long on-station time, cruise speeds adequate to penetrate large scale ocean circulation, small to moderate payload volume, small to moderate hotel loads, deep dive capability with neutral hull compressibility. Potential transitions and applications for this functional class include:

> *Long Range Surveillance
> *Deep Water Perimeter Patrol
> *Re-Configurable/Recoverable Vertical Arrays
> *Deep Water Sentry with Terminal Homing & Identification
> *Deep Water Perimeter Defense or Barriers
> *Fuzing for Novel Tagging and Weapon Concepts in Deep Water
> *Gliding Depth Charge
> *Oceanographic Environmental Characterization
>   Ocean Soundings
>   Current Monitoring
>   Acoustic Experiment Monitoring
>   Fisheries Monitoring
>   Pollution Monitoring
>   ~waste fields from ocean outfalls
> *Optical Environmental Characterization

Above Surface (Atmospherics)
Below Surface (Ocean Optics)

5.2 *Depth Limited Roaming:* This functional class requires cross-country capability within a limited depth regime. This constraint arises when operations are required in the shallow water regimes of the littoral zone, or when the vehicle must operate in a prescribed sector of the water column such as the sound channel or avoid penetration across the thermocline. The Slocum has design adaptations for this role such as it's piston pump that allows it to rapidly reverse dive cycles in close proximity to the free surface or seabed in confined shallow water operational regimes. Design adaptations for this role require some or all of the following capabilities: flat glide slope (high L/D) capability to maximize range for a minimum number of dive cycles, high cruise speeds to penetrate strong coastal currents, small to moderate payload volume, small to moderate hotel loads, rapid high resolution pitch and roll response to avoid broaching or grounding in confined depth regimes, adequate control authority for suppressing wave induced flight oscillations and avoidance measures for fishing trawlers. Potential transitions and applications for this functional class include:

> *Patrolling Sonabuoy (Station Keeping in the Sound Channel)
> *Shallow Water ASW (Detection & Neutralization of
>   Enemy 206's and 209's)
> *Sentry and Round-Trip Coastal Patrol
> *Target Reconnaissance & Coastal Surveillance (above water
>   surveillance, monitoring of enemy experiments, biochemical testing
>   of coastal emissions)
> *Coastal Perimeter Defense and Barriers
> *Upward Looking Traffic Surveillance
> *Virtual Periscope (Safety for Surfacing Submarine)
> *Terminal Homing, Identification, Novel Tagging and Fuzing
>   Concepts (ala Ramora Penetrations into Enemy Harbor)
> *Dumb Mine hunting and Neutralization (ala Kamikaze Swarms)

5.3 *Virtual Station Keeping* : Station keeping requires the ability to maintain position at a prescribed point. Other than the case of free drifting in stagnation flow or grounding on the seabed, UW gliders must execute depth excursions in order o maintain station at a fixed latitude and longitude. Hence, the

station keeping ability is 2-dimensional and is referred to as *virtual* station keeping. All three legacy gliders have demonstrated virtual station keeping for long periods of time, some within a watch circle of several meters for several weeks time when the vehicle are trimmed for stationary flight in an opposing current. Some station keeping roles may require the glider to profile the water column at a fixed latitude and longitude, which would require maximum cruise and dive speed capability. Other station keeping roles may require that the glider maintain station in a certain depth regime, which would require that the glider have minimum sink rate properties. In either case, the glider requires adequate cruise speed to penetrate and hold station against ocean currents. In addition the glider may be required to hold station on the seabed, in which case it will need the ability to generate sufficient negative net buoyancy or have provisions in its hull and wing shape for anchoring it against currents. Other vehicle qualities for station keeping would be high endurance, long on-station capability, small to moderate payload volume, small to moderate hotel loads, rapid high resolution pitch and roll response to execute grounding maneuvers or maneuvers near the seabed, adequate control authority for suppressing wave induced flight oscillations when operating near the surface, and avoidance measures for fishing trawlers. Potential transitions and applications for this functional class include:

> *Re-configurable/Recoverable Array Concepts: vertical array
> concepts in the water column or grounded on the bottom (aperture
> forming, with collective, dispersal and redeployment capabilities)
> *Expand Vision of Already Established Arrays
> *Trip-Wire Sentries, for choke points and strategic waterways
> *Magnebuoys
> *Traffic Surveillance (upward or downward looking)
> *Fixed-Point Profiling of ocean properties

5.4 *Payload Delivery:* The stealthy, high endurance potential demonstrated by legacy gliders suggests that delivery of deployable payloads would be logical function when delivery time is not required in a matter of hours to a few days. Among the most important characteristics for this bread of UW glider would be the ability to move large payloads point to point at an efficient transport economy using minimal numbers of dive cycles. This may require both deep water and depth limited operational capability with adequate cruise speeds to penetrate both large scale ocean circulation and coastal currents. In addition, large payload

volume is required using minimal hotel loads. Potential transitions and applications for this functional class include:

*Long Range Clandestine Delivery (point-to-point)

*Littoral Penetration (Unmanned Alternative to SSN), Delivery of Large Payloads to Hostile Littoral Zones (eg: Deploy Mine Fields or Sea Floor Torpedoes, Lay Down Large Sapper Charges Against Moored Ships & Shore Facilities, Deploy Monitoring Networks, Pre-Position Offensive Assets)

*Long Range Swimmer Delivery Vehicle (SDV) for SPECWAR Operations

*Mother Vehicle for Insertion of Conventional SDV's

*Mother Vehicle for delivery of AUV's to Mine Search and Patrol Areas

5.5 *Level Flight Hybrids:* This concept is posed to compensate for two of the most important limitations of UW gliders: the inability to maintain depth and slow cruise speeds relative to conventional surface and sub surface vehicles. In essence it is a glider with an auxiliary motor driven screw. The concept of a motorized hybrid is envisioned for circumstances where operations are required in very narrow depth regimes, when level flight is required or when short term burst speed capability is needed. Level flight capability may be required for proper operation of certain upper end sensors like mine hunting and seafloor mapping sensors, or for operations in very shallow water such as enemy harbors. Burst speed capability may be required for certain avoidance maneuvers or for penetration in strong shallow water currents such as encountered navigating through chokepoints. The concept entails conventional glider operations at low energy consumption levels while executing long range insertions and extractions from operational or denied access areas, and then motorized runs with active screws while performing level flight or high speed sprints within those areas. In many respects, the Hybrid glider provides a concept for a long range, high endurance AUV. Long range transit ability can be augmented by extraction of thermal energy from ocean stratification, and harvesting kinetic energy from velocity shear and wave induced flow. Design adaptations for this role require many of the same characteristics of depth unlimited roaming, including: flat glide slope (high L/D) capability to maximize range for a minimum number of dive cycles while in transit to and from the target region, low drag with high cruise speed to maximize powered flight performance, small to moderate payload

volume, small to moderate hotel loads, rapid high resolution pitch and roll response to avoid broaching or grounding in confined depth regimes, adequate control authority for suppressing wave induced flight oscillations and avoidance measures for fishing trawlers and other shallow water traffic. Potential transitions and applications for this functional class include:

*Reconnaissance and Surveillance in Enemy Harbors, Bays, Estuaries, Coastal Rivers and Other Inland Waterways
*Mobile Mine Countermeasures, Pattern Searches, Identification, Marking and Neutralization
*ASW Patrol/Detection
*Surface Ship Detection and Traffic Surveillance
*Seafloor mapping where motion compensation would otherwise be required for pure gliders that can not maintain constant depth
*Terminal Homing in Harbors and Coastal Waters (Long Range Torpedo)

6. Scaling Rules and Leading Order Variables

Analytic surveys of natural and man-made flyers provide a logical starting point for identification of present operating regimes of the legacy gliders and rules of scale to extrapolate to other performance regimes from those gliders. The practice of design surveys in aeronautical design and bio-mechanics has produced a number of useful works for this purpose, including: McMasters, (1974, 2003), Pennycuick, (1966, 1971, 1973 and 1992), Schmidt-Nielson, (1972), Tucker (1968), Tennekes (1997) and Withers (1997). Table 6.1 gives a summary of gross characteristics of the complete spectrum of natural and man-made flyers, ranging in scale from insects to jet transports. A separate listing for birds only with selected performance data is found in Appendix A.

6.1 Energetics: A distillation of the analytic flight survey literature reveals that the leading order variable controlling regimes of scale is the loaded mass, M, applied to the wing, where $Mg = B =$ the net buoyancy force and g is the acceleration of gravity (Figure 4.2). In the underwater glider application, the loaded mass is supplied by the buoyancy engine. The legacy gliders typically operate at a loaded mass on the order of 100g, placing them in a regime of scale comparable to bats (see Table 6.1). The loaded mass (net buoyancy/g) is the scale-controlling factor of the *net transport economy* (*NTE*), a measure of the cost of transport in terms of the energy consumed per meter traveled for each kilogram of loaded mass in air or net buoyancy underwater,

$$NTE = P/(Bu) \quad = \quad P/(Mgu) \qquad (6.1)$$

The net transport economy is dimensionless and smaller values indicate less incremental energy consumption is required per meter traveled in order to transport each kilogram of loaded mass and therefore more efficient transport. By convention, the dimensionless *NTE* is commonly compared to the loaded mass in kilograms, (Pennycuick, 1966, 1971, 1973). The next to last column on the right hand side of Table 6.1 give numerical estimates of net transport economies for host of natural and man-made flyers as compiled by Boeing engineer, John McMasters, (see McMasters ,1974).

Type	Wing Span $2b$ (m)	Wing Area A (m)	Aspect Ratio Nr	Load Mass M (kg)	Wing Load B/A (N m²)	Cruise Speed u (m/s)	NTE/u (W/kg)	E_e (W-S) (N-m)	Ref.
Insects:									
1. House fly (Musca)	0.013	2×10^{-5}		1.2×10^{-5}	5.9	2.0	166		26,34
2. Butterfly (Papillio)	0.082	3.6×10^{-3}	1.87	3×10^{-4}	0.82	3.5			8
3. Locust (Schistocerca)	0.10	2×10^{-3}	5.0	2×10^{-3}	9.8	4.15	87		11,32
4. Blue Dragonfly (Aeschna)	0.10	1.85×10^{-3}		1.5×10^{-4}	0.8	10			6
Birds:									
5. Pigeon (Columba)	0.65–0.25	0.063–0.038	6.7–1.6	0.4	62–102	12.4	67.5	0.185[+]	14
6. Fulmar petrel. (Fulmaris)	1.09	0.102	11.7	0.725	69.5	12.2		0.120[+]	13
7. Black vulture (Coragyps)	1.32	0.323	5.4	1.79	54	12.5		0.088	39
8. White-backed vult. (Gyps)	1.44	0.364	5.7	2.30	62	15		0.045	12
9. Rüppel's Griff. vult. (Gyps)	2.2	0.69	7.0	5.4	76.5	13	(3.64)[+]	0.066	15
10. Wand. albatross (Diomedae)	2.5	0.83	7.55	7.5	88.5	14.5		0.0625	16
	3.5	0.60	20.4	9.2	150	20		0.050	43
	3.45	0.725	16.5	9.8	132	16		0.052	41
Bats:									
11. Dog-faced bat (Rousettus)	0.461	0.04	5.32	0.119	20.6–29.2	8		0,156	17
	0.554	0.057	5.42						
Pterosaur:									
12. Pteranodon	7	4.2	11.5	16	37	9		0.050	48
	7.6	4.6	12.5	11.3	24	8		0.087	3,47
Anemophilous Seed:									
13. Zinonia	0.15	6.2–3	3.63	3–4	0.475				50
	0.115	5–3	2.65	1.75–4	0.343				6
Hang Gliders:									
14. Typ. Std. Rogallo	6.58	18.4	2.36	81.5	43.5	10		0.25	4
15. Eipperformance "Quicksilver B"	9.15	10.75	2.65	81–118	74–108	9.8		0.143	4
16. Kiceniuk "Icarus V"	9.75	14.9	6.4	100	65.8	10		0.1	4
17. Volmer Jensen VJ-24	11.1	15.15	8.15	141	91	9		0.1	4

Table 6.1. Vehicle Characteristics

Type	Wing Span 2b (m)	Wing Area A (m)	Aspect Ratio Nr	Load Mass M (kg)	Wing Load B/A (N m²)	Cruise Speed u (m/s)	NTE/u (W/kg)	E_e (W-S) (N-m)	Ref
Man-Powered Aircraft:									
18. Hatfield "Puffin II"	28.4	36.3	22.2	132	35.7	8** (8.7)	14.3** (17.5)	0.028** (0.032)	52
19. Herts. "Toucan"	37.5	55.8	25.2	240	42.2	8.25** (9.2)	13.1** (17.4)	0.025** (0.030)	52
20. Weybridge "Dumbo"	36.7	44.6	30.2	127	27.9	7.45** (8.0)	11.0** (13.8)	0.023** (0.027)	52
Motor Glider:									
21. Scheibe SF-27M	15	12.1	18.6	370	300	34.2		0.032	Zacher 55
Sailplanes:									
22. Schweizer 1-26	12.2	14.9	10	270	178	21.6	39.5	0.0465	56
23. Schempp-Hirth "Std. Cirrus"	15	10.0	22.5	333	326	26.2	29.6	0.0264	56
24. Schleicher AS-W-12	18.3	13.0	25.8	412	311	24.6	22.6	0.0231	56
25. VVG	18.6	10.25	33.8		477	30.5			
Design Study	19.0	16.3	22.3	500	300		27.6	0.0230	3
General Aviation:									
26. Piper PA-18 "Super Cub"	10.76	16.58	7.0	794	479	32	157	0.09	
27. Beech "Bonanza"	10.2	16.8	6.2	1417	830	48	192	0.075	
28. Cessna 310F	10.9	16.3	7.3	2190	1320	56	209	0.071	
Jet Transports:									
29. McD.-Douglas DC-9-20	28.4	93.1	8.7	4×10^4	4200	190	580	0.055	
30. Boeing B-707-320	44.4	274	7.2	1.22×10^5	4400	210	523	0.059	
31. Boeing B-747	59.6	511	6.95	2.8×10^5	5400	240	420	0.059	

** Flight in ground effect at 3 m height

+ Power-off glide

++ Half fuel weight

Note: All numbered data points on Figures 6 and 10-13 correspond to the entries in Table 1.

Table 6.1 Continued. Vehicle Characteristics

Figure 6.1 plots the dimensionless net transport economy over 12 orders of magnitude variation in loaded mass, covering regimes of scale from insects to jet transports. The numbered points correspond to the entries in Table 6.1. The *NTE* values in Figure 6.1 are based on total power consumption including both the external flight energy spent overcoming drag ($P_e = DU$) as well as internal energy consumption (P_0), which includes basal metabolic rates in the case of natural flyers and all sub-system energy consumption in the case of man-made flyers (*hotel loads*). Tucker (1970) made some estimates of the basal metabolic rates of birds based on the body mass and came up with an empirical formulation of *NTE*:

$$NTE = 0.898(Mg)^{-0.227} \qquad \text{(Tucker Flyers)} \qquad (6.2)$$

Schmidt-Nielsen (1972) examined a limited set of data on birds and derived a similar empirical relation:

$$NTE = 0.914(Mg)^{-0.293} \qquad \text{(Schmidt-Nielsen Flyers)} \qquad (6.3)$$

These two empirical relations are indicated by the solid sloping lines in Figure 6.1. The most apparent scale dependent feature of these empirical relations and the *NTE* data is that the energy consumed per meter traveled decreases for each additional kilogram of loaded mass as the loaded mass is increased, ie bigger flyers (greater loaded mass) are more efficient flyers.

The legacy gliders presently operating in the range of 100-300 g of loaded mass are overlaid on Figure 6.1 as a red triangle. It appears that the legacy gliders are consuming relatively higher levels of energy per meter traveled than their bird/bat counterparts operating at equivalent loaded mass. Natural flyers are used as a standard for ultimate efficiency because natural selection tends to eliminates all but the most efficient mutations (Welty, 1962). One contributor to the disparity in efficiency of legacy gliders relative to birds is the extra energy that is consumed when having to glide through ocean stratification, particularly when crossing the thermocline. Density changes in the ocean water mass cause corresponding changes in net buoyancy B, resulting in additional rate of working by gravity as defined by the right hand side of equation 4.1. Hull compressibility resulting from depth changes in the ocean cause additional changes in net buoyancy and in work rates by gravity that ultimately factor against the total power consumption of the UW glider. There is no counterpart to this increment of energy consumption for birds flying in air.
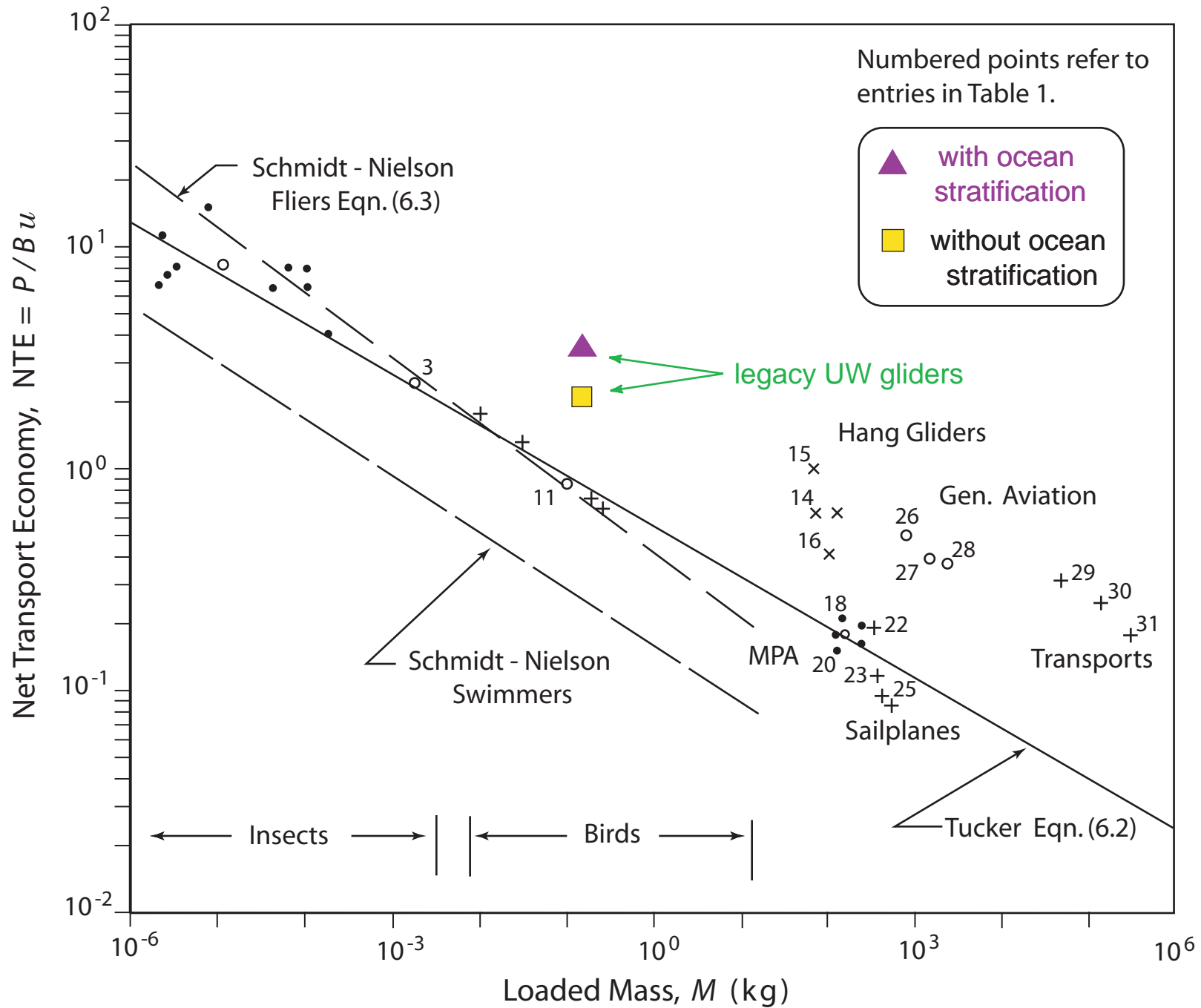
Figure 6.1. Net Transport Economy (NTE) for natural and man made flyers verses the legacy underwater gliders with and without ocean stratification. Based on total energy (external + internal) consumption.

To estimate the extra incremental energy consumption required for gliding in the ocean vs in air, consider the net buoyancy of a glider as given by:

$$B(z) = \rho(z)g \, V_0 \, (\, 1 - kp + \kappa T) - gm_0 + \rho(z)g \, \delta V(t) \qquad (6.4)$$

Here: m_0 = vehicle mass, V_0 = displaced volume of the vehicle at the surface with buoyancy engine oil retracted, k=hull compressibility, p is the external hydrostatic pressure, κ = temperature coefficient, $rho(z)$= vertically varying density of a stratified ocean, δV = net buoyancy volume due to the amount of oil pumped in and out of the pressure hull by the buoyancy engine and $p\delta V$ = the pump work done by the buoyancy engine. To maintain a constant speed U_0 (with constant sink/rise rate w_0), then the buoyancy must be maintained as:

$$B(z) = B_0 \; = U_0 \, D \, / \, w_0 \qquad (6.5)$$

As a rigid hull glider (less compressible than seawater with small k) initially executes an ascending glide from depth from depth $z = Z_0$, it selects a net buoyancy volume $dV(z=Z_0)$ that gives $B(z=Z_0) = B_0$. However, as the glider ascends higher in the water column and the pressure relaxes, it becomes less buoyant because the hull is less compressible sea water. Consequently the buoyancy pump must create an additional increment of buoyancy volume δV 'in order to maintain the buoyancy B_0 necessary for a steady state glide. Similarly, as the ascending glide path crosses the thermocline and the seawater density decreases, the buoyancy is further reduced, requiring an additional expenditure of pump energy $p \, \delta V$" to maintain a steady state glide. Neglecting hydraulic inefficiencies of the pump itself, the pump energy expended during an ascending glide must balance the flight energy associated with the vertical excursion Z_0 through the water column, or:

$$p \, \Sigma\delta V = B_0 Z$$
$$(6.6)$$

where: $\Sigma\delta V = \delta V(z=Z_0) + \delta V' + \delta V"$

On descending glides the same incremental energy exchanges associated with compressibility *(p δV')* and density stratification *(p δV")* occur in reverse; and if the buoyancy engine were a perfect thermodynamic system, there would be

no net change in the energy budget due to these effects at the completion of a steady state dive cycle. However, the present technology buoyancy engines used in the legacy gliders have no provision for recovery of these energy increments during a descending glide. An advanced buoyancy engine would bleed oil back inside the pressure hull through a generator during a descending glide which would let us recover the $p\, \delta V'$ and $p\delta V''$ work increments. Instead, this work gets thrown away, and we end up paying the price. We pay for it in two ways: we throw away the energy, and we also must carry around more oil to compensate for the full range of δV required.

To estimate how much energy might be wasted in this way, consider Levitus temperature/salinity (T, S) profiles from three ocean environments that give a high degree of variability in density stratification, namely at: 52 N, 145W, 36 N, 125 W, and 7 N, 120 W, see Figure 6.2. We consider a numerical computation of a complete dive cycle for the legacy glider Spray, gliding down to 1000 m depth and back to the surface, adjusting the surface buoyancy such that the average horizontal speed on descent is 25 cm/s. On ascent, δV is adjusted to maintain the 25 cm/s speed, and then pump energy is integrated to give the total energy required. These computations were repeated for a full range of compressibility.
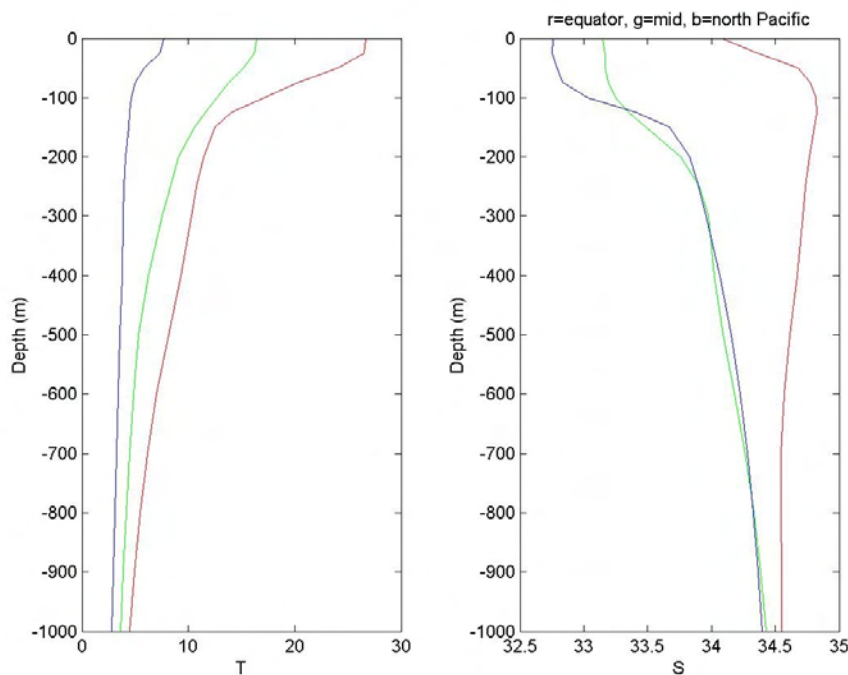
Figure 6.2: Levitus temperature profiles (left) and salinity profiles

(right).The red curves are from the equator, green is the mid-Eastern Pacific, and blue is the Northeast Pacific. After Sherman (2003).

Figure 6.3 shows the starting surface buoyancy, and the value at the 1000 m dive apogee for the three locations (based on Equations 6.4 & 6.5). A Buoyancy value of B_0=113 gms is required for 25 cm/s horizontal speed. For the Spray (k=3e-6), at the equator it starts B(z) ~330 gms heavy at the surface and ends up B(z)~70 gms heavy at 1000 m, for an average horizontal speed of 25 cm/s. If the Spray had the same compressibility as sea water (k~4.4e-6), the buoyancy swing would be B(z)~280 gms at the surface, reducing to B(z)~100 gms at 1000m depth. Again we find that for a glider with the same compressibility as sea water operating in a homogeneous ocean ($\rho(z)$ = constant), all buoyancy goes into flight energy (Equation 4.1), and the pump energy expended at the dive apogee is $p\,\delta V = B_0 Z$, where the net buoyancy volume for steady glide is simply $\delta V = B_0\,/(\rho g)$.
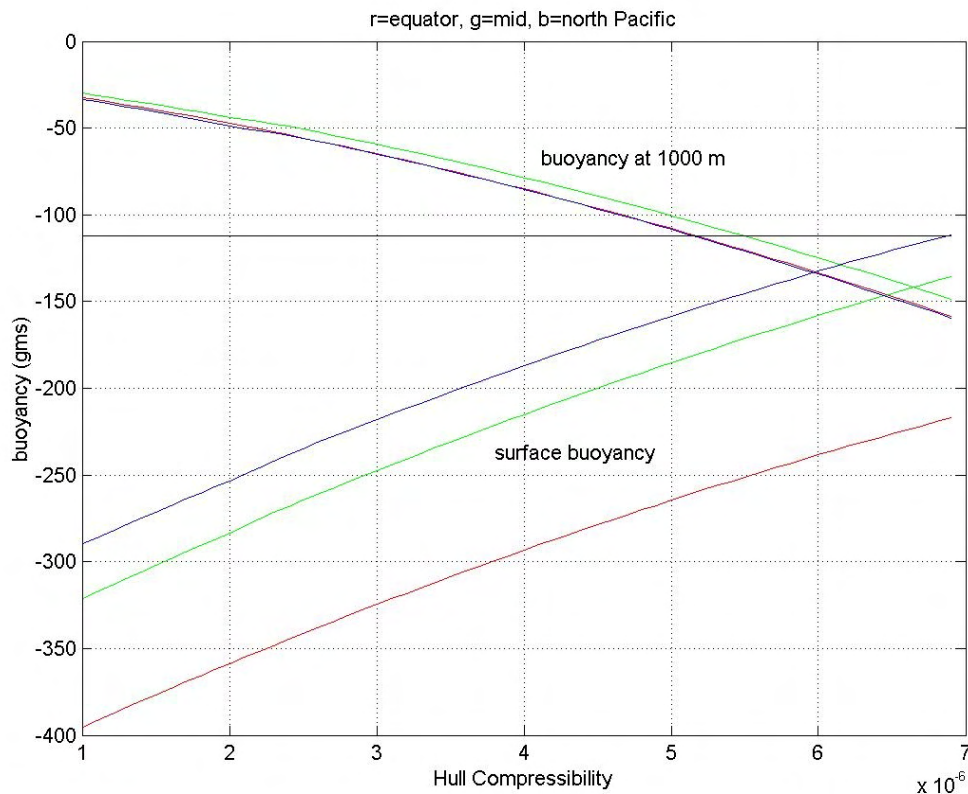
Figure 6.3: Computed buoyancy changes between surface and 1000m depth as a function of hull compressibility (k) in three ocean environments : equator (red), mid-latitudes (green) high northern latitudes (blue). From Sherman (2003)

Figure 6.4 gives computations of the energy that is wasted due to the lack of energy recovery capability of present buoyancy engines when operating in stratified ocean environments with pressure hulls that do not match seawater compressibility. The results are expressed in terms of the ratio of the total pump energy expenditure to the flight energy during a 1000m gliding dive cycle. Note that a hull slightly more compressible than sea water gives the minimum pump energy expenditure, as it somewhat compensates for the higher density below the
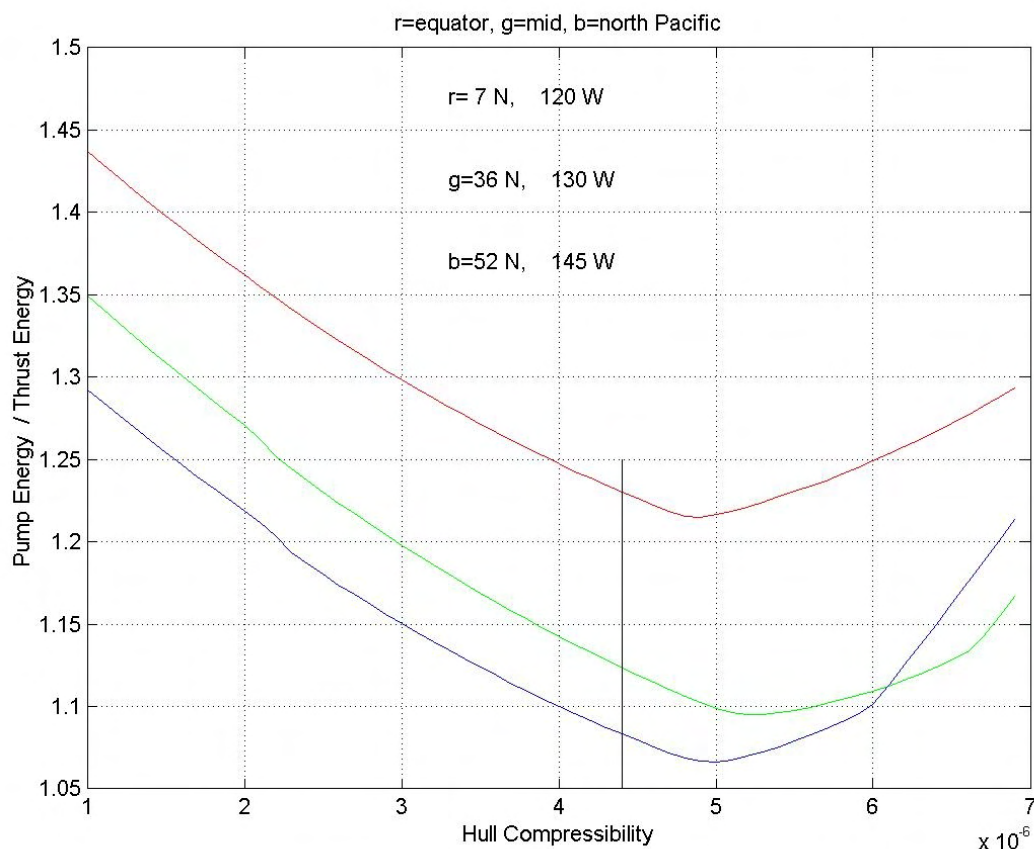
Figure 6.4: Ratio of buoyancy pump energy consumption to flight (thrust) energy as a function of hull compressibility (k) during round trip gliding dives to 1000m depth in three ocean environments : equator (red), mid-latitudes (green) high northern latitudes (blue). From Sherman (2003)

thermocline (this advantage is slight). For the Spray compressibility of k=3e-6, we pay ~6% higher energy cost over a hull with k=4.4e-6. The energy cost due to the density gradient varies from ~8 % of the flight (thrust) energy (at k=4.4e-6) in high latitude environments to as much as 23% in equatorial environments. This result is tempered by the fact that the seasonal thermocline is shallow in Figure 6.2, but the penalty in not recovering the *P dV"* work during descending glides in more strongly stratified coastal environments (as found near major rivers) may be considerably higher

If we correct the net transport economy calculations for the legacy glider in Figure 6.1 to remove the 23 % higher energy consumption due ocean stratification and the 6 % higher consumption associated with hull compressibility, then we get a new data point represented by the blue square. Although this correction places the legacy gliders in a more similar environmental context with natural flyers in air, we find that the legacy gliders still can not match the transport efficiency small birds, bats and bio-swimmers (Schmidt-Nielson). So the question arises, how much of this disparity is due to the aero/hydro-dynamic efficiency of the flying shape and how much is due to other forms of energy consumption not directly associated with flight energy. Those other forms of consumption are termed *internal* energy consumption (P_0), and include the basal metabolic rates in the case of natural flyers and all sub-system energy consumption in the case of man-made flyers. For underwater gliders, these sorts of internal forms of energy consumption are referred to as *hotel loads,* and include the power consumed by sensors, payloads, and navigation, communication and data link systems.

To normalize for differences in internal energy consumption between legacy gliders and flyers in air and to reveal relative differences in efficiency of the flying shapes, we compare *specific energy consumption (E_e)*, which is a transport economy formulation based only on the rate of expenditure of flight energy required to overcome drag ($P_e = DV = Bw,$), see Tennekes, (1997). Figure 6.5 shows the data from Figure 6.1 recalculated in terms of specific energy consumption. Again, the numbered data points in Figure 6.5 correspond to the various entries of natural and man-made flyers listed in Table 1, and the legacy gliders are calculated without energy expenditure to overcome ocean stratification. We find that the disparity between legacy gliders and natural flyers at a comparable loaded mass still exists. From analysis of observational measurements of birds in wind tunnel and in natural environments, Tucker (1970) has extracted an empirical relation for specific energy consumption of natural flyers based on body mass (*M* in kg):

$$E_e = 0.109(Mg)^{-0.185} \qquad\qquad (6.7)$$

Legacy gliders are simply less efficient flyers (larger E_e) than Tucker's equation would predict (see Figure 6.5). Hence, it appears that the present underwater gliders are consuming an excessive amount of flight energy compared with the possibilities demonstrated in Nature and that the shapes or the operational regime (as selected by loaded mass) can be further improved.

　　To explore the sources of this aerodynamic inefficiency it is helpful to make a simple analytic formulation of specific energy consumption using classical aerodynamics. From The force and speed triangles of Figure 4.2 and Equation (4.1) we write:

$$E_e = DU/Bu = Bw/Bu \sim D/L = C_D/C_L \qquad\qquad (6.8)$$

C_D and C_L are the drag and lift coefficients, normalizing drag D and lift L respectively to the wing area A:

$$D = 1/2\rho\, C_D AU^2$$

$$L = 1/2\rho\, C_L AU^2$$

The drag coefficient is made up of two terms: a Reynolds number (Re) dependent profile drag term (C_{D0}) and an induced drag term C_{Di} that increases with increasing lift coefficient and decreases with wing aspect ratio, Nr, or:

$$C_D = C_{D0} + C_{Di} = K_0\, R_e^{-a}(A_t/A) + KC_L^2/(\pi\, Nr) \qquad\qquad (6.9)$$

Here, K is a constant, typically $K/\pi = 0.38$ for flyers in air; and the aspect ratio is $Nr = 2b/c = 4b^2/A$, where $2b$ is the wing-span and c is the mean cord of the wing. The Reynolds number dependent profile drag term is largely due to friction acting on the total wetted area (A_t). Here the power law dependence of profile drag is $a = \frac{1}{2}$ for a completely laminar, unseparated boundary layer over the vehicle; and $a = 1/5$ for completely turbulent unseparated boundary layer. While the Reynolds number increases linearly with glide speed, both glide speed, U, and sink rate, w,
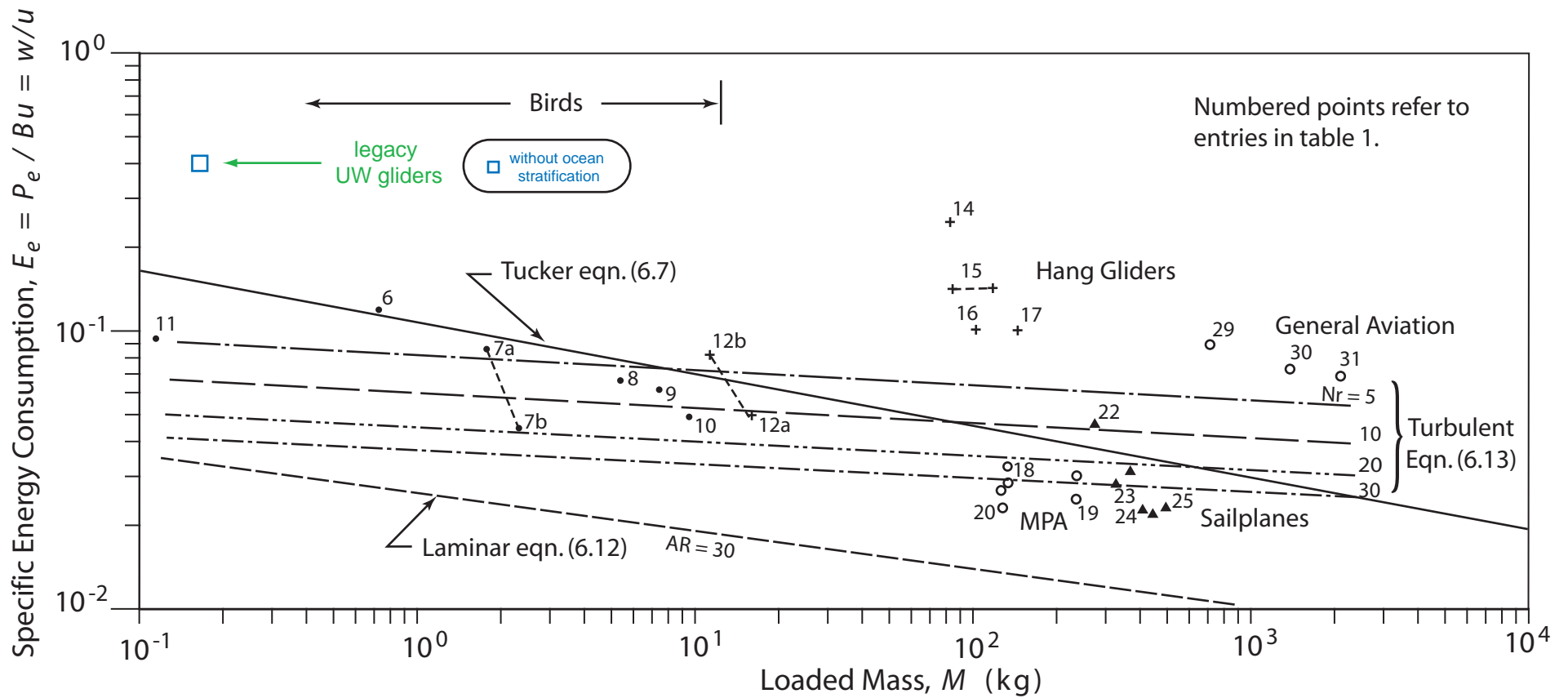
Figure 6.5. Specific Energy Consumption (E_e) for natural and man-made flyers verses the legacy underwater gliders based on external energy consumption [after McMasters, 1974].

The following equations appear within the figure:

$$E_e \sim (A_t/A)^{4/7} \ (Nr)^{-2/7} \ (M)^{-1/7} \qquad \textit{pure laminar boundary layer}$$

$$E_e \sim (A_t/A)^{10/19} \ (Nr)^{-8/19} \ (M)^{-1/19} \qquad \textit{pure turbulent boundary layer}$$

Where: A_t = total wetted surface area
A = wing planform area
Nr = wing aspect ratio
M = loaded mass

increase with the loaded mass (*M* in kg*)* per unit wing area:

$$U = (2Mg/\rho \, C_L A)^{1/2} \sim (B/A)^{1/2}$$

and

$$w \sim (2MgC_D / \rho \, C_L^{3/2} A)^{1/2} \sim (B/A)^{1/2} \qquad (6.10)$$

The factor $B/A = Mg/A$ is commonly referred to as the *wing loading* (force per unit area applied to the wing) . Substituting the wing-loading dependent cruise speed into the Reynolds number formulation gives:

$$Re = Uc/\nu = (2/\rho\nu^2)^{1/2} (Mg/C_L Nr)^{1/2}$$

With (6.9) and (6.7) inserted in (6.5) an analytic solution for the specific energy consumption is obtained:

$$E_e = K_0 \, (\rho\nu^2/2)^{a/2} \, C_L^{-(1-a/2)} (Nr/Mg)^{a/2} (A_t /A) + KC_L^2/(\pi \, Nr) \qquad (6.11)$$

or, more generally:

$$E_e \sim (M)^q (A_t/A)^r (Nr)^s$$

where: $q = -a/(4-a)$
$\quad\quad\quad r = 2/(4-a)$
$\quad\quad\quad s = -2(1-a)/(4-a)$

Two limiting forms of (6.11) result from the selection of the exponent a in the Reynolds number dependent friction drag:

$$E_e \sim (M)^{-1/7} (A_t/A)^{4/7} (Nr)^{-2/7} \quad \text{all laminar boundary layer} \qquad (6.12)$$
$$(q = -1/7; \, r = 4/7; \, s = -2/7)$$

$$E_e \sim (M)^{-1/19} (A_t/A)^{10/19} (Nr)^{-8/19} \quad \text{all turbulent boundary layer} \qquad (6.13)$$
$$(q = -1/19; \, r = 10/19; \, s = -8/19)$$

These solutions are indicated by the monotonically declining straight lines

in Figure 6.5. Both the laminar and turbulent state solutions show dependence on *B* that indicates flight at higher loaded mass is more efficient, consuming less flight energy per meter traveled for each additional kilogram (Newton) of payload. The efficiency improves more rapidly with increasing loaded mass if the boundary layer remains laminar, $(M)^{-1/7}$ vs $(M)^{-1/19}$ for the turbulent boundary layer. The wing aspect ratio exerts a somewhat stronger influence, with the specific energy consumption decreasing with increasing aspect ratio as $(Nr)^{-8/19}$ for a turbulent boundary layer and as $(Nr)^{-2/7}$ if it is laminar. Turbulent solutions from (6.13) are plotted for varying wing aspect ratios ranging from *Nr = 5 to 30*. In the turbulent regime, increasing the wing aspect ratio from 5 to 30 reduces consumption of flight energy by 50%. An aspect ratio of 30 is approaching the structural limits for supporting bending and torsional loading. Consequently, the laminar solution shown in Figure 6.5 for an aspect ratio of 30 approximates the most efficient of utilization of flight energy that is possible with existing materials technology. Natural flyers (which have an aspect ratio of no more than *Nr* = 18 and more typically 5 to 8) appear to be operating in a mixed regime that is intermediate between pure laminar and all turbulent states. The other shape-related factor that strongly effects the specific energy consumption is the amount of wetted surface area that is generating lift, as expressed by the ratio of wetted area to the wing area A_t/A. The consumption of flight energy goes up rapidly for both the laminar and turbulent states as more and more non-lifting surface area is added to the vehicle. The smallest A_t/A ratios are associated with flying wing geometries, such as utilized by birds for which A_t/A *= 2.2 to 2.4.*This shape adaptation may in large part explain the superior flight efficiency of birds in the size (mass) regime in which they operate.

The apparently excessive consumption of flight energy by the legacy gliders (Figure 6.5) can now be understood. By operating at such a small loaded mass (*M* ~ 100 – 300 g) legacy gliders are in a scale regime that is intrinsically less flight efficient. Utilization of the dead space volume in these vehicles to increase the net buoyancy to say 1-3 kg would reduce the specific energy consumption by 72% in an all- laminar state and by 89% in an all-turbulent state. This would be a considerable increase in efficiency for essentially no change in vehicle configuration. A further indication that the legacy gliders are not heavily loaded enough in relation to their volume is that the wetted area to wing area ratio is A_t/A *=19 – 27,* about an order of magnitude greater than the small birds and bats operating at the same loaded mass. About 90% of the wetted area of the legacy glider is due to the body volume that produces essentially no lift. In essence the

legacy glider is closer to being a gliding blimp than a bird. Because E_e goes up at roughly the ½ power of the A_t/A ratio, an order of magnitude larger A_t/A for legacy gliders translates into a three fold larger consumption of flight energy than their bird counterparts. At first glance, a possible reconciliation for this energy penalty might be to consider fitting legacy gliders with larger wings in order to reduce the A_t/A ratio.

Figures 6.6 and 6.7 compare the wing dimensions of the legacy glider to the natural and man-made flyers on the basis of equivalent loaded mass. Wing dimensions scale with loaded mass by a principle known as the *square-cubed law* originally posed by aviation pioneer, Cayley, and critiqued later in the *Journal of Aircraft* by Cleveland (1970). Based on dimensional analysis, the basic law specifies:

Wing Semi-Span: $b \sim M^{1/3}$
Wing Area: $A \sim 0.165 \, M^{2/3}$ *(6.14)*

Where M is loaded mass in kg. Inspection of Figure 6.6a indicates the wing semi-span of the legacy gliders may be a bit excessive for the loaded mass at which they operate, but that the wing area of the legacy gliders in Figure 6.6b compares closely with Nature , fitting almost exactly the square-cube law formulation in (6.14) refined by Tucker (1970 and 1972) from measurements of birds. Hence the lack of comparable efficiency of the shapes of the legacy gliders revealed by Figure 6.5 appears not to be due to insufficient wing area, but rather, because the loaded mass M is too small or the wetted surface area A_t is too big, or both . So the next question arises, how little B is too small and how much A_t is too much? To find this parametric balance we write the normalized total derivative of the specific energy consumption from (6.11):

$$\mathrm{d}E_e/E_e = q \, \mathrm{d}M/M + r \, \mathrm{d}A_t/A_t + s \, \mathrm{d}Nr/Nr \qquad (6.15)$$

The loaded mass (net buoyancy/g) depends on how much variable buoyancy volume ($V_{buoyancy}$) can be packed into the vehicle and is proportional to the total vehicle volume V_0 by what shall be referred to as a *lung capacity factor, n_b*

$$M = \rho n_b V_0 \sim n_b \ell^3 \tag{6.16}$$

where $n_b = V_{buoyancy}/V_0$ and ℓ is some characteristic dimension that is a measure of vehicle size. Similarly the wetted surface area is related to total vehicle volume by the cross section factor, n_r:

$$A_t = n_r V_0^{2/3} \sim n_r \ell^2 \tag{6.17}$$

The wing semi-span b is related to the characteristic length by the wing stretching factor $b = n_w \ell$ such that the aspect ratio scales as:

$$Nr = (4n_w \ell)^2 / \ell^2 = 4n_w^2 \tag{6.18}$$

Hence the aspect ratio is independent of vehicle size at lowest order. With (6.16) through (6.18) inserted in Equation (6.15), the size dependence of the specific energy consumption is given by:

$$dE_e/E_e = q(3n_b \, d\ell/\ell + dn_b/n_b) + r(3n_r \, d\ell/\ell + dn_r/n_r) + s \, dNr/Nr \tag{6.19}$$

Equation (6.19) reveals that a percentage increase in vehicle size, $d\ell/\ell$, will only make a percentage reduction in the flight energy consumption if the vehicle is sufficiently packed with variable buoyancy such that

$$n_b^* > 2r \, n_r/(-3q)$$

or

$$V^*_{buoyancy} > V_0 \, 2r \, n_r/(-3q) \tag{6.20}$$

Inserting the surface area and dimensional data of the 50 liter legacy gliders into Equation 6.20 gives a threshold buoyancy volume $V^*_{buoyancy} = 188$ cc ($n_b^* = 0.37\%$) for laminar flow and $V^*_{buoyancy} = 510$ cc ($n_b^* = 1.0\%$) for turbulent flow. Presently, legacy gliders operate at a lung capacity factor of about $n_b = 0.2\%$ to 0.5%. Since the legacy gliders are presently using a variable net buoyancy volume of 100-150 cc, simply making them proportionately bigger may or may not make them more transport efficient depending on the percentage of laminar flow which their shapes will support. A more direct approach is to first increase the lung capacity factor of those gliders in order to achieve a higher efficiency with greater
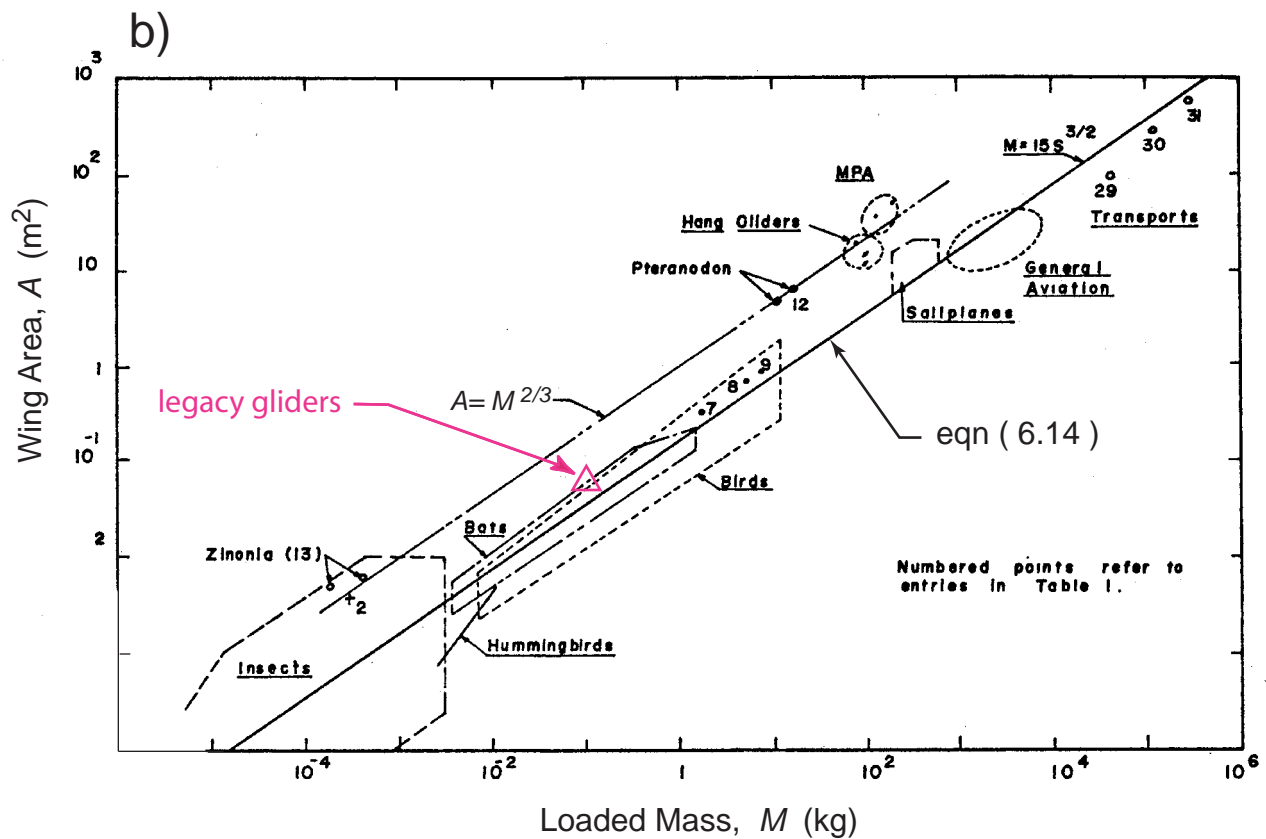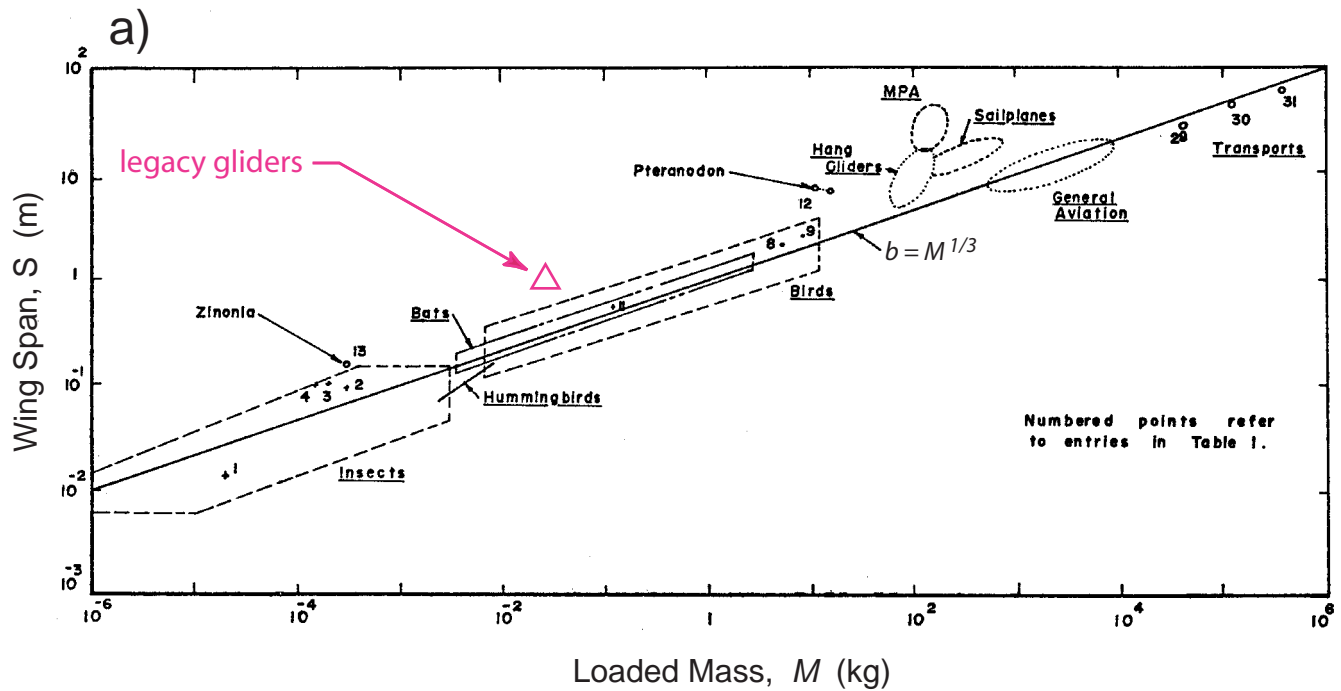
Figure 6.6. Characteristic wing dimensions as a function of loaded mass (*M*) for: a) Variation in wing semi-span (*b*) with loaded mass, and b) Variation in wing area (*A*) with loaded mass, [from McMasters , 1974].

size. The approach is evaluated in Sections 10 and 11.

 Although (6.19) suggests that E_e can be reduced indefinitely by ever larger wing aspect ratios, Nr, there is in fact a size limitation to achieving performance improvements by this design approach. Specific energy consumption declines as the lift to drag ratio (L/D) increases; but L/D suffers a catastrophic decline if the wing section cord is made too small in an effort to achieve a high aspect ratio. Figure 6.7 shows that this L/D crisis occurs when the wing section Reynolds number, $Re = Uc/\nu$ drops into the mid 10^4 regime. This phenomenon occurs because of laminar separation on the suction side of the wing section, which destroys a large percentage of the lift. Legacy gliders with their present 10-20 cm wing cords and 30 cm/sec cruise speeds are operating within the laminar separation regime where their wings will not be able to realize a higher L/D and lower E_e by simply flying them at higher angles of attack, α, see Figure 4.2. This suggests a need to go to bigger wing cords and get above the mid 10^4 Reynolds number regime in order to improve the efficiency of the legacy gliders. Since nature indicates in Figure 6.6 that the wing area of legacy gliders is properly sized, these larger wing section cords would reduce the wing aspect ratio. The aspect ratio of the legacy gliders varies from a maximum of $Nr = 9.75$ for Spray to a minimum of 4.4 for Seaglider. Table 1 entries for birds and bats at equivalent loaded mass seem to suggest an optimal aspect ratio of $Nr < 4$. This is contrary to the guidance given by the aspect ratio dependent terms in equations (6.11) and (6.19) , but these terms are the result of the original inviscid lifting line formulation of Prandtl (1936). However such improvements in efficiency through aspect ratio reduction are unique to the particular size regime of laminar separation ($Re < 10^5$). Figure 6.7 shows that for size regimes above the mid 10^4 Reynolds number regime , the L/D of the wing section increases with Reynolds number commensurate with the reduction in friction drag, ala the first term on the right hand side of (6.9). At these larger sizes, the advantages of high aspect ratio wing geometry are fully realized in accordance with (6.19). Nature seems to agree, for the larger soaring birds such as the wandering albatross utilize aspect ratios as large as $Nr = 18$ to 20.

 Together, Equations (6.12), (6.13) and (6.19) tell us there are 4 distinct adjustments that can be made to vehicle characteristics to get energetically more efficient than the legacy gliders: 1) increase the lung capacity factor, n_b, to at least a value that satisfies equation (6.20) by maximizing the internal volume dedicated to the buoyancy engine, 2) once (6.20) is satisfied, make the UW gliders bigger, 3) reduce cross section factor n_r to the maximum extent possible by reducing the
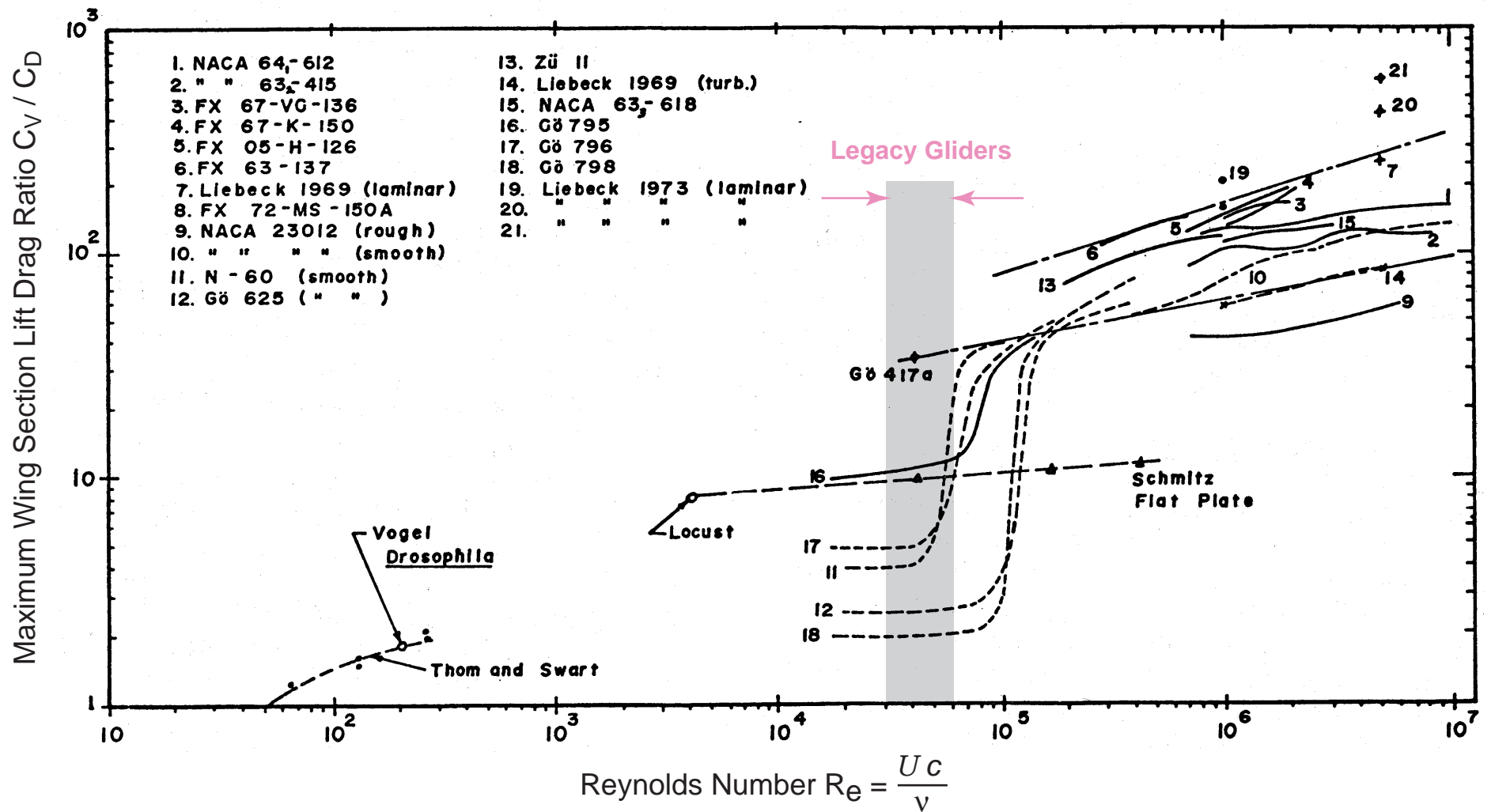
Figure 6.7. Variation in maximum airfoil section lift-drag ratio with Reynolds Number [after McMasters, 1974]

Figure 6.8. Blended-Wing-Body Geometry to Minimize Relative Wetted Area (A_t / A)

3.63 m

3.45 m

0.97 m

Pressure Hull
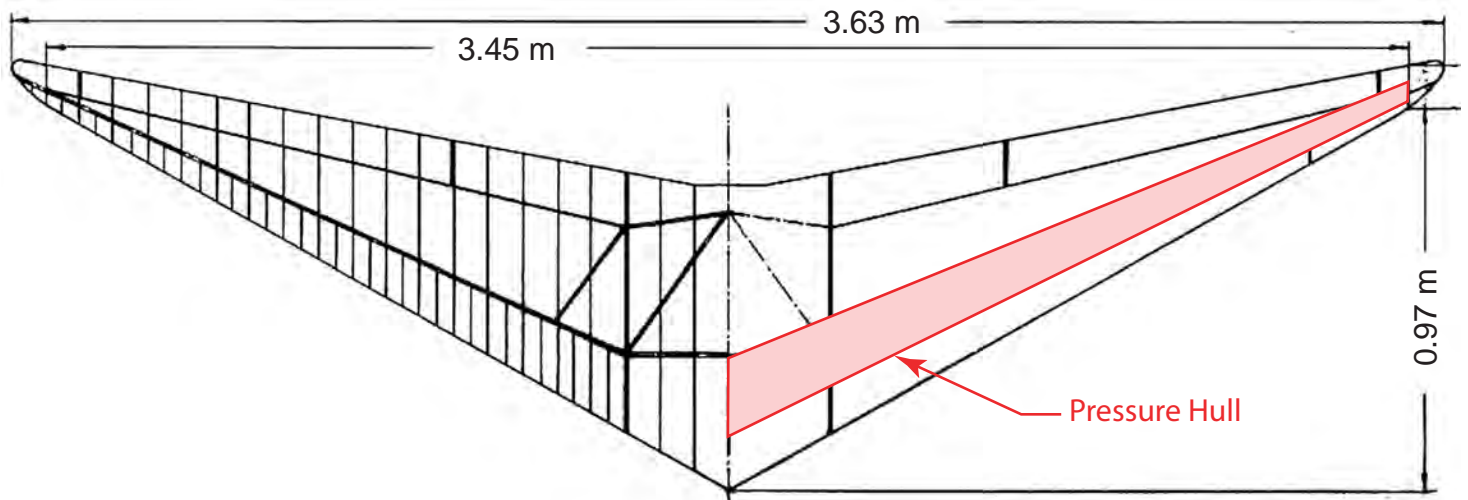
a. Horten H-II Surrogate at equivalent internal volume (21.6% scale).
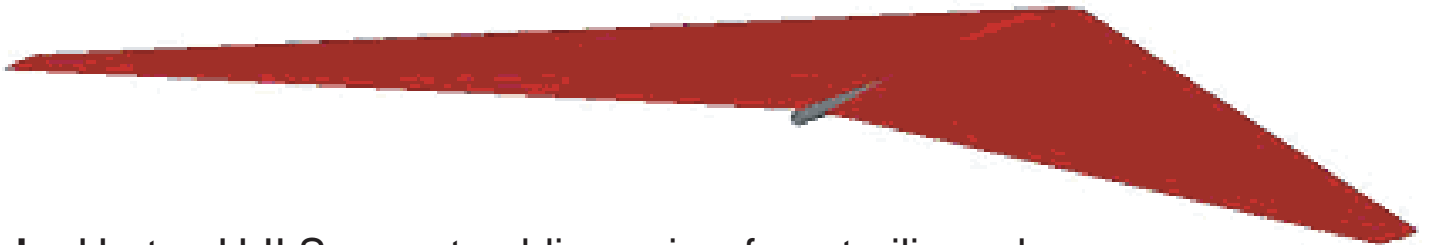
b. Horten H-II Surrogate oblique view from trailing edge.

Pressure Hull

Static Pressure Oriface (46 Total, 26 Upper, 20 Lower)

.088m (t/c = 28.8%)

.5

x/c

1.0

Strut Section View

.305m
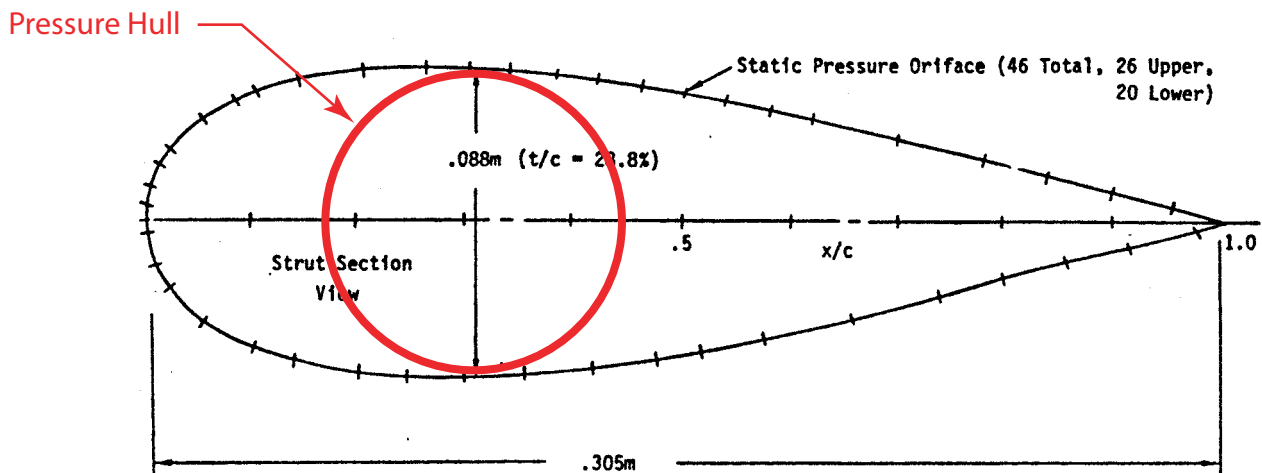
c. Thick, low-Reynolds number wing section [after McMasters, 1981].

amount of body and tail surface area that contributes to the total wetted area, A_t, and 4) increase the wing high aspect ratios to the maximum extent possible without reducing wing cord to such a degree that it operates in the mid 10^4 Reynolds number regime. The wetted area could obviously be reduced by copying birds and repackaging the legacy glider in a flying wing body shape. Figure 6.8 shows a 50 liter legacy glider repackaged in the planform of a Horten H-II flying wing glider (Bullard, 1997) using a thick low-Reynolds number wing section developed by McMasters (1981). This configuration reduces the wetted area ratio to $A_t/A = 2.2$, which by equation (6.12) should reduce the specific energy consumption of to $E_e \sim 0.1$ for a UW glider operating with a legacy glider equivalent loaded mass of 100 to 300 gm. Such a reduction in flight energy consumption would place the flying wing morph of the legacy glider slightly below Tuckers equation (6.5) and close to Equation (6.13), comparable to bird flight efficiency in this scale regime. These sorts of performance extrapolation will be examined in greater detail in Sections 9 & 10 with the aid of numerical flight simulation models.

   6.2 Glide Speed: Flight efficiency is not just a function of vehicle characteristics, but also a function of how the vehicle is flown. Returning to the basic definition of specific energy consumption in equation (6.6) it is apparent that flight energy consumption is minimized by maximizing the lift to drag ratio, *L/D*. The *L/D* is maximized by the combination of the appropriate vehicle characteristics as described above and the selection of the glide path angle β at which the glider is flown. From the proportionality between the force and speed triangles in Figure 4.2, a unique relation exists between the maximum *L/D* achieved and the angle of the glide path. This relation is plotted in Figure 6.9 wherein the glide path angle is measured with respect to a horizontal plane. Since the legacy gliders are flown at glide path angles of between 20 and 30 degrees in order to profile the gradients of ocean temperature and salinity field, they will not achieve a specific energy consumption any better than $E_e \sim 0.3 – 0.5$ no matter how optimal their physical characteristics are made. So, this is an example where the requirements of the functional class of the vehicle (*Depth Unlimited Roaming* as an ocean sounding instrument) will limit the achievable flight efficiency. However, there are other functional classes where maximum flight efficiency is essential, such as: *Depth Limited Roaming* where it is necessary to travel a long distance in a confined vertical space, *Payload Delivery* where many kilos of payload must be transported a long distance, or *Level Flight Hybrids* where a very flat glide path angle is required to minimize the expenditure of energy on auxiliary
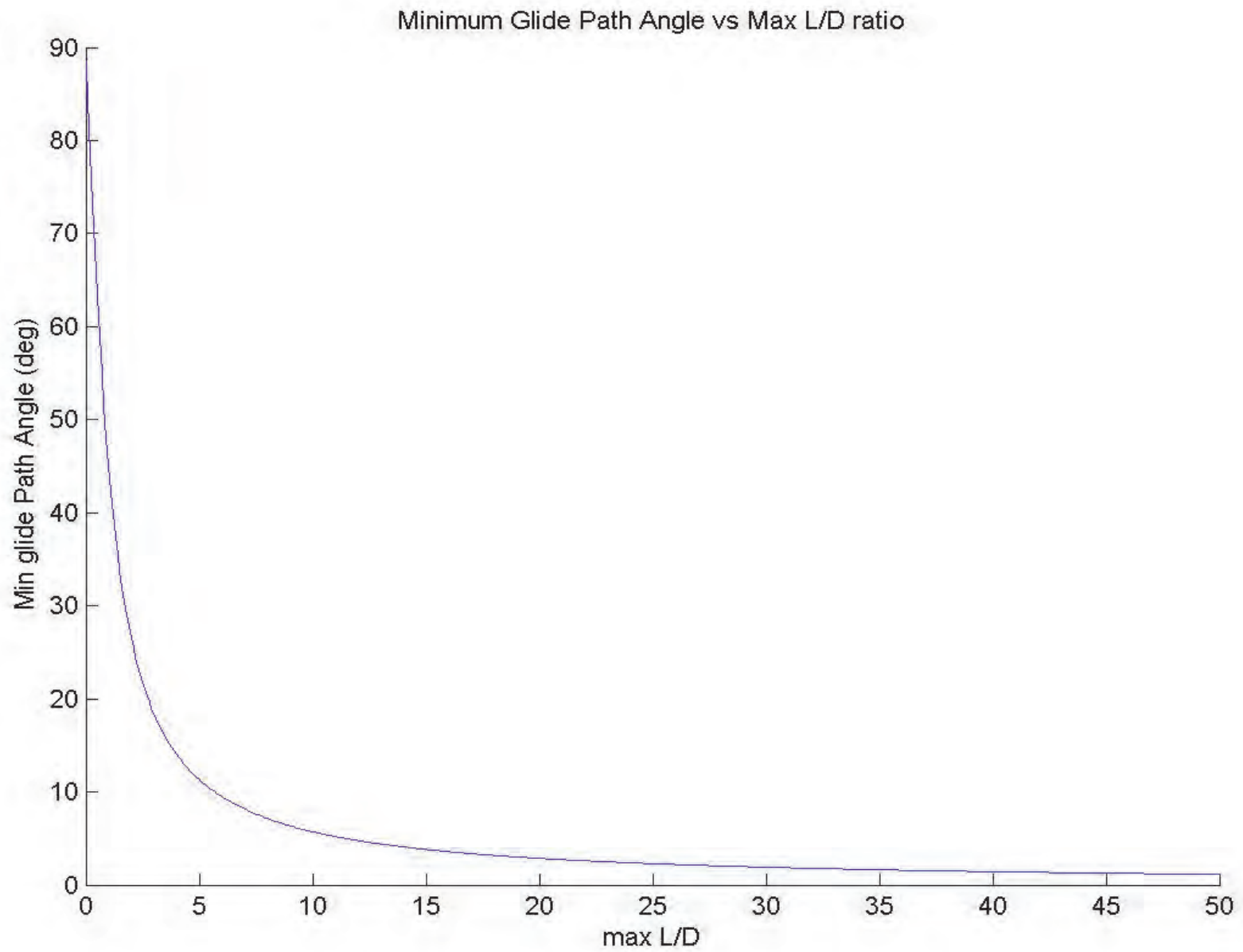
Figure 6.9. Minimum glide path vs Max L/D [from Graver, 2003, see Appendix].
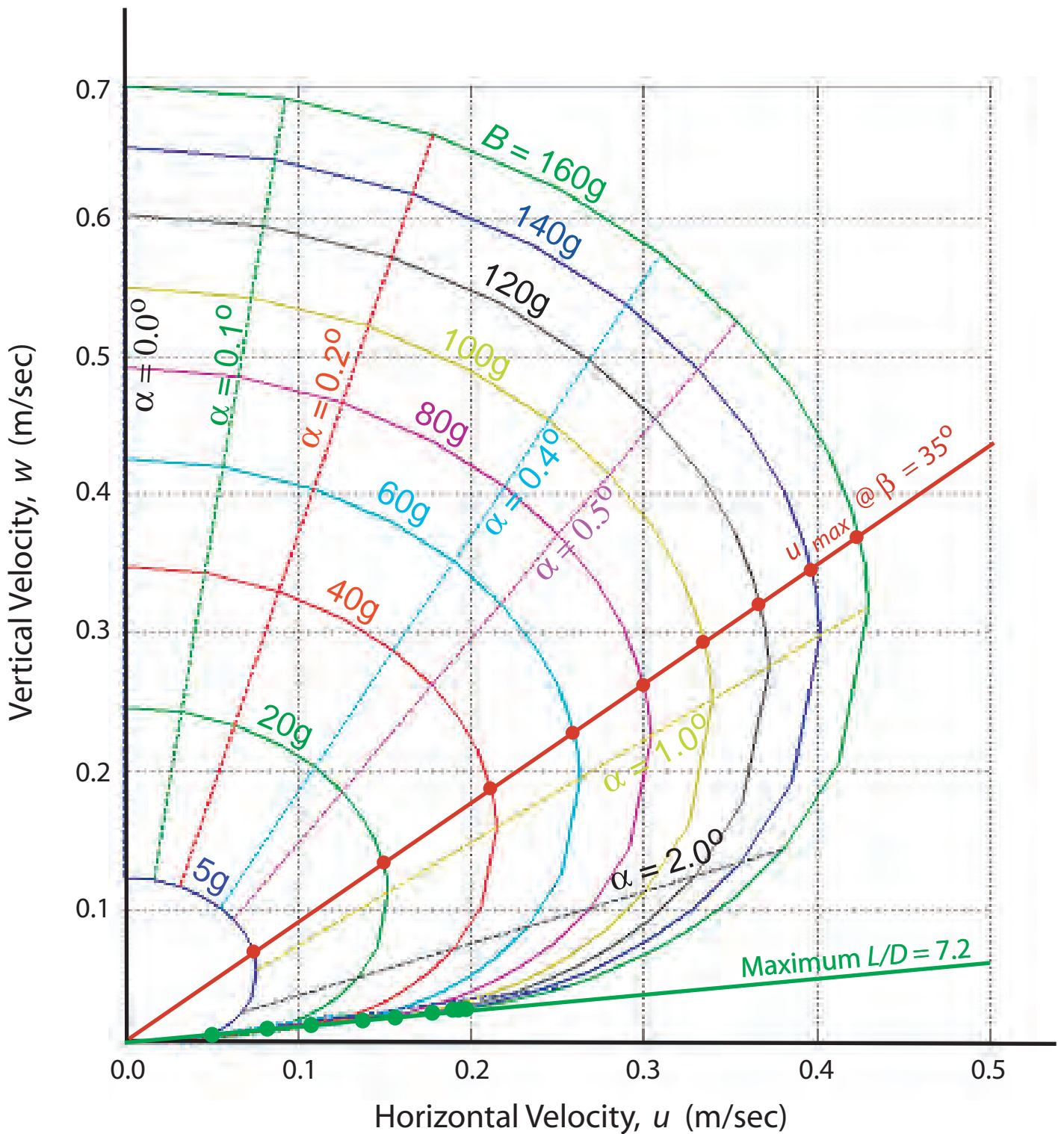
Figure 6.10. Glide polar (spider plot) of legacy glider [after Humphreys & Smith, 2003]. Polar contours appear as concentric solid curves for loaded mass $B = 5$ to 60 g. Dashed radial lines are contours of constant angle of attack, α. Intersections of the radial red line with glide polar contours give maximum cross country speed, u_{max}. Intersections of the solid green tangent line to glide polars give speed for maximum L/D.

propulsion. All these types of applications for under water gliders require minimum *NTE* and E_e, and hence maximum *L/D*.

While the L/D varies with glide path angle as in Figure 6.9 there is a corresponding change in the proportions of the speed triangle in Figure 4.2. This proportional change in the speed triangle with changing glide slope angle yields a continuous relationship between the horizontal and vertical components (*w versus u*) of the vector glide velocity, *U*. This relation is known as the *glide polar* and a generalized example scaled to the legacy gliders is shown in Figure 6.10. An analytic expression for the glide polar can be derived from (4.1) and (6.9) giving:

$$w = (C_D / C_L)u = K_3 u^{3-a} + K_4 / u \qquad (6.21)$$
$$\text{where} \quad K_3 = (\rho A K_1) / 2Mg$$
$$K_4 = (2MgK_2) / (\rho A)$$
$$K_1 = K_0 A_t c / (v A) \qquad K_2 = K / (\pi N_r)$$

The glide polar contains all the information defining the performance of the glider. According to (6.21) there is a different glide polar for each potential value of loaded mass, *M*, and selected polars are shown Figure 6.10 for values of *M* ranging from 5 to 160 grams, designated by the solid concentric lines of different color. The maximum L/D is found at the points where the green line projected from the origin meets the points of tangency (green dots) with the various polar lines. The glide speed at which maximum *L/D* occurs is given by these points of tangency because they represent the locus of points having the biggest u for the smallest w. The vector sum of these (u,w) pairs from the green tangent points is often referred to as *speed-to-fly* or *best L/D speed*. For instance, when the loaded mass is *M* = 160 g, the speed-to-fly for maximum *L/D* is *U'* = 19.7 cm/sec (horizontal velocity *u* = 19.5 cm/sec, vertical velocity *w* = 2.7 cm/sec). An analytic approximation of the best L/D speed can be obtained from the from a Taylor series expansion of (6.22) about some cruise speed less than maximum glide speed , *u* = *U'*. The first three terms of this expansion give:

$$w \to f_2 u^2 + f_1 u + f_o$$
$$\text{where } f_2 = (3-a)(2-a)K_3 U_1 - a + (2K_4 / U_3)$$
$$f_1 = (3-a)K_3 U^{2-a} - (K_4 / U) - 2U f_2$$
$$f_0 = K_3 U^{3-a} + (K_4 / U) - f_2 U^2 - f_1 U$$

(6.22)

Taking $d(L/D)/du = 0$ of (6.22) at $u = U'$ gives the best L/D speed as:

$$U' = \frac{(f_2 f_o)^{1/2}}{f_2}$$

(6.23)

By Equation (6.23) speeds for maximum L/D increase in proportion to $M^{1/2}$. The corresponding sink rate of the UW-glider at best L/D speed also increases aproximately as $M^{1/2}$ since $a < 1$. However, at loaded mass comparable to the legacy gliders ($M = 100$-150 gm), these best L/D speeds are about 40% - 50% slower than the cruise speeds at which they have been typically operated (about 30 cm/sec). The maximum L/D that the legacy gliders might obtain if operated at these slower best L/D speeds would be about 7. Operating them in this way would reduce specific energy consumption to about $E_e \sim 0.14$, making them almost as efficient as their bird counterparts. Hence achieved flight efficiency is strongly controlled by how the UW glider is flown, which in turn may be constrained by the purpose (functional class) for which the glider is employed.

Natural and man-made flyers are not always flown at best L/D speed, but rather at some *cruise speed* which is best suited to a particular flying activity (functional class). Even among soaring birds of equivalent size there is often a 50% difference in cruise speed; for instance, between the low speed circling glides (at 10 m/sec) of the turkey vulture in small diameter land thermals versus the high speed straight line glides (at 20 m/sec) flown by the wandering albatross in the air-sea boundary layer, (Pennycuick, 1966, 1971, 1973 and 1992). These different functional performance adaptations among natural and man-made flyers produce the scatter in Figure 6.11. In spite of this scatter a remarkably tractable relation is found between the immersed weight (net buoyancy, *B,* in force units) and the cruise speed *U* across 11 orders of magnitude in scale . This relation has come to be known as The Great Flight Diagram (Tennekes, 1997). The solid black

line is simply Equation (6.10) with C_L set at 0.131 to achieve a best fit to the data. To compare the underwater gliders with the flyers in air we must account for the density difference between air (ρ_a) and water (ρ_w). This is done by the normalization method of *equivalent airspeed, U_a*, whereby:

$$U_a = U_w(\rho_w / \rho_a)^{1/2} \qquad\qquad (6.24)$$

Inspection of Figure 6.11 reveals that the cruise speed of the legacy gliders expressed in terms of *equivalent airspeed* is comparable to moderate sized birds, (Franklin's gulls and pigeon hawks), although the best L/D speed is clearly at the low speed edge of the envelope of scale. If we project toward higher speeds along a parallel to the fit line of the Great Flight Diagram, we find that the net buoyancy (immersed weight, *B*) of the legacy gliders would have to increase by a factor of 1000 to achieve cruise speeds of 2 knots in the ocean (given the present lung capacity factors , $n_b = 0.002$ to 0.005). To achieve a best L/D speed of two 2 knots, the Great Flight Diagram suggests that the net buoyancy of the legacy gliders would have to be increased by a factor of 10,000.

In addition to efficient energetics, it is essential in the underwater applications that a glider achieve sufficient glide speed to penetrate against ocean currents, otherwise functions such as station keeping, round trip excursions and vehicle recovery will not be possible. Equations 4.1, 6.9 and 6.10 can be solved for the maximum horizontal (cross country) speed:

$$u_{max} = (Bsin\ \beta\ /\ \tfrac{1}{2}\ \rho\ C_D)^{1/2}\ cos\ \beta \qquad\qquad (6.25)$$

where again, $B = Mg$ is the net buoyancy force. In Figure 6.12, non-dimensionalization of Equation 6.25 reveals that maximum along coarse speed, u_{max} ,is always obtained at a 35 degree glide path angle, regardless of vehicle shape or other hydrodynamic properties. This is also evident in each of the glide polars in Figure 6.10, where the maximum horizontal velocity component of each polar is found along the red line corresponding to a glide path angle of $\beta = 35^0$. At $u = u_{max}$ the trigonometric glide path factor $(sin\ \beta\ )^{1/2}\ cos\ \beta$ is always 0.6, (Graver, 2003). In the numerator of (6.25) $B = Mg$ is related to vehicle volume V_0 by the lung capacity factor, n_b , according to Equation (6.16); while C_D in the denominator is proportional to $V_0^{2/3}$ by Equations (6.9) and (6.17). Hence the maximum glide speed has a parametric scale dependence on vehicle volume and capacity factor:
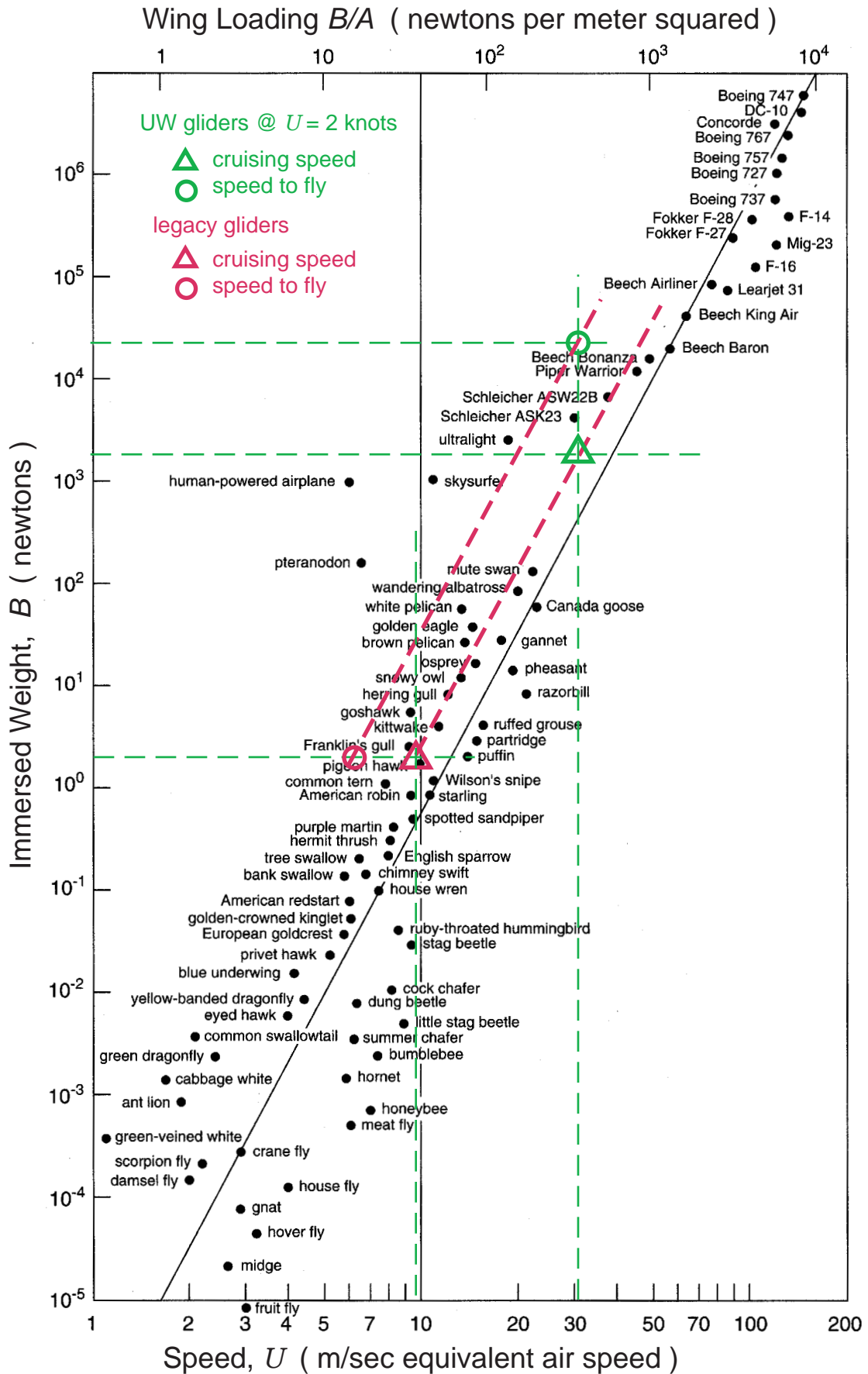
Figure 6.11. The Great Flight Diagram. Cruising speed and sped to fly of legacy gliders was converted to equivalent air speed by multiplying speeds in water by the sqaure root of the density ratio of water to air.
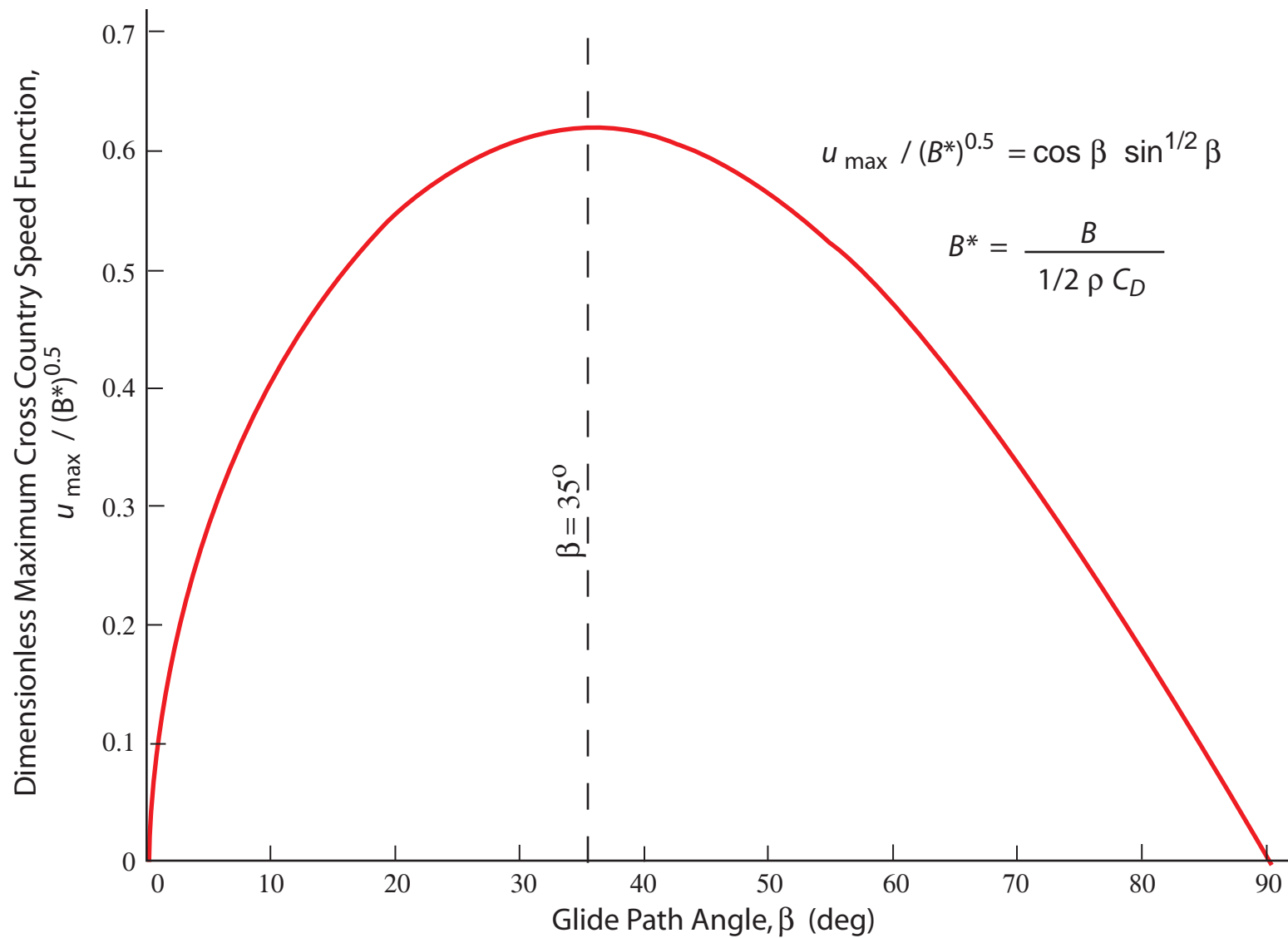
Figure 6.12. Speed Function, $\cos \beta \, \sin^{1/2} \beta$ vs glide path angle β [from Graver, 2003, see Appendix].

$$u_{max} \sim 0.6 \; (55.6 \; g \; n_b)^{1/2} \; V_0^{1/6} \qquad\qquad (6.26)$$

Equation (6.26) is plotted in Figure 6.13 showing u_{max} versus glider volume V_0 for a selection of constant lung capacity factors ranging from $n_b = 0.005$ for the present configuration of Slocum legacy glider to a potential advanced vehicle concept wherein as much as 40% of the vehicle volume is dedicated to the buoyancy engine capacity, $n_b = 0.4$. Maximum glide speed increases relatively slowly (as $V_0^{1/6}$) with increasing vehicle volume for fixed lung capacity factors. However, larger incremental increases in maximum glide speed are possible by improving the buoyancy capacity of a given size vehicle ($u_{max} \sim n_b^{1/2}$). The largest gains in high speed performance will be achieved by increasing lung capacity and vehicle size together. increases with increasing, and increasing, as plotted in Figure 6.13. Hence, increasing the capacity of the buoyancy engine and the size of the vehicle will achieve faster gliders as well as more transport efficient gliders (see Equation 6.20).

Another choice for flying the UW glider would be at the speed which results in the minimum vertical velocity, w. This choice would be whenever sensors might require near-level or hovering flight or when station keeping in hovering flight against an opposing current was required. This is referred to as *speed to fly for minimum sink*, u_{wmin} and is found taking *dw/du = 0* from the glide polar equation (6.21) which yields:

$$u_{wmin} = \left[\frac{K_4}{(3-a)K_3} \right]^{1/(4-a)} \qquad\qquad (6.27)$$

Speed to fly for minimum sink occurs at speeds less than the best L/D speed, where drag is a minimum, see Figure 6.14. Inserting (6.26) into the polar equation gives the minimum sink rate as :

$$w_{min} = \left[\frac{4 v^{-a} B^{2-a} C_D^{2-a}}{(3-a)K_o c^{-a} \rho^{2-a} A^{2-a} C_L^{3-a}} \right]^{1/(4-a)} \qquad\qquad (6.28)$$
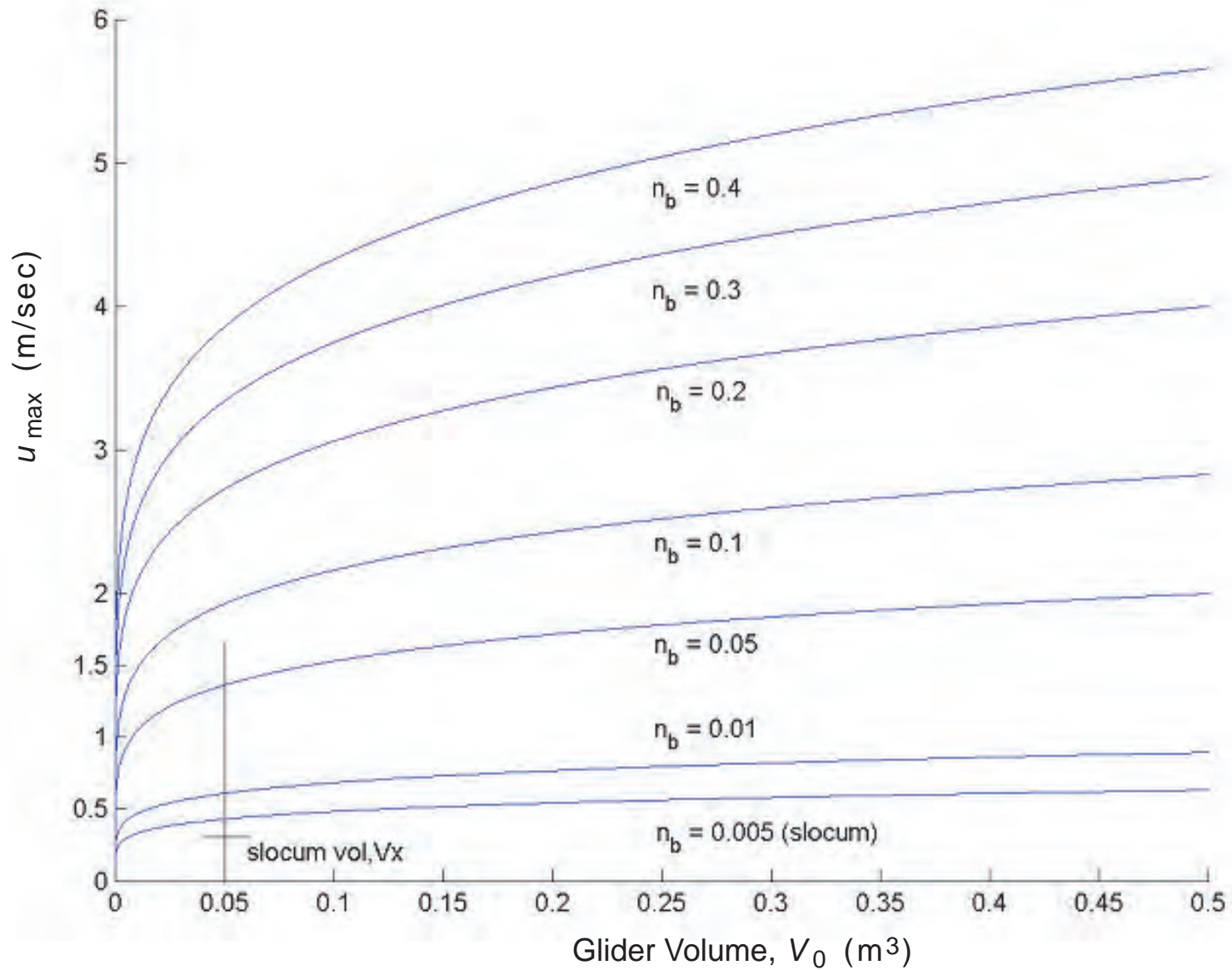
Figure 6.13. Maximum cross country speed u_{max}, as a function of total vehicle volume, V_0, for various lung capacity factors, n_b; where, $n_b = V_{buoyancy} / V_0$. [from Graver, 2003, see Appendix]

When $U = u_{wmin}$, the drag is predominately due to induced drag as shown in Figure 6.14. The induced drag coefficient C_{Di} from (6.9) is independent of Reynolds number at lowest order, and hence independent of the parameter, a. Therefore we take $C_D \sim C_{Di}$ in (6.28) and set $a \sim 0$, which gives:

$$w_{min} \sim (B/A)^{1/2} \ (C_L^{3/2}/C_D)_{max}^{-1/2} \hspace{4cm} (6.29)$$

The minimum sink rate and the speed to fly for minimum sink decrease with both decreasing wing loading B/A and with increasing $C_L^{3/2} / C_D$. The parameter $C_L^{3/2} / C_D$ is known as the *endurance factor* because a glider at a given altitude can remain aloft longer as the endurance factor increases. The minimum sink rate is achieved by the maximum endurance factor of the wing section, $(C_L^{3/2}/C_D)_{max}$. From Figure 6.14 it is apparent that the total drag is large at minimum sink rate glides, when $U / u_{wmin} = 1.0$. Figure 6.15 shows that $(C_L^{3/2}/C_D)_{max}$ results from high lift, rather than low drag. Consequently minimum sink glides are not the energetically most efficient speeds to fly. Many of the vehicle characteristics which promote minimum sink performance run contrary to those which promote low rates of energy consumption (small *NTE* and E_a). Low net buoyancy (immersed weight, B) and large wing areas help to reduce a glider's minimum sink rate; but as we have seen in Equations (6.12) & (6.13), these same vehicle characteristics are mutually exclusive with high speed and high transport efficiency. In other words, flying at minimum sink rate will maximize the glide duration, but the achieved glide range will be less than that resulting from flying faster at best L/D speed. Nonetheless, where on-station time or near-level flight characteristics are a priority, optimizing vehicle properties for minimum sink and flying minimum sink speed to fly strategies have a well defined *niche*.

There is another issue of concern with flying at minimum sink rates besides poor energetics. That additional concern is maintenance of pitch stability of the glider. The lower left hand panel of Figure 4.2 shows a schematic of how the flow circulation which the wing section generates to create lift also produces a reaction torque on the glider opposite to the sense of rotation of the flow circulation. This reaction torque is referred to as the *wing pitching moment*. During a descending glide when lift is acting upward, the pitching moment acts to pitch the glider nose down. During an ascending glide with lift acting downward, the pitching moment acts to induce nose-up pitching of the glider. To balance the pitching moment in order to maintain stable flight, birds and conventional gliders in air are fitted a
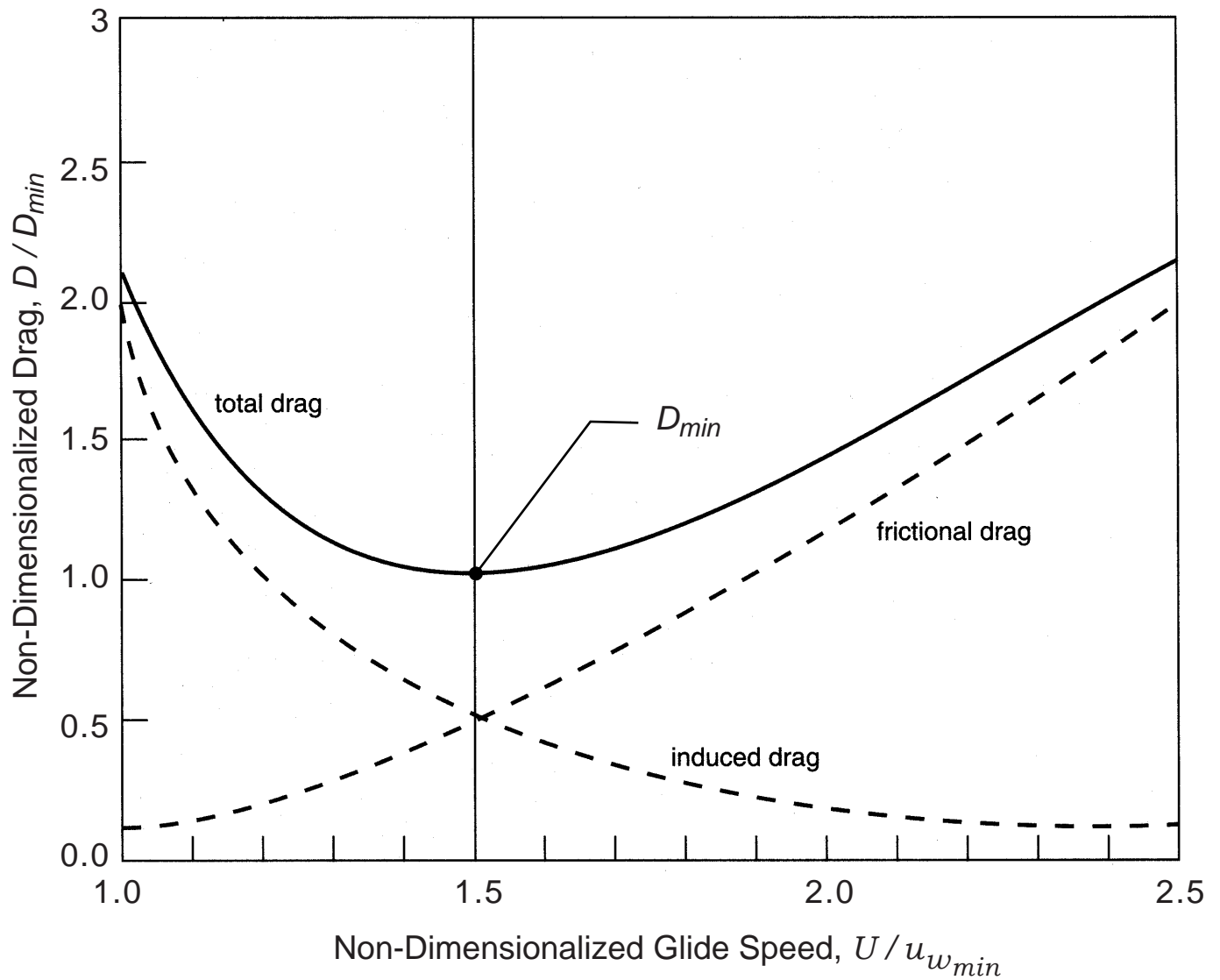
Figure 6.14. Variation of drag with glide speed. Drag is non-dimensionalized by D_{min}. Glide speed is non-dimensionalized by speed-to-fly at minimum sink rate, $u_{w_{min}}$ from Equation 6.27. [after Tennekes, 1997]
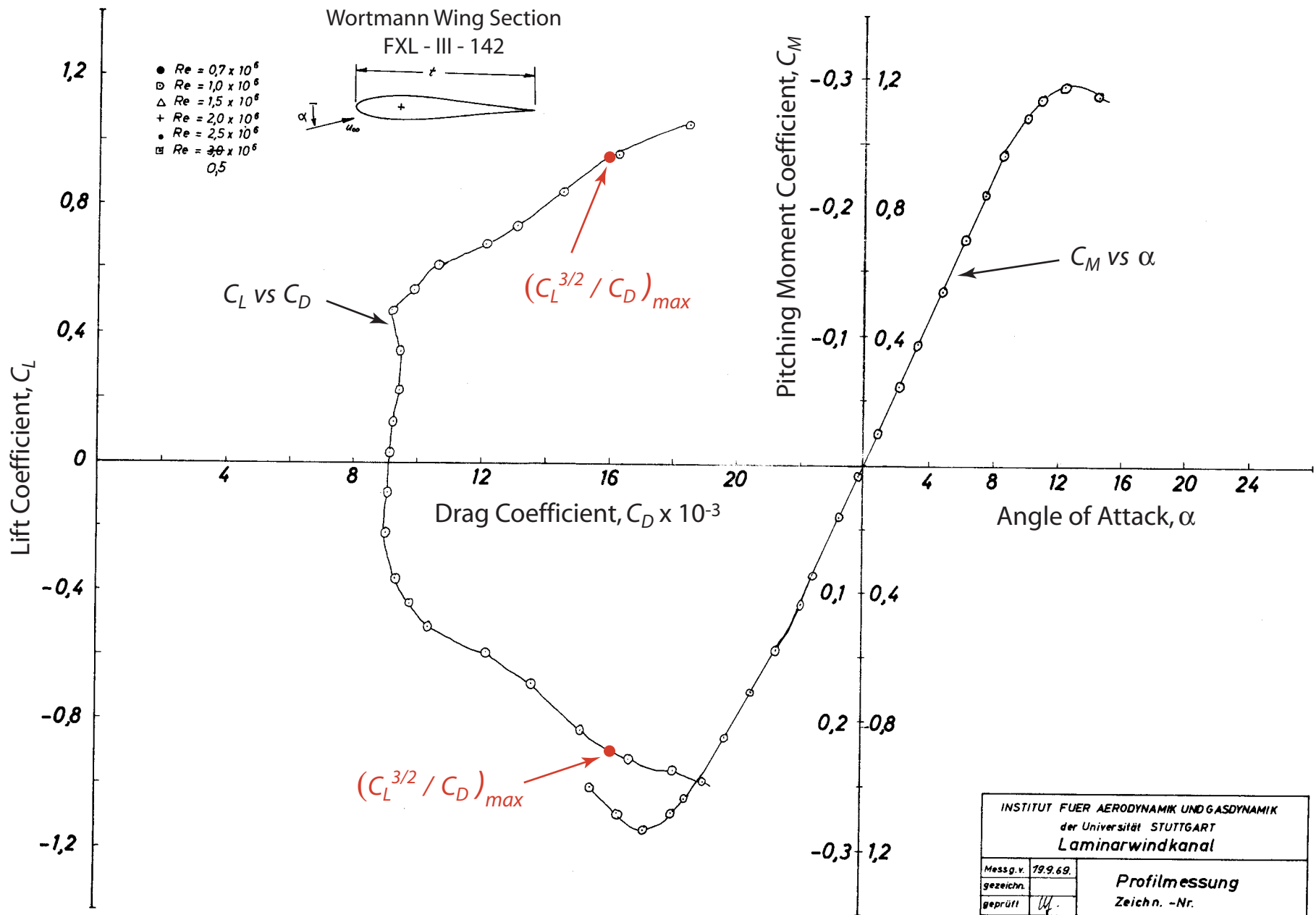
Figure 6.15. Polars of lift coefficient, C_L vs drag coefficient, C_D (left) and pitching moment coefficient, C_M vs angle of attack, α (right) for a symetrical Wortmann wing section.

horizontal tail. The tail produces lift in the opposite direction to the lift generated by the wing in order to generate a counter torque to balance the pitching moment. The additional induced drag of the tail causes another source of drag referred to as *trim drag*. The underwater glider has the advantage of being able to selectively place the center of buoyancy relative to the wing by means of internal mass shifting in order to generate a compensating torque to the pitching moment. Consequently UW gliders do not require a horizontal tail and do not suffer from the energetics degradation associated with trim drag. Regardless, the mass shifter must have sufficient resolution to perfectly balance the pitching moment which has the general parametric formulation:

$$\tau = 1/2\rho \; C_M A c U^2 \qquad\qquad (6.30)$$

where C_M is the moment coefficient. By convention, τ and C_M are referenced about the quarter cord of the wing section, referred to as $c_{1/4}$. Figure 4.15 shows C_M as a function of angle of attack, α, for a symmetric wing section such as used in bi-directional gliding underwater. We see that moment coefficient progressively increases with increasing angle of attack, and hence with increasing lift coefficient. As a result large C_M are realized at $(C_L^{3/2}/C_D)_{max}$. Moreover, a rapid rate of change in C_M sets in at the high angles of attack where $(C_L^{3/2}/C_D)_{max}$ is realized. This behavior makes the maintenance of stable pitch attitude somewhat challenging during glides at minimum sink rate, and requires high resolution and rapid response from the mass shifter buoyancy moment control mechanism. The demands placed on this system during such low speed glides can be mitigated somewhat with wing sections having low $(dC_M/d\alpha)$ properties.

6.3 Pressure Hull Compressibility: Displacement Versus Weight

This section works towards a relation of hull weight versus operating depth and slenderness ratio (X_L/d), yielding design rules of the available payload versus operating depth and X_L/d. As the goal is to provide general direction, assumptions will be allowed which yield simplified analytical results, giving more intuitive insight to the design process (for instance sea water density $=1$ gm/cc for displacement calculations). The basic hull shape will be assumed to be a cylinder with hemispherical or prolate ellipsoid end caps.

6.3.1. Definition of Fractional Payload : The pressure vessel of weight W_0 displaces a certain volume of water, V_0, resulting in an available payload $V_0 - W_0$,

or as a fraction of total volume, *FPL = (V₀ - W₀)/V₀= 1 - W2V*, where *W2V = W₀/V₀*. To maximize payload, it is clear that W2V needs to be minimized. For geometries of constant thickness, *t*, and where the radius, *R*, is large enough to consider t to be thin-walled (*t/R <<1*), then

$$W2V = k_A \, \rho_h \, t/R \qquad k_A = 3 \text{ for a sphere, } k_A = 2 \text{ for a cylinder} \qquad (6.31)$$

where ρ_h is the hull material density. For an ellipsoid, k_A varies from 3 to .75π as the major/minor axis ratio varies from 1 to infinity. Note a cylinder is lighter as it does not have any end caps associated with it.

6.3.2. Plastic Failure: When the operating pressure causes material stress to rise above the yield stress (σ_Y), plastic flow will lead to hull failure. Let P_{max} denote this maximum pressure:

$$P_{max} = k_B \, \sigma_Y \, t/R \quad k_B = 2 \text{ for a sphere, } k_B = 1 \text{ for a cylinder} \qquad (6.32)$$

An ellipsoid stress will be greatest at the base (the ellipsoid-to-cylinder joint), with k_B varying between 1 and 2, depending upon the eccentricity. For all cases, P_{max} varies linearly with *t/R*. Substitution into (6.31) yields

$$W2V = k_C \, \rho_h \, P_{max} / \sigma_Y, \quad k_C = k_A / k_B, \qquad (6.33)$$

where $k_C = 1.5$ for a hemisphere, $k_C = 2$ for a cylinder, and somewhere in between for an ellipsoid. This comes as no surprise: a sphere minimizes the weight/volume ratio, thus maximizing payload. The other lesson is that the penalty in payload loss is linear with P_{max}, which is only dependent upon *t/R*, and not the absolute value of r. At this stage, X_L/d does not matter.

6.3.3. Buckling: A long thin cylinder under external pressure will not fail by plastic yield, but will buckle due to modal instabilities. For a cylinder that is supported at some spacing length X_{LS}, the maximum operating pressure, P_{buckle}, is given by:

$$P_{buckle} = 0.807 \mathcal{E} (t / X_{LS}) (t/R)^{1.5} \ (1 - \Pi^2)^{-0.75} \qquad (6.34)$$

where $\mathcal{E}$ is the Young's Modulus and Π is the poisson ratio. To maximize the ring stiffener spacing, P_{buckle} is set equal to P_{max}, yielding

$$X_{LS} / t = C_1 (t/R)^{0.5} \qquad C_1 = .807 (1\text{-}\Pi^2)^{-0.75} \, \mathcal{E} \, / \sigma_Y \qquad (6.35)$$

Note that in a design process, P_{max} sets t/R, which in turn sets the X_{LS}/t value. The lesson is that the thinner the wall, the closer the stiffeners must be, until we have plastic failure instead of buckling.

The stiffener must be stiff enough to keep itself from buckling, and have enough material to keep it from failing. We will model the stiffener as a simple ring frame of width y_b and height h, such that the frame's inner radius is given by $(R - t - h)$. The frame carries part of the cylinder load, yielding a higher effective pressure on the frame, P_{eff},

$$P_{eff} = P_{max} (y_b + Q)/ y_b \qquad (6.36)$$

where Q is the effective length of the cylinder loading, modeled here as

$$Q = 1.56 (Rt)^{0.5} \qquad (6.37)$$

Note this is a simplification of Q, as it really depends upon the stiffness of the frame itself. The frame stress is the same as in the cylinder hoop stress, but with thickness $h + t$, giving the maximum stress in the frame, σ_f,

$$\sigma_f = P_{eff} \, r/(h+t) \qquad (6.38)$$

where $\sigma_f = \sigma_Y$ at failure, yielding the minimum value of h required to not have ring failure:

$$h = R P_{eff} \, / \sigma_Y - t . \qquad (6.39)$$

The next concern is to keep the frame from buckling, which will occur at

$$P_{eff} = 0.25 \, \mathcal{E} \, (1 - \Pi^2)^{-1} [(h + t) / R]^3 \qquad (6.40)$$

which can be solved for a second value of h, equal to the minimum to keep the frame stiff enough to resist buckling. The largest value of h is chosen to guarantee the frame does not fail by either stress or buckling.

6.3.4 Hull Compressibility Scale Rules

At this stage, for a given P_{max} and radius R, the thickness t is defined to not allow plastic failure, which also defines the ring spacing. The stiffener size (width and height) is set to avoid ring failure (independent of ring spacing). We can now calculate the cylinder pressure housing weight, as well as available payload. Conversely, for a given P_{max}, length and diameter, we can calculate the required hull thickness and stiffener spacing and size, thus defining the overall weight and fractional payload. Calculations were run for 6061-T6 for a cylinder with (2, 4, 8)" radius (w2v2p.m). It was additionally constrained to have a minimum hull thickness of 1/8". These calculations reveal the following scaling rules for pressure hull design in underwater gliders:

1) The t/R ratio increases linearly with P_{max}, (see Figure 6.16 upper panel). Minimum thickness constraint makes it difficult to optimally design at shallow depths.
2) Bulkhead / Diameter versus P_{max} is independent of hull radius, R (see Figure 6.16 lower panel).
3) By constraining the stiffener ring width to twice the hull thickness, ring stiffener ring size (ID / diameter ratio) becomes independent of hull radius. (See Figure 6.17, upper panel).
4) For a fixed desired payload of 1000 cc, hull weight is independent of hull diameter, until the 1/8" minimum thickness is encountered (see Figure 6.17 lower panel).
5) The Fractional Payload $FPL = (V_0 - W_0)/V_0$ is independent of hull diameter, and hull length to diameter ratio, X_L /d (see Figure 6.18). The least-squares-fit to FPL in Figure 6.18 for a cylinder with no endcaps yields:

$$FPL = 0.99 - (1.9 \times 10^{-4})P_{max} \text{ [dBar]} \tag{6.41}$$
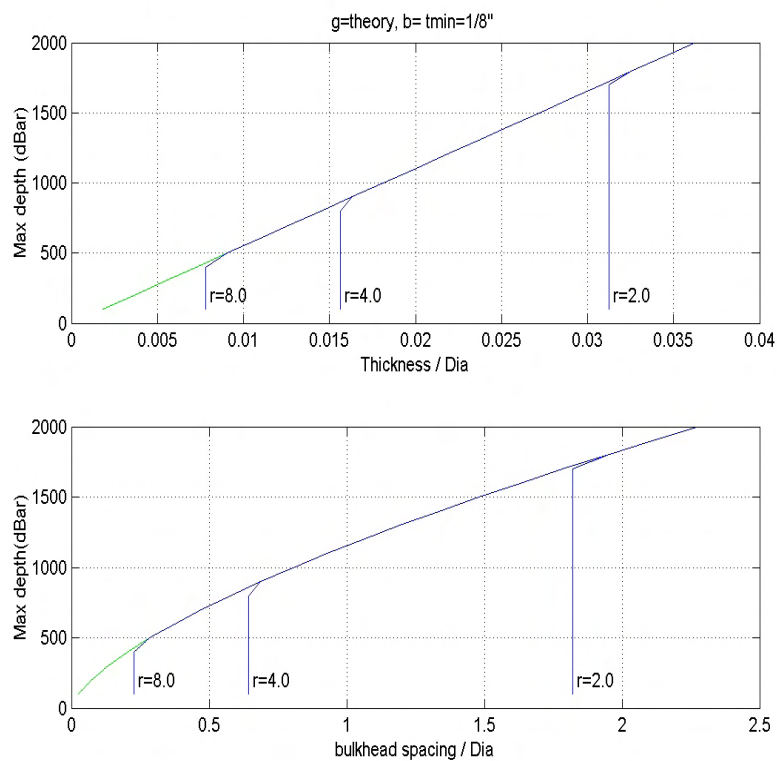
Figure 6.16: Depth dependence of the pressure hull wall thickness to hull diameter ratio (upper panel), and bulkhead spacing to hull diameter ratio (lower panel). From Sherman (2003)
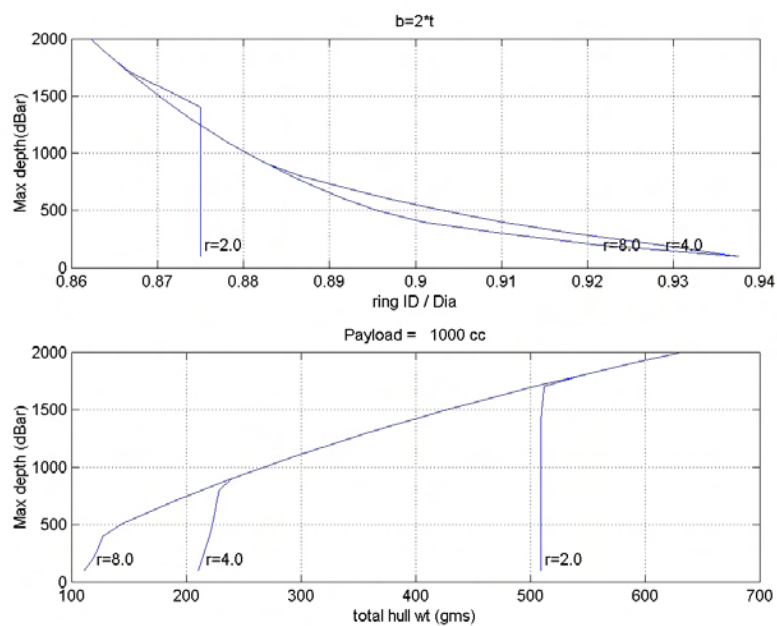
Figure 6.17 Depth dependence of stiffener ring size (upper) and total hull weight (lower). From Sherman (2003).
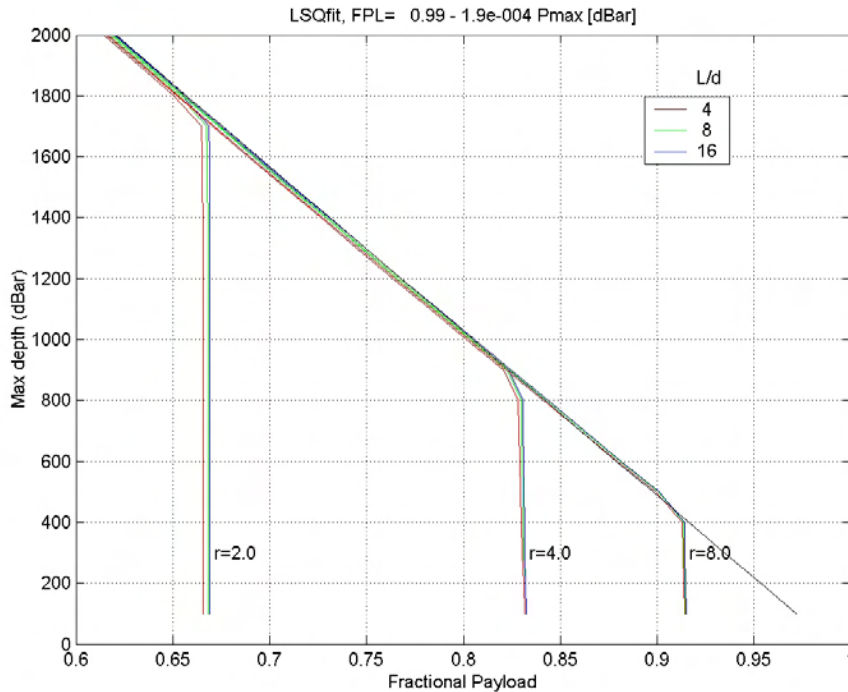
Figure 6.18: Depth dependence of the fractional payload for various hull length to diameter ratios . From Sherman (2003).

7) If hemisphere endcaps are added (which are the most efficient), the results are virtually unchanged, with:

$$FPL = 0.99 - (1.8 \times 10^{-4})P_{max} \text{ [dBar]} \qquad (6.42)$$

Hence, we conclude that there is no optimum hull diameter and length to diameter ratio X_L/d to minimize hull weight. Shallow vehicles will be constrained by a minimum hull thickness, which is set by handling and machining constraints. The major design obstacle will be the packaging ability around the ring stiffeners, in order to thus provide maximum use of all internal volume.

6.4 Cost Scaling:

Production costs are somewhat difficult items to forecast especially in an adolescent instrument with build sets of less than 10 on average and we will no

doubt be feeling our way along in the year to come. Sensors suites are often a higher cost than the vehicle itself and except for CTD are thus left out of this consideration.

Usual in economics, as the quantities produced increases, the cost associated with production decreases. The glider teams have come from the base assumption that these instruments will be used in large numbers – large at least in the sense of oceanography, with targets of high hundreds of units. Therefore the market pricing as it stands today is targeted aggressively at ~ $60,000 each, based on a larger production run than is realized at the moment. The impetus is to make numbers of these instruments reasonably available so as to get them in the field. It is recognized that to bring this technology to life there has to be a number of user groups with quantities of gliders at their disposal.

This is a cost that does not allow for much research and development and presumes an upfront investment from the developer and in these cases ONR. AUV's are complex and presently evolving vehicles, as they get to design maturity there will certainly be an easing in production costs. Presently customer support with a prototype-to-production system is a large component of the initial investment, as is payload additions, and developmental software. The goal is to continually improve performance and ease of use, until the vehicle itself simply fades to the background. And, of course, we will continually be looking to reduce the costs to provide a better dollar value for data.

Maintenance comes primarily in replacing any damaged structures, sensor recalibration, and re-powering. Of these, re-powering is usually the recall from the field unless there has been a technical issue. This tends to drive the time base for the rest of the overhaul and can be estimated at 10% of the vehicle cost. Investing in a rechargeable energy system, with the tradeoff of shorter duration runs, can reduce the costs to 5% of the vehicle cost.

Where gliders are being scaled to up to 10,000 times their buoyancy drive, the scaling of volume to cost is a consideration. Since there are no examples of a variety of glider sizes in production to examine, the comparable propeller AUV world was examined to provide a benchmark to work against. Existing, on the market, AUV's included in the study were stripped to the base vehicle - removing any sensor systems not necessary for vehicle operation. It must be noted that this is a general curve set where allowances have not been made for type of battery chemistry, durations, speed, special handling equipment, depth ratings, quantity produced or necessary personnel and ship support. It is simply a cost per liter based on liters of displacement of a base operational instrument.

There is a fundamental set of components that defines an instrument as an AUV, and gliders are no exception. Items such as navigation, propulsion devices, controllers, actuators, and communications are ubiquitous in such vehicles. Scaling a vehicle up and beyond these items typically is to increase payload whether it be for energy, sensors suites, or delivery capacity. Thus, the original hotel structure is a fixed cost and the scaling pertains to greater hull capacity, energy requirements, and greater thrust to move the volume through the water. The graph below shows a rapid decrease of cost/liter instrument displacement as the total instrument volume displacement increases, and then a knee where the costs flatten out significantly. Of course the total cost of the larger vehicle increases, as do costs associated with handling and ship support. The general finding is that the smaller instrument, while it may be more expensive per liter makes up with lower operating costs.

Gliders have been aggressively priced early on with the expectations of production quantities in the future. With a price of $60,000 per 50 liters, the legacy gliders fit the below curve at $1200/liter, roughly half the price as the cost scaling propeller AUV curve would indicate. It is not that the costs between a propeller AUV and a glider are significantly different. The glider teams have come from the base assumption that these instruments will be used in large numbers – large at least in the sense of oceanography, with targets of high hundreds of units. Therefore the market pricing as it stands today is targeted aggressively, based on a larger production run than is realized at the moment. The impetus is to make numbers of these instruments reasonably available so as to get them in the field. It is recognized that to bring this technology to life there has to be a number of user groups with quantities of gliders at their disposal.

From a limited set of cost data on AUV's built to date, an incremental cost function was prepared in Figure 6.16, relating the cost per liter of vehicle volume to the total vehicle volume, V_0. Because the cost function in Figure 6.16 does not appear to be converging to any asymptotic limit for large vehicles ($V_0 = 3500$ liters or larger), it does not seem to be a viable tool for making cost estimates of vehicles 100, 1000 or 10,000 times larger than legacy class gliders. Therefore the study does not attempt to make cost estimates for the complete scale regimes of underwater gliders
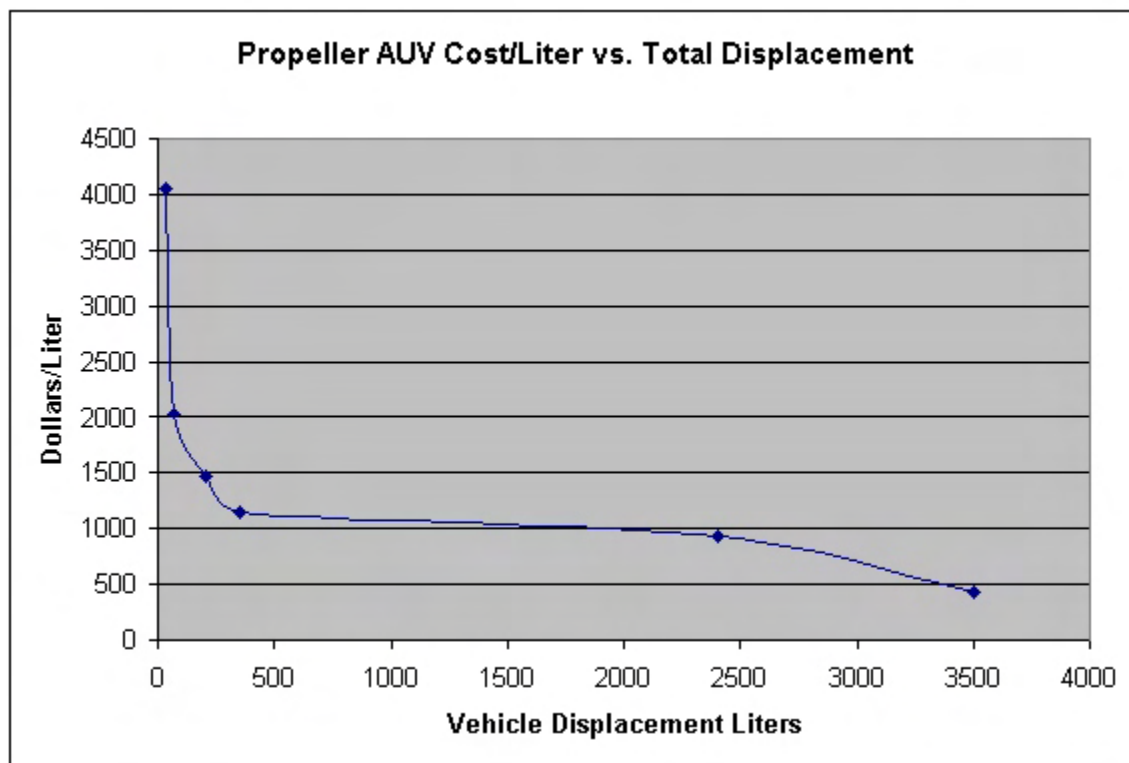
Figure 6.19: Incremental cost function for propellor driven AUV's

7. Computational Methods:

The extrapolations of scale from the legacy gliders to the scale regimes of the functional classes were performed by coupling two distinct sets of computational methods: 1) a suite of numerical models referred to as *VCT Tools* that were used to predict hydrodynamic performance and control variables; and 2) a spreadsheet analysis that accepts the hydrodynamic predictions and combines them with a multitude of system variables to produce the end-to-end integrated systems computations of power consumption and range characteristics of the new breads of UW gliders. These methods are detailed in this section.

7.1 VCT Tools™ (Exerts from Humphreys, et al, 2003)

The vehicle characteristics used in VCT developed simulations are modeled with hydrodynamic forces and moments computed for individual contributions from the body, the various fins and the propulsor[1]. Figure 7.1 shows the relationships between the various major programs in VCT Tools™. More than 225 vehicles have been designed or analyzed using the methodology of flow-decomposition into component features; an approach that has been in continual development and application for many years[2,3].

In the new methodologies, contributions to the body and fin surfaces are computed using a combination of techniques that are CFD-based and semi-analytical in that the models have a theoretical/analytical basis but include factors that are evaluated from a parametric experimental database. Interference effects (such as fin-to-fin, body-to-fin and fin-to-body) are computed using CFD-based models.

Validation of the VCT prediction techniques has been a continuous process over the past 30 years. Because of this, the new CFD-based methodologies are added with confident, experimentally-validated steps. Hydrodynamic model predictions have been validated against tow tank, water tunnel, wind tunnel, planar motion mechanism (PMM), rotating arm (RA), radio-controlled model (RCM) and full-scale test data. Test facilities used in these validations include David Taylor Model Basin (DTMB), Tracor Hydronautics, ARTEC, University of Maryland

[1] Watkinson, K.W., D.E. Humphreys, T.F. Tureaud, N.S. Smith, "Integrated Vehicle Control Design for an Unmanned Underwater Autonomous Vehicle (UUAV)," International UUV Symposium, April 24-28, 2000.

[2] Humphreys, D.E., "Dynamics and Hydrodynamics of Ocean Vehicles," Proc. IEEE Oceans 81 Conference, Boston, September 1981, pp. 88-91.

[3] Humphreys, D.E. and K.W. Watkinson, "Methods of Estimating Vehicle Transfer Functions Requiring Only Geometric and Inertial Characteristics," Proc. IEEE Oceans 72 Conference, September 1972, pp. 220-231.

Glenn L. Martin Wind Tunnel and NASA Ames Wind Tunnel. Validation has been made against many types of Navy vehicles including torpedoes, submarines, UUVs, towed mine countermeasure vehicles, towed ASW vehicles, Swimmer Delivery Vehicles (SDV), as well as Air Force aircraft and towed vehicles. Many of the more than 225 vehicle designs that used the VCT techniques were unusual shapes with large asymmetric components for which no hydrodynamic database existed prior to the design analysis.
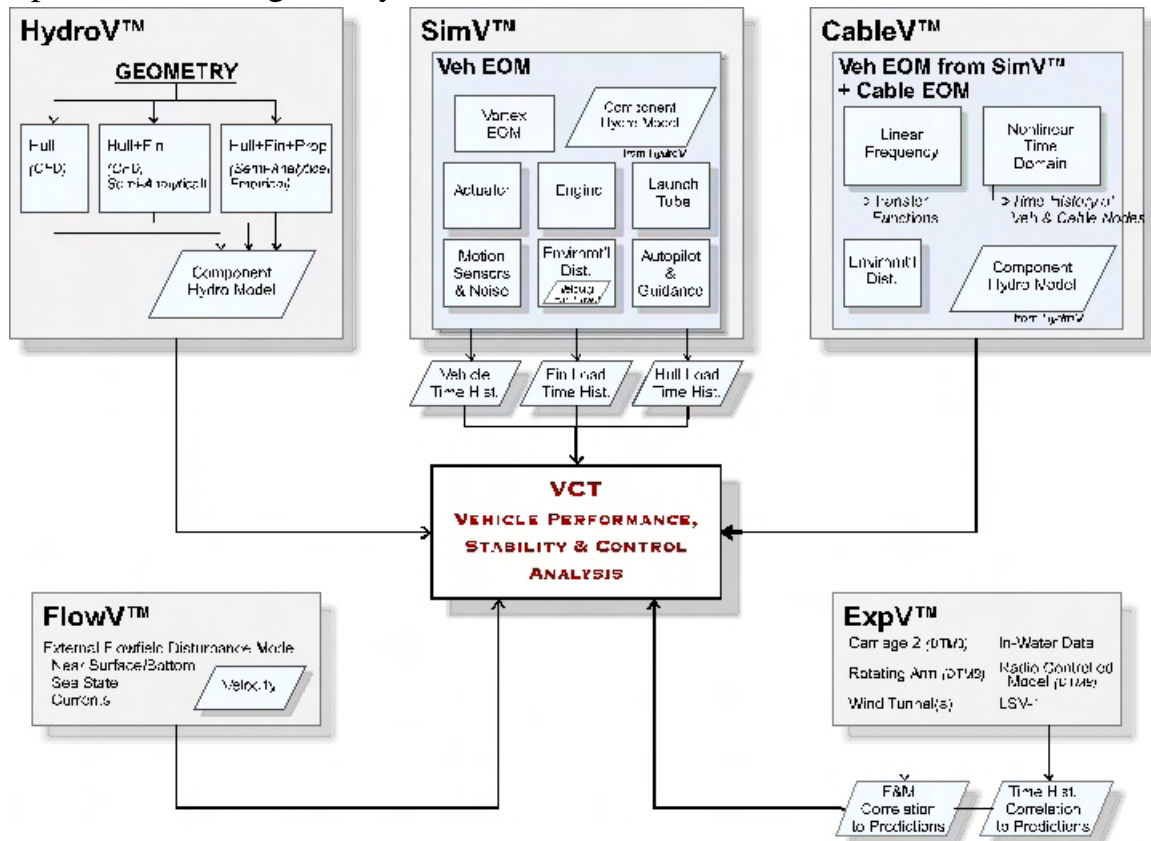
Figure 7.1 · VCT Tools™ for Vehicle Design and Analysis

The key to obtaining models with a low level of uncertainty for use in control system design is the development of a model that accurately predicts the complex linear and nonlinear hydrodynamic forces and moments acting on the vehicle. Vehicle hydrodynamic forces and moments in nonlinear (and many linear) maneuvers are dominated by the vorticity field about the vehicle. The dominant flowfield is created by vorticity shed from the hull and from the various lifting appendages.

Under the VCT methodology, all linear and nonlinear hydrodynamic effects appearing in the EOM representing hydrodynamic forces and moments are computed in a consistent framework with individual contributions due to the body, the horizontal fins, the vertical fins, the asymmetric fins and the propulsor. This includes static, dynamic, acceleration and control contributions. Figure 7.2 and Table 7.1 present the range of geometry parameters that VCT Tools™ has been validated against, along with an example of VCT predictions versus wind tunnel data.

Applicable to a Broad Class of Geometries		
Hulls	$3 \leq$ L/D ≤ 17	BOR, Noncircular
Fins / Wings / Flaps	$0.25 \leq$ AR ≤ 20	Flap Types; TE, Tip, Split
Interactions	$0.5 \leq K_B + K_W \leq 4.0$	Thick and Thin BL
Configurations	+, X, Y, invert-Y, hi, lo, fwd, aft	Up to 17 fins
Stores	Up to 10	Full 6-DoF model for Missile on Wing Tip, Sonar Arrays, LBL, ACDP, etc.
Angle of Attack Range		
Linear	$< 4°$	Excellent
Nonlinear	$4° < \alpha < 20°$	Good
High alpha	Up to 90°	Fair
Astern Maneuvers	90° to 180°	Propulsor-dependent
Unsteady Aero/Hydrodynamics		

Table 7.1 · VCT Tools™ Range of Applicability
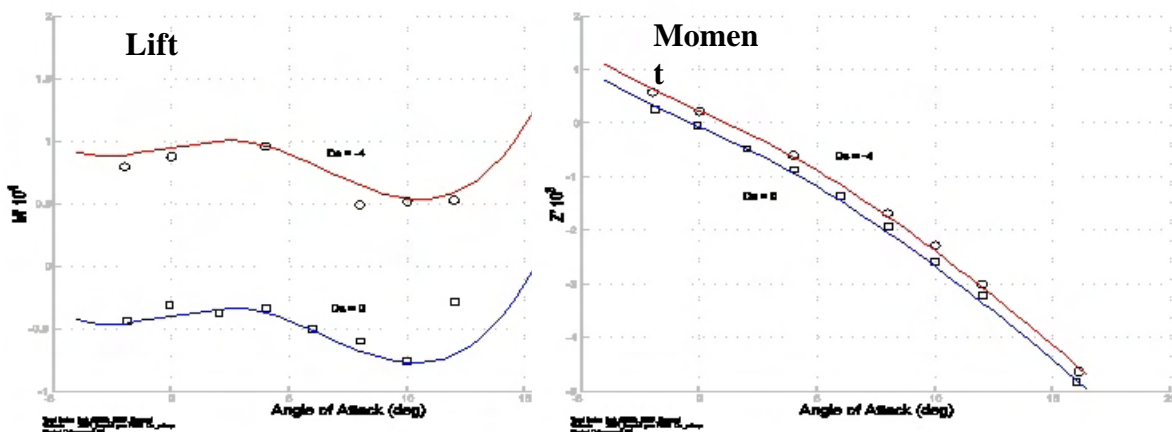
Figure 7.2 · Example of VCT Predictions vs Wind Tunnel Data, Combined Angle of Attack and Control Surface Deflection

7.1.1 Isolated Body Static Force and Moment

The normal force on an isolated body of revolution at an angle of attack is made up of contributions resulting from vorticity lift and viscous crossflow effects. At small angles of attack, the normal force is well represented by potential flow theory and is essentially linear with angle of attack. Crossflow separation starts at the base of the body at an angle of attack between 2° and 4°. With increasing angle of attack the location of this crossflow separation moves upstream so that eventually most of the body is in separated crossflow. Validation against approximately 50 hull configurations has shown that the total normal force can be successfully described by a combination of potential flow theory with viscous wake models (Fgures 7.3 & 7.4) and a second nonlinear term derived from the crossflow-drag analogy.

The pitching moment on a body of revolution is obtained by integrating the axial distribution of the normal force. As in the case of the normal force, it can often be described adequately by a potential flow (linear) term and a crossflow drag (nonlinear) term. For very low speed maneuvering, the local flow velocities are used to compute the crossflow characteristics appropriate for the local Reynolds number.
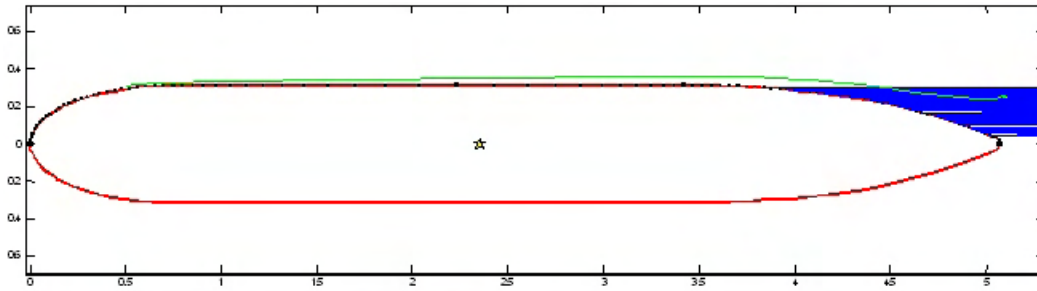
George221_10_Cd027: L/D = 8.1		Breaks [ft]				Slopes [Degrees]		Panels [ft]			
BHF-File	George221_10_Cd027	B	N	X	R	SB-	SB+	HB-	HB+	Np	Tp
Length	5.0562	1	1	0	0		84.61		0.019	27	1
Diameter	0.625	2	28	0.75	0.313	0.94	0	0.049	0.047	14	1
Volume	1.2811	3	42	2.231	0.313	0	0	0.197	0.198	11	1
Surface area	8.8814	4	53	3.417	0.313	0	-0.02	0.048	0.05	52	1
Frontal area	0.3068	5	105	5.073	0	-87.69		0.02		0	0
Xncb	2.35	6									
Prismatic coef.	0.826	7									
Panels [A,C]	[104, 40]	8									
Breaks	5	9									
Wakes	[64:101]	BREAKS		PANELS	EXTERNAL	MODGEO		*SAVE*		*RESTORE*	
Kutta		Hull flow		P	Va	Vc	Viscous cross		Flow output		Summary data	

Figure 7.3 · Hull-Alone CFD Results – Body Wake
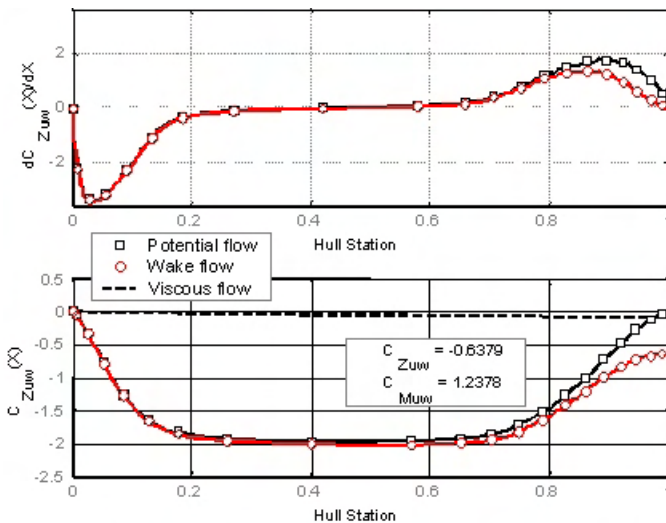
George221-10-Cd027: L/D = 8.1: dC_z/dX and $C_z(X)$ loads for the UW mode

Figure 7.4 · Hull-Alone – Pressure and Load Distribution

Drag as a function of Reynolds number and equivalent sand grain diameter (SGD) is shown in Figure 7.5. At a speed of 0.5 KTS, the Reynolds number (Re No.) for the hull is $9x10^4$. At this speed, the drag coefficient (based on $Vol^{2/3}$) is 0.0195 for zero roughness and 0.032 for SGD=0.25.
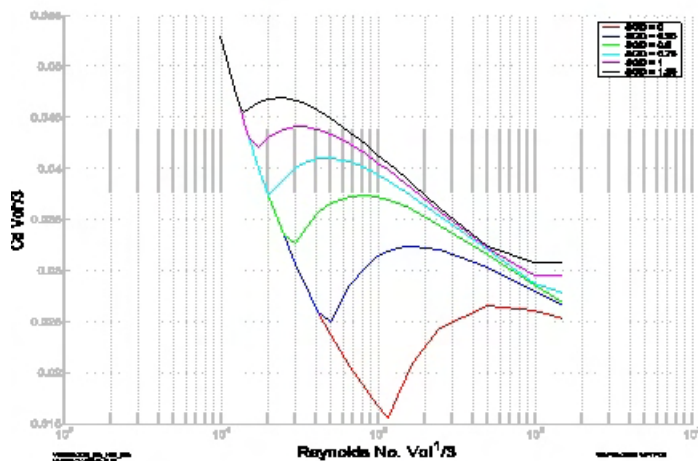
*Figure 7.5 · Reynolds number and SGD Effects on Drag Coefficient –
Hull Alone High Drag*

7.1.2 Fin Lift and Moment

The lift force generated by the fins is an important parameter for the performance and stability of any underwater vehicle. Lift varies as a function of angle of attack and flap deflection for a given planform geometry. The lift is first computed for an isolated fin that is not mounted to a body. When the fin is mounted to a body, its lift is changed by the carryover lift from the body to the fin plus the carryover lift from the fin to the body. Carryover is computed using both CFD and semi-analytical methods. Both the hull vorticity wake and the full viscous boundary layer affect the lift carry over, which can vary from 0.8 to 4.0 times the fin-alone lift. Lift carryover is a function of the fin location on the hull, the ratio of fin span to local body radius, fin taper ratio and afterbody shape.

The geometric parameters that affect isolated fin lift are; aspect ratio, sweep angle, taper ratio, flap chord ratio, flap span ratio and flap span location (Figure 7.6).

`   The lift curve slope, $c_{L\alpha}$, is largely a function of sweep angle and aspect ratio. Major gains (a factor of 3) can be made by increasing the aspect ratio from 0.5 to 2.0, which is a typical range for underwater vehicle fins. For these low aspect ratios, sweep has less effect in decreasing the lift than other parameters. For an aspect ratio of 3.0, a sweep angle of 30º reduces lift by only 6%.

FHF File: George221-221-10-Cd027-tft.geo

Vehicle 221-10 d027ft.geo: Equivalent wall fin loads
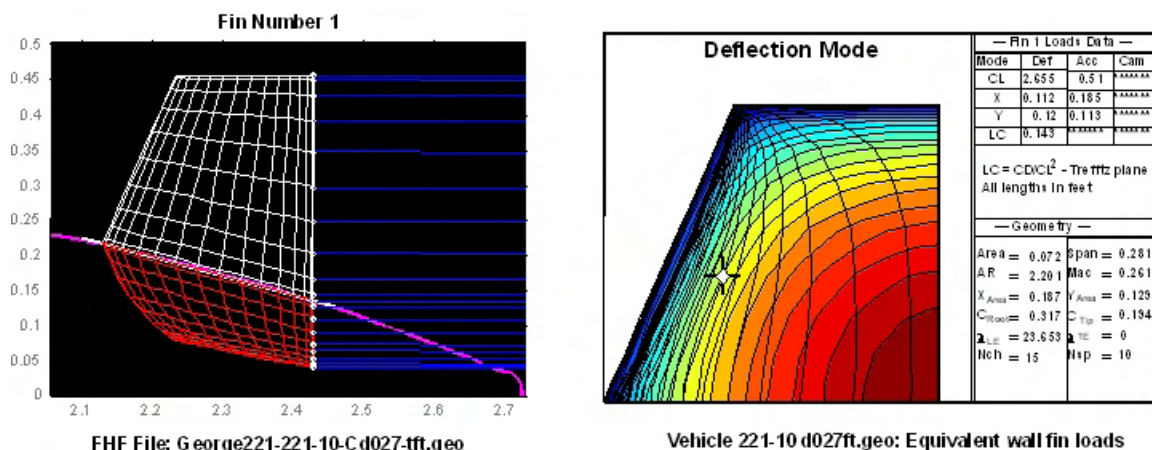
Figure 7.6 · Hull-Fin CFD Results

7.1.3 Wing Downwash Effect on Aft Fins

For vehicle configurations (airplane, missile, submarine, etc.) that have both forward and aft lifting surfaces, the vorticity shed from the forward surfaces can induce significant loads on the aft fins (and to a lesser degree on the hull or fuselage). As an example, consider the loads induced on a vehicle's aft fins (rudders, stern planes, dihedrals) by the vorticity shed by the wing. The local angles of attack induced by the wing on each tail fin panel depends on the vortex's strength and location with respect to each panel. This results in a decrease in lift for the aft fins as well as an induced roll moment due to the panel-panel angle of
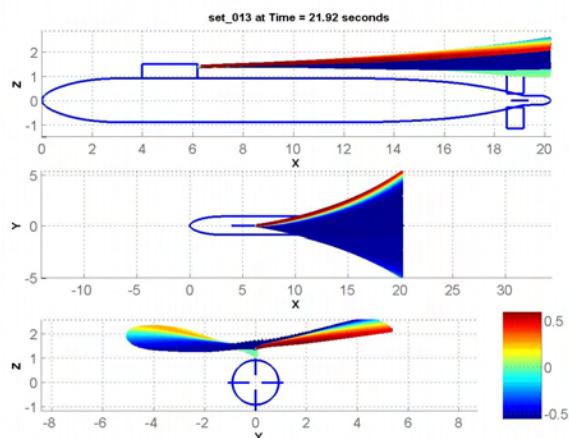
Figure 7.7 · Vortex Path during Horizontal Overshoot Maneuver

attack variation. The strength and position of the vorticity (Figure 7.7) depend, in a nonlinear fashion, on the motion state of the vehicle and on its motion time history; these vortex-induced effects are generally nonlinear even for steady state motion conditions. A coefficient representation of these vortex-induced lift and roll moment effects is not adequate, although various attempts have been made in the past to use such a representation (e.g., 2510 equations of motion). Classical downwash models (e.g., $d\varepsilon/d\alpha$) treat the downwash from the wing onto the tail assuming the following:

> wing span is significantly greater than the control fin span
> control fin's x-separation from the wing is large relative to the span of the wing
> wing tip vortex is fully rolled up.

These assumptions are valid for conventional aircraft, but break down for most underwater depressor designs like the AQS-20 and, in some cases, buoyant control glider designs.

The remaining assumption is that the vortex sheet is fully rolled up. To remove this assumption requires the use of multiple wake vortices shed from the wing's trailing edge, allowing them to roll up as they progress downstream. Such an improvement is a planned upgrade in the VCT model. As such, the new VCT model requires an adjustment to the wing-tip vortex strength. For a fully rolled up vortex at an infinite distance downstream, this value is 1.0. For a value just aft of the wing trailing edge, the theoretical value is 0.50. Thus, the correlation value is expected to be between 0.50 and 1.0.

With the VCT vortex-tracking model, we capture much of the nonlinearity that is exhibited in depressor data (Figure 7.8a). Classical $d\varepsilon/d\alpha$ models exhibit very little of this nonlinearity (Figure 7.8b).

These considerations also apply to other types of vehicles, such as a UUVs with canard controls. The particular behavior of the vortex-induced effects depends upon the geometric configuration of the vehicle, but the physics governing these effects is the same across all types of configurations. The physics of vortex motion and vortex-induced loads are implemented in VCT's component hydrodynamic and aerodynamic models.
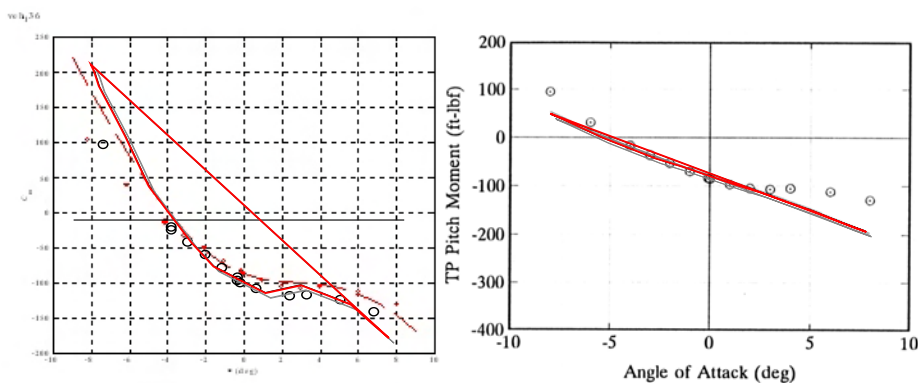
Figure 7.8 & Figure 7.9. VCT Vortex Model vs dε/dα Model

7.1.4 Numerical Modeling Procedure:

Utilizing the VCT database of over 230 vehicles and its modeling and simulation program, referred to as VCT Tools, hydrodynamic models of the Seaglider vehicle were developed using inputs of geometry and mass characteristics. The vehicle model is a full 6-DoF non linear rigid-body model that consists of individual geometry components that react to flow conditions in each geometry component's local angle of attack/sideslip. All hydrodynamic models required for the simulation have been developed by VCT under this task.

Static performance measures consisting of classical C_L C_D , C_L/C_D and $C_L^{2/3}/C_D$ plots as a function of angle-of-attack and glide angle are reported along with spider type performance plots. Spider plots are a single plot that shows a map of glider performance, taken after Osse[4] with the horizontal velocity (u-component of total speed, U) plotted on the x-axis and vertical velocity (w-component of total speed) plotted on the y-axis are used to compare the VCT model to in water static performance data. Lines of constant net buoyancy and lines of constant angle of attack and/or X_{CG} location are overlaid on the plot to show the relationship between glider configuration and performance. Once a satisfactory match was obtained between the VCT predicted static performance and the legacy gliders in water data, VCT Tools was then used to extrapolate a composite surrogate of each functional class over all practical regimes of scale.

These extrapolated data were then throughput to the spreadsheet analysis for the final systems integration analysis of the functional classes.

7.1.5 Trajectory Simulation Model (SimV™)

VCT trajectory simulations are performed using SimV™, a computer program developed by VCT, based on the legacy code TrjV™. SimV™ is a digital computer program coded in both FORTRAN™ and C™ languages. Specialized versions of TrjV™ were developed in the past for the simulation of specific classes of vehicles. Examples of these are TRAJN, a submarine simulation, TRJTORP, a torpedo simulation and TRJUUV, an Unmanned Underwater Vehicle simulation. The current version of SimV™ incorporates the most recent developments in vortex models and the full range of angle of attack up to 180°. It is applicable to all types of air and submerged vehicles. A block diagram of the program structure is shown In Figure 7.10 below.
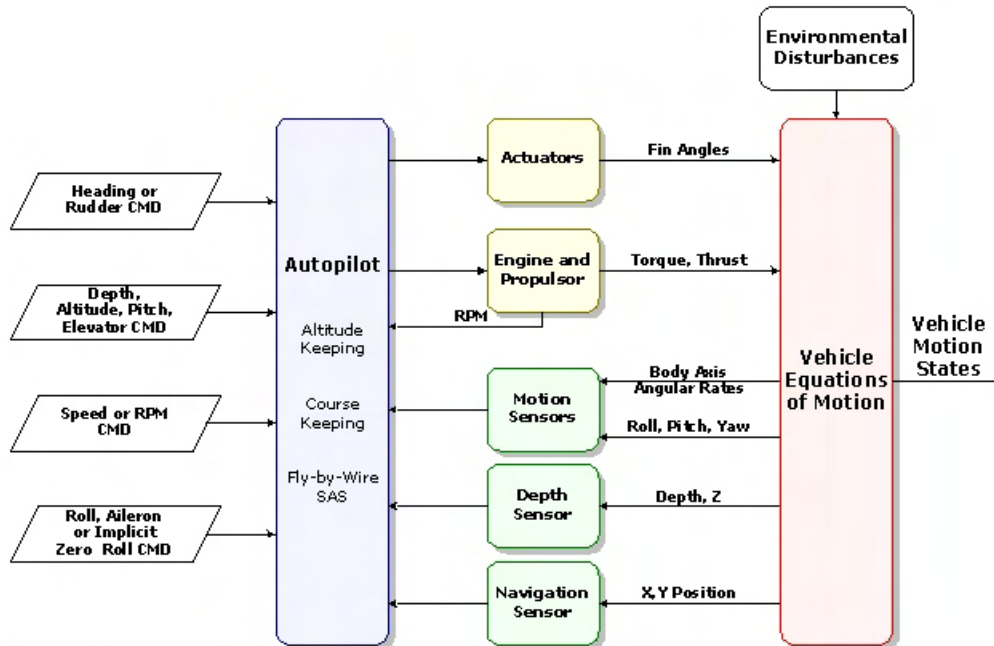
Figure 7.10: Time Domain Vehicle Simulation Tool (SimV™)

SimV™ models the dynamics of the vehicle in both deeply submerged and shallow water conditions. The equations of motion in SimV™ reference a body-fixed system of axes, which is defined with respect to inertial space by the standard Euler angles. The standard SNAME conventions are used. The origin of the body-fixed axis system is arbitrary and not restricted to the body's center of gravity or center of buoyancy. The inertial frame of reference and Newton's Laws of Motion are the basis of this set of equations.

7.1.6 Validation for Legacy Gliders

Field data on the legacy glider performance was provide by contributing authors, Jim Osse , Clayton Jones and Jeff Sherman and was to validate the VCT numerical simulations. Seaglider maneuvering data detailed one complete depth excursion cycle to a depth of 1000m depth executed at about a 20° pitch angle. The dive cycle duration eas about 20,000 seconds, or 5½ hours. For the Slocum glider the data set used for comparison to simulation is we01-2003-013-36. It has three depth cycles to 50m. Each cycle took about 450 seconds (7.5 minutes). Figure 10.13-10.17 presents plots of the data set. One complete depth excursion cycle was provided for Spray. It was a 100m depth change with about an 18° pitch angle. The cycle took about 2,200 seconds, or 37 minutes.

Simulated glide polars for legacy gliders Slocum, Seaglider and Spray were validated at discrete points in the solution space as shown in Figures 7.11, 7.12 and 7.13, respectively. In the glide polar (spider) plots shown on the right hand side of each figure, validation control points derived from the field data are indicated by solid diamonds and those produced by model simulation are indicated by open diamonds. For the angle of attack (a = AoA) variations of C_D, C_L, C_L/C_D and $C_L^{3/2}/C_D$ appearing on the left hand side of these figures, data derived estimates are shown as circles and model derived values are diamonds. In most instances, the agreement between data and simulation are so close that the two sets of symbols are indistinguishable.

Flight simulations were performed using a 231-07 vehicle model for Seaglider, 231_05 for Slocum, and 236_05 for Spray. Buoyancy changes and pitch mass movements are entered as piecewise linear representations of the data time histories. This can be seen in the center and lower panels of Figure 7.14 for Seaglider, Figure 7.16 for Slocum and Figure 7.18 for Spray. The resulting depth time history is shown in the upper panels of these figures and the comparison between simulated depth excursions and measured excursions is quite close. The

depth rate and pitch angle time histories are shown in Figures 7.15, 7.17 and 7.19 for Seaglider, Slocum and Spray, respectively. Again, the agreement between simulation and measurement is extremely good.

In summary, the legacy gliders were succesfully modeled using VCT hydrodynamic and simulation tools (VCT Tools™). Vertical plane maneuvering data from field observations compared well to simulation data. This match validates the fidelity of the vehicle hydrodynamic modeling methods and the simulation model. Plots showing the legacy glider performance were developed for the full range of operating buoyancies and pitch angles. These indicate, that typically a maximum horizontal velocity of about 37 cm/sec can be obtained with the nominal buoyancy of 200 grams for glide angles of 35^0. Cruise speeds for legacy gliders are typically less and performed at glide angles of typically 20^0. Performance for other values of buoyancy and pitch and glide angles were found. Therefore, the application these numerical simulation methods to UW glider performance is regarded to be sufficiently validated to extrapolate performance in other scale regimes. It is customary to use tow tank force and moment data to validate simulation models and to guide the adjustment of key hydrodynamic parameters. The excellent match between the data and the VCT simulation was achieved without tow tank data for the legacy. This achievement is made possible by the continuous improvement to VCT flow phenomena models throughout the past 30 years and the preponderance of previous validation efforts using tow tank, wind tunnel, rotating arm and full-scale in-water data.

Veh 231-07 Seaglider In Water Drag
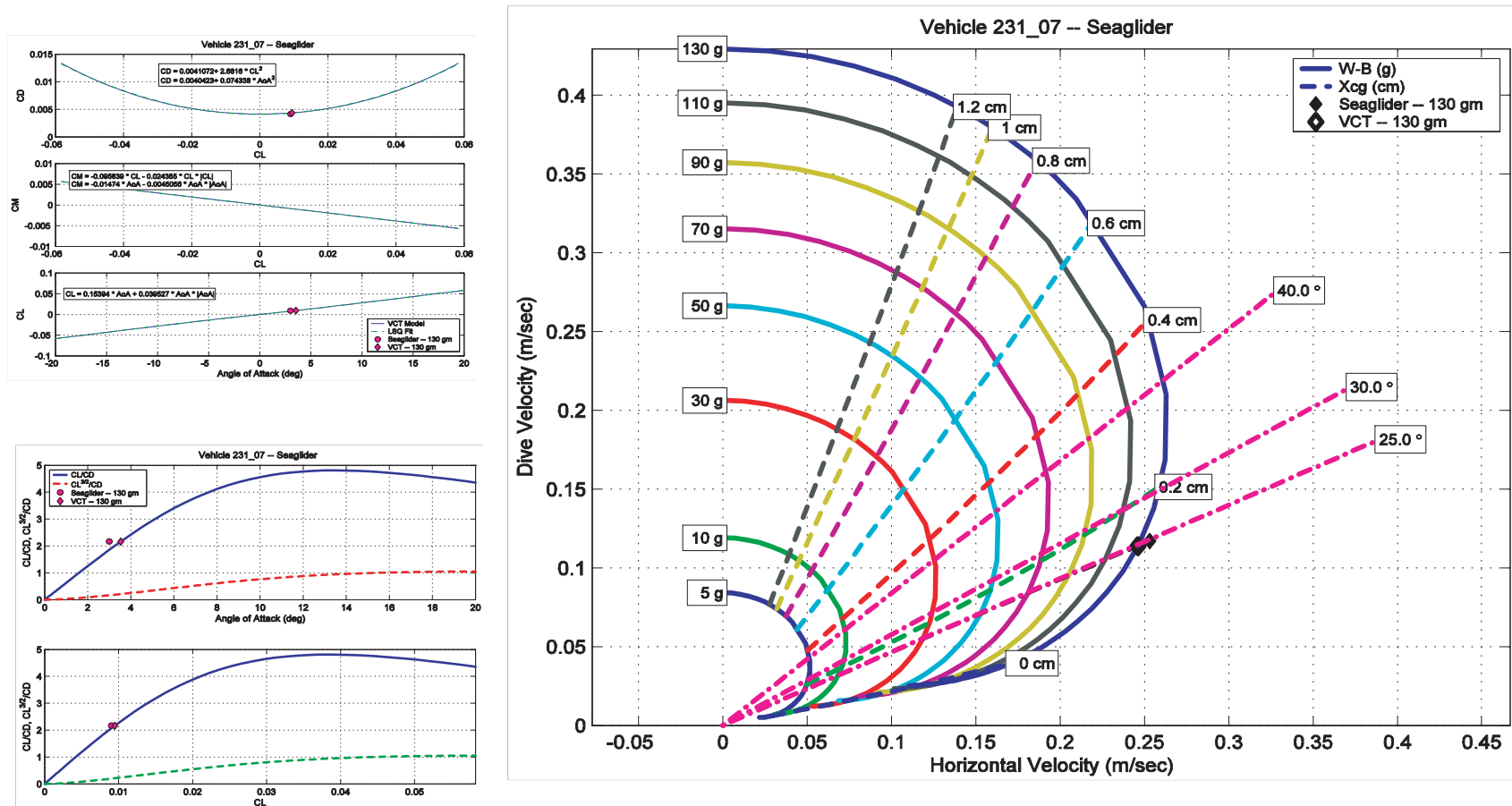
Figure 7.11. Calibration of VCT simulated glide polar for legacy glider (Seaglider). In the left hand panel, validation control points are indicated by circles for values derived from field data and diamond for VCT simulated values. In the right hand panel, data are solid diamonds and simulated points are open diamonds. [from Humphreys et al., 2003].

Veh 235-05 Slocum
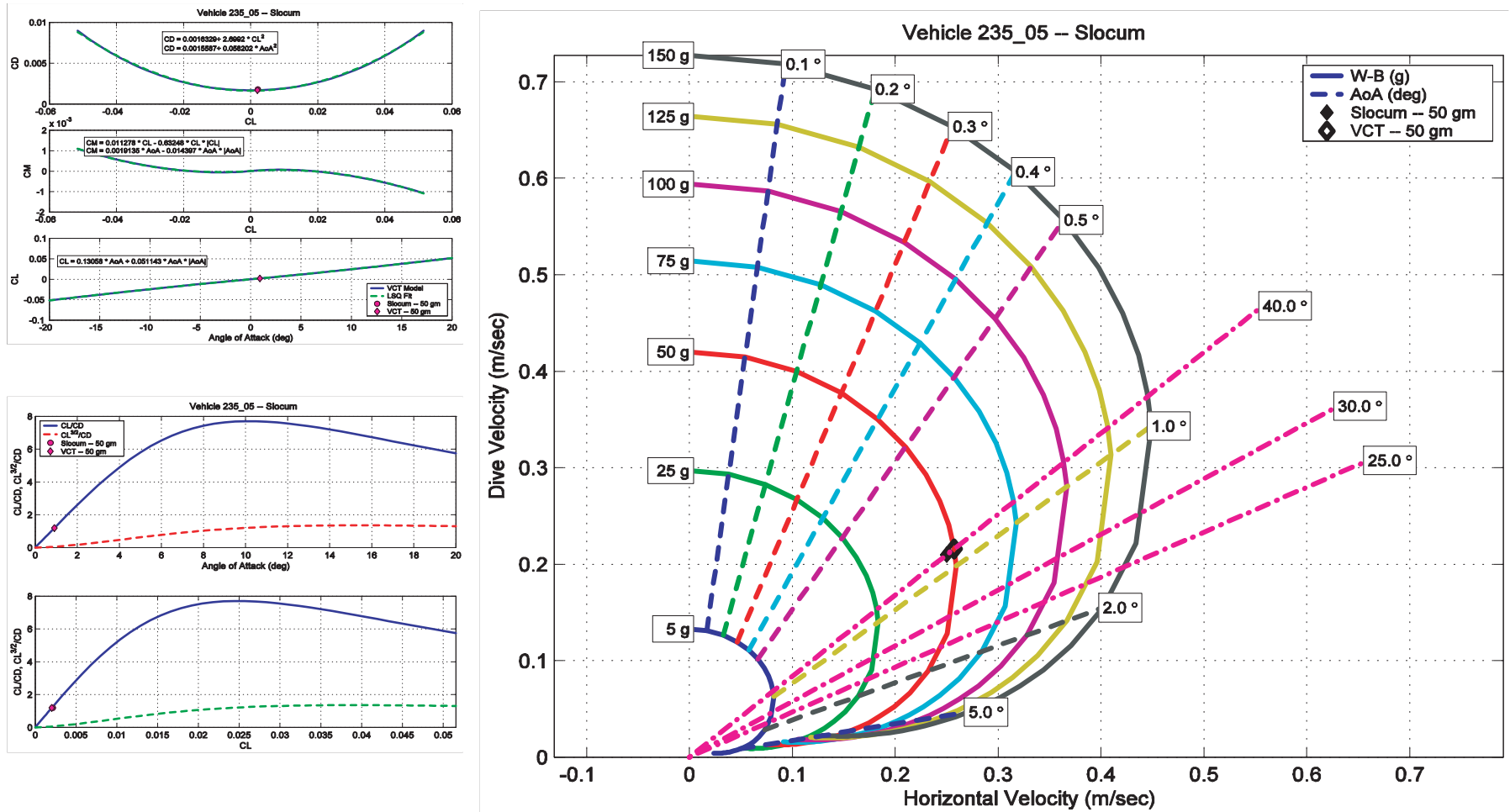
Figure 7.12. Calibration of VCT simulated glide polar for legacy glider (Slocum). In the left hand panel, validation control points are indicated by circles for values derived from field data and diamond for VCT simulated values. In the right hand panel, data are solid diamonds and simulated points are open diamonds. [from Humphreys et al., 2003].

Veh 236-04 Spray
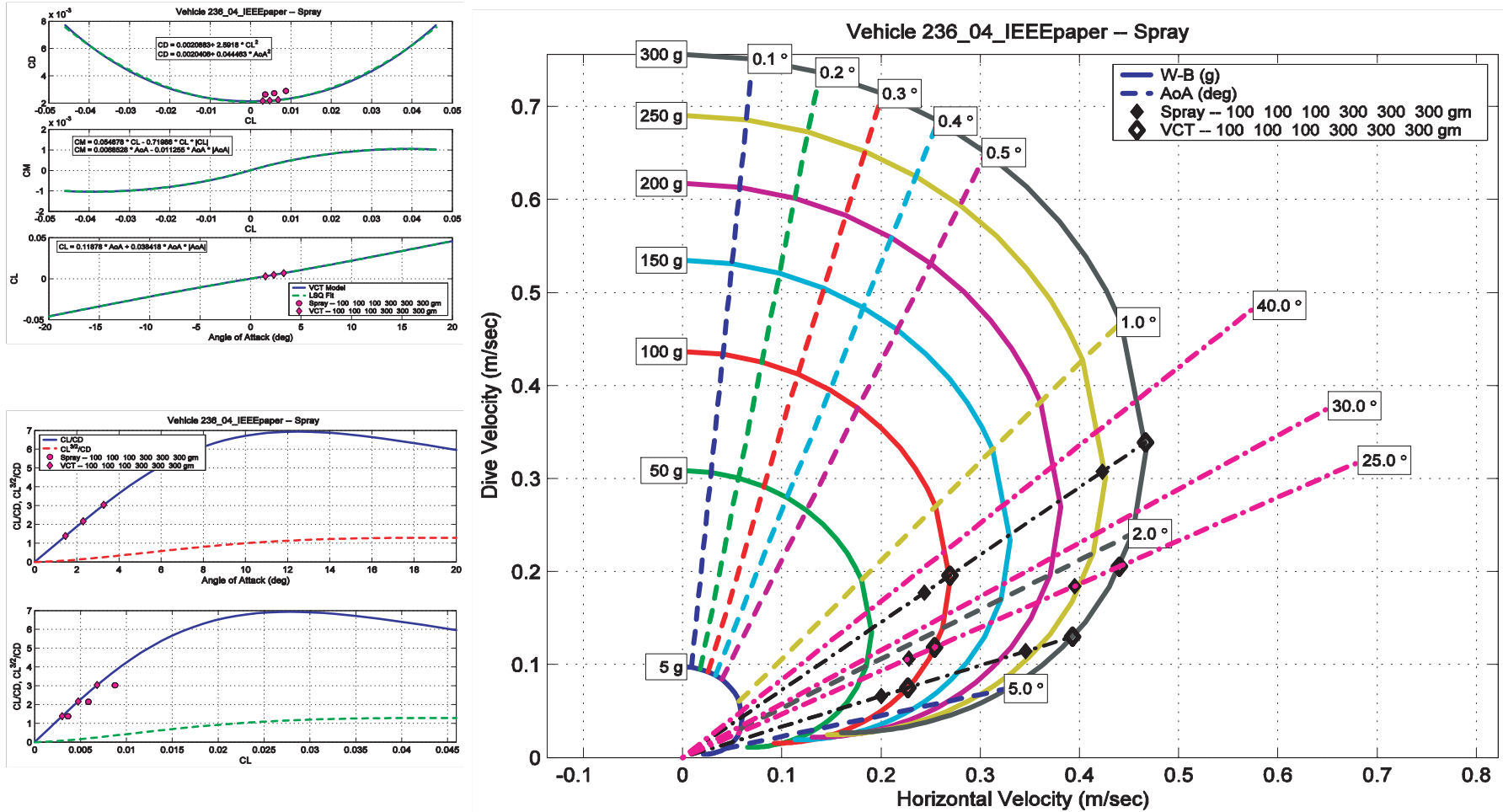
Figure 7.13. Calibration of VCT simulated glide polar for legacy glider (Spray). In the left hand panel, validation control points are indicated by circles for values derived from field data and diamond for VCT simulated values. In the right hand panel, data are solid diamonds and simulated points are open diamonds. [from Humphreys et al., 2003].
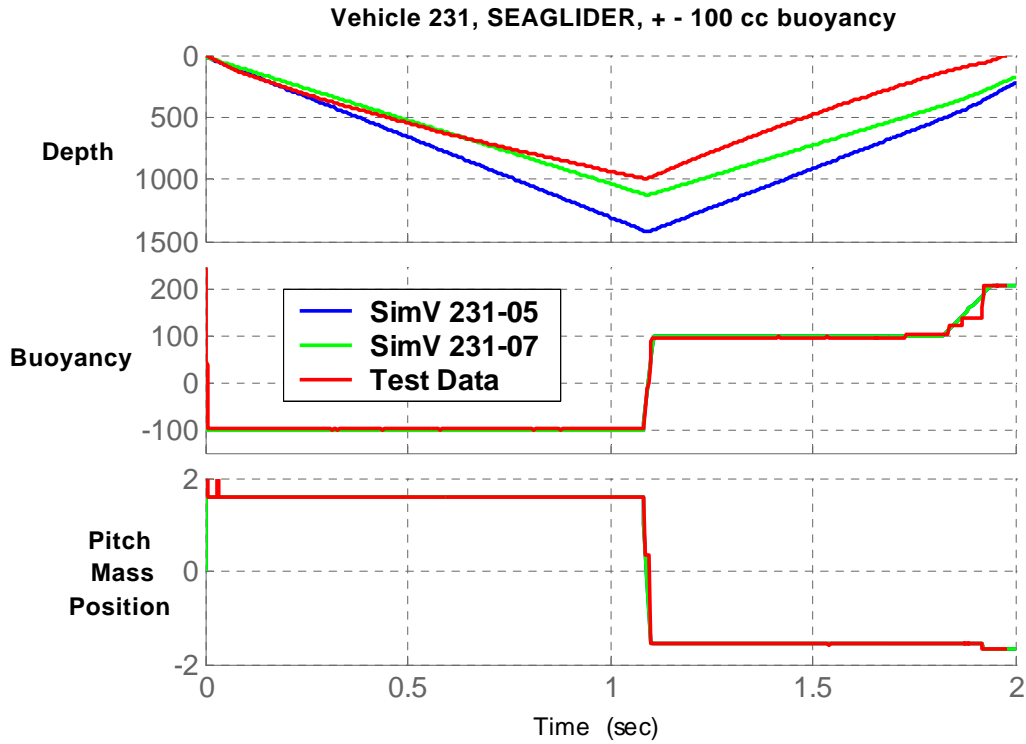
Figure 7.14. Seaglider maneuvering data versus simulation: depth, buoyancy & pitch mass position.
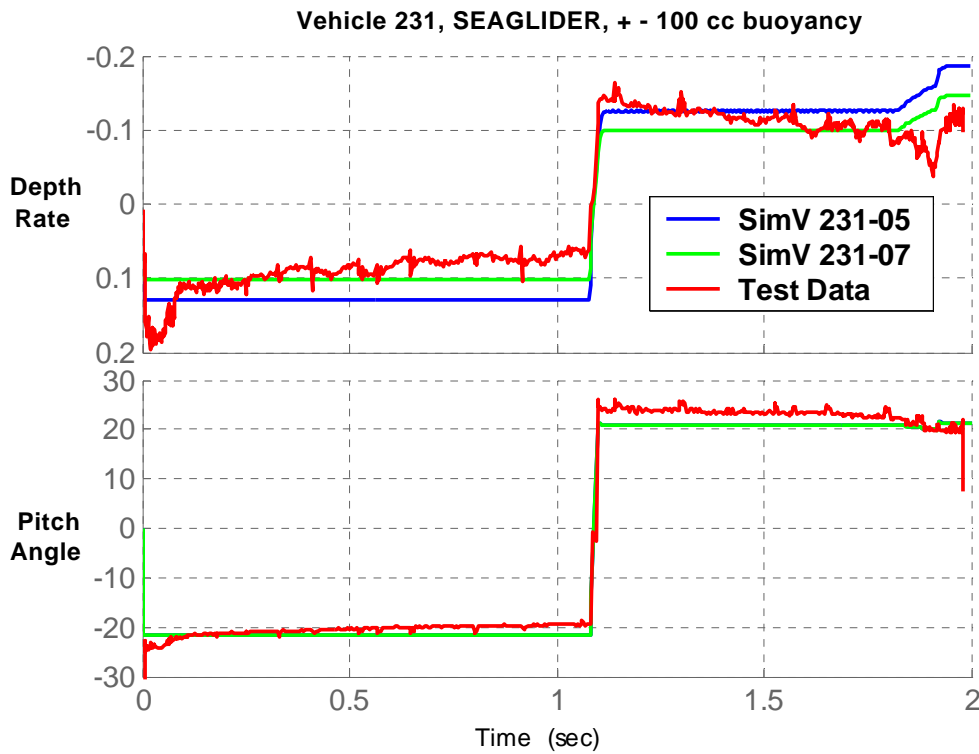
Figure 7.15. Seaglider maneuvering data versus simulation: depth rate & pitch angle.
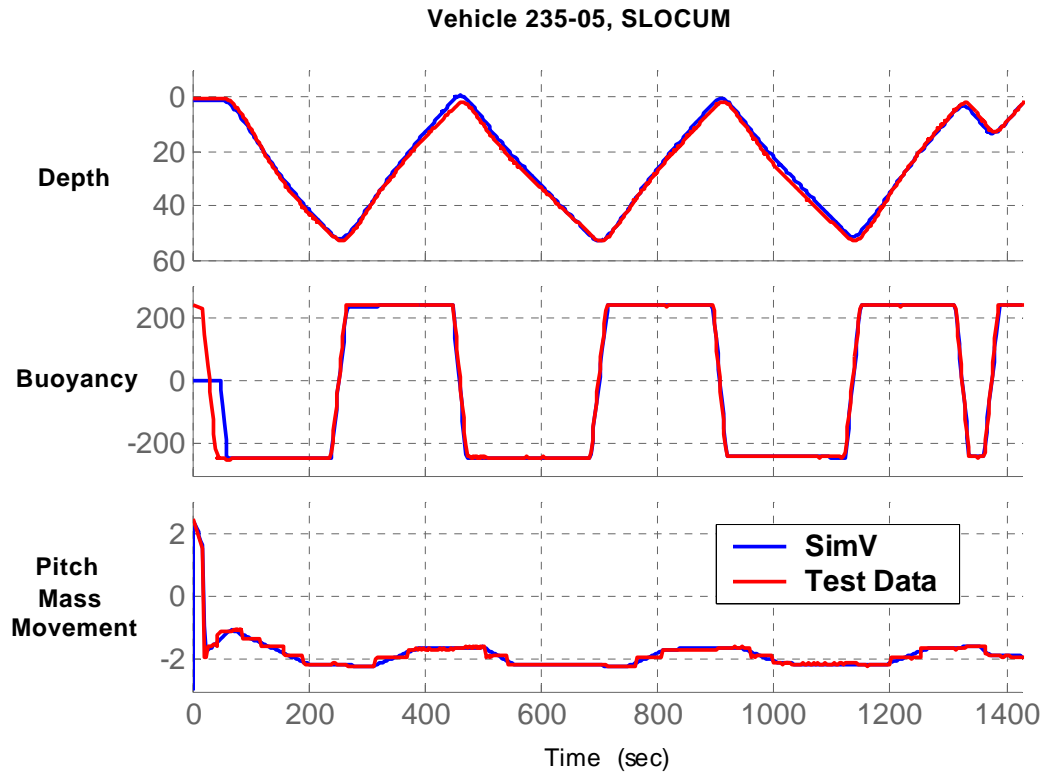
Figure 7.16. SLOCUM simulation versus data: depth, buoyancy and pitch mass movement.
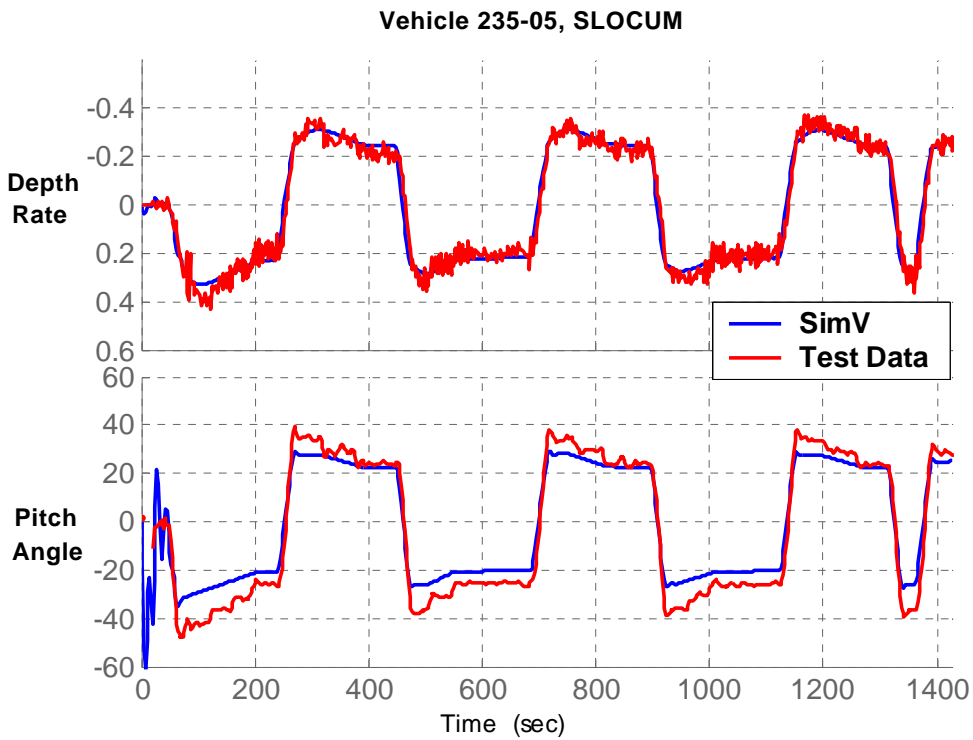
Figure 7.17. SLOCUM simulation versus data: depth rate and pitch angle.
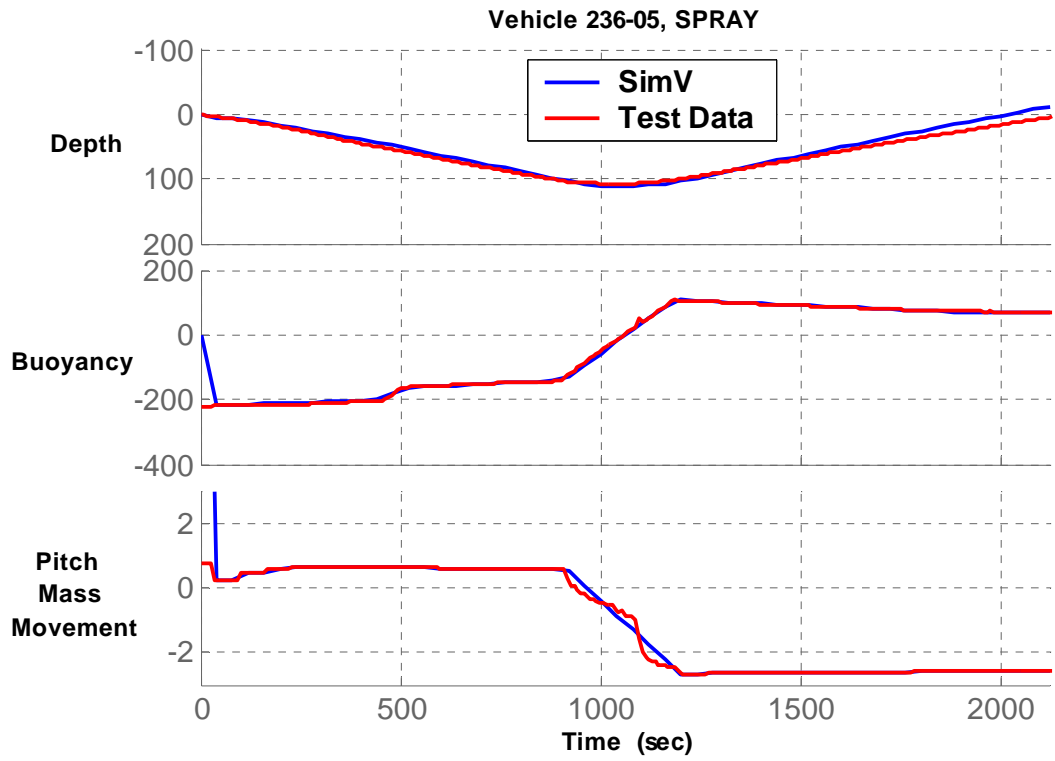
Figure 7.18. Spray data versus simulation: depth, buoyancy and pitch mass movement.
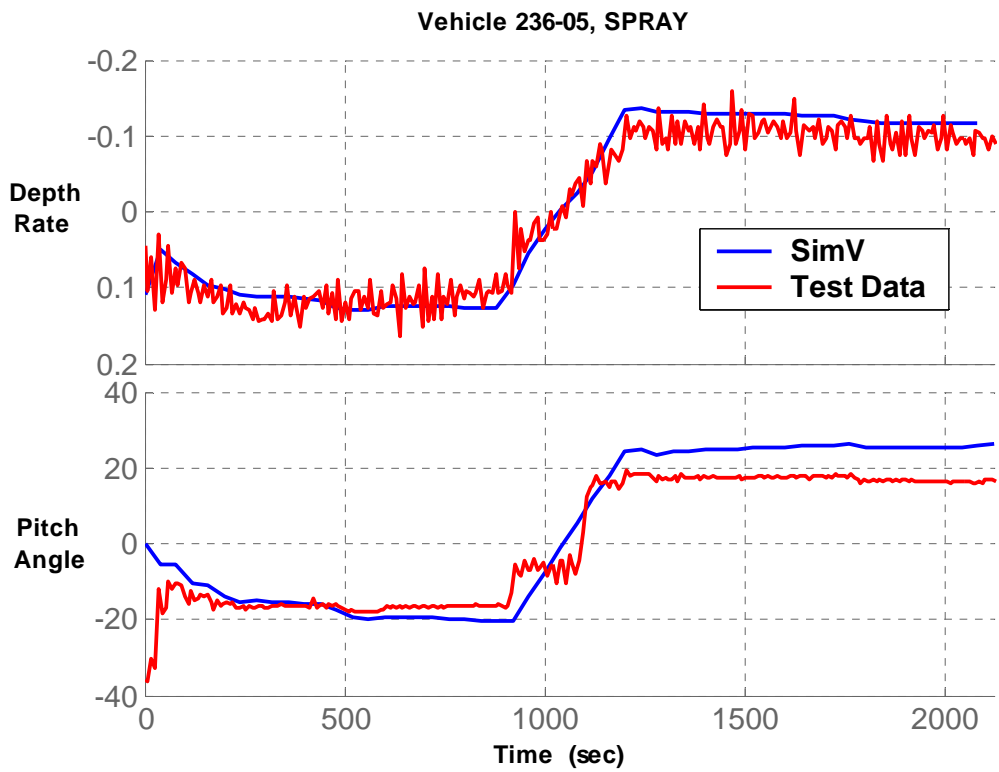
Figure 7.19. Spray data versus simulation: depth rate and pitch angle.

7.2 Spread Sheet Analysis (Exerts from Osse, 2003)

The spreadsheet analysis excepts key hydrodynamic parameters from the VCT numerical model simulations and combines those data with a host of systems information to ultimately calculate the energetics of the UW-glider. The original intent of the spreadsheet model was to answer the questions of how far can a glider of a given size travel or how long can it remain flying, given a payload of known power requirements and weight/volume. It has since been reformatted to calculate NTE, Ea and a vareity of other energetics specific parameters used in flight survey and scale regime analysis. Calculation of these parameters distills down to simple bookkeeping, but it involves many disciplines of engineering, from modeling guidance and control to pressure hull design to battery technology. All must be synthesized to answer the questions above.

The spreadsheet model has been the primary engineering design tool in the development of the Seaglider AUV since 1995. It began as a hydrodynamic performance model when conducting initial wind tunnel test. It has since evolved to include all power consumers in the vehicle including buoyancy engine and all hotel loads. The primary inputs are listed in the summary Performance worksheet in Table 7-2, and include the variables available to the operator to fly the glider. From knowledge of the target distance and depth to operate, one chooses a given net buoyancy for a dive and by distance to a target a pitch angle is set.

The spreadsheet model does not include pitch moment balancing, but does solve for total velocity given a net buoyancy and a specified lift and drag coefficients. Given a specified data sampling scheme of the science sensor suite, and a specified Guidance and Control duty cycle, add in the energy needed to telemeter the data via the Iridium satellite data link, and the spreadsheet can compute a total energy cost per flight profile.

The control of the glider is modeled by controlling attitude with longitudinal and transverse center of gravity. Glide path control is accomplished with adjustments to the variable net buoyancy volume. Because buoyancy variation constitutes a dominant fraction of the energy needs, the model of the hydraulic pump efficiency is important. There are five different models of traditional hydraulic pumps, and five models of single stroke piston pump. In general the positive displacement, axial piston design have similar efficiencies and superior weight efficient designs to single stage large bore single stroke

piston pumps. A pump model was adapted from the Seaglider, with similar performance to the Spray glider. The spreadsheet model computes the additional buoyancy volume increments needed to overcome ocean stratification and hull compressibility effects as described in Section 6.1.

The spreadsheet model was run for the different glider sizes evaluated by VCT Tools. For each size, and for a specified maximum depth, the model computes an estimate hull weight based on an average of the specific strength per unit weight of payload within the legacy gliders. It then tallies the weights of other components, some of which vary with vehicle size, such as the fairing that scale with the length ratio squared, to electronics weight which does not change at all with size or depth. The payload of science sensors or other AUVs such as REMUS are then added, and the remaining is given to energy stores (batteries). Each sensor sums it data requirements into the total energy budget. Both overhead and per byte transmit cost are accounted for in the energy budget. A duty cycle from 10 to 100% is assigned to each sensor, including both data acquisition and G&C rate periods, as done in the Seaglider. The total energy on board divided by the per dive energy cost yield the sustainable number of dives (duration). The number of dives factored against the glide slope gives and depth yield the range.

From an imbedded Visual Basic program the spreadsheet model computes a sweep of net buoyancy versus depth. This presents most of the tradeoffs for a given configuration. From these we compute 6 dependant variables, which are plotted on two separate plots (using the data graphics package Igor). These six dependant variables are:

- Number of Dives: Pressure hull weight increases with depth, reducing available payload for energy storage, and reducing the number of dives. However the percent fraction of time spent during apogee pump and surface telemetry benefits the endurance of deeper dives.

- Range (km): total range for a given battery pack. This is estimated using Lithium Thionyl Chloride batteries. These are the highest energy density batteries commercially available; hence range is reduced for other battery chemistries.

- Dive Time (hours): round trip dive time between surfacing, not including apogee pump times.

- Effective horizontal Velocity (cm/s): this accounts for lost time during apogee pumps and surface communications, where the glider is assumed to be stationary. Alternatively the cross country speed, *u*, is calculated per dive cycle without consideration of on-surface loitering.

- NTE : Net Transport Economy based on Equation (6.1).

- Thrust Fraction: the ratio of energy consumed by the buoyancy engine to the total energy consumed (including all hotel loads).

An example of the spreadsheet model output is shown in Table 7.2. An explanation for certain critical entries is as follows:

1. **Surface Buoyancy**: the minimum buoyancy needed at the surface to elevate the antenna as computed at surface pumping efficiency rates.

2. **Density Range:** density over a specified apogee depth (i.e. the same range of density whether a 100 meter or a 1000 meter dive)

3. **Temperature Range :** Temperature over a given dive depth regime (i.e. same range of temperature whether a 100 meter or a 1000 meter dive)

4. **Apogee depth**: Deepest point of a dive cycle

5. **Hull Compressibility:** set to 75% of seawater

6. **Length to diameter ratio** : Hull length divided by hull diameter =6.86, used for scaling factors relative to the legacy glider average.

7. **Packing Factor:** a ratio of enclosed volume to displaced volume. All the gliders have varying degrees of a flooded fairing, for carrying payloads in separate pressure housings to protection of the external bladder. Default setting is 90%. Should not be confused with lung capacity factor, n_b = ratio of net buoyancy volume to displaced volume.

8. **Data rate**: typically 30 seconds for oceanographic sensors, 100% duty cycle for INU's while diving, 10% duty cycle for magnetometers, etc.

9.   **G&C Update rate** :typically 5 minutes or shorter SatComm Telemetry rates, assuming our experience with the Iridium satellite network.

10.   **Pump rates** : derived from extensive field dive modeling of the Seaglider hydraulic pump. Monitoring of pump current continually has given good data on this style pump to 1000 meters depth. It is identical to the deep versions of the Slocum gliders, and similar to some versions of the Spray glider.

Table 7.2_p1. ONR Glider Study Performance Calculations				Version		3.3			
Insert Fields that are RED						Date	4/9/2003		
Comments	VCT 23x_22 ; improved pump model of Parker PGP PGM 511 6 cc/rev piston pump at 1500 RPM;								
Pilot Settings	corrected NTEB per Jenkins memo 4/6/03, Osse notes of 4/8/03								
Apogee Depth	**500**	meters	725	psi					
Angle of Attack	**1.00**	degrees							
Net Buoyancy	**50,000**	cc	2 x pumped at apogee depth						
Compressibility effect	3190	cc	to accommodate compressibility; pumped at avg. depth						
Density effect	17618	cc	to accommodate variations in SW density and temperature						
Temperature effect	0								
Maximum dive buoyancy (-)	70807	cc	represents maximum negative displacement for one dive from neutral at surface						
Maximum surface buoyancy (+)	**20,000**	cc	total surface buoyancy			0.31%			
Total VBD capacity	40807	cc	total required VBD volume per dive			0.31%			
						101.9531	cc/sec		
Environmental parameters						6.2242	cu in/sec		
Temperature range	0	C				0.0269	gps		
Water Density	1.0200	gm/cc				1.6167	gpm		
Seawater Density range over profile	0.003	Range				6.1192	lit/min		
Hull characteristics									
Enclosed Volume of hull	**6,525**	liters	267 for 1000						
Displaced Volume	5872.5	liters	207.475	cf	13,320	lbs			
Length to Diameter of hull	**6.857**		same as VCT L/D						
Hull diameter	123	cm	AEMT Fineness Data of 6.0 L/d		48.27	inches			
Hull Length	841	cm	AEMT Length to Volume Data		330.98	inches			
Packing Factor	90%		Ratio Displacement to Enclosed Volume						
Length Ratio re: Seaglider	4.67								
Flight Data									
Total # of Dives, based on energy	1663	at x dives/day this takes	24.82	days	0.827	months			
Time for Round-trip; dive only	0.26	hours	15.84	minutes	950	seconds			
Time for Round-trip incl pumping and s	0.36	hours							
Distance travelled over ground	**2833**	km		**3285**					
Effective horizontal velocity	132.1	cm/sec							
Total Velocity	207.95	cm/sec	4.04	knots					
Horizontal Velocity, u	179.3	cm/sec	3.49	knots	74%				
Vertical Velocity, w	105.3	cm/sec			26%				
					100%				
Lift/Drag Ratio	1.85								
Glide Angle	31.4	degree from horizontal							
Pitch Angle	30.4	degree from horizontal							
NTE Performance factor; Total W	**0.01119**	non-dminesional							
NTE Performance factor; Net B	**1.31411**	non-dminesional	**0.44064**						
NTE B; theoretical	**0.53047**	theoretical flight power/horiz speed/thrust							
vector sum lift+drag	49030.4	grams							
Power; Flight only	475.5	Watts		475.5					
Percent Thrust energy / Total energy	71%								

Table 7.2 p2. Hydrodynamic Model			Version	3.3					
Dynamic Pressure, q	22.504	gm-sec^2/cm	46.05086	psf		2205.4	kg/m-sec^2		
Volume Reynolds #	2,368,185								
Length Reynolds #	########	hull length							
Angle of attack	3.0	degrees		3.4deg gives about max obtained glide slope of 3.3:1					
Reference Velocity	50	cm/s	Hubbards Baseline specification			Original AEMT			
Reference Planform Area	314	sq. cm	Hubbards Baseline						
Reference Chord	8.48	cm	Hubbards Baseline	3.34	inches	4.326531	cm	1.703359	inch
Reference Span	42.90	cm	Hubbards Baseline	16.89	inches	21.88776	cm	8.617226	inch
Reference Aspect Ratio	4.37		Hubbards Baseline	1.72	inches				
Reference Semi-Span of Rudder	18.52	cm		7.29	inches				
Tailboom Diameter	18.28	cm		7.20	inches				
Fin Characteristics	Wings	Rudder		Wings	Rudder				
Fin Chord Scale Factor	1.40	0.68							
Fin Semi-Span Scale Factor	1.47	1							
Chord	11.87	5.77	cm	4.67	2.27	inches			
Semi-Span	27.22	18.5	cm	10.72	7.29	inches			
Total Span	100.00	40.6	cm	39.37	16.00				
Aspect Ratio	7.73	7.73							
Area, span planform	646	214	cm^2	100.2	33.1	sq in			
Scale Factor Planform	2.06	0.68							
Hull Characteristics									
Body Radius	14.61	cm @	0.66	X/L					
Geometric Span	83.67	cm							
Minimum Pitch Angle	27.09	degrees							
Lambda from WRC	15.29	non-dimensional							
Eriksen Performance factor, Lambda	265.12								
Minimum Glide Slope	0.12								
Lift									
Lift, Body and Fin	1656.00	gms, from theoretical							
Lift Coefficient from "Tunnel"	0.00558558	CLalpha ref:length^2							
Fudge Factor based on Wash Cost ops	1.19	lift is reduced by this amount							
Effective Lift Coefficient	0.00469376		0.004694						
Lift from Tunnel data	**74653.44**	gms							
Lift Curve Slope from Eriksen Model	0.0030061	CE's a							
Lift Coefficient from Eriksen Model	0.0030061								
Fudge Factor based on VCT model	1.00								
Lift from Eriksen Model	**47811.49**	gms							
Lift Coefficient from VCT Info	**0.002711**								
Lift from VCT Info	**43122.63**	gms							
Total Lift	**43122.63**								
Body Drag									
Body Drag; theoretical	682.58	gms	Horiz	Vertical					
Fin Drag, 4 semi-spans	323.67	gms	205.540	118.132					
Body+Fin Drag ONLY	1006.25	gms, from theoretical							
Drag Coefficient from "Tunnel"	-0.0013165	ref: L^2	-0.0266	ref Vol^2/3	0.002331				
Fudge Factor based on Wash Cost ops	0.70	drag is multiplied by this amount							
Effective Drag Coefficient	-0.0009216								
Drag from Tunnel data	**-14657.60**	gms	-3.262						
Drag Coefficient from Eriksen Model	0.0098915	CE's b							
Fudge Factor based on VCT model	1.00	0.71	1.08						
Adjusted by FF above	0.0098915								
Drag from Eriksen Model	**23332.76**	gms	2.049114						
Drag Coefficient from VCT Info	**0.0015911**		**25306.89**						
Drag from VCT Info	**25306.89**	gms	1.703987						
Induced Drag									
Induced drag constant, k	55.0000								
Induced drag coefficient; theoretical	4.9867E-05								
Induced Drag from theoretical estimates	**793.12**	gms							
Induced Drag Coeff. From Eriksen Model	2.3614E-05	CE's c							
Drag from Eriksen Model, (included above)	**375.58**								
Total Drag	**23332.76**	gms	(Using VCT Coeff)						
Total Drag Coefficient	0.0015	reference: Length ^2							
Total Drag Coefficient	0.0297	reference: enclosed vol^.66		0.0009	barebody Cd				

Table 7.2_p3. Hydrodynamic Model (cont.)

Cd Theoretical	0.0072	curve fit from Autosub paper ref: vol^.66		-3.7113618		
Fudge Factor	1.43	was 2.0 x body only; Hubbard at 1.43				
Drag Coefficient, ref: Volume^.66	0.0103	Revised;Hubbard's Memo#2 Cd of 0.515 for 45l@50cm/s				
Lift/Drag Ratio	1.85					
Glide Angle	28.4	deg				
ERIKSEN INFO						
Q	2785.716	1.97955551	54041.91			
Total Velocity	10.294	m/s	1029.39	cm/s	4.042	kts
Total Velocity						
eriksen total force	53201.095					
VCT INFO						
Vel from VCT spreadsheet	48.800	cm/s	input direct from spreadsheet			
Glide Angle from VCT spreadsheet	35	degrees	input direct from spreadsheet			
Glide Angle from VCT using Drag/Lift	30.4	degrees				
Lift/Drag Ratio	1.70	ratio of Cl/Cd				
Glide Angle from VCT using Cd/Cl	30.4	degrees	gamma			
Pitch Angle	31.4	degrees	theta			
Qdynamic	22.50	gm/cm^2				
Velocity	208.0	cm/s				
u, horizontal velocity	179.3	cm/s				
w, vertical velocity	105.3	cm/s				
Pitch Moments						
Static moment from trim						
gamma	30.4069	pitch angle minus alpha				
for pure couple of CB to CG						
psi prime	#NAME?	angle of vcg to lcg from Trim				
x prime	#NAME?	straight line distance from CB to CG				
horizontal X1	#NAME?	horizontal component of x prime, cm				
moment about CB	#NAME?	gm cm				
for torque due to excess weight						
psi dbl prime	#NAME?	angle of vcg to hull centroid				
x dbl prime	#NAME?	straight line distance from VCG to hull centroid				
horizontal X2	#NAME?	horizontal component of x double prime, cm				
moment about CB due to THRUST	#NAME?	gm cm				
Dynamic moment from Hydro						
Pitch Moment, nondimensional	-0.0008	from !Hydro				
Pitch Moment, dimensional	-11109929	gm-cm				
Total Moment	**#NAME?**	**gm-cm**				

There are a total of 10 worksheets involving engineering calculations. Table 7.2 lists the first 2 worksheets among the following contained in the spreadsheet model:

1. Performance; the executive summary here most data is entered and results tabulated.

2. Hydro; originally included the wind tunnel model, supplanted by the Eriksen model, and finally built around the VCT model for glider performance.

3.Power; A summary of total energy needs per dive

4.VBD; The most reliable model due to Eriksen data analysis is used

5.ONR Trim; based on averages of the 3 legacy gliders, a reduced version of the Seaglider trim sheet invoking data from the other two legacy gliders

6.Data; data acquisition rates and sensors data quantity requirements

7. Tunnel; a database of original wind tunnel model data for the ½ scale Seaglider

8.Hull; separate but more sophisticated analysis as function of Factor of Safety

9.Battery; originally designed around the split primary cell pack used in the Seaglider, devolved to a single pack, de-rated to 77% for service temperature and historical seaglider experience relative to vendor data.

10. Piston Pump; A summary of UW, WRC, and Scripps experience in designing and building a single stroke piston using a mechanical lead screw, dynamic piston seals, a holding mechanism, and a position feedback sensor. Overall these systems seem to be only preferred in shallow water operation of more limited pump volume.

In addition there are 6 supporting data base worksheets:

a.Cal: where all glider specific calibrations can be kept

b. Seaglider Trim: a detailed 2 dimensional static trim and balance sheet

c. Antenna: a model to compute antenna height versus displaced volume

d. Material: a database of material properties

e. Cost-Part: a database of the last build of 5 Seagliders

f. Cost-Labor: a database of the last build of 5 Seagliders

The 6 plot matrix of range, number of dives, dive time, horizontal velocity(cross-country speed) net transport economy and thrust fraction, are also individual worksheets as part of the spreadsheet. In addition, model data from wind tunnel tests are also found under the Eriksen data base work sheets together with extensive field trials data.

8. Payloads, Navigation, Steering and Communication Systems (exerts from Clem et and Carroll, 2003 and Jones, 2003):

The analysis of surrogates for the functional classes is driven in large part by the size, weight, and power requirements of the payloads and sensors which the gliders must carry to perform in those classes. A suite of non-acoustic payloads and sensors was considered. These payloads and sensors were treated in 2 configurations: 1) As single payloads consisting of 1 dedicated sensor type and 2) bundled or mixed payloads consisting of combinations of multiple sensors. The single payloads represent minimal useful payload packages for bracketing the high speed, high endurance end of potential vehicle performance, whereas, the mixed payload packages represent heavy payloads for examining the high end of load carrying capacity and transport efficiency.

In the vein that data issues will replace vehicle concerns, an important consideration is the payload sections of gliders. Weight and its relative position, in an inherently balance-sensitive instrument such as a glider, takes great care in planning and design. Present legacy gliders have been designed around certain sensor payloads such as CTD, oxygen, and optical sensors. One recent advance is a modifiable payload section integrated in the center portion of a glider, giving the least amount of impact on the fore/aft balance and allowing for ease in expandability. This payload section is modular; and thus it is easy to swap in or out for recalibration or to change the sensor payloads dependant on the mission given. Present examples of payload sections are: BrevBuster (red tide detection), acoustic modem, Hydroscat 2, CTD, optical packages, hydrophone sampling, and various others. Mechanical modifications to the center hull are sometimes necessary to accommodate the new sensors with, for instance windows, yet costs are kept down by not requiring a full vehicle hull redesign. Other approaches have been to leave a faired wet area of the vehicle to allow for external addition of payload. These "wet" areas tend to be located in the ends of the gliders necessitating a greater constraint on balance issues.

Divided science/payload control architecture is preferable, set up in such a way that the science controller is separate from the flight controller. This may simply be a bus system or another control unit, although processor power considerations weigh in heavily. Software development is one of the leading costs of an AUV, and as a result of this architectural division science code can be modified without changing the main glider application. This reduces costs and allows for users to write their own application code without potentially

jeopardizing the health of the necessary flight control operations.

Payload consumption of energy is the major contributor to hotel loads and is always foremost in design considerations with an AUV, especially one where endurance is being maximized. There are choices about powering from the same bus or separate power sources. Either way energy must be considered as a component of the payload of the vehicle, and as the volume of the vehicle increase so must the drive force to maintain an optimal forward speed.

8.1 Non-Acoustic Sensors and Glider Applications:

Here our primary interest is non-acoustic sensors that can be considered for UW glider payloads for a variety of naval applications. The emphasis is on sensors with small size and ultra-low power requirements. Three classes of non-acoustic sensors are included: electro-magnetic sensors, optical sensors and chemical sensors. One or more sensors are included for each category. This section includes descriptions of selected sensors and identifies applications and modes of operation that provide enhancements to present Naval war fighting capability. The study initially investigates individual non-acoustic sensors but later combines one or more sensors with an acoustic sensor and other essential system support elements to define new system concepts that maximize UW glider capability for a given mission.

The discussion of each sensor class includes identification of the target phenomenon of interest for the most important naval applications, a description of the applicable non-acoustic sensor, a description of the application concept and identification of processing, navigation or communication equipment required to achieve mission performance. Applications that require precision navigation capability are identified as well as applications that require additional vehicle control beyond that of a basic glider.

In selected missions a glider may require added propulsion capability to overcome sea currents and tides for limited periods. In those cases the addition of small motor creating a hybrid "motorized" glider may be required to perform the mission. Missions where more complex vehicle control is required are identified. In applications where fine vehicle control is required over long periods, even hybrid gliders may not be suitable. In those applications gliders may be best employed to provide clandestine delivery of separate, fully motorized AUVs to shallow water regions. The AUVs could then be deployed to perform the final application phases of their mission.

Each sensor area is investigated to identify the types of sensors needed and to identify one or more application roles particularly in the littorals. Sensor configurations are described as well as the system architecture required to provide the Navy with useful information or to perform a useful task. Special operational requirements are identified as necessary. Furthermore, elements of data management are discussed and concepts, where onboard processing is feasible or necessary, are identified. Forms of the final product are identified as well as requirements and concepts for data transmission.

A limited number of Naval glider functional applications are in the deep-water regime. These include performing surveys to collect wide area environmental measurements and deep-water surface and sub-surface vessel sentry duties. The majority of glider sensor applications investigated in this study focus on applications in shallow waters in the near-shore littoral area. Broad areas of shallow water UW glider application investigations include: (1) glider delivery/deployment of re-configurable and recoverable sensor arrays (virtual station keeping); (2) shallow water glider surveillance and coastal patrol operation (depth limited roaming); and (3) glider clandestine payload delivery of swimmer delivery vehicles, mine hunting search and neutralization systems, and mine/torpedo/sapper deployment systems (payload delivery).

Five types of non-acoustic sensors were considered in combinations with inertial navigation systems and advanced 2-way communication systems and data links. The non-acoustic sensors include:

Passive magnetic sensors
Passive optic and electro-optic sensors
Electric field sensors
Active electromagnetic sensors
Chemical (Biochemical) sensors
Inertial navigation systems

8.1.1 Passive Magnetic Sensors: Passive magnetic sensors are used by the Navy to detect targets of interest such as surface vessels, submarines and sea/surf/land mines that are constructed of magnetic materials such as steel. These targets behave as bar magnets and generate detectable magnetic fields. Passive magnetic sensors can be used as fusing sensors for sea mines, when they are configured to detect the magnetic field of an approaching submarine or surface vessel. Furthermore, passive magnetic sensors that measure low frequency fields, typically less than 5 Hz, can be configured as stationary nodes in an underwater

barrier system to detect passage of submarines and surface craft. When configured properly, passive magnetic sensors can be used in a search mode to locate submarines or sea mines. For search applications the magnetic sensors typically transit the search area in a "mow the lawn" pattern by either an airplane or boat. Magnetic detection of targets by barriers or search modes is commonly referred to as magnetic anomaly detection. Stationary and search magnetic sensors can be constructed in multiple sensor array configurations measuring target magnetic field components and magnetic gradients and sensor outputs processed to provide precise target location and magnetic size. The target magnetic size can be used as a classification tool to distinguish targets from clutter (e.g., mine versus oil drum). Real time processing of magnetic sensor data for target location and size requires modest computational capability.Magnetic detection ranges vary with magnetic size of the target and sensitivity of the magnetic sensor. The range versus a particular target dictates the spacing of a barrier or the separation of search tracks. For state of the art sensors and large targets, detection ranges of a thousand feet or more are feasible. For smaller, mine-sized targets, the detection ranges are tens of feet but, importantly, magnetic sensors can detect mines that are buried below the sea bottom, a particularly plaguing problem in sea mine detection.

Primary magnetic sensor types are vector magnetometers, total-field magnetometers, and gradiometers synthesized from either of the two magnetometer types. Sensor selection will depend on mission, operational scenario, and glider capability. Candidate magnetic sensors are categorized for this study according to several important parameters including size, weight, power, functional use, detection range, and sensing fidelity.

Primary applications for magnetic sensors in low cost, power limited UW gliders typified by current glider prototypes should include (1) oceanographic and sea-bottom geologic environmental characterization, in a fixed-point or roaming mode, and (2) bottom nodes in distributed networks for monitoring surface and sub-surface sea traffic. Other applications for this baseline class of gliders include sentry, capitalizing on virtual station keeping in the water column, or perimeter patrol. Total-field magnetometers or vector magnetometers integrated into individual gliders are projected as the primary sensor classes for these applications. Higher performance sensors are desirable for the distributed network applications for traffic monitoring in order to keep the numbers of units down to a tractable number. Long-baseline gradiometer/array signal processing will be used in these applications in order to reduce temporal environmental noise that is coherent over the node spacing. With the exception of environment

characterization, computational capabilities typical of 386-to-586 PC processors will be required to manage the signal processing for all applications described in this and the next paragraph. Hence, the vehicle computers in the current baseline class of gliders will not be adequate to manage this payload signal processing on top of its primary vehicle functions.

Because of the limited range of magnetic sensors compared to acoustic sensors, upper end magnetometers and/or gradiometers are likely required on missions involving mobile target reconnaissance and surveillance. For example, ASW or minehunting are two such missions, where upper end magnetometers would be desirable. These types of missions would require more sophisticated gliders, which can provide precision navigation, high vehicle motion stability, and power budgets 50 to 100 times greater than payload energy budgets for the baseline class of gliders. In particular, hybrid (motorized) gliders, which have capabilities while under propulsion comparable to those of unmanned underwater vehicles, such as the Woods Hole Oceanographic Institute Remote Environmental Monitoring Unit System (REMUS) or the Bluefin Robotics Battlespace Preparation AUV (BPAUV), are likely required. Moreover, magnetic sensors can be used in a similar manner for fusing of gliding depth charges and other weapons.Several candidate magnetometers are shown in Figure 8.1a and gradiometers in Figure 8.2a. Size, weight, and power requirements of these magnetic sensors in addition to special isolation requirements are listed in the tables in Figures 8.1b and 8.2b.

The primary constraint in packing these magnetic sensors in the underwater glider is that they must be isolated from the other electrical and electronic systems needed for vehicle control, buoyancy pump operation, and communication and navigation systems, as shown schematically in Figure 8.3. In the case of winged-bodies-of-revolution these magnetic sensors need to be isolated in the nose or tail section of the body, separated from the external electronics by a distance of 35.75”. For measuring magnetic field gradients, sensor transducers must be separated by a minimum distance of 6.52” around the longitudinal axis of the body. In the case of flying wing geometries, these isolation and separation distances are easily satisfied by placing the sensor transducers in the outboard sections of the wing with the remaining external vehicle systems packed in the root section of the wing. In summary, the passive magnetic sensors require that the electronics be separated from the sense head, which increases the volume required for the magnetic sensor for glider application.

a)
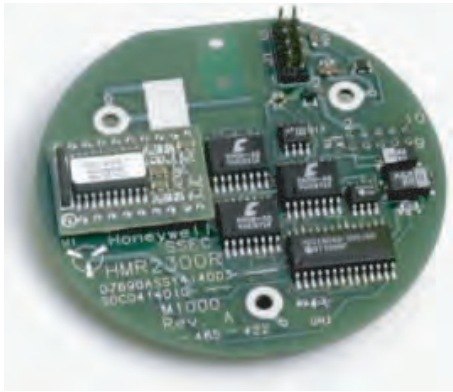
Axis Magnetoresistive
Vector Magnetometer
Honeywell Model HMR2300r

Single Channel Overhauser
Scalar Magnetometer
UW Tow Configuration
Marine Magnetics SeaSPY

Single Channel
Optically Pumped
Scalar Magnetometer
UW Tow Configuration
Geometrics Model G-880

b)

Technology	Power (Watts)	Sensor Weight Dimensions	Electronics Weight Dimensions	Sensor Electronics Separation	Functional Use Capability
Magnetoresistive Vector Magnetometer *Three-Channel Sensor* *Analog Output*	0.7	$S_w = 0.04$ kg D = 7 cm L = 1.3 cm	N/A Contained On Sensor Board)	13 cm	Geomagnetic Measurement Magnetic Anomaly Detection *Stationary Array* *Low to Moderate Detection Range*
Overhauser Scalar Magnetometer *Single-Channel Sensor* *Analog Output*	3	$S_w = 1.8$ kg L = 30 cm D = 8.3 cm	$E_w = 0.34$ kg 9 cm W = 5 cm H = 5 cm	75 cm	Geomagnetic Measurement Magnetic Anomaly Detection *Stationary Array or Very Slow Mobile Operation* *Applications requiring only Low Sample Rates* *Low-to-Moderate Detection Range* *Low Fidelity Classification/localization*
Optically-Pumped Scalar Magnetometer *Single-Channel Sensor* *Digital Output*	12	$S_w = 0.34$ kg L = 15 cm D = 6 cm	$E_w = 1.6$ kg L = 15 cm W = 8 cm H = 20 cm	50 cm	Geomagnetic Measurement Magnetic Anomaly Detection *Mobile Operation* *Moderate-to-High Detection Range* *Low Fidelity Classification/localization*

Figure 8.1. Candidate magnetometers for UW Gliders [from Clem et al, 2003].

a)
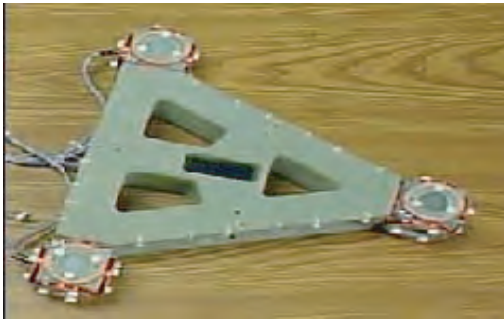
Realtime Tracking Gradiometer
(Quantum Magnetics - CSS)

Laser-Pumped He4 -Vapor
Scalar Gradiometer (Polatomic - CSS)

b)

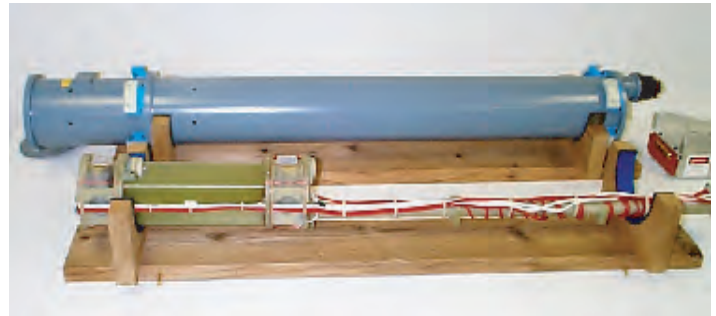| Technology	Power (Watts)	Sensor Weight Dimensions	Electronics Weight Dimensions	Sensor Electronics Separation	Functional Use Capability
Magnetoresistive Tensor Gradiometer *Five-Channel Sensor* *Digital Output*	0.5	S_w = 1.4 kg D = 30 cm L = 7 cm	E_w = 1.4 kg D = 30 cm L = 18 cm	30 cm	Magnetic Anomaly Detection *Mobile Operation* *Low Detection Range* *High Fidelity Classification/Localization*
Fluxgate Tensor Gradiometer *Five-Channel Sensor* *Digital Output*	30	S_w = 2.2 kg D = 30 cm L = 7 cm	E_w = 1.4 kg 30 cm L = 18 cm	48 cm	Magnetic Anomaly Detection *Mobile Operation* *Moderate Detection Range* *High Fidelity Classification/Localization*
Optically-Pumped Scalar Gradiometer *Three-Channel Sensor* *Digital Output*	19	S_w = 3.3 kg D = 30 cm L = 60 cm	E_w = 1.9 kg D = 30 cm L = 18 cm	58 cm	Magnetic Anomaly Detection *High Detection Range* *High Fidelity Classification/Localization*

Figure 8.2. Candidate gradiometers for UW gliders [from Clem, et al., 2003].
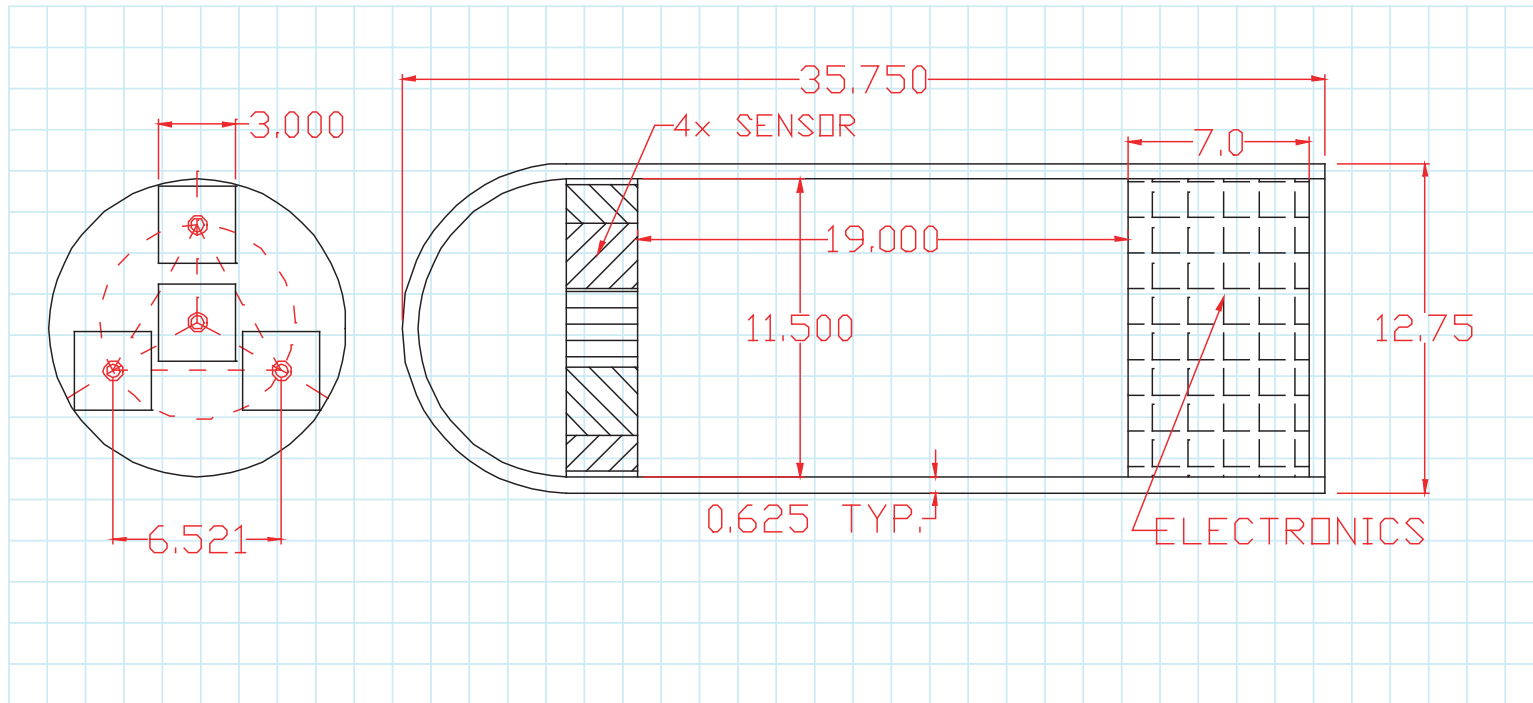
Figure 8.3. Magnetic sensor isolation [from Clem, et al., 2003].

8.1.2 Electric field Sensors: The U.S. Navy has demonstrated that electric field sensors can be used to detect surface and subsurface craft at distances on the order of hundreds of meters or greater. These detection ranges are short compared to acoustic detection ranges. However, shallow water conditions can cause acoustic environmental noise sources to increase, which deceases their effective detection range, so that alternative sensor detection ranges can be comparable or superior. Electric field sensors can serve as effective surface and subsurface vessel surveillance sensors under shallow water conditions and can be configured as a continuous, uninterrupted barrier. In shallow water surveillance application electric fields sensors are configured electrode pairs positioned stationary on the ocean bottom to detect the low frequency electric fields resulting from corrosion currents generated by the surface or subsurface craft. Corrosion currents are caused by electrochemical action between the dissimilar metals of the steel hull, the bronze screws/drive shaft, and the sacrificial zinc anodes of the vessel. The most prominent electric field signals from transiting vessels are the low frequency (0.001-0.01 Hz) signal from the vessel dc electric field moment as the vessel transits a site and the slightly higher frequency (8-20 Hz) field caused by the vessel shaft rotation that modulates the dc electric field. Ambient noise of electric fields is of the order of 10^{-9} volts/meter at low frequencies.

Compact low noise, e-field sensor systems have been developed and demonstrated that could form the basis of a shallow water e-field surveillance barrier sensor deployable using glider technology. Figure 8.4a shows a pair of Polyamp carbon fiber PA3001 electrodes and high performance signal amplifier module that are the building blocks of a robust, low noise E-field sensor array package. Figure 8.aa also shows a set of three electrode pairs configured as a three-axis E-field array that could be used with appropriate signal processing to determine characteristics of a detected vessel. Figure 8.4b lists the characteristics of the Polyamp electrode sensor and amplifier. A compact, multi-axis E-field sensor formed from these components could provide nanovolt/meter/root Hz performance in a 30 liter, 8-watt package.

A primary glider concept employing electric field sensors would be based on using gliders to clandestinely deploy a set of stationary, underwater e-field sensor systems in a barrier to detect the surface and subsurface ship traffic passing an area. The limited range of the e-field sensors would require a number of e-field sensor systems to provide complete barrier detection. Each glider would transit to a sensor deployment location and deploy an e-field system. The glider could transit to more than one location and deploy a multiple sensor barrier.

Pair of Polyamp carbon fiber
electrodes PA3001

UEP
Signal
Amplifier
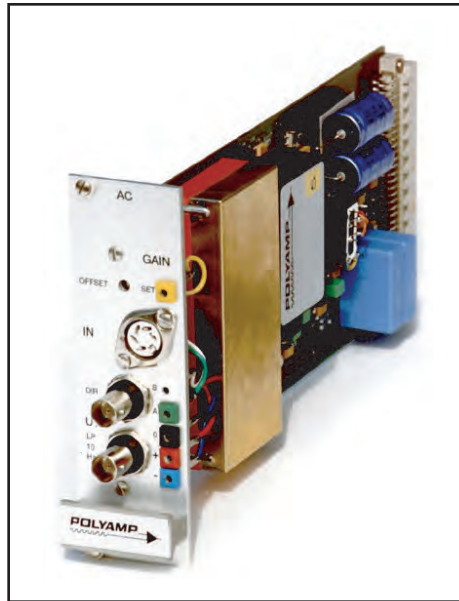
3 Axis E-Field Polyamp Platform

a)

b)

Type	Sensor Size (kg) (cm)	Power (Watts)	Sensitivity	Sensor Maturity
Carbon Fiber Electrodes	Electrode 0.150 Diam=5 Length=15; Electronics 1.0 Eurocassette 12 x 4.5 x 23.2	1.3 per electrode	< 2 nv/root Hz at 1-1000Hz, Typically 1 /root Hz	Mature

Figure 8.4. Candidate E-field sensors for UW gliders [from Carrol, et al., 2003].

Furthermore, the glider might loiter in the barrier area and serve as an acoustic communications link for several barrier sensors. Moreover, the glider could resurface periodically and RF link/report traffic results to remote command and control locations.

8.1.3 Active Electro-Magnetic Sensor: Active electromagnetic (EM) sensors, such as metal detectors, can be used to detect metallic/conducting objects buried below the surface on land or underwater. Active EM sensors generate low frequency EM fields using a set of drive coils. These fields induce eddy currents in a conducting object, which are detected using a second set of detection coils. Active EM drive coils and detection coils are typically coaxially collocated in the sensor head and detection ranges of 1-2 meters are common for operating frequencies of a few Hz. The low frequency EM field can penetrates the land or sea bottom and detects conducting targets buried beneath the ground or the sea bottom. The most basic types are pulse 8X metal detectors (Figure 8.5a).

More advanced active EM sensors, such as Geophex GEM-3, can measure the broadband spectrum of the secondary field from the detected object at several frequencies (8-30 Hz) and obtain a distinct spectral signature that may be used to uniquely identify the buried object. This concept is referred to as electromagnetic induction spectroscopy (EMIS). A GEM-3 system shown in Figure 8.5a has been used to demonstrate detection of unexploded ordnance (UXO) buried underwater in the harbor bottom at Mare Island in San Francisco Bay. The table in Figure 8.5b provides details of the size and power requirements for the J.W. Fisher Pulse 8X Sensor and the Geophex GEM-3 Sensor.

The system on the far right hand side of Figure 8.5a includes two GEM-3 sensors positioned at the bottom of poles separated by approximately 8 feet to expand the search width of the two-sensor system. Study of the in-phase and out-of-phase detected response of each sensor indicates that the EMIS method can reveal characteristics of the size and shape of the buried conducting objects, characteristics that can be used to identify the buried object as UXO or mine-like and significantly reduce the rate of false alarms.

New concepts are currently being investigated to assess the utility of using active EM sensors as a reacquisition and identification (R&I) sensor against buried sea mines. In one concept an autonomous underwater vehicle (AUV) with an acoustic low frequency sensor initially searches, detects and locates a suspected buried mine. Coordinates of the mine detection are communicated to a second AUV with an active EM sensor. The active EM sensor AUV transits to the

a)

Active EM Coils
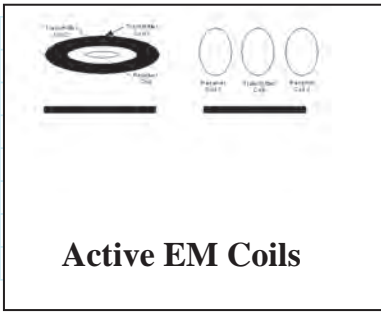
J.W. Fisher Pulse 8X Metal Detector

Geophex GEM-3 Sensors Configured for UW Search

b)

Type	Sensor Size (kg), (cm)	Electronics Size	Power (Watts)	Sensitivity	Sensor Maturity
J.W. Fisher Pulse 8X Metal Detector	3 kg (total); 45cm diam coil x 56cm		1.2	ppm	Mature
Geophex GEM-3 UW Detector 30Hz-24kHz	4 kg (total); 40cm diam coil; 11x25x5 46 cm long		Few (est.)	ppm	Mature

Figure 8.5. Candidate active EM sensors for UW gliders [from Carrol, et al., 2003].

coordinates of the detected, suspected buried mine and executes an R&I search. The R&I search requires that the AUV execute a parallel track search pattern with the AUV operating a few feet above the bottom. In this concept the output of the active EM sensor is processed on board the AUV and compared to a library of sea mine templates to confirm sea mine detection/identification. The processed results would be acoustically linked to an RF link to report mine detection coordinates to a remote command and control location.

The proposed application of active EM sensors as the primary sensor in a buried sea mine R&I operation would require that the sensor vehicle perform intricate search patterns and maneuvers that require a high degree of vehicle control. Sea gliders in their current configuration probably would not be the proper vehicle to perform detailed search patterns required for sea mine R&I. A more realistic alternative would be to use the glider to clandestinely deliver one or more self propelled AUVs (with active EM sensor package) to an area and have the AUV conduct the detailed R&I search.

8.1.4 Optical Sensors: Two types of optical sensors were investigated: (1) Cameras that operate above water for collecting images of the seaside activity and (2) optical devices designed to operate underwater to capture images of detected underwater objects (e.g., sea mines).

A survey of electro-optic (EO) imaging sensors was performed. Electro-optic sensors, which could be useful to Naval missions in the littoral area and could be deployed from an UW glider, were investigated. Several classes of EO imaging sensors were considered and it quickly became clear that several classes have common features of small size, low mass and low energy consumption that are attractive for an UW glider payload.

One EO imaging concept that emerged was that of an UW glider with an EO sensor package that would transit clandestinely from over the horizon and perform coastal patrol surveys in selected littoral areas. The EO sensors would be used to gather images of enemy forces ashore including placement of defensive equipment and force activity and provide vital near real-time intelligence, reconnaissance and surveillance (IRS) information via satellite to a remote U.S. command. Of particular importance, the glider could be remotely commanded to loiter in a given area with high or important activity and provide continuous, uninterrupted images of the unfolding enemy activity.

Electro-optic imaging sensors that were considered included: a color digital camera; a bank of two/three CCD cameras with narrow band filters; a 3-CCD

a)

Supercircuit
PC-104C CCD
Monochrome Video
Camera

Panasonic GP-US522
3-CCD Color Camera with DSP

Indigo MERLIN
Microbolometer Imager

b)

CAMERA	WEIGHT (kg)	SIZE (cm)	POWER (Watts)	USAGE
Monochromatic CCD Camera	**1.0**	L = 5.0 W = 5 D = 2.5	1.4	Narrow Band Filtered Images
3-CCD Color Camera	1.73	L = 6.5 Dm = 2 L = 20 W = 4 D = 25	3	Color Image
320 x 240 Focal Plane Array IR Microbolometer 8-12 microns	1.6	L = 10 W = 11 D = 20	1.5	Thermal Imager 12° x 9° Field of View

Figure 8.6. Candidate above-water optical surveillance cameras for UW gliders [from Carrol, et al., 2003].

color camera with individual outputs; and an infrared imager. Figure 8.6a shows examples of a CCD monochromatic camera, a 3-CCD color camera and an IR imager. The table in 8.6b shows the size and power characteristics of three of the EO imaging cameras. All are small, compact and low power.

The choice of the optimal cameras/imager package would depend on image resolution requirements and size of the imager package. The coastal patrol surveillance mission will require that the EO sensor(s) be positioned well above the average wave height (assume ~ 6 feet) to provide clear visibility to the shore. One concept would have the camera imager or lens at the end of a slender mast that is deployed vertically above the glider, when the glider is on the surface. The imager lens would be positioned to point toward the shore as the glider moves parallel to the shore. The imager would take single frame images that could be temporarily stored on a hard disk or flash memory card until the image is RF transmitted to a remote U.S. command.

At present it would seem desirable to include two imagers, one camera and one IR imager to provide total 24-hour image coverage. However, this sensor packaging may present complications in the mast camera design. One solution for the camera is to place the imaging lens on the mast and then transfer the image to an onboard CCD through a fiber optic cable. However, this approach may not be feasible for an IR imager. System design studies would be required to resolve this important design issue as well as additional factors such as mast motion

8.1.5 Underwater Passive Optic and Electro-optic Sensors: Passive and active optic and electro-optic sensors were investigated to consider sensors that could be useful to the Navy for underwater target identification. Representative sensors considered included an environmental sensor, several cameras and two active electro-optic imaging sensors shown in Figures 8.7a and b with characteristics listed in the table in Figure 8.7c.

The C-Star transmissometers shown in Figure 8.7a are compact environmental sensors that measure the optical properties (e.g., water clarity) during area surveys. The water clarity is an important indicator of the water visibility and the imaging range of underwater cameras and imaging sensors. Imaging ranges for cameras (passive sensors) vary from fractions of a meter to several meters as a function of the water clarity and turbidity. Often, clarity decreases and turbidity increases in shallow water and surf zone areas, environments where Navy targets of interest are located, such as sea mines. Figure 8.7a also shows a CCD Camera and underwater light kit that can be

a)

**C-Star
Transmissometers**

**BENTHOS
4200 CCD CAMERA**

ULK-2
UNDERWATER LIGHT KIT

b)
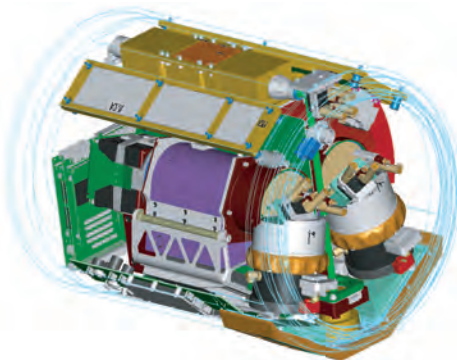
**15.5" dia, 19.5" long
154 lbs weight (sensor + shell)
762 watts power (max)**
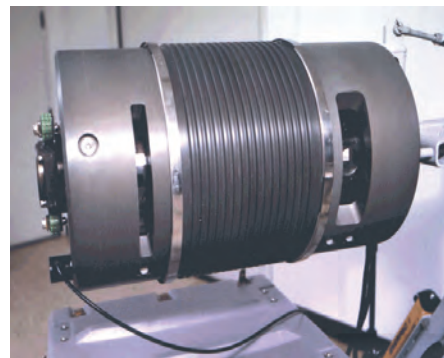
**28 in. Long, 16.5 Diameter
110 kg
< 250 W Power (typical)**

c)

CAMERA	WEIGHT (kg)	SIZE (cm)	POWER (Watts)	USAGE
Transmissometer	4.4	L = 49.5 D = 32	0.4	Measurement of Water Quality
CCD	9.7	L = 25.4 D = 9	3	High Light Level Clear/Moderate Water Clarity
ICCD	11	L = 33 D = 10	10 -12 W	Low Light Level Clear/Moderate Water Clarity
Underwater Light Source			16 AA batteries	For Usage when Visibility Is Greater than 10 Feet
Laser Line Scanner (LLS)	110	L = 50.4 D = 48.3	100 W	Minimum of 10 -Ft Range Range of 5 Attenuation Lengths
Sreak Tube Imaging LIDAR (STIL)	339	L = 45.7 D = 40.6	762 W	Comparable to LLS

Figure 8.7. Candidate sub-surface camers and laser imaging devices for UW gliders [from Clem, et al., 2003].

employed in a short range search for underwater targets. The light kit is useful to extend camera searches to night operations. The active electro-optic sensors shown in Figure 8.7b are more complex sensors that employ laser sources with gating and scanning techniques to extend the imaging range of the sensor. Employing techniques that reduce backscatter, the active sensors can extend target imaging ranges by factors of 5-10 beyond those of passive EO sensors. Under limiting water clarity conditions active EO sensors can provide images for target identification not feasible with simpler passive cameras.

All UW optical imaging sensors have a very limited range and are primarily candidates for target identification missions. Presently, only the environmental sensor and the smaller cameras are consistent with any feasible glider sensor package. The active EO sensors are presently too large, too power consuming and too costly to be considered viable glider sensor candidates. Currently, camera sensors are available at hundreds or few thousand dollars whereas the active EO sensors are several hundred thousand dollar systems.

8.1.6 Chemical Sensors: There are a variety of chemical sensors with size and power requirements low enough to be considered for deployment on a glider. The main contenders are optical and electrochemical sensors. Gas chromatography with electron capture detection is also a possibility for a select number of compounds.

The prime application using chemical sensors in gliders would be in ASW and/or surface ship patrol and/or detection. In this application the glider would perform fixed point or roaming detection of submarine or surface craft affluence. In the roaming mode the glider/chemical detector would move through the affluence and once detected could trail the detected target. This concept would likely require a hybrid glider with some minimum ability to control the glider direction after detection.

The identification of the most useful detectable target affluence would require additional analysis. The range of chemical sensors identified below indicates, that there are a wide variety of candidate target affluence types ,which could be detected.

Figure 8.8a shows three candidate chemical sensors for glider application, that come in compact forms. The electrochemical sensor, shown in schematic form, can be instantiated in two forms of interest: (1) an electrochemical sensor with ion selective electrodes that detects chloride, fluoride, potassium and phosphate and (2) a polarographic sensor that detects transition metal ions,

a)

Diagram of the In Situ Sensor

Electrochemical Sensor

SEAS-1 Spectrophotometer

MEMS-based GC Sensor

b)

Type	Phenomenon	Key Components	Size/Power
Ion Selective Electrode	Selective uptake of ions through barrier; Measure potential due to charge separation	Electrode, Membrane or barrier	Few square inches; < 1 Watt
Polarography	Analyte oxidation causes observable voltage plateau	Electrodes	Few square inches; < 1 Watt
Spectro-photometer	Reduction in photodiode output	Electrodes, lamp, pump	11cm dia; 46cm long; Lamp/diode array 1-2 Watts; Pump ~ 10 Watt
Gas Chromatography	Differences in adsorption of analytes in coated column - > to characteristic peaks	Sample column, MEMS electrodes, gas cartridge	Wafer 5x5cm; < 1 Watts

c)

Type	Sensor Size (kg), (cm)	Electronics Size	Power (Watts)	Sensitivity	Sensor Maturity
Electro-chemical	< 1 kg; 5cm x 5cm		~1	~ 1 ppm	Mature
Spectro-photometry	2.7 kg; 11cm diameter; 46 cm long		~6	~0.5 nmol	Mature
Gas Chromotography (GC)	3.6 kg; 20cm x 13cm x 8 cm		24	35 ppb	P'type
UW Mass Spectrometer	38 kg Dia = 19 L = 125	N/A	95	Few ppb	P'type

Figure 8.8. Candidate chemical sensors for UW gliders [from Carrol, et al., 2003].

oxygen, hydrogen and CO. The spectrophotometer (SEAS-1) detects inorganic analytes (Fe^{2+}, PO_4^{3-}, Ni, Cd, Cu, NH_3, Mn, NO_2^-, NO_3^-). The gas chromatogram (MEMS-based) primarily detects explosives, fluorocarbons and solvents. Further analysis would be required to determine the most useful chemical sensor.

The table in Figure 8.8c lists details on the size and power requirements of four different classes of chemical sensors that are candidates for glider application. Two of the sensors, the electrochemical and spectrophotometry sensors, are developed in mature forms. The gas chromatography and mass spectrometer fig 8.8 sensors are presently developed in prototype form. The prototype sensors are substantially larger and require more power than the electrochemical and spectrophotometry sensors. The costs for most of the chemical sensors are in the range of a few thousand dollars. Furthermore, when fully developed, the mass spectrometer could still be several times the cost of the others.

8.2   Navigation Sensors

Currently, existing glider systems, Seaglider and Slocum Glider, navigate by dead reckoning between GPS navigation fixes. The Seaglider navigation system employs a Precision Navigation, Inc. Model TCM2-80 attitude sensor package and a Garmin 25HVS GPS receiver to measure its position and control the vehicle dynamics during dive cycles. Glider navigation to a new position multiple miles ahead is accomplished by dead reckon navigation toward the final objective position on each dive cycle. GPS glider position data is updated after each dive cycle and glider heading is adjusted to guide the glider toward the next interim waypoint. Thus, glider position is corrected during each dive cycle to achieve navigation to the final destination point.

A number of the proposed naval glider applications do not require navigation to precise locations but rather navigation to a point in the vicinity of a desired location. For example, a glider that is transporting sensors or AUVs payloads to a given area may be required to deliver them to the specific area but the precise sensor location is not important. For example, a barrier sensor could determine its actual location after deployment with GPS. A glider performing a coastal patrol likely does not need to know its location beyond GPS accuracy of the glider at the time that an imaging sensor collected its image. In these applications, the existing glider navigation systems would likely provide sufficient vehicle position accuracy.

Figure 8.9. The iXSEA U-phin Inertial Navigation System

Figure 8.10. Kearfott 6050 Inertial Navigation System

Other glider applications may require higher vehicle position accuracy. Selected search applications require increased navigation accuracy if the vehicle is not able to take periodic GPS fixes during a search pattern. Higher navigation accuracy can be achieved employing inertial navigation systems (INS).

A study was conducted to identify candidate INS for glider applications. Figures 8.9 and 8.10 show the iXSEA U-phin and Kearfott 6050 units, which are two of the smaller, compact INS systems. Inertial navigation systems investigated are listed in Table 8.1 and include data on the size, weight, power consumption, and navigational accuracy of the INS units The iXSEA U-phin appears to be the most attractive unit for glider applications that require INS. It is compact, low mass and has a competitive navigational accuracy. Moreover, the iXSEA U-phin has the lowest power consumption rating, a premium on gliders. INS units in Table 8.2 generally cost 12-15K except Navigator - 75K.

8.3 Payload Packages

Here we consider using single payload packages or combinations of sensors that could be bundled together to provide functional class applications as listed in Sections 5.1 through 5.5. Several factors must be considered:

It is likely that the upper end sensors are not particularly compatible with glider applications such as ASW or MCM search missions. Several factors contribute to this assessment. Upper end sensors typically require relatively high power by glider standards (in excess of 10W for passive sensors, 50W for active sensors. Dedicated searches may require tempos exceeding glider capabilities. Level flight is desired to avoid complex motion compensation. Upper end INS are required for precise target localization.

Hybrid "motorized" UW gliders may provide one cost effective exception to this general rule. During ASW or MCM search missions UW gliders can glide to and from operational areas and run under power during primary search operation.

All glider sensor applications require data storage during the mission. Applications that require storing multiple images have the greatest storage requirements. Images can be temporarily stored on a hard disk or flash memory card until the image is RF transmitted to a remote U.S. Command.

In regards to the data storage burden cited above, adaptive sampling can limit the proliferation of data and raise its information quality. Adaptive sampling

INS	Power (Watts)	Weight (kg)	Dimensions (cm)	Position Accuracy
Kearfott KN-5051	35	35	18 X 18 X 28	20 meters/hr CEPR
Kearfott KN-5053	35	44	18 X 18 X 28	3 meters/hr CEPR
iXSEA U-phins	12	39	L = 20 D = 19	< 3m/hr
Kearfott KN-6051	50	125	L = 46 D = 23	0.5% distance traveled
Kearfott KN-6053	50	130	L = 46 D = 23	0.05% distance traveled
Cornerstone Navigator	60	22	14 X 16 X 18	0.3 % distance traveled

Table 8.1. Candidate high fidelity INS's for UW Gliders [from Clem et al, 2003].

is the key of targeted data collection using a number of influences to direct resources. This is done presently on the human scale where resources are allocated, moved, and redirected based on a set of criteria that is being optimized. The goal is to move that to an automated network that makes intelligent decisions such as a Bayesian Network System. Three approaches seem promising:

A)Vehicle Internal: Internal adaptive sampling for gliders involves a predetermined known target value that the internal glider sensors seek. The mission adapts its flight commands depending on the sensor inputs relating to the field structure and characteristics. The functionality of way points, inflection depth, and dive angle can be modified to follow a warm water eddy for example, or to learn the thermocline limits and fly above or below it. Here the science/payload processor can change mission parameters and feed them to the flight controller, within the allowable flight constraints.

B)Vehicle external: In this case the glider adaptively follows an area of interest and may call on other gliders in the vicinity for cooperation so that the requisite field structure is covered. However, the source of adaptive parameters is external to the glider and may come from satellite imaging, acoustic sound sources or user command-center. The Command/Control Center becomes the postmaster, collecting and delivering mission parameter letters that are posted by other agents.

C)Inter-vehicle sampling: Inter-vehicle sampling comes into play if gliders are capable of two-way communication with each other. In this case, one glider in a region of interest is capable of calling gliders in the vicinity and commanding their positions, flight patterns, waypoints or sampling criteria. Work is being done to model these dynamics based on group behaviors seen in fish activity, and inter-vehicle communications are considered in Section 8.5 below.

Tables 8.2 through 8.4 below summarize potential Naval applications using underwater gliders, classified under the functional classes: Depth Unlimited Roaming, Depth Limited Roaming, Virtual Station Keeping, and Payload Delivery. One or more potential sensor suites are identified for each individual mission. This information along with the information in Section 8.1 on the individual sensors may be used to guide future development of system concepts for Naval application. The following are some specific examples assembled from these payload package tables:

A) *Basic Sentry or Recon Package:*

    Overhauser Magnetic Sensor

    X SEA U-phins INS Package

        Magnetic Sensor (including electronics):

        Volume - 2100 cc (2.1 liters);

        Weight (Mass) – 2.14 kg;

        Power Required - ~ 3 watts

    INS Package

        Volume – 5670 cc (5.7 liters);

        Weight (mass) – 39 kg;

        Power Req – 12 Watts

    Totals for Basic Package:

        Volume – 7.8 liters

        Weight – 41 kg

        Power – 15 watts

	Depth Unlimited Roaming	
Concept/Mode	Deep Water Sentry ASW Target Detection	Research Platform Environmental Sensor
Prime Glider Mode/Capability	Conduct ASW Search of general area; Some direction control required	Glide into general area Perform environmental measurements
Hybrid	Need	Need
Magnetic	Gradiometer- ASW localization/ID	
Active EM		
E-Field		
Chemical	Need -TBD	
E/O ID		
E/O Camera		
Other Sensor	Active Acoustic	Environmental
INS	No	No
Coms	RF Coms	RF Coms

Table 8.2. Depth Unlimited Roaming Payload Packages

B) Enhanced Sentry Package

Add an Above Water Optics Package:

3 CCD Camera

Volume – 2.0 liters;

Weight – 1.7 kg;

Power – 3 Watts

IR Sensor (320 x 240 Focal Plane Array)

Volume – 2.2 liters

Weight – 1.6 kg

Power – 1.5 watts

Fiber optic antenna (est)

Volume – 1 liter

Weight - < 1 kg

Power – NA

Add an ASW Sonar for Submarine Detection (Augment ASW Sentry)

Depth Limited Roaming					
Concept/Mode	Shallow Water ASW Patrol	Shallow Water ASW Barrier	Round -Trip Coastal Patrol/Snooper	MCM Survey	Mine Neutralization
Prime Glider Mode/Capability	Glide to Choke Point or Search General Area; control required	Glide to Barrier location; Position on bottom	Conduct Patrol of general area; direction control required	Conduct MCM Search of general area; direction control required	Glide to MCM Search Area; fine direction control required beyond hybrid
Hybrid	Need	Need	Need	Need	Need
Magnetic	Gradiometer - ASW localization/ID	Gradiometer - ASW localization/ID		ID – Buried Mines	Gradiom - local/ID
Active EM				ID - Buried Mines	
E -Field		E-Field Array			
Chemical	Need - TBD				
E /O ID				ID – Proud/Buried Mines	
E /O Camera			Above Water - Color and IR		
Other Sensor	Active Acoustic	Passive Acoustic	Active/Passive Acoustic	Active/Passive Acoustic SSS/SAS, DIDSON	Deliver Crawlers
INS	Yes	Yes	No	Yes	Yes
Coms	RF Coms	RF Coms	Buoy Mode/RF Coms	Buoy Mode/RF Coms	RF Coms

Table 8.3. Depth Limited Roaming Packages

	Virtual Station Keeping		Payload Delivery	
Concept/Mode	Barrier/Array Multiple Gliders	Trip Wire Sentry	Long Range Clandestine Delivery	
Prime Glider Mode/Capability	Glide to general area; Anchor at selected position; direction control required	Glide into general area	Glide to general MCM search area; Deploy AUVs; direction control required	Glide to ASW Patrol or Barrier area; deploy AUVs or barrier arrays; direction control
Hybrid	Need	Need	Need	Need
Magnetic	Gradiometer- ASW localization/ID		ID – Buried Mines	Gradiometer- ASW localization/ID
Active EM			ID – Buried Mines	
E-Field	ASW Detection			E-Field Array
Chemical	Need - TBD			Need - TBD
E/O ID			ID – Proud/Buried Mines	
E/O Camera	Above Water - IR			
Other Sensor	Up Looking Sonar	Trip Wire??	SSS, SAS, DIDSON	Passive Acoustic
INS	No	No	No	No
Coms	Buoy Mode/RF Coms	Buoy Mode/RF Coms	RF Coms	RF Coms

Table 8.4 Virtual Station Keeping & Payload Delivery Packages

C) Sanitization Package "The Bus"

For larger payload packages we consider multiple REMUS AUVs for conducting coordinated MCM surveys missions. Each AUV is self-contained from a power requirement point of view. Current REMUS AUVs specifications are:

Volume ~ 45.6 liters
Weight ~ 36.3 kg

Currently two REMUS AUVs are required to perform MCM detection and identification by operating as a coordinated survey search pair. One REMUS operates a Klein Side Scan Sonar (5400) and CAD/CAC HW/SW and performs mine detection and a second REMUS operates a DIDSON forward looking imaging sonar conducting coordinated reacquisition and mine identification. Search and ID of ~ 1.9 nmi^2 or 6.27 km^2 areas could be achieved by each REMUS

AUV pair: Volume: ~ 90 liters; Weight ~ 73 kg. This would require a payload of 2x the standard 50 liter package.

Area MCM search rates could be increased by increasing the glider payload in multiples of 90 liters and 73 kg. A 10x glider payload could carry and deploy 5 REMUS AUV pairs; a 100x glider payload could carry and deploy 50 REMUS AUV pairs. The above estimates do not include the acoustic/RF link buoy. The buoy is equivalent in size to one REMUS AUV pair of vehicles. However one buoy could service multiple pairs of REMUS AUVs.

8.4 Control Systems:

Steering and attitude techniques being used are internal weight shift, controlled external planes, and realizing symbiotic simultaneously adjusted pitch with buoyancy drive. All of the early gliders accomplished steering through a radial mass shifter (usually some subset of the batteries) to roll the vehicle to induce a turn. Depending on wing placement, the flow acts on different surfaces resulting in steering control. If the wings are placed far aft on the glider, then in descent the glider's port wing is dropped so that lift on the wing drives the stern to port, overcoming lift off the tail fin (vertical stabilizer), and realizes a turn to starboard. In ascent, the opposite is true, the starboard wing is dropped to turn to starboard. Hydrodynamic lift on the side-slipping hull produces the centripetal force to curve the course. If the wings are placed closer to the middle of the glider the lift force is realized on the tail fin of the glider. In descent, to turn to starboard the starboard wing is dropped and the lift force on the tail fin results in a starboard side turn of the glider and the opposite for the ascent. An advantage of the internal mass shift steering is that there are no external moving parts. The turning radius is on average 25 meters and having to change roll at each inflection causes some counter steering force. This is typically not an issue where there is a great water depth and inflections are infrequent, and turning quickly is of no great advantage.

In shallow water, however, where the glider is inflecting frequently and it is important to recover heading after surface communication a tail fin control surface as a rudder gives the benefit of no counter steering during inflections, a turning radius reduced to 7 meters, and the capability to remain level in flight. Level flight is important to some optical sensors and to the altimeter used for bottom avoidance and bathymetry measurements.

Glider pitch is achieved also by using a mass shifter. This mass can be either the same mass used for steering change or a mechanism of two separate masses for pitch and roll. Some gliders are designed so that the major pitch change is symbiotically achieved by the already necessary buoyancy drive change for inflections thus maximizing on energy conservation. A pitch vernier adjust, the mass shifter, is still necessary for fine-tuning yet the movement (energy) needed is greatly reduced.

8.5 Communications Systems (excerpts from Berry, 2003, and Jones, 2003)

Bi-directional communication is a vital element in the operation of an autonomous platform. The goals are to provide command/control and to have near real time data available to the user. Gliders as drag sensitive buoyancy driven instruments have limited surface expression at the surface. There are a variety of methods to raise an antenna out of the water including a supplemental air bladder to increase buoyancy, careful surface pitch control, a variety of stings or booms to lift out the least amount of volume, and rotating the vehicle to expose a wing section outfitted with the antenna elements. A significant effort has been to develop pressure and waterproof antennas to accommodate the various communication systems. In all cases, the gliders initiate the communication when surfaced for the a radio frequency system, the underwater acoustic systems can be initiated either by the vehicle or the host.

8.5.1 Communications Systems Tested in Buoys, Drifters and Underwater Gliders:

RF modem: Line of sight 900 MHz and 2.4 GHz spread spectrum modems have provided a local high-speed communication link at 5700 bytes/sec and 3 J/Mbyte. Range limits are determined by antenna height and wave shadowing of the glider antenna can be a problem. Airborne repeaters have been successfully demonstrated.

ARGOS: This 401 MHz satellite system has a very small bandwidth of .1 bytes/sec, yet is a robust proven communication system that is used for recovery situations reporting GPS position when available. The ARGOS service is also capable of using Doppler to provide its own position after post processing. Due to non bi-directionalality of the traditional ARGOS satellites the messages cannot be

acknowledged as having been received, the vehicle is transmitting for a number of hours at the surface to catch satellite passes, and no commands can be sent to the vehicle - thus the energy cost is high at 3,250 J/Kbyte and this is not considered a command/control communication path.

Note, however, just online is a new ARGOS satellite operating at 401 and 466 MHz with the capability of bi-directional higher speed communications and it will have to be seen how this plays in the future. The constellation of the low earth orbit (LEO) satellites will be sparse resulting in data packet transfers rather than real-time communication.

Iridium: Out of bankruptcy this 1625 MHz US military supported satellite system has worldwide coverage linking at 180 bytes/sec and 30 J/Kbyte. This is the primary communication path for two of the three legacy gliders as it is a large constellation real-time direct modem link or an internet link depending on the user setup.

Orbcomm: Operating at 137 and 148 MHz this LEO system is used by one of the legacy gliders as a fairly low data rate .5 bytes/sec and 400 J/Kbyte data packet transfer.

Globalstar: A geostationary satellite system operating at 1610 and 2484 MHz, it is a direct modem link but only operational in spot zones particularly targeted to the US and Caribbean area. There are financial long term concerns about its viability.

Cellular: Real-time communication at 450 bytes/sec and 26 J/Kbyte, but with the obvious coverage limitations and the non-control of power settings. The cellular host side towers are capable of selecting between three handset power levels to gate system noise and activity, thus during high activity cellular usage times being in the wave shadowed fringe may result in no connects.

Acoustic Modem: Incorporating an acoustic modem in a glider allows for connectivity with other gliders, underwater networks or the Command Center. The acoustic link is a low bandwidth method 300 bytes/sec with varying power levels of wireless underwater communication. Gateway functionality has been demonstrated where the glider either ferries information between above sea

centers to undersea nodes or sits on the surface and is able to communicate with both simultaneously providing a conduit.

8.5.2 Communications Systems Trade Space (excerpts from Berry, 2003)

Selection of communications package for autonomous gliders involves a complex trade space that includes the specific glider mission and sensor package. Glider technology is very attractive across the following factors used to assess surveillance system concepts:

- · Operating Depth
- · Deployment Duration/ Sustainability
- · Deployment Observability
- · Operational Observability
- · Cost

The glider technology is also attractive for missions that require modest speed deployment to operational area, modest mobility, and modest re-locatability.

The communications package should fit with the mission niches that the glider is likely to occupy. In general, a number of different communications packages may required to meet some or all of the following attributes matched to the glider mission niches:

- · Communications with glider at depth vs. surfaced glider comms
  - o Some missions may be best accomplished by immediate reporting of events of interest. Reporting while glider is still at depth could be attractive.
  - o Some missions may require low observability. Exposure of the glider for communications purposes may pose risk that can be countered by communications at depth
- · Low power communications to enhance deployment duration. (Intermittent vs. continuous comms, low vs. high bandwidth)
  - o Gliders are very attractive based on their low power operation and resulting long duration. Communications must be tailored to missions to minimize power consumption.
  - o Intermittent, low bandwidth (data rate), and low power communications from a glider is most attractive to minimize power requirements.
  - o Continuous communications requires both communications at depth and significant power expenditure.

- o High bandwidth continuous communications requires more power and/or a more complex directional antenna system
- · Low observable communications
  - o Exposure of the glider for communications purposes may pose risk that can be countered by communications at depth, movement of the glider to a separate communications terminal, or deployment of a separate communications package
- · Low cost communications
  - o Gliders can be attractive for some missions simply due to their low cost. Gliders can be a cost-effective way to continuously deploy and provide long-term surveillance based on a small per unit cost relative to long term fixed surveillance concepts.
  - o Communications costs per glider need to be small. A low cost per glider communications package could be supplemented with a central communications glider or buoy to cost effectively provide communications at the glider "field" or "swarm" level.

8.5.3 Evaluation of Current Approaches

The current generation of Glider technology uses low data rate (2.4-9.6 kbps) satellite technology (such as Iridium or Globalstar) for its 2-way data link. LEO satellites already optimize power requirements due to low earth orbit constellation and low bandwidth. LEOs occupy the niche market choice for low data rate, low power communication. Configurations have been customed-developed to simultaneously use multiple Iridium or Globalstar phones to increase bandwidth. Power consumption and available bit rate are directly proportional to the number of phones used. A single commercial system < 1 pound, ~ 1/2 liter with battery can provide 2 or more hours air time. Custom designs have achieved greater size, weight, and power performance envelopes.

Inmarsat options, while time-tested and reliable for remote or marine-based communications, also provide 2.4 kbps and higher data for 2+ hours in portable configurations. Inmarsat is less attractive for the same reasons as other military higher earth orbit satellites. Inmarsat requires larger size, greater weight, a directional antenna, and more power. The smallest commercial, self-contained INMARSAT portables are about 3L volume, 2.2. kg, consume 20W for data transmit and have a manually stabilized directional antenna. Inmarsat also offers

more expensive, higher data rate options with larger antenna and power requirements. The antenna is flat, but substantial and requires manual pointing towards the satellite (7X28X37cm terminal and 37X77X1.2cm antenna). The system weighs only 3.9 kg. A variety of INMARSAT options exist, but the units are expensive (low $1000's), high data rate service is expensive ($6-$11/min for 64 kbps data), and units are relatively bulky.

Global LEO delivery of voice and data does not have a successful history considering the number of satellites required for LEO coverage and current financial status of companies such as Globalstar, Iridium, and Teledesic. Other location specific phone services maybe appropriate for glider deployment. Thuraya (geosynchronous) for the Mediterranean and Middle East claims commercial data rates of 9.6 kbps in a handheld size system (220 grams) with 2-4 hours of talk time (and integrated GPS). Thuraya handsets switch between local (GSM) cellular and satellite depending on coverage. Other local satellite solutions are available in the "littorals" of other regions of interest.

Clusters of multiple satellite phones can be used to achieve bandwidths in the 19.2-76.8 kbps range for an 8 phone configuration. Glider communications on commercial LEOs is attractive for achieving communications under the following system and mission constraints:
- Surfaced glider with broached antenna
- Low power, intermittent, on-demand communications
- Low bandwidth (<9.6 kbps per "phone")
- Modest cost ($3.00/min Iridium or less)
- Communications cost per glider is modest at ($ hundreds), not quite at the disposable level.

For time critical communications, communications at depth, or low observable communications; Gliders may also consider disposable comms packages that consist of a launched comms device (modified portable phone) to the surface.

8.5.4 Increasing Data Rate: Satellite Communications Options:

Higher data rates may be achievable in specific locations with specific LEO, MEO or GEO satellite constellations. However, as owners of DirecTV or DirecPC know, higher bandwidth 2-way asymmetric communication is possible but requires highly directional antennas with precise alignment requirements.

Upgrading satellite communications to higher rates (and likely utilizing medium earth orbit (MEO) or geostationary orbit (GEO) satellites) typically requires increased power and a larger, directional antenna with stabilization. More power or large aperture solutions are not consistent with many of the Glider mission niches and capabilities.

For example, global coverage commercial marine satellite systems considered to be "breakthrough" in size for shipboard use include Harris Corporation's Shipboard Very Small Aperture Terminal (VSAT) that require 1 rack of satellite equipment and a 4+ foot stabilized antenna delivers 512 kbps downlink and 256 kbps uplink in C-band. High data rate shipboard military satellite communications systems use the Defense Satellite Communications System (DSCS) backbone of Super High Frequency (SHF) satellites in geosynchronous orbit. These systems, currently in use by the Navy, use a 3-foot antenna to achieve 64-128 kbps. Seven-foot antenna systems achieve up to 2048 kbps. The submarine service is in the process of upgrading its satellite communications capabilities. Submarines share common engineering issues with Gliders in the desire for small size. The submarine high data rate antenna (SubHDR) is a 16-inch satellite antenna that extends on a mast to support multiple band (EHF, SHF, and commercial band) satellite communications in the 128 to 256 kbps range.

Using direct Glider to satellite communications at increased data rate is unattractive for Gliders due to the aperture and power requirements for typical MEO and GEO satellite constellations. Clusters of LEO or GEO satellite phones can achieve a significant fraction of data rates achievable by VSAT alternatives.

8.5.5 Increasing Data Rate: Radio Frequency (RF) Alternatives

Alternatives for increasing data rate involve communicating "Line of Sight" (LOS) or "over the horizon" (OTH) to modest range (10-100 mi) to a manned or unmanned aircraft, ground receiving station, or a communications buoy. Exploration and development of these communications alternatives has been conducted by ONR and other DoD entities for communications with unmanned aerial vehicles (UAV), manned aircraft, submarines, autonomous underwater vehicles (AUV), and other remote systems.

These RF alternatives involve decreasing the demands of direct Glider to satellite communications by limiting communications range required. A Glider

communications system could communicate to an intermediate receiver in the local area such as a

- · SH-60R helicopter
- · P-3 Maritime Patrol Aircraft (MPA)
- · Receiving Relay Buoy or Glider
- · UAV or manned aircraft

Radio frequency systems in the UHF/VHF band are currently in use for communication from sonobuoys to Navy ASW helicopters and MPA. Radio frequencies require a clear path between radio receivers known as a "line of sight". At sea, line of sight is typically calculated based on the line of sight to the horizon based on antenna height. The line of sight from an antenna at 3 ft height to a 5000 ft aircraft is on the order of 100 mi. Current A-sized systems can achieve the equivalent of 50-100 kbps. Current A-size sonobuoys that include in-buoy acoustic processing and digital communications achieve 6 hours of communications at this rate. The current A-size (39 lb) system could be modified to a fraction of its size and weight with duration extension as an example of currently achievable line of sight communications. The approach has the advantage of existing Fleet receivers but is for the most part one-way from buoy to aircraft.

Another alternative involves the concept of communication to a communications node in the form of a buoy or communications glider. This strategy offloads above water communications requirements to a communications gateway node. The ONR Gateway Platforms concept highlights the trade space and available technologies directly related to upgrading communication with AUV, gliders, and other autonomous sensors. In January 2001, ONR held a workshop and concluded a top-level tradeoff analysis. Results are reiterated here and the final report includes detailed size weight and power trades for acoustic and RF communications:

"…missions share a need for gateways that are difficult to detect and remove and can be installed without using a surface vessel. These requirements make most of the gateways that have been used to date, which typically have been moored surface buoys deployed from ships, less than ideal.

The optimal gateway platform designs are gliders, AUVs, and pop-up moored systems that remain submerged except when sending data via the RF channel. They are deployed by subsurface means (i.e., submarine, AUV or

diver/diver vehicle) and operate over periods from a few hours to about 1 month. They collect data from remote, acoustically linked sensors and telemeter that data over the horizon (OTH) during their relatively infrequent visits to the surface. They may surface as few as 10 times or as many as 100 times during a deployment, depending on the mission requirements.

Gateway RF communication modules include line of sight (LOS), over the horizon (OTH), and satellite systems. The LOS option is available COTS and can provide adequate burst data rates (56 Kbps) for most missions. The OTH option can be met with an aircraft relayed LOS link or with an HF system operated in ground wave mode. The HF system can, in theory, provide throughput similar to the LOS link at reasonable power, though these HF systems are not in widespread use. Concerns about HF antenna size, hardware size and weight, and the reliability of the communications channel need to be addressed. Satellite links are also potentially useful in gateways, if reluctance by the users can be overcome. Users have expressed concerns about latency, throughput and timely access to the satellite bandwidth.

The horizontal range of existing acoustic modems operating in the 10-20 kHz band varies from about 0.5 to 6 miles depending on the water depth, noise levels, propagation channel, output power, data rate and specific site conditions. Data rates vary between about 50 and 10,000 bits/sec, depending on the variables above as well as the transducer bandwidth, modulation technique and receiver array configuration. One approach to addressing the range of these values in a single gateway design is to develop an adaptive acoustic modem that automatically chooses between several clear choices in data rate and power to meet the needs of the user. As an example, an acoustic modem operating in the 10-20 kHz range, might be configured to negotiate between 100, 1000 and 10,000 bps using 15 Watts of transmit power. This approach would cover most of the operational scenarios.

Thus, the conceptual gateway design consists of a variety of potential platforms that each contain identical RF, acoustic and control modules with a battery pack designed for the mission duration and operating cycle. The gateway provides reliable underwater connectivity at ranges typically between 0.5 and 3 miles with a minimum reliable acoustic data rate of a few 100 bps. It has an RF range of order 6 to 12 miles (LOS) or 120 miles OTH and a burst data rate of the order of 50 to 100 kb/s."

Many of these technologies are in ongoing development and the conclusion reached in 2001 for technology development still apply:

"First, existing acoustic modems, such as those in use at WHOI and those produced by Benthos, have the capabilities needed by first generation gateway platforms. Development of adaptive versions of these modems should be pursued along with packaging for use with gliders, AUVs, and small moored systems.

Second, present COTS LOS UHF radio links, such as Freewave modems, can be used for LOS or OTH (with aircraft relay) applications. Implementations with special purpose controllers and special antenna configurations need to be developed. Ground wave HF transceivers and L/C band satellite transceivers that are optimized for low power and small antennas need to be investigated more fully to determine the best approach for OTH situations where aircraft relays are impractical or too costly. The major issues here are packaging, power, antenna size, and data reliability.

Third, existing glider and AUV designs need to be configured with gateway electronics and acoustics to test how they work in operational scenarios. Pop-up moorings that self-deploy need to be developed for use in VSW. These moorings need to be packaged for diver and aircraft deployment. The aircraft version would also be useful in deeper water. An aircraft version (A-size) of a low-cost surface moored gateway should be developed for applications requiring widely spaced gateways that are not too sensitive to detection issues. Fourth, a network topology needs to be defined that will allow gateways and sensors of all types to operate in various configurations with a variety of data rates and duty cycles. The Freewave RF modems may provide a reasonable model for this network definition. An internet-based TCP/IP protocol is recommended for the network with a simpler, but well-defined interoperability standard(s) for the acoustic communication subnet. A first generation acoustic interoperability standard is in place and has been implemented on the WHOI and Benthos acoustic modems."

There are a number of candidate solutions for RF and well as acoustic/RF gateway communications. The RF to aircraft or UAV solution is attractive because of the minimal engineering but requires an aircraft to receive the broadcast. The HF groundwave solution is attractive because the transmission has the potential to reach the 100 mi range but is "over the horizon" and can be

received by ships or relay gateway nodes rather than aircraft.   While HF is theoretically attractive, various parts of the HF band are particularly finicky, and shipboard HF communications systems have typically overcome this challenge by applying more power.

8.5.6 High End Solution

Communication from Gliders to UAVs represents a high end solution to the Glider communications problem worthy of further exploration.   Communication to UAVs is attractive because there is so much new development and new capability. Since the UAV operation and data relay is predicated on communication, UAV community has been embarked on developing a common, very capable network.   UAV communications networks are designed for 2 way communications to ground stations or ships as well as relay among ground stations, ship stations, other air, and satellites. The links are designed for command and control, data relay, and high data rate imagery downlink. Getting Glider data to UAVs would provide options for instant relay to tactical forces. Two of the UAV communication options are described here. The first option, already described above, includes adding a LOS RF system such as sonobuoy receiver from current SH-60R / P-3 aircraft.   The second option explores connecting the Glider into the Common Data Link architecture (CDL).

Manned air vehicles (U-2, JSTARS) and unmanned air vehicles (Predator, Outrider) use the Common Data Link (CDL) or Tactical Common Data Link (TCDL), see Figure 8.9.   The CDL architecture is being applied to as many aircraft types as can supported on a $40 million/year budget with all UAVs directed to have CDL capability. Publicly available information on CDL and TCDL is included below (Federation of American Scientists, L3 Communications, and Harris).

CDL is a full-duplex, jam resistant spread spectrum, point-to-point digital link. The uplink operates at 200kbps. The downlink can operate at 10.71 Mbps, 45 Mbps, 137 Mbps, or 234 Mbps. The Common Data Link (CDL) program is designed to achieve data link interoperability and provide seamless communications between multiple Intelligence, Surveillance, and Reconnaissance (ISR) collection systems operated by armed services and government agencies. CDL provides full-duplex, jam resistant, digital microwave communications between the ISR sensor, sensor platform, and surface terminals.

TCDL Airborne Terminal
Link Interface: 3"x6.75"x10"
Microwave Modem: 3"x12"x10"
Weight: 15.5 lbs
        including omni antenna

- **Common Data Link (CDL): DoD standard for us in imagery and SIGINT**
  - *Ku band (14.5 - 15.35 GHz)*
  - *Secure, jam resistant uplink @ 200 kbps*
  - *Downlink @ 10.71 Mbps (secure), 45, 137 or 274 Mbps*

- **Tactical Common Data Link (TCDL): family of CDL-compliant, interoperable, secure, full-duplex digital data links for use with reconnaissance aircraft**
  - *Uplink: 15.15 - 15.35 GHz @ 200 kbps*
  - *Downlink 14.4 - 14.83 GHz @ 10.71 Mbps*

- **High Integrity Data Link (HIDL): NATO sponsored full-duplex, narrow band, jam resistant data link operating in broadcast mode**
  - *UHF (223 - 400 MHz) link with 100 kbps bandwidth*
  - *Can control 2 or more UAVs simultaneously*
  - *Operable with wideband TCDL*

UNCLASSIFIED

Figure 8.9. Tactical data links [from Worley and Berry, 2003].

The TCDL program has developed a family of CDL-compatible, low-cost, light weight, digital data links with the capability to support a wide range of Intelligence, Surveillance and Recognizance (ISR) applications (Figure 8.9). The initial TCDL design was targeted for unmanned aerial vehicle UAV applications (e.g., Predator and Outrider). TCDL design is expected to be extended to additional manned and unmanned applications (e.g., Guardrail, Rivet Joint, Reef Point, ARL, Joint STARs (JSTARs), SH-60R, and EP-3). The TCDL operates in Ku band and is interoperable with the existing CDL at the 200 Kbps forward link and 10.71 Mbps return link data rates. In addition, the TCDL is capable of operation in other frequency bands and operation with variable forward and return link data rates.

TCDL provides near-real-time connectivity and interoperability between multiple TCDL collection platforms, TCDL surface terminals, and currently fielded Common Data Link (CDL) interoperable systems operated by the armed services and Government agencies. The architecture is intended to be modular in construction so that, as new sensors and users are introduced, the system architecture can accommodate them without a complete restructuring of the data link.

The engineering that has been accomplished to provide airborne lightweight (15.5 lbs), very capable TCDL terminal (6"X12"X10") with modest directional antenna for 2 way UAV communications (125 W) may represent a future path for high data rate communications from gliders or relay communications buoys. Ground terminals for TCDL application have a larger antenna aperture and physical size than the airborne segment. The next step to explore this potential high end solution for remote system communications is to assess just how flexible the TCDL design is. Several changes might be considered to adapt the TCDL air segment to Glider use: feasibility of using the airborne terminal as a small, lightweight uplink terminal, assessing the resulting link equation, exploring adaptations of system to lower data rates, and ability to use link on demand vice dedicated point-to-point.

8.5.7 Summation of Communication Systems Options

There are a number of attractive communications solutions for the Glider missions. The most attractive match for the Glider capabilities and many mission niches is the widely available low bandwidth, low power, service on demand satellite phone solutions. Local geosynchronous phone solutions, such as

Thuraya if working as advertised, should be considered as the air time and system costs may be more attractive or more available in the future relative to global LEO solutions such as Iridium.

High bandwidth satellite solutions are expensive in size, weight, and power. Clusters of 8 satellite phones can provide up to half of the data rates achievable from lower end 3 ft aperture satellite systems.

Radio frequency solutions in the line of sight (LOS) (UHF/VHF band) to aircraft or UAVs or over the horizon (OTH) (HF groundwave) to ship, shore, gateway node or buoy relay can achieve up to 100 nmi coverage. LOS RF solutions have pedigree and existing Fleet receivers. OTH HF systems need to demonstrate capability and reliability under a variety of (HF frequency dependent) atmospheric conditions and have some pedigree with existing large mast, higher power shipboard HF communications systems.

A closer look into UAV data links such as Tactical Common Data Link (TCDL) is recommended to see if the autonomous sensors can possibly take advantage of the developments in size, weight, power, and performance already in service for manned and unmanned air vehicles. Tapping into the common data link architecture could provide higher data rate bridge into common Fleet networks. Glider use of TCDL requires a number of link issues to be addressed and will likely stress the flexibility of the TCDL design.

9. Performance Envelopes (model results by Douglas Humphreys, 2003; spreadsheet analysis by Serman,2003; Jones,2003 and Osse,2003)

The methods identified under Section 7 are applied to vehicle performance modeling computations of 5 distinct glider types that span a scale regime ranging across three to four decades in vehicle volume, from about a 2/3 scale of the legacy glider volume to as much as 10,000 times larger. The analysis was based on 2 general classes of payloads: 1) a single (small) payload based on the *Basic Sentry Package* described in Section 8.3 (consisting of the Overhauser Magnetic Sensor with the X SEA U-phins INS Package) and 2) a bundled or mixed (heavy) payload that was represented for the small to mid-sized scale regimes by the *Enhanced Sentry Package* described in Section 8.3 with the marine magnetics package of the basic sentry design supplemented by an Above Water Optics Package containing a 3 CCD Camera, IR Sensor (320 x 240 Focal Plane Array) with Fiber optic antenna. For the largest scale regime of bundled payload (1000 times larger than the legacy regime) the Enhanced Sentry Package was supplemented by a set of REMUS AUV pairs occupying a free flooding compartment of the glider. These payload types were applied to 2 basic classes of vehicle shapes: 1) a winged-body-of-revolution, typified by a scaled up composite of the legacy gliders in Figure 4.1, and 2) a flying wing concept as shown in Figure 6.8 and re-scaled for multiples of the various volume sizes.

A serial numbering scheme was developed within the file protocol of the VCT computers and shall be carried over into this report to insure version control. By that scheme, the winged body of revolution designs for single payload will by designated 23x_03 through 23x_43 and 23S_03 through 23S_43; the winged-body of revolution designs for bundled (heavy) payloads will by designated 23x_02 through 23x_42 and 23W_03 through 23W_43; the flying wing designs for bundled (heavy) payloads will by designated 238_02 through 238_42 and 238_03 through 238_43; the flying wing designs for single payload will by designated 238_04 through 238_44.

9.1 Winged-Body-of Revolution for Single (small) Payloads: The study objective of this class of vehicle was to determine the upper end of speed and transport efficiency that would be possible from a legacy type shape using minimum payload volume and increased net buoyancy volume (at present assessment of maximum practical lung capacity factor, $n_b = 0.05$). The hydrodynamic performance of this class was evaluated explicitly by VCT modeling for a size regime that varied between a 31 liter vehicle and a 2024 liter

vehicle, but was extrapolated by spreadsheet analysis to V_0 = 8257, 19760, and 82,394 liter vehicles based on drag results for the 2,024 liter vehicle. The dimensions and physical specifications used for explicit modeling of the winged-body of revolution of revolution for single payloads is found in Table 9.1. The 31liter vehicle measured 1.47 m in length and had a body diameter of 0.21 m, with a wing span of 0.88 m. At the large end of the size spectrum, the 2024 liter vehicle was 5.91 m in length, had a body diameter of 0.86 m and a wing span of 3.53 m. The larger scale extrapolations used a length of 9.7 m for the 8257 liter vehicle, 13.0 m length for the 19760 liter vehicle, and the of 89,252 liters vehicle had a length of 20.9 m.

The computed glide polars, (w versus u), from explicit modeling of the 31 to 2024 liter vehicles are found in Figures 9.1-9.3. Variations of lift to drag ratio (C_L/C_D) and endurance factor ($C_L^{3/2}/C_D$) extracted from these polars are presented in the middle and lower panels of these figures. These polars indicate that the single payload winged-body-of-revolution is capable of maximum lift to drag ratio of L/D_{max} = 6.3 in the small size regime and L/D_{max} = 7.8 for larger vehicles. These L/D_{max} values correspond to specific energy consumption that varies from E_e ~ 0.16 for the small gliders and improves to E_e ~ 0.13 for the large gliders. These best E_e and L/D_{max} were obtained at an angle of attack α =10° for the 31 liter glider and α = 9° for the 2024 liter glider (see the middle panel of Figure 9.1 versus Figure 9.3). Since the glide path angel is β = - 9° for the small glider, the pitch angle at L/D_{max} remains nose level at 0°. For the larger 2,024 glider, the pitch angle is nose-high at +1.7^o when flying descending glides at L/D_{max}. (The sign of these angles of attack, glide and pitch angles reverses for ascending glides).

The maximum along course speeds, u_{max}, vary from as little as 0.385 m/sec at a loaded mass of M = 100 g for the 31 liter vehicle (Figure 9.1), to a maximum of 2.75 m/sec at a loaded mass of 13.5 kg for the 2024 liter vehicle (Figure 9.3). In these plots the loaded mass, M, is varied by an order of magnitude with each value indicated in grams in the rectangular boxes along the u = 0 axis. Extrapolations to larger vehicles (V_0 =19,760 liters for M = 1,000 kg) indicates that the maximum along course speed increases to u_{max} = 5.8 m/sec. In all cases the maximum along course speed was obtained at a glide path angle of β = -35° for which the angle of attack of varied from α = + 1.4^o for the small 31 liter glider to α = + 0.9^o for the 2,204 liter vehicle. The pitch angle for u_{max} is nose down in a descending glide at 33.6^o to 34.1^o. (A summary comparison of u_{max} versus loaded mass for the single payload winged-body of revolution against other glider types evaluated is found at the end ot this section in Figure 9.15). For cruise speeds intermediate between best L/D speed and u_{max}, a glide path angle of β = - 12° to β = - 20° is selected,

**Table 9.1a.** Summary of dimensions of winged-body-of revolution for single (small) payloads.

Method		23x Inches Sim	23S-03 Feet Froude	Sim	23S-13 Feet Froude	Sim	23S-23 Feet Froude	Sim	23S-33 Feet Froude	Sim	23S-43 Feet Froude	Sim
Hull Length (INCHES or FT)		72.000	4.837		5.090		5.428		9.225		19.395	
Diameter (INCHES or FEET)		10.5	0.705		0.742		0.792		1.345		2.828	
Hull Lnose (INCHES or FEET)		43.7	2.934		3.088		3.293		5.596		11.765	
Hull Ltail (INCHES or FEET)		28.020	1.883		1.981		2.112		3.590		7.548	
hub len (INCHES or FEET)		0.305	0.020		0.022		0.023		0.039		0.082	
dia TE (INCHES or FEET)		2.5	0.168		0.177		0.188		0.320		0.673	
slope (Deg)		0.0	0.0		0.0		0.0		0.0		0.0	
Total Length (INCHES or FT)		72.000	4.837		5.090		5.428		9.225		19.395	
L/D		6.857	6.857		6.857		6.857		6.857		6.857	
Volume FT^3)		1.9577	1.026	1.107	1.195	1.290	1.449	1.569	7.115	7.690	66.124	71.500
Swet (FT^3)		11.369	7.750		8.586		9.772		28.200		124.680	
Pr (Prismatic Coeff)		0.5426	0.5428		0.5428		0.5428		0.5428		0.5428	
Wing												
XNTE (FT)	4.5677	4.5677	3.683		3.875		4.132		7.023		14.765	
BTE (FT)	1.3544	1.3544	1.092		1.149		1.225		2.082		4.378	
CR (FT)	0.71125	0.71125	0.573		0.603		0.643		1.094		2.299	
Upper Vertical Tail												
XNTE (FT)	5.7342	5.7342	4.623		4.865		5.188		8.816		18.536	
BTE (FT)	0.563	0.563	0.454		0.478		0.509		0.866		1.820	
CR (FT)	0.28425	0.28425	0.229		0.241		0.257		0.437		0.919	
Lower vertical Tail												
XNTE (FT)	5.7342	5.7342	4.623		4.865		5.188		8.816		18.536	
BTE (FT)	0.563	0.563	0.454		0.478		0.509		0.866		1.820	
CR (FT)	0.28425	0.28425	0.229		0.241		0.257		0.437		0.919	
Acoustic Pinger												
XNTE (FT)		4	3.225		3.393		3.619		6.150		12.930	
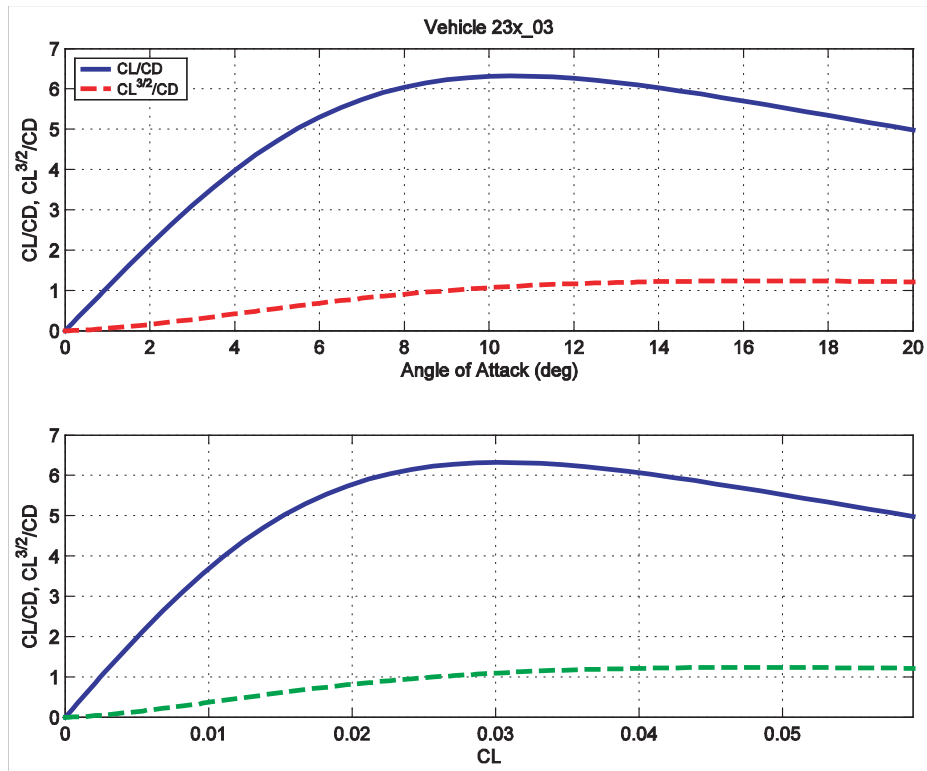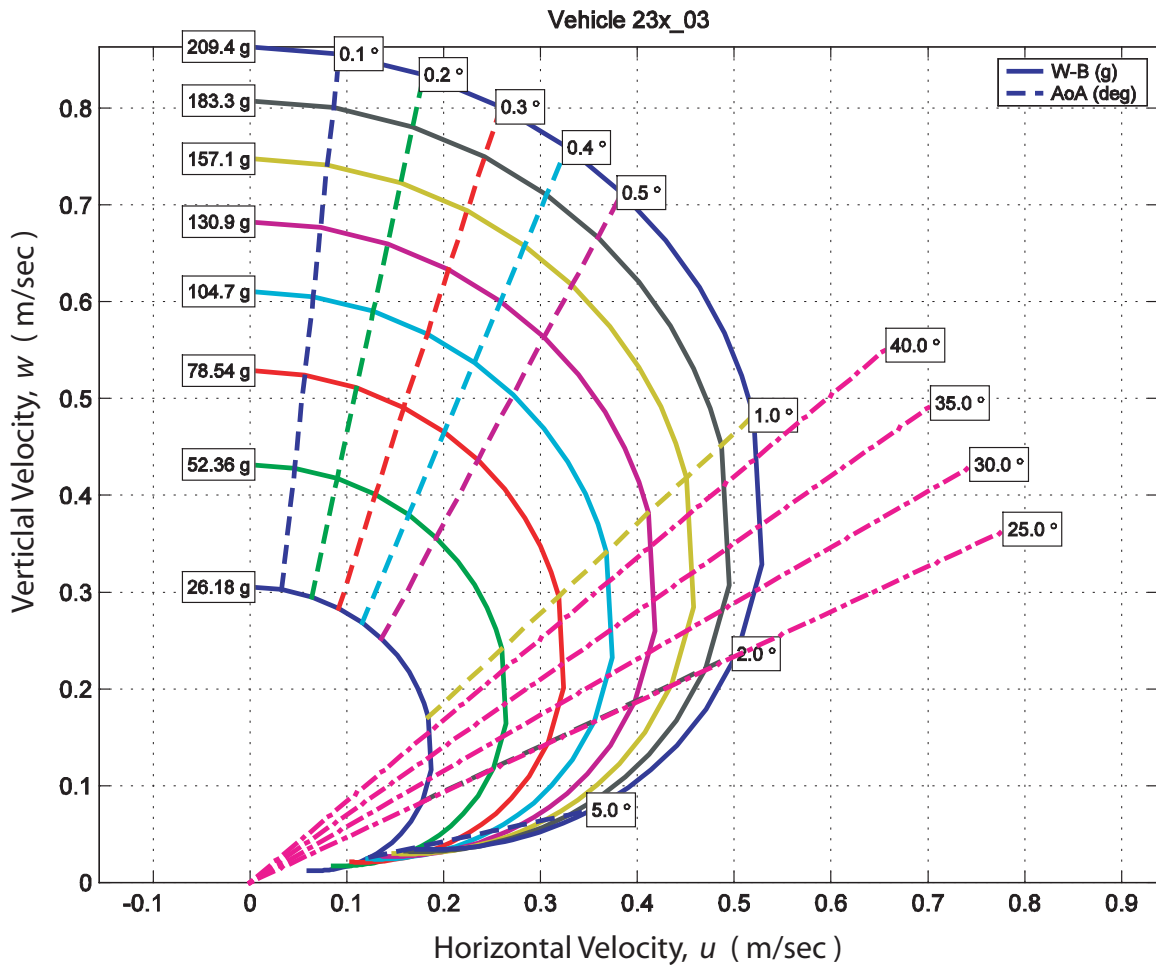
Figure 9.1. Glide Polar (upper), lift-to-drag and endurance ratios vs angle of attack (middle) and vs lift coefficient (bottom) for single payload winged-body of revolution. Length = 1.47 m, Body Diameter = 0.21 m, Span = 0.88 m, Total Volume = 31.35 liters.
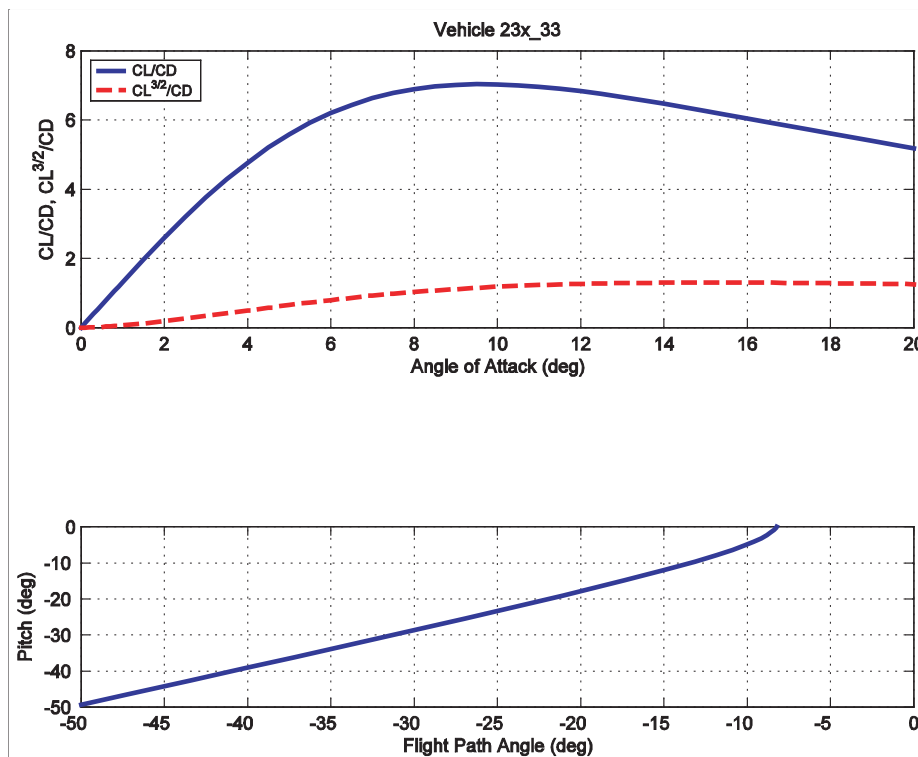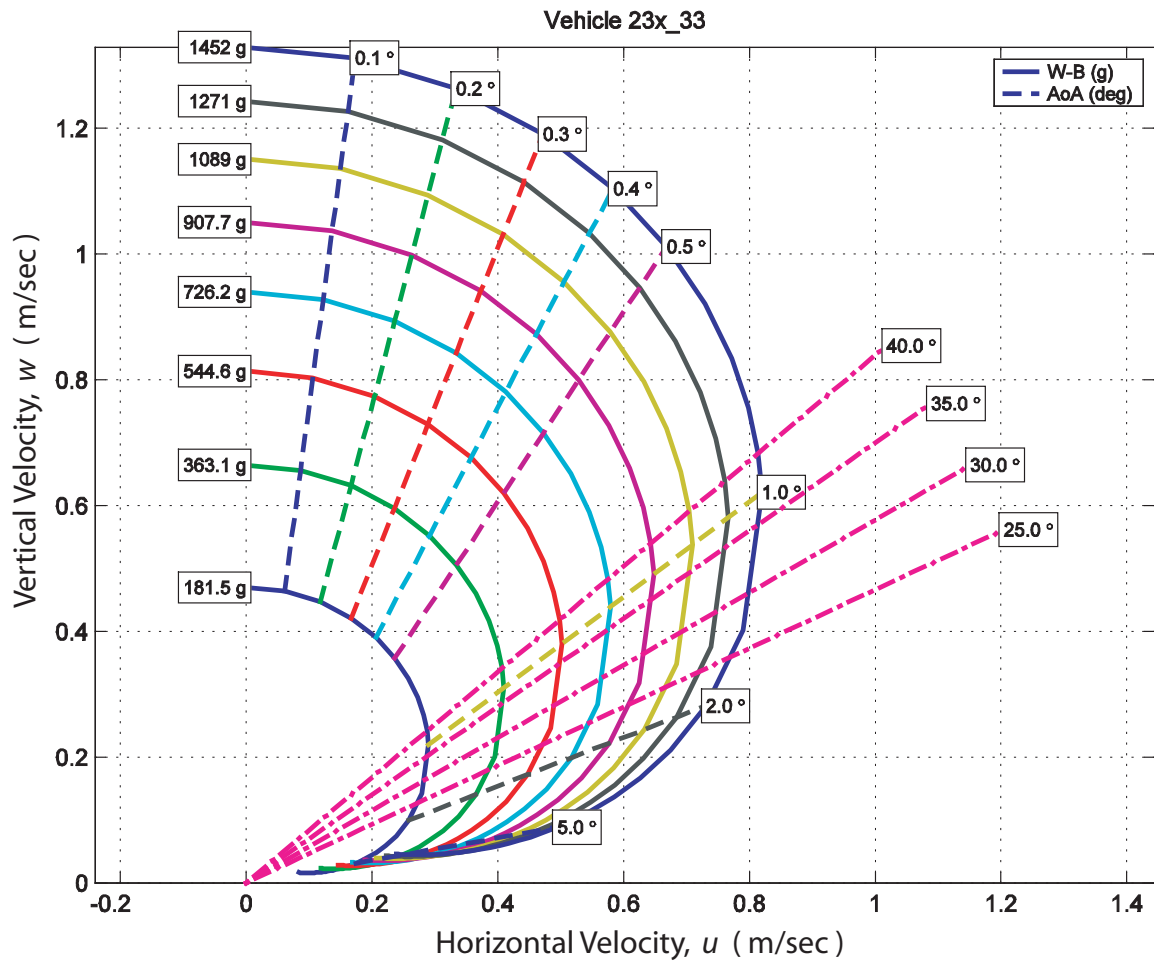
Figure 9.2. Glide Polar (upper), lift-to-drag and endurance ratios vs angle of attack (middle) and vs lift coefficient (bottom) for single payload winged-body of revolution. Length = 2.81 m, Body Diameter = 0.41 m, Span = 1.68 m, Total Volume = 217.76 liters.
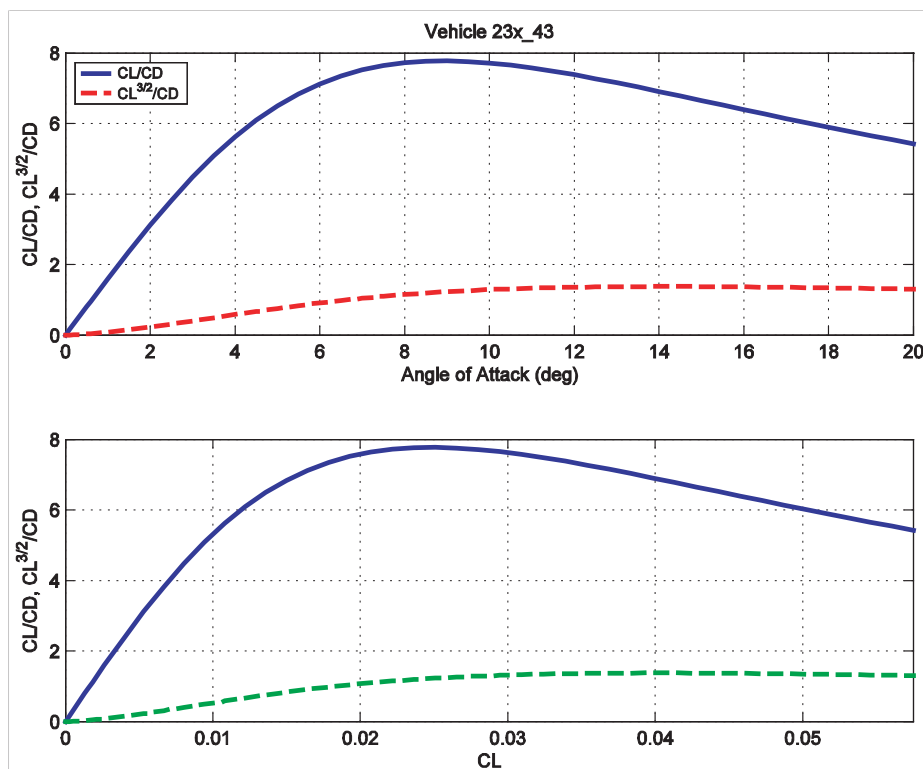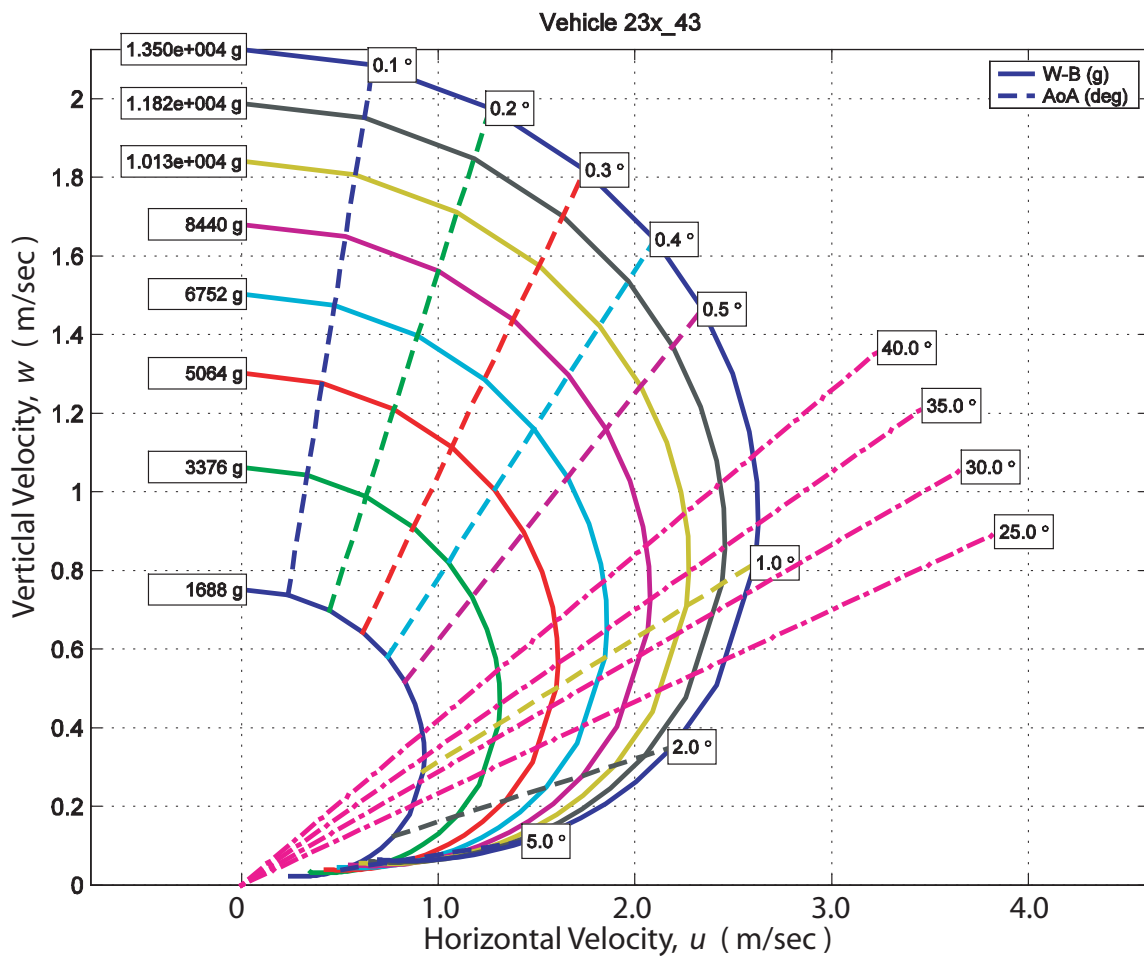
Figure 9.3. Glide Polar (upper), lift-to-drag and endurance ratios vs angle of attack (middle) and vs lift coefficient (bottom) for single payload winged-body of revolution. Length = 5.91 m, Body Diameter = 0.86 m, Span = 3.53 m, Total Volume = 2024.67 liters.

requiring an angle of attack that would typically be on the order of $\alpha = +3.5^0$ to $\alpha = +2^o$, respectively giving a 8.5^0 to 18^0 nose down pitch angle during a descending glides. Typically cruise speeds range from 0.22 m/sec for the 31 liter glider at $M = 100$ g , to 2.49m/sec for the 2,024 liter glider and ultimately 5.0 m/sec for the largest glider at $V_0 =19,760$ liters for $M = 1,000$ kg. Minimum sinking speeds range from .03 m/sec for the 31 liter glider at $M = 100$ g , to .08 m/sec for the 2,024 liter glider.

Based on the explicitly modeled glide polars, (*w* versus *u*) in Figures 9.1 through 9.3, spreadsheet analysis produced the following estimates of energy consumption at cruise speed as measured by net transport economy (*NTE*). Spreadsheet analysis of *NTE* did not admit to calculations at best L/D speed , $\beta = (L/D)_{max}^{-1}$, because of controller limitations in high angle of attack flight, (see Section 11). The following *NTE* were obtained using $\beta = - 12^o$ and $\beta = - 20^o$

Range = 3500 km , glide angle = 12 degrees

Vol	Len	Net Buoy	u	w	Range	Total_Pwr	NTE	Re	Cd
Liter	m	Liter	cm/s	cm/s	km	MJ		Vol^1/3	Vol^2/3
54.5	1.8	0.15	22.8	4.8	3500	11.4	2.22	7.3e+004	0.079
108.6	2.3	1.50	58.2	12.4	3500	27.7	0.54	2.4e+005	0.076
846.2	4.5	15.00	100.2	21.3	3500	243.7	0.47	8.1e+005	0.065
8257.9	9.7	150.00	172.0	36.6	3500	2415.7	0.47	3.0e+006	0.048
82393.8	20.9	1500.00	273.6	58.1	3500	24142.9	0.47	1.0e+007	0.041

Range = 3500 km, glide angle = 20 degrees

Vol	Len	Net Buoy	u	w	Range	Total_Pwr	NTE	Re	Cd
Liter	m	Liter	cm/s	cm/s	km	MJ		Vol^1/3	Vol^2/3
55.8	1.8	0.1	25.6	9.3	3500	12.2	3.55	8.7e+004	0.062
57.4	1.9	0.2	36.0	13.1	3500	12.6	1.83	1.2e+005	0.062
73.6	2.0	0.5	52.8	19.2	3500	18.6	1.08	2.0e+005	0.060
115.8	2.3	1.0	65.1	23.7	3500	31.8	0.93	2.8e+005	0.059
916.5	4.7	10.0	112.7	41.0	3500	283.2	0.82	9.7e+005	0.049
8946.4	10.0	100.0	195.7	71.2	3495	2803.8	0.82	3.6e+006	0.036
89252.4	21.4	1000.0	302.5	110.1	3495	28020.6	0.82	1.2e+007	0.032

Range = 500 km, glide angle = 20 degrees

Vol	Len	Net Buoy	u	w	Range	Total_Pwr	NTE	Re	Cd
Liter	m	Liter	cm/s	cm/s	km	MJ		Vol^1/3	Vol^2/3
30.7	1.5	0.1	31.3	11.4	500	1.4	2.87	8.7e+004	0.062
31.7	1.5	0.2	43.8	16.0	500	1.5	1.54	1.2e+005	0.062
36.0	1.6	0.5	67.1	24.4	500	2.5	1.00	2.0e+005	0.060
43.8	1.7	1.0	90.1	32.8	500	4.3	0.87	2.8e+005	0.059
214.0	2.9	10.0	183.0	66.6	500	38.9	0.79	9.7e+005	0.049
1990.4	6.0	100.0	322.9	117.5	500	386.5	0.79	3.6e+006	0.036
19760.1	13.0	1000.0	500.0	182.0	500	3863.6	0.79	1.2e+007	0.032

Increasing the loaded mass increases the cruise speed at $\beta = -20^o$ and improves the net transport economy in the low to mid range of the vehicle size regime:

```
Range = 3500 km , glide angle = 20 degrees
     Vol    Len  Net Buoy u      w     Range  Total_Pwr  NTE    Re        Cd
    Liter    m    Liter  cm/s   cm/s    km       MJ            Vol^1/3  Vol^2/3
     55.9   1.8    0.15   31.4  11.4   3500     12.1     2.34 1.1e+005   0.062
    159.7   2.6    1.50   72.4  26.4   3500     45.5     0.88 3.5e+005   0.058
   1362.8   5.3   15.00  123.7  45.0   3500    423.4     0.82 1.2e+006   0.047
  13407.8  11.4  150.00  217.3  79.1   3495   4204.6     0.82 4.6e+006   0.033
 133865.2  24.5 1500.00  323.6 117.8   3495  42030.0     0.82 1.5e+007   0.032


Range = 500 km , glide angle = 20 degrees
     Vol    Len  Net Buoy u      w     Range  Total_Pwr  NTE    Re        Cd
    Liter    m    Liter  cm/s   cm/s    km       MJ            Vol^1/3  Vol^2/3
     31.1   1.5    0.15   38.1  13.9    500      1.4     1.94 1.1e+005   0.062
     51.7   1.8    1.50  105.5  38.4    500      6.2     0.84 3.5e+005   0.058
    312.6   3.3   15.00  202.0  73.5    500     58.2     0.79 1.2e+006   0.047
   2977.5   6.9  150.00  358.8 130.6    500    579.7     0.79 4.6e+006   0.033
  29627.7  14.8 1500.00  535.0 194.7    500   5795.2     0.79 1.5e+007   0.032
```

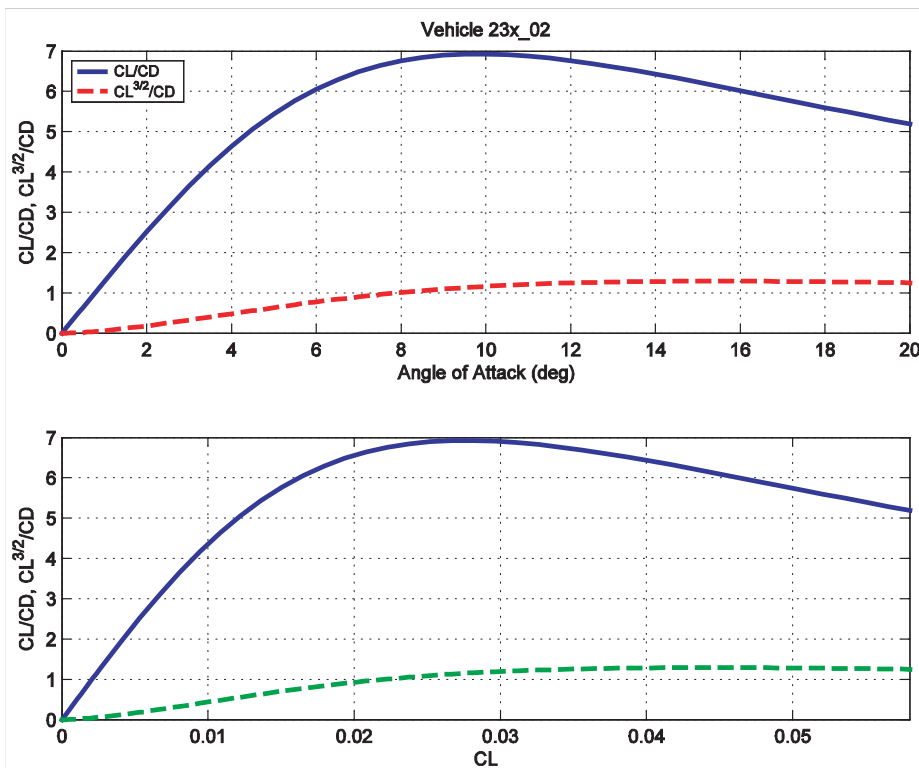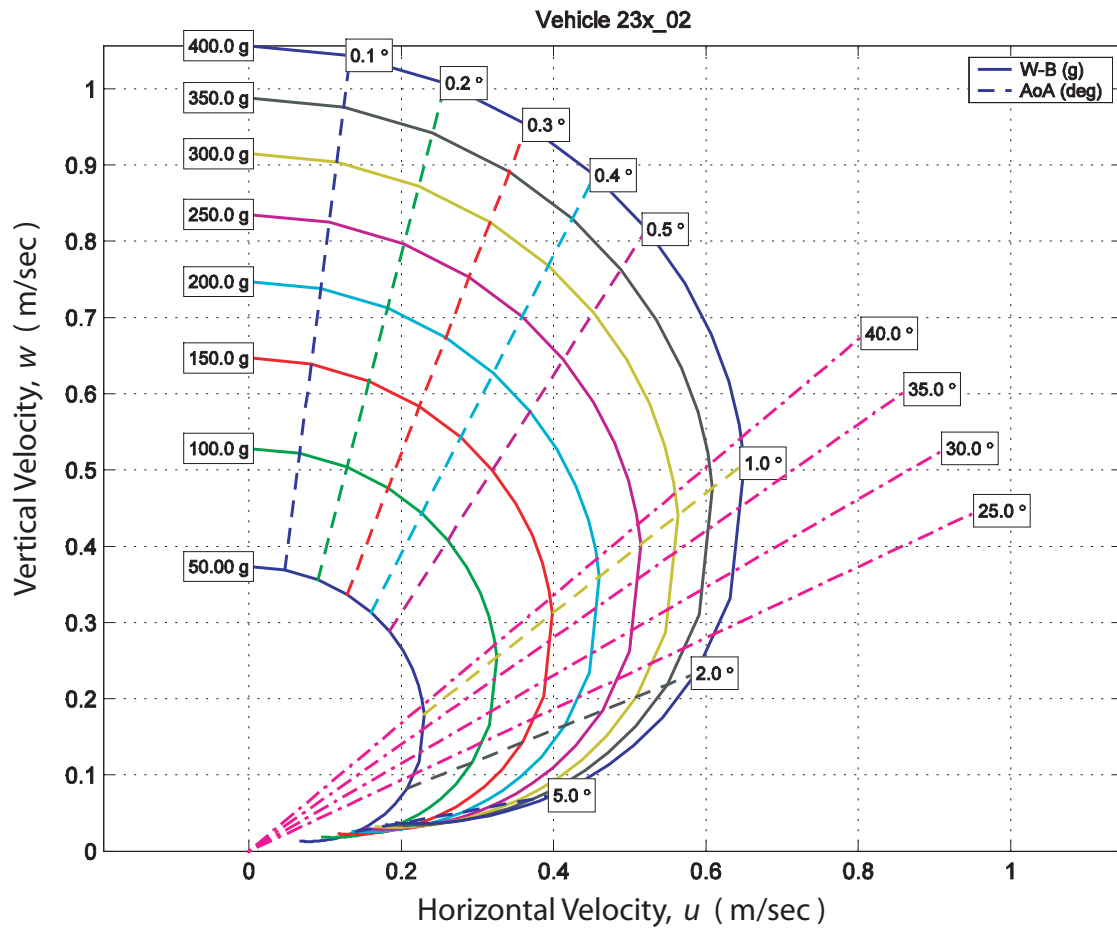**9.2 Winged-Body-of Revolution for Bundled (heavy) Payloads(*The Bus*):** This class of vehicles was posed to evaluate the transport economy and speed potential of a large payload hauling underwater glider based on the conventional legacy glider shape. Because of the requirement to dedicate a large fraction of the internal volume of these vehicles to payload space, the lung capacity factor of the buoyancy engine was not large; in fact it was on the order of the present generation of legacy gliders, ranging from $n_b = 0.002$ for the small vehicles to $n_b = 0.007$ for the large vehicles. The dimensions and physical specifications used for explicit modeling of the winged-body of revolution for bundled (heavy) payloads is found in Table 9.2. The size regime ranged from a 55 liter vehicle to a 554,000 liter vehicle. The 55 liter vehicle had dimensions similar to the legacy gliders, with a body length of 1.83 m, a body diameter of 0.27 m, and a span of 1.09 m. The large end of the size spectrum evaluated a 39.4 m long vehicle with a body diameter of 5.47 m sufficient to house large bulk payloads such as REMUS vehicles. The wing span of the 554,000 liter vehicle measures 23.5 m, roughly the same as an open class, high-performance sailplane. Intermediate between these 2 size regimes were vehicles measuring 3.9 m, 8.5 m , 18.3 m in length with wing spans of 2.4m, 5.1m and 10.9 m, respectively.

Glide polars (*w* versus *u*), lift to drag ratios *(C_L/C_D)*, and endurance factors *($C_L^{3/2}/C_D$)* are found in Figures 9.4 thru 9.8 for the *The Bus,* with vehicle volumes ranging from $V_0 = 55$ to 554,000 liters. For any particular size vehicle, the loaded

Figure 9.2a. Summary of dimensions of winged-body-of-revolution for bundled (heavy) payloads.

| Method	23W-02 (Inches) Sim	23W-10x-12 Sim	23W-10x-12 (Feet) Froude	23W-100x-22 Sim	23W-100x-22 (Feet) Froude	23W-1Kx-32 Sim	23W-1Kx-32 (Feet) Froude	23W-10Kx-42 Sim	23W-10Kx-42 Froude	Sim
Hull Length (INCHES or FT)	70.886	72.000	12.926		27.845		59.986		129.226	
Diameter (INCHES or FEET)	11.8	10.5	1.885		4.061		8.748		18.846	
Hull Lnose (INCHES or FEET)	43	43.7	7.841		16.891		36.388		78.390	
	0.53									
Hull Ltail (INCHES or FEET)	27.586	28.020	5.030		10.836		23.344		50.290	
hub len (INCHES or FEET)	0.3	0.305	0.055		0.118		0.254		0.547	
dia TE (INCHES or FEET)	2.565	2.5	0.449		0.967		2.083		4.487	
slope (Deg)	0	0.0	0.0		0.0		0.0		0.0	
Total Length (INCHES or FT)	70.886	72.000	12.926		27.845		59.986		129.226	
L/D	6.0	6.857	6.857		6.857		6.857		6.857	
	145									
Volume FT^3)	2.27	1.9577	19.572	19.579	195.745	195.755	1957.099	1956.870	19564.195	19564.877
Swet (FT^3)	1731	11.369	52.775	52.762	244.924	244.862	1136.596	1136.377	5274.868	5273.783
Pr (Prismatic Coeff)	0.5	0.5426	0.5428		0.5428		0.5428		0.5427	
Wing										
XNTE (FT)	4.5677	4.5677	9.840		21.198		45.666		98.378	
BTE (FT)	1.3544	1.3544	2.918		6.286		13.541		29.171	
CR (FT)	0.71125	0.71125	1.532		3.301		7.111		15.319	
Upper Vertical Tail										
XNTE (FT)	5.7342	5.7342	12.353		26.612		57.329		123.502	
BTE (FT)	0.563	0.563	1.213		2.613		5.629		12.126	
CR (FT)	0.28425	0.28425	0.612		1.319		2.842		6.122	
Lower vertical Tail										
XNTE (FT)	5.7342	5.7342	12.353		26.612		57.329		123.502	
BTE (FT)	0.563	0.563	1.213		2.613		5.629		12.126	
CR (FT)	0.28425	0.28425	0.612		1.319		2.842		6.122	
Fairwater (CTD Fairing)										
XNTE (FT)		4	8.617		18.564		39.991		86.151	
CG										
XcG (FT)		0	0		0		0		0	
ZcG (FT)	0.01483	0.0115	0.025		0.053		0.115		0.248	
ZcB (FT)	-0.000951	-0.001	-0.002		-0.005		-0.010		-0.022	

Figure 9.4. Glide Polar (upper), lift drag and endurance ratio vs angle of attack (middle) and vs lift coefficient (bottom) for bundled payload winged-body-of-revolution *(The Bus)*. Length = 1.83 m, Body Diameter = 0.27 m, Span = 1.09 m, Total Volume = 55.43 liters.
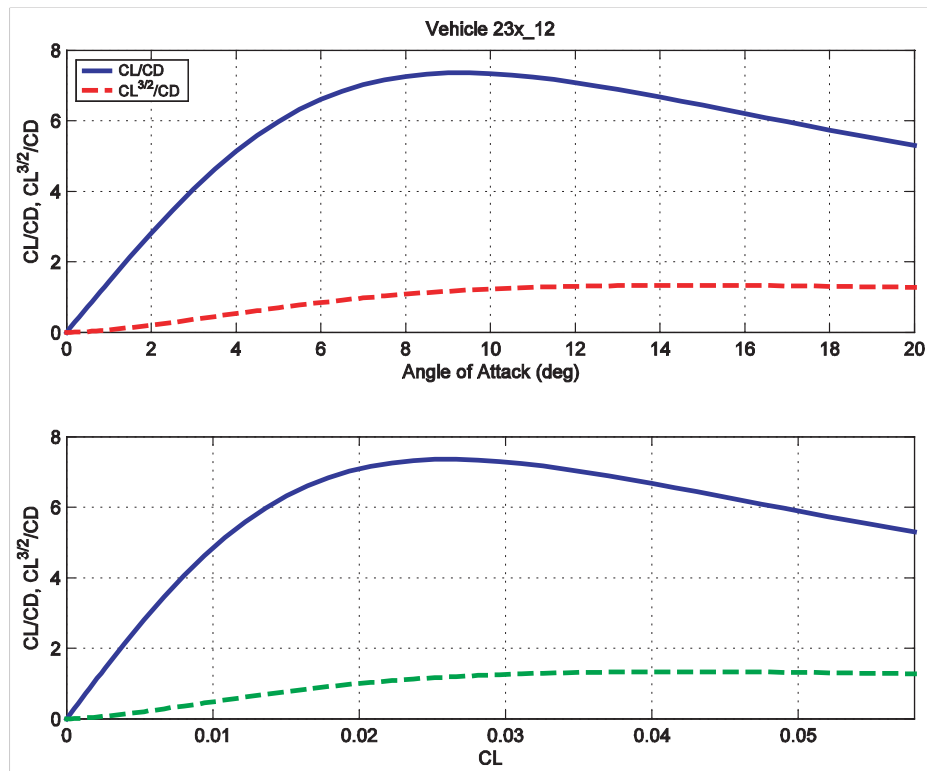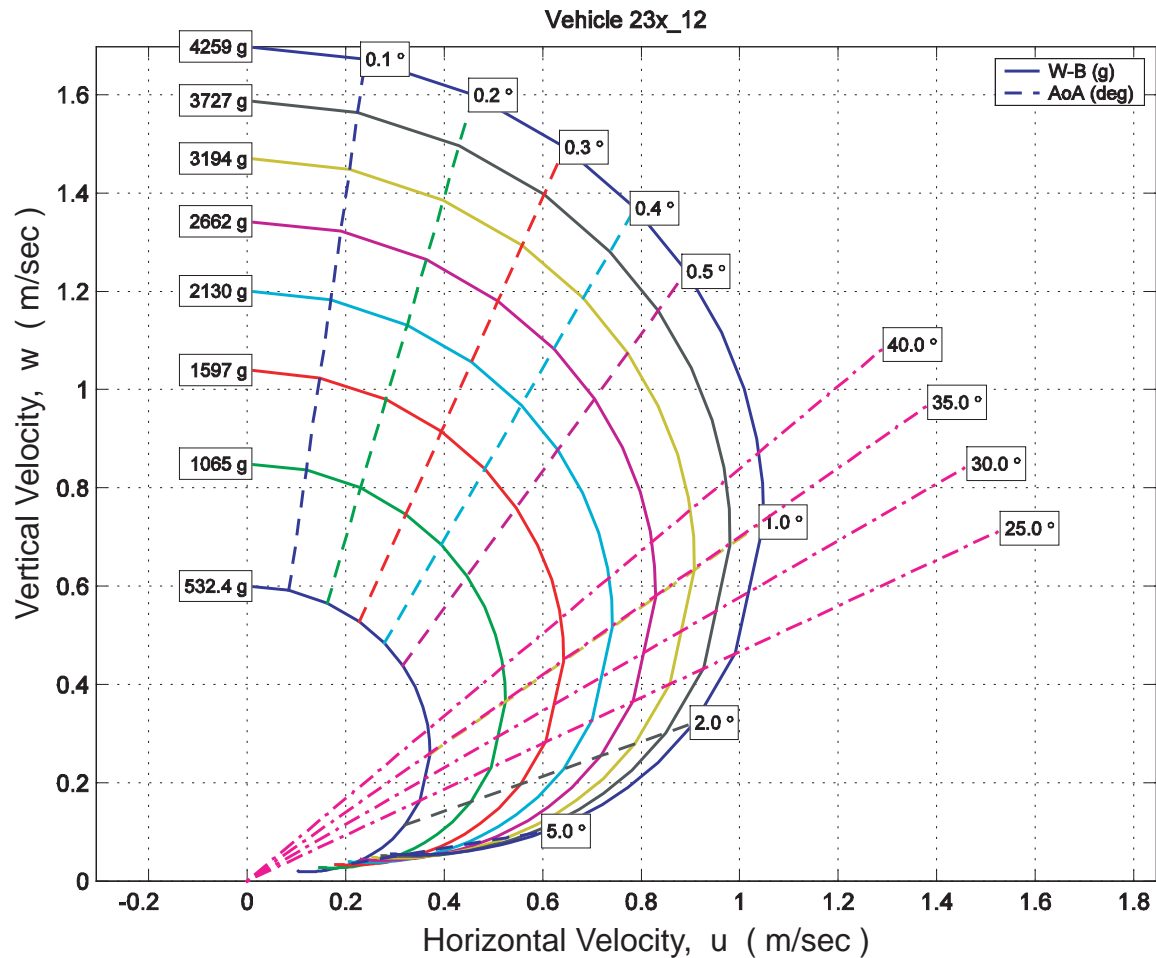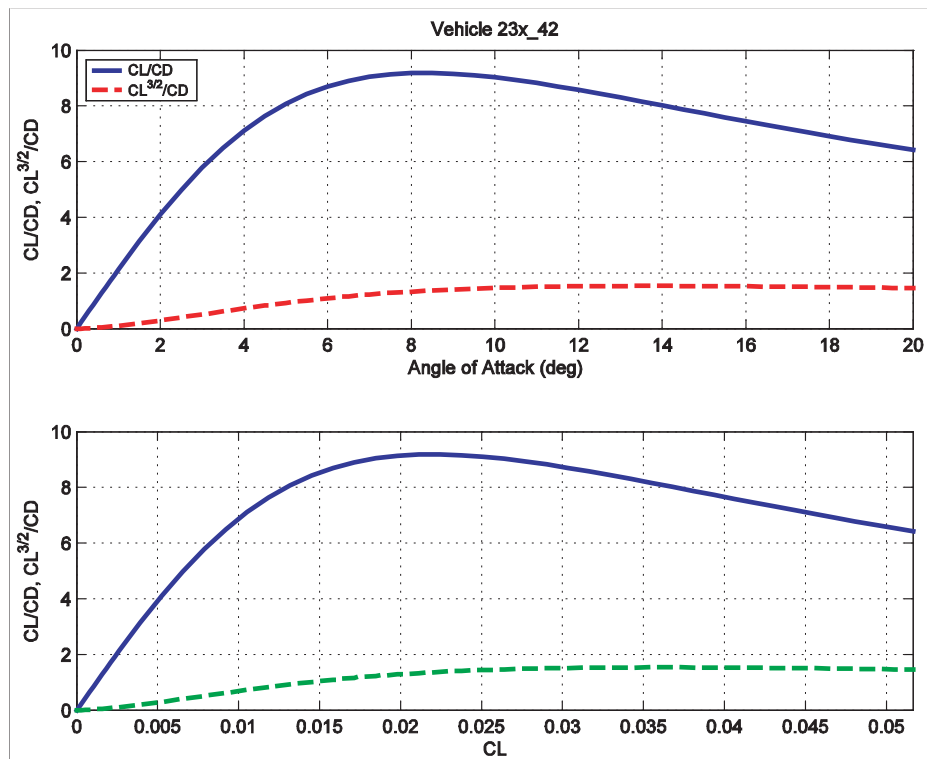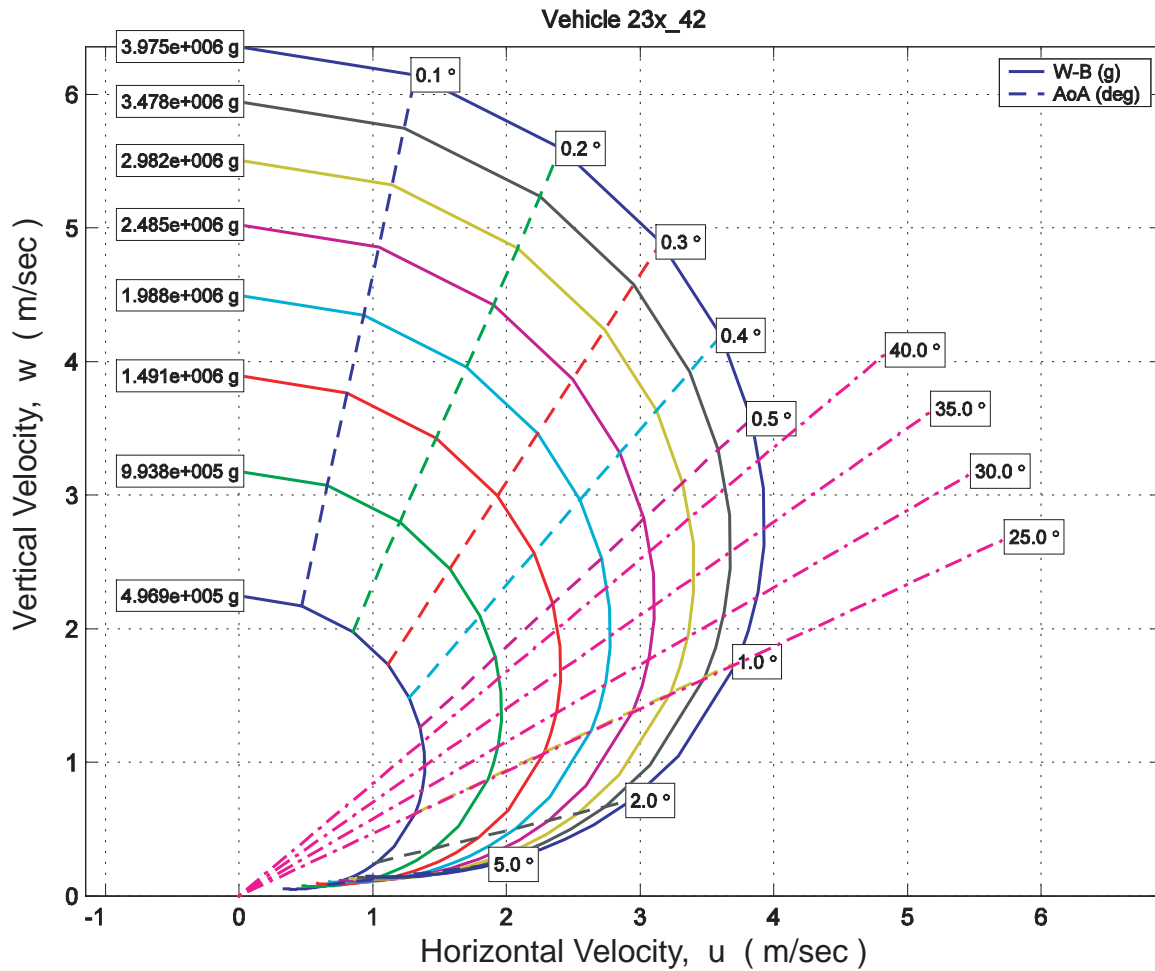
Figure 9.5. Glide Polar (upper), lift-to-drag and endurance ratios vs angle of attack (middle) and vs lift coefficient (bottom) for bundled payload winged-body-of-revolution *(The Bus)*. Length = 3.94 m, Body Diameter = 0.57 m, Span = 2.35 m, Total Volume = 554.22 liters.
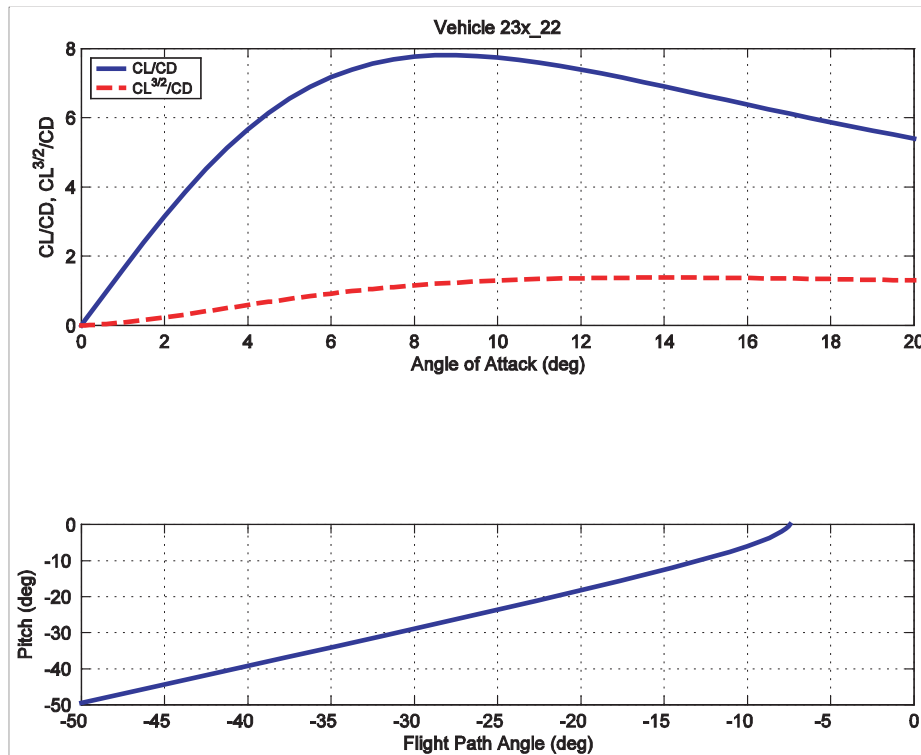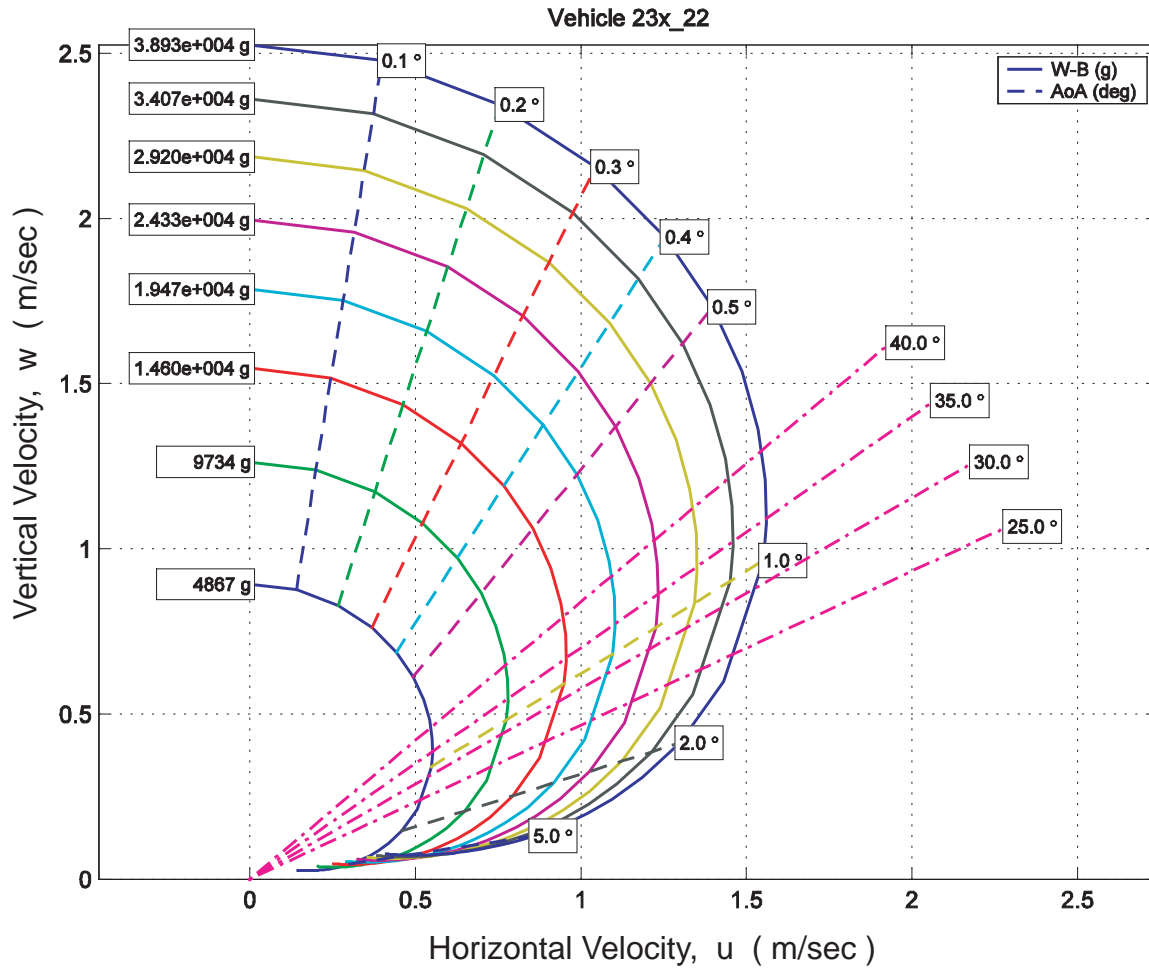
Figure 9.6. Glide Polar (upper), lift-to-drag and endurance ratios vs angle of attack (middle) and vs lift coefficient (bottom) for bundled payload winged-body-of-revolution *(The Bus)*. Length = 8.49 m, Body Diameter = 1.24 m, Span = 5.07 m, Total Volume = 5542.9 liters.
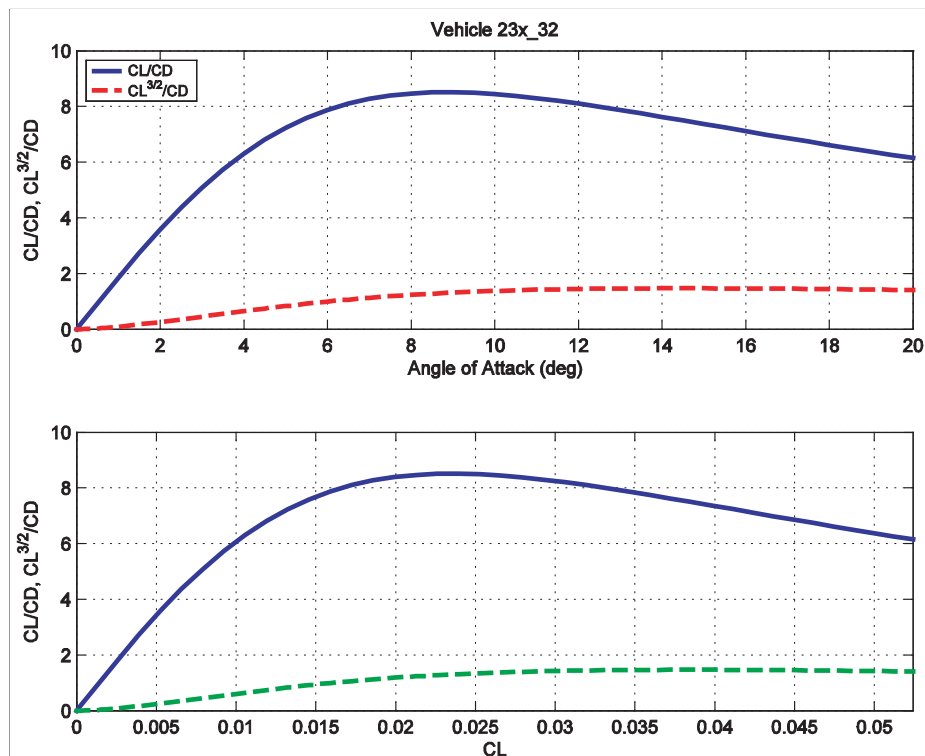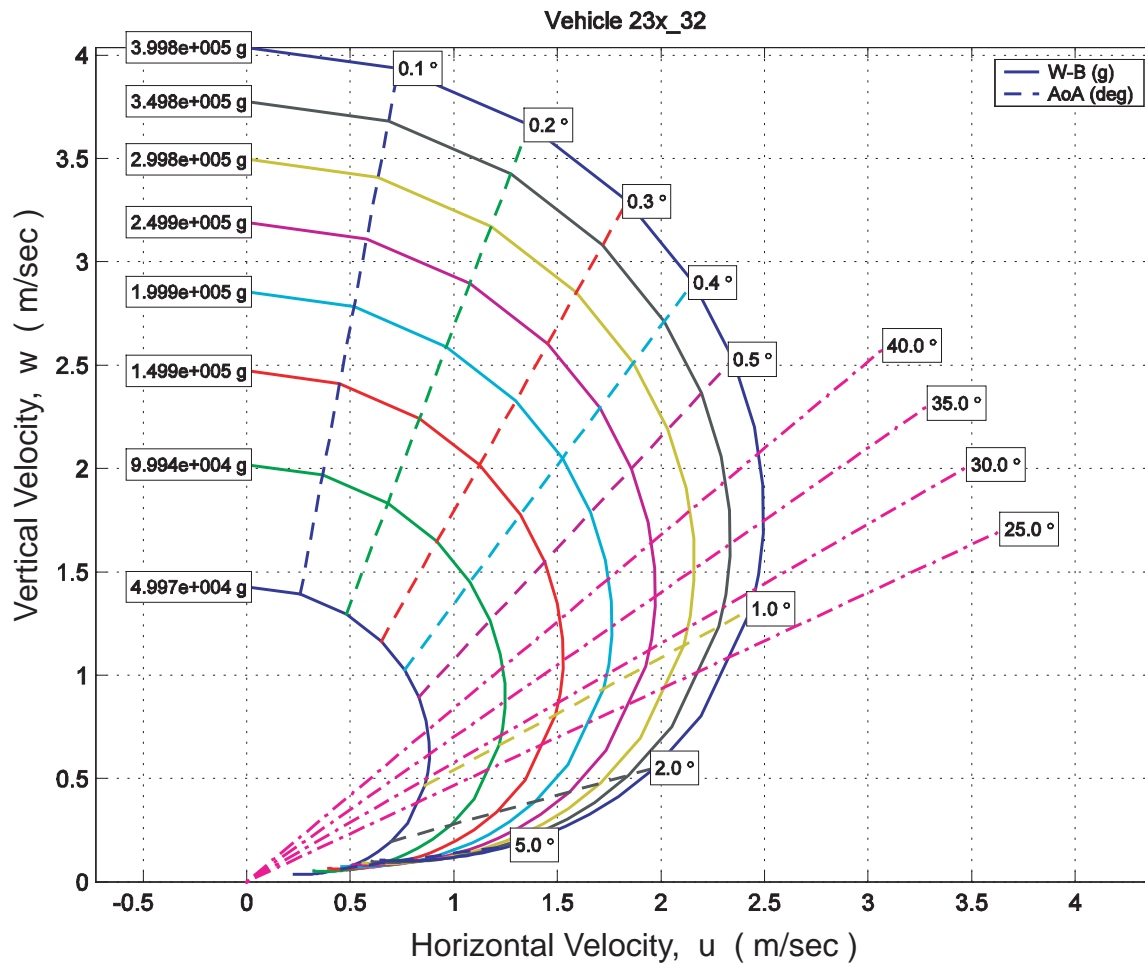
Figure 9.7. Glide Polar (upper), lift-to-drag and endurance ratios vs angle of attack (middle) and vs lift coefficient (bottom) for bundled payload winged-body-of-revolution *(The Bus)*. Length = 18.28 m, Body Diameter = 2.67 m, Span = 10.92 m, Total Volume = 55416.67 liters.

Figure 9.8. Glide Polar (upper), lift-to-drag and endurance ratios vs angle of attack (middle) and vs lift coefficient (bottom) for bundled payload winged-body-of-revolution *(The Bus)*. Length = 39.38 m, Body Diameter = 5.74 m, Span = 23.52 m, Total Volume = 553999.8 liters.

mass, M, was varied by an order of magnitude giving a separate polar curve for each choice of M as indicated by the rectangular boxes along the u = 0 axis. This gave an evaluation of glide performance for a range of buoyancy engine lung capacity spanning roughly $0.0007 < n_b < 0.007$. At the small end of the size spectrum (Figure 9.4), the maximum L/D of The Bus is equivalent to the single payload vehicles, measuring L/D_{max} = 6.9 at an angle of attack of α = + 10°. This results in a glide angle of β = - 8.2^o giving a nose-up pitch angle of +1.8^o during a descending glide. For the large Buses (eg Figure 9.8), the maximum L/D increases to L/D_{max} = 9.2 at a angle of attack of α = + 8°; but because the glide path angle flattens to β = - 6.2^o, a nose-up pitch angle is still maintained at +1.8^o during descending glides. (The sign of these angles of attack, glide and pitch angles reverses for ascending glides). The L/D_{max} values of *The Bus* correspond to specific energy consumption that varies from E_e ~ 0.14 for the small Buses and improves to E_e ~ 0.108 for the 554,000 liter Bus

The large Bus in Figure 9.8 (V_0 = 554,000 liters) achieves an impressive maximum along course speed of u_{max} = 3.9 m/sec at a glide path angle of β = − 35°, with an angle of attack at α = +0.7^o during descending glides when the loaded mass is increased to M = 3,975 kg. Smaller versions of The Bus have slower maximum speed capabilities in accordance with Equation (6.26), with the smallest version achieving only u_{max} = 0.63 m/sec with a loaded mass of M = 400g (Figure 9.4). A summary comparison of u_{max} versus loaded mass for the single payload winged-body of revolution against other glider types evaluated is found at the end of this section in Figure 9.15 . In all cases the maximum along course speed was obtained at an angle of attack of between α = + 0.7^o and α = + 0.8^o which gives a steeply nose-down pitch angle of between 34.2^o and 34.3^o in a descending glide. Cruise speeds for the Bus approach u_{max} since its primary application would be depth unlimited roaming in which little restriction is placed on vertical excursions through the water column. However, for long range transport economy of large payloads, best L/D speeds may be desirable speeds to fly. Best L/D speed for the Bus is about ½ cruise speed, ranging from U' = 0.21 m/sec for the 55 liter legacy sized Bus to U' = 1.90 m/sec for the largest version (V_0 = 554,000 liters). Because of the relatively low n_b values for *The Bus* minimum sinking speeds remain fairly low even for the large vehicles. Minimum sink is only w_{min} = 0.1 m/sec at a glide speed of u_{wmin} = 0.5 m/sec for the largest Bus (V_0 = 554,000 liters) operating at M = 1,000 kg and declines to w_{min} = 0.013 m/sec at u_{wmin} = 0.06 m/sec for the 55 liter glider at M = 100 g.

The modeled glide polars, (*w* versus *u*) in Figures 9.4 through 9.8 provided input to the hydrodynamic sheets of the spreadsheet analysis for the energetics of

the bundled payload variant of the winged body of revolution. Spreadsheet analysis of *NTE* did not admit to calculations at best L/D speed , $\beta = (L/D)_{max}^{-1}$, because of controller limitations in high angle of attack flight, (see Section 11). A detailed analysis of the energetics is found in Figures 10.5 through 10.12 in Section 10 for the complete size regime as a function of diving depth and range. A summary of the of the net transport economy (*NTE*) at cruise speeds for $\beta = -20^{o}$ is found in the following listing of vehicle size for the heavy payload hauling winged-body of revolution.

Length Ft	Wing Span Ft	Volume Cu Ft	Loaded Mass (Net Buoyancy) Grams	Cruise Speed Kts	Best L/D Speed Kts	Net Transport Economy
6.0	3.6	2.0	150	0.95	0.41	4.49
12.9	7.7	19.6	1,500	1.5	0.76	1.30
27.9	16.6	195.7	15,000	2.3	1.22	1.04
60.0	35.8	1957.0	150,000	3.6	1.58	0.88
129	77.1	19,569	3,975,000	7.3	3.7	0.88

9.3 Flying Wing for Bundled and Single Payloads : For a winged body of revolution legacy-type glider as evaluated in Sections 9.1 and 9.2 above, the maximum lift/drag ratio is limited by the constraints on the glider geometry. Drag resulting from flow over the body limits the gliding performance at low glide path angles and high angles of attack. On the other hand, flying wing designs offer improved lift/drag performance for gliders. In a flying wing, the full volume of the glider is contained within the wing section. By eliminating the body of the glider it is possible to significantly lower the wetted area ratio of the glider ($A_t/A \sim 2.2$) and improve its maximum lift/drag ratio. This gives better gliding performance at shallow glide path angles than existing designs.

Two variants of flying wings are evaluated for the underwater glider functional classes outlined in Section 5. One is for bundled (heavy) payloads (Series 238_x2) to be flown at cruise speed intermediate between best L/D speed and u_{max} in depth unlimited environments. The other flying wing variant (Series 238_x4) is for single payloads flown near best L/D speed in depth-limited environments. Both types are scaled from the Horten H-II surrogate shown in

Figure 6.8. using the McMasters 28.8 % thickness to cord wing section. The dimensions and physical specifications used for explicit modeling of the heavy payload variant of the flying wing are found in Table 9.3; and for the small payload variant in Table 9.4. Together, these two sets of flying wing dimensions spanned a considerable range in vehicle volume, from $V_0 = 37$ liters for the smallest single payload variant to $V_0 = 622,408$ liters for the largest heavy payload variant. At the high end of the size spectrum the 622,408 liter vehicle had a root chord dimension of 15 m, a root wing section thickness of 4.37 m, a wing span of 68.93 m, and a wing area of 592.37 m^2. The Smaller flying wing examples were evaluated for spans of 2.2 m, 2.75 m, 4.58m, 6.89 m, 9.6m, 14.85 m, 20.9m and 32 m. In addition, spreadsheet analysis interpolated to a number of intermediate sized vehicles, including $V_0 = 15,532$ liters, 19,514 liters, 30,920 liters, 58,485 liters, 82,394 liters and 133,865 liters.

Because the VCT numerical modeling and spreadsheet analyses remained well behaved and self consistent across the many permutations of scale for studied the flying wing, we shall present glide polars (w versus u), lift to drag ratios (C_L/C_D), and endurance factors $(C_L^{3/2}/C_D)$ for the Series 238_x4) single payload vehicles in Figures 9.9 through 9.13. Collectively, these polars span the entire range of loaded mass evaluated by all methods, from $M = 04.$kg to 4,000 kg, or a range in buoyancy engine lung capacity of $0.006 < n_b < 0.26$. Inspection of the glide polars in Figure 9.9 indicates that the small, single payload flying wing ($V_0 = 36.8$) liters is capable of a rather impressive value of maximum L/D equal to about 17.8, achieved at an angle of attack of $\alpha = 10^0$. Since the glide angle is only $\beta = -3.2°$ due to the high value of L/D_{max} the pitch angle in a descending glide is very nose-high at 6.8^0. At the large end of the size spectrum (Figure 9.13), the maximum L/D's were obtained at an angle of attack, $\alpha = 7°$ but at a higher maximum L/D of $L/D_{max} = 23.5$. Therefore, the pitch angle of the largest flying wings at L/D$_{max}$ is less nose-high at 4.6°. The L/D_{max} values of the flying wing correspond to specific energy consumption that varies from $E_e \sim 0.057$ for the small Buses and improves to $E_e \sim 0.04$ for the 622,000 liter wing.

If the large single payload flying wing in Figure 9.13 ($V_0 = 15,500$ liters) is ballasted to a relatively high loaded mass ($M = 4,000$kg), then a very impressive maximum along course speed of $u_{max} = 6.7$ m/sec can be obtained at a glide path angle of $\beta = -35°$ using a low angle of attack of $\alpha = 0.25^0$ (pitch angle in a descending dive nose-down at $-34.75°$). This was the highest u_{max} obtained in any of the simulations but is primarily an artifact of the very high buoyancy engine lung capacity assumed for this result, $n_b = 0.26$. To achieve such a high n_b would probably require the placement of the batteries in free-flooding sections of the

**Figure 9.3a.** Summary of dimensions of flying wings for heavy payloads.

	238_02	238-10x		238-100x		238-1000x		238-10Kx
	-02	-12		-22		-32		-42
	Ft	Feet		Feet		Feet		
Method	Sim	Froude	Sim	Froude	Sim	Froude	Sim	
Hull Length (FEET)	2.300	4.955		10.674		22.995		49.537
WingPlanForm Area(2-panels) (FEET^2)	13.747	63.8		296.1		1374.1		6376.9
Volume (FEET^3)	2.2	22.0		220		2198		21980
Wing								
XNTE (FEET)	2.3	4.955		10.674		22.995		49.537
BTE (FEET)	5.25	11.310		24.365		52.488		113.073
CR (FEET)	2.3	4.955		10.674		22.995		49.537
Upper Vertical Tail								
XNTE	0	0.000		0.000		0.000		0.000
BTE	0	0.000		0.000		0.000		0.000
CR	0	0.000		0.000		0.000		0.000
Lower vertical Tail								
XNTE	0	0.000		0.000		0.000		0.000
BTE	0	0.000		0.000		0.000		0.000
CR	0	0.000		0.000		0.000		0.000
Fairwater (CTD Fairing)								
XNTE	0	0.000		0.000		0.000		0.000
CG								
Xcg	0	0		0		0		0
Zcg	0	0.000		0.000		0.000		0.000
Zcg	0	0.000		0.000		0.000		0.000

Figure 9.4. Summary of dimensions and hydrodynamic parameters of flying wings for light payloads.

**Veh 238 Iter-2: 3.2 DEG Glide Slope FLYING WING**   **(Sherman)**

Vehicle	238 -04	238 -14		238 -24		238 -34		238 -44	
Method	Sim	Froude	Sim	Froude	Sim	Froude	Sim	Froude	Sim
Scale	0.86	0.86		1.430		3.000		6.560	
Net Buoyancy-base (GRAMS)	150	1,500		15,000		150,000		1,500,000	
Speed m/sec	0.073	0.239		0.561		0.981		1.556	
Speed Kts	0.14	0.46		1.09		1.91		3.02	
Length Total (FT)	1.98	1.98		3.29		6.90		15.09	
Disp Weight Lbs	82.7	94.9		389.4		3,539.6		35,104.7	-
AoA (Deg)	0.4	0.35		0.2		0.2		0.7	
Flight Path Angle (Deg)	3.2	3.2		3.2		3.2		3.2	
Cd(SB)	38.4	37.0		91.0		264.9		1266.6	
SB (ft^2) Hull	0.0055	0.0055		0.0055		0.0055		0.0055	
CdA =	0.211365	0.203225		0.5005		1.45695		6.9663	
Cd(L^2)	0.05402	0.05194		0.04627		0.03060		0.03060	
L^2 - Root Chord	3.91	3.9		10.8		47.6		227.6	
Cd(WingPlanform)	0.0208	0.0200		0.0178		0.0117		0.0117	
Wing PlanFormArea(2-panels)	10.16	10.16		28.14		124.04		593.60	
Cd(Vol^2/3)	0.1781	0.1562		0.1501		0.1002		0.1037	
Vol^2/3	1.187	1.301		3.335		14.536		67.149	
CdA =	0.211	0.203		0.501		1.457		6.966	
Volume	1.29	1.48		6.08		55.31		548.51	
Ratio Cd_0/Cd_scaled	1	1.04		1.17		1.77		1.77	
Re(Vol_1/3)	2.1.E+04	7.2.E+04		2.7.E+05		9.8.E+05		3.4.E+06	
Re(Vol_1/3) (Geo)	1.4.E+04	4.8.E+04		1.8.E+05		6.6.E+05		2.3.E+06	
Re(L)	3.80.E+04	1.2.E+05		4.9.E+05		1.8.E+06		6.2.E+06	
Re (L) (Geo)	2.53E+04	8.30E+04		3.28E+05		1.20E+06		4.18E+06	
L (Geo) MAC	1.31E+00								

	238_04	238-14		238-24		238-34		238-44	
	Ft	Feet		Feet		Feet			
Method	Sim	Froude	Sim	Froude	Sim	Froude	Sim		
Hull Length (FEET)	1.978	1.978		3.289		6.900		15.088	
Hull Length (Inches)	23.736	23.736		39.468		82.800		181.056	
WingPlanForm Area(2-panels) (FEET^2)	10.16	10.160		28.140		124.0		593.6	
Volume (FEET^3)	1.29	1.48		6.08		55.31		548.51	

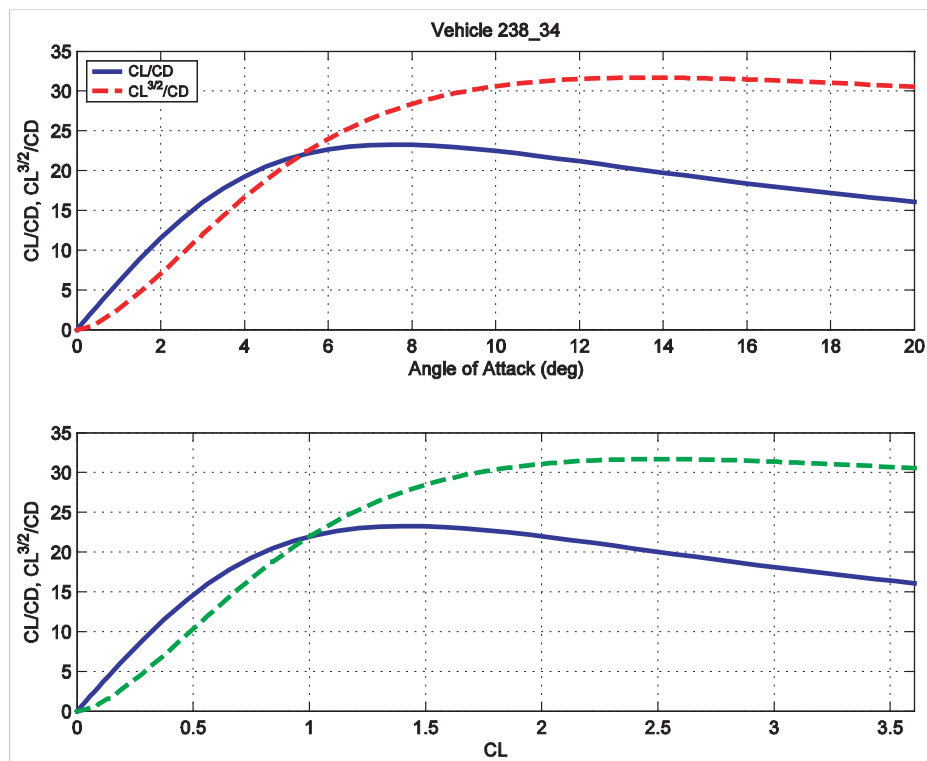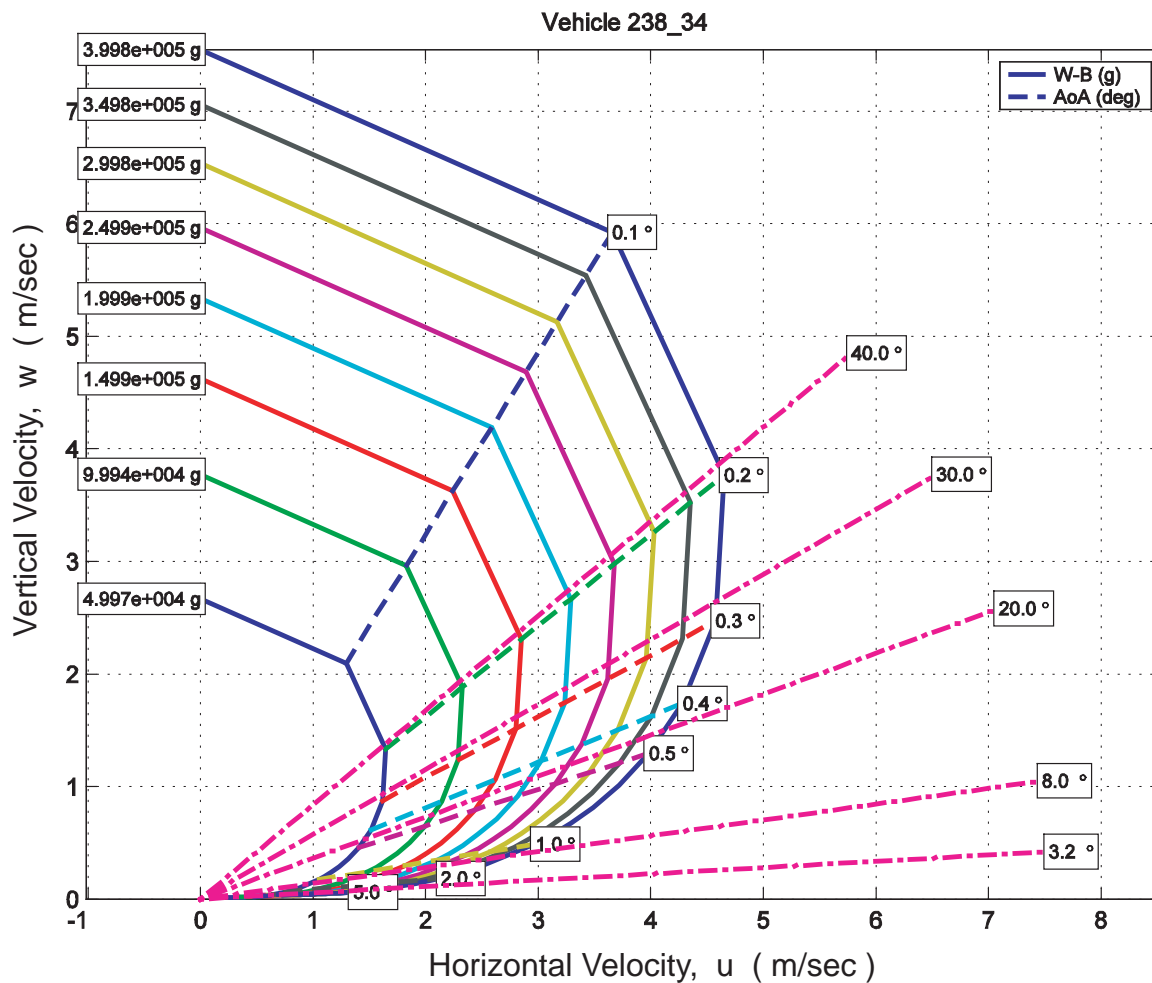| Wing									
XNTE (FEET)	1.978	1.978		3.289		6.9		15.088	
BTE (FEET)	4.515	4.515		7.5075		15.75		34.44	
CR (FEET)	1.978	1.978		3.289		6.9		15.088	
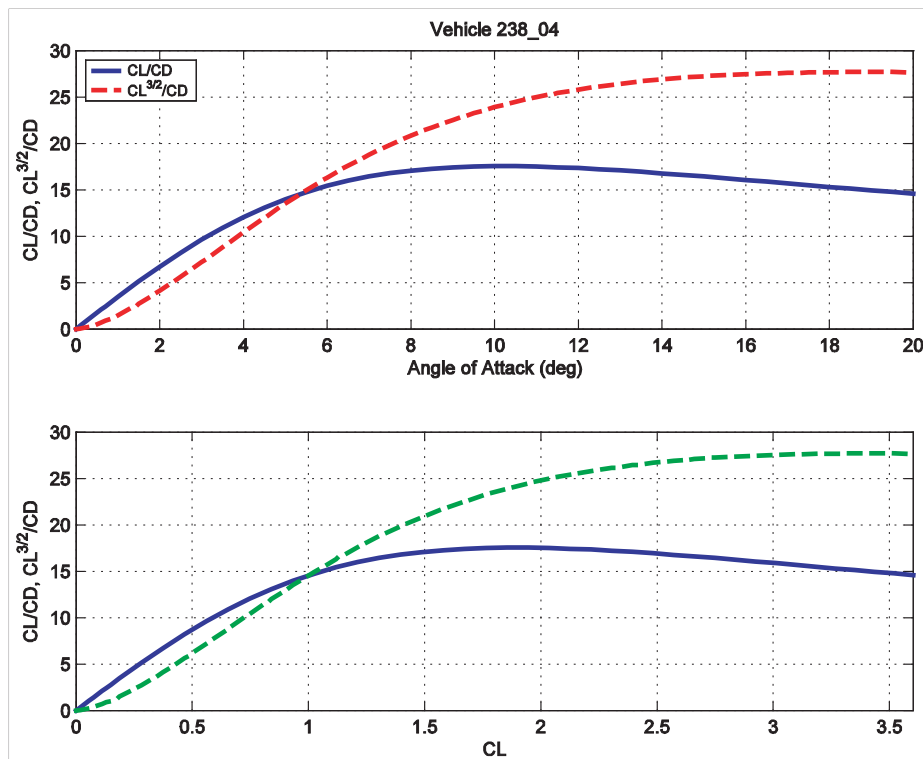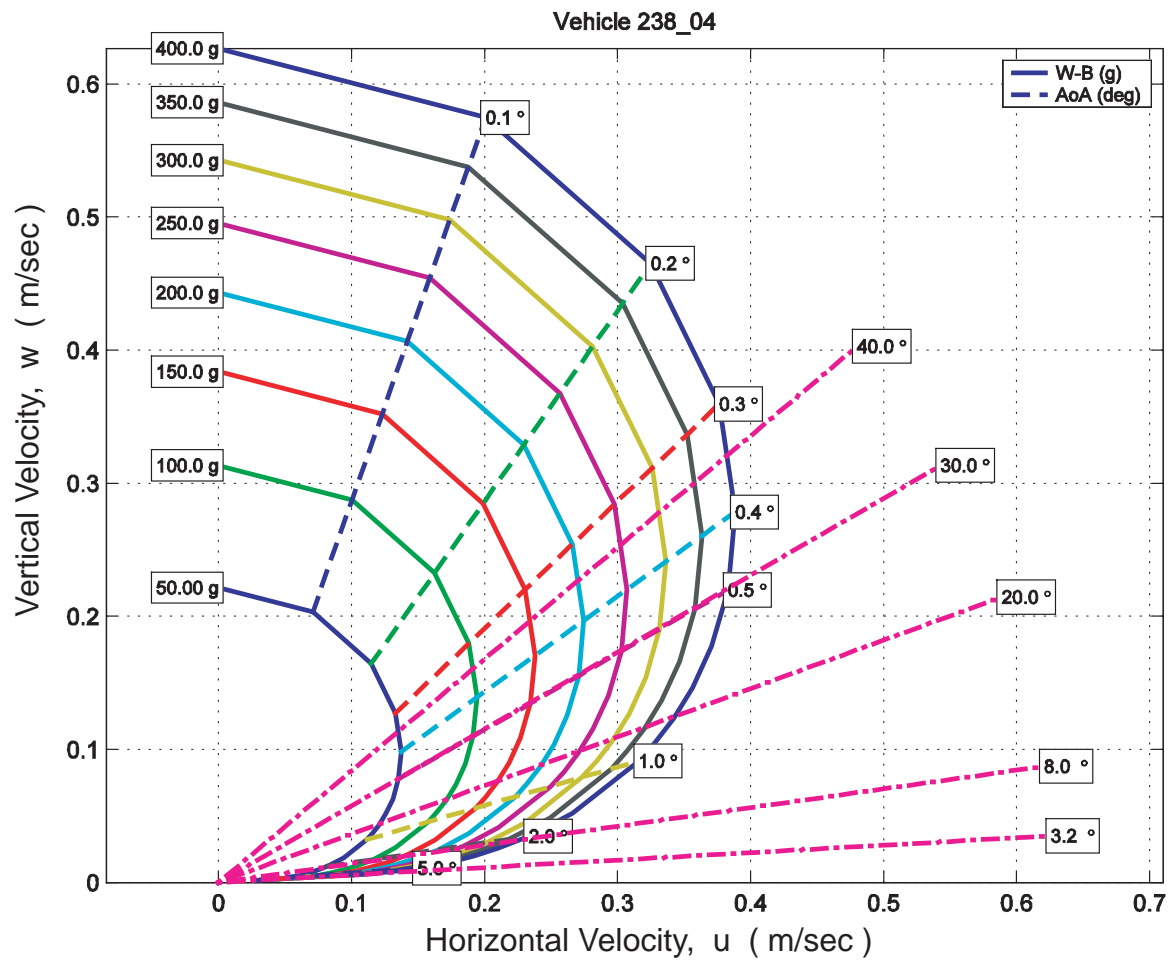
Figure 9.9. Glide Polar (upper), lift drag ratio and endurance ratio verses angle of attack (middle) and verses lift coeffiecent (bottom) for single payload flying wings. Root Cord = 0.60 m, Root Section Thickness = 0.17 m, Span = 2.75 m, Wing Area = 0.94 m2, and Volume = 36.8 liters
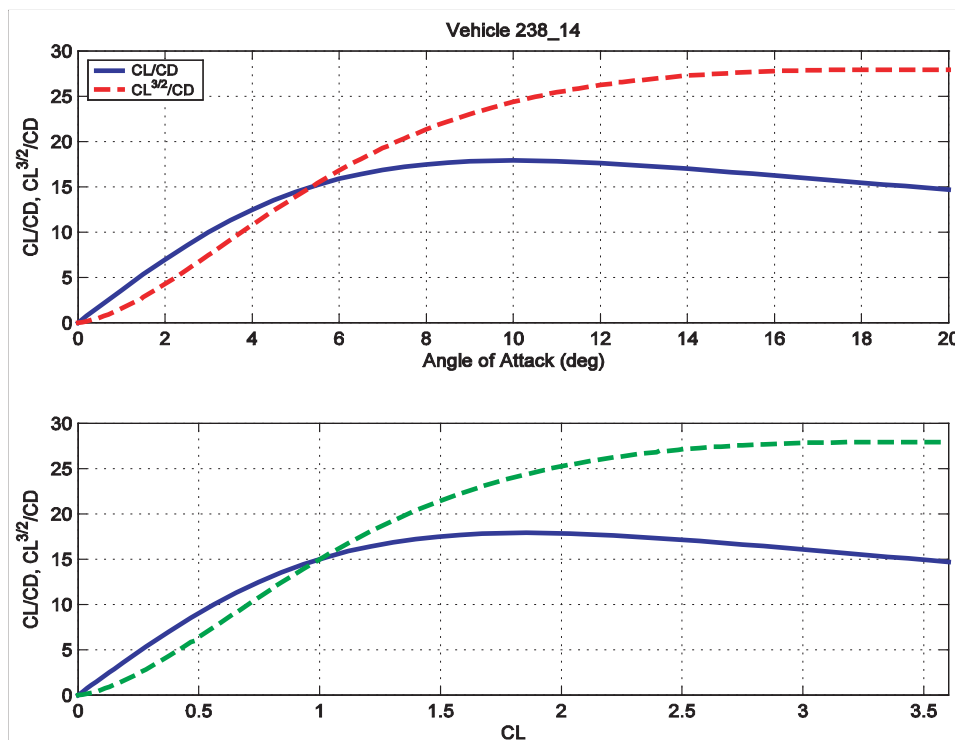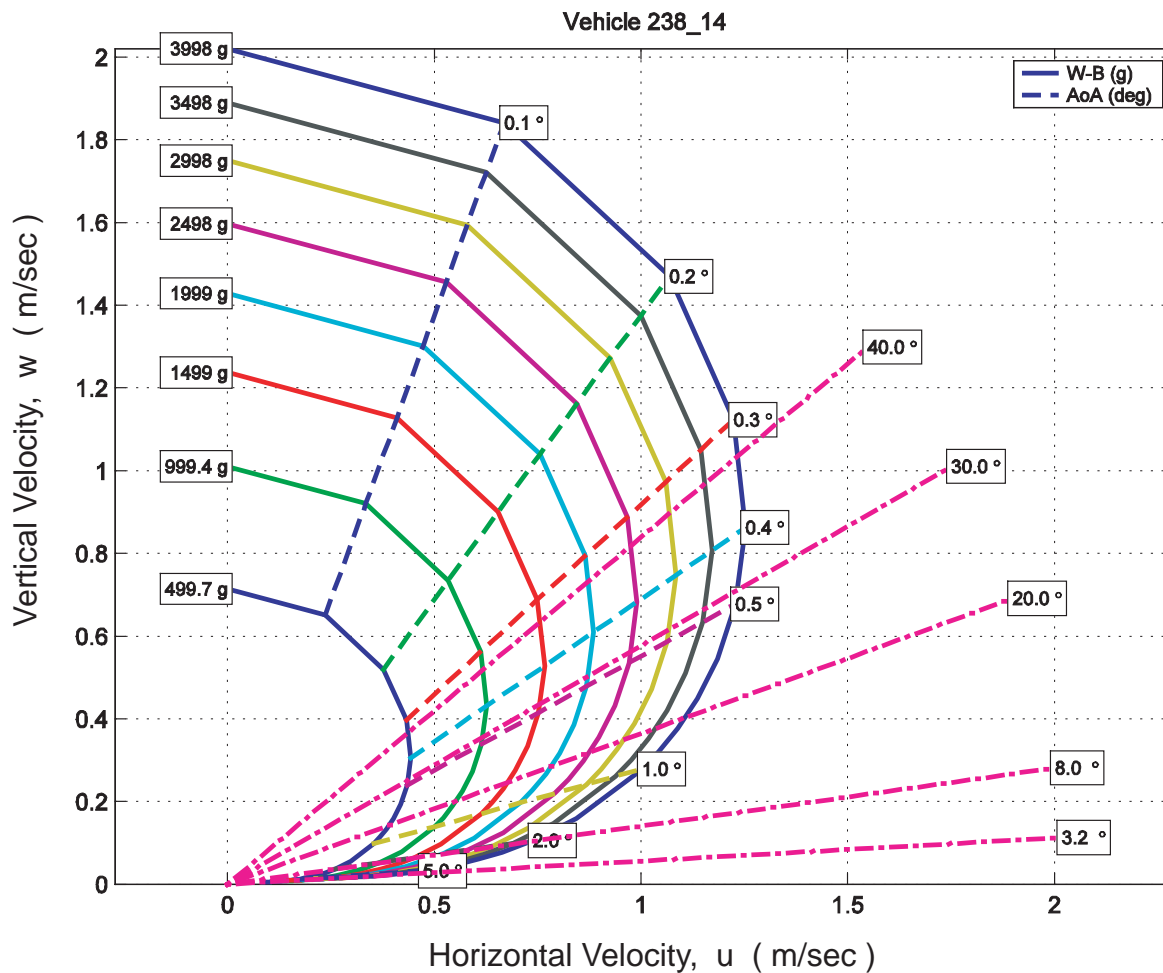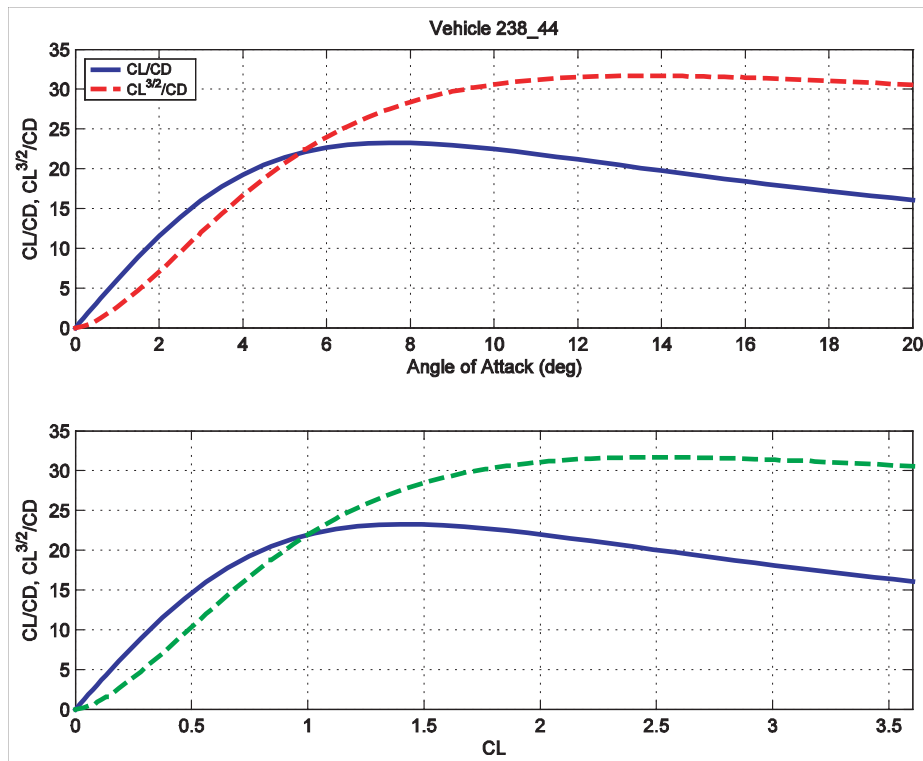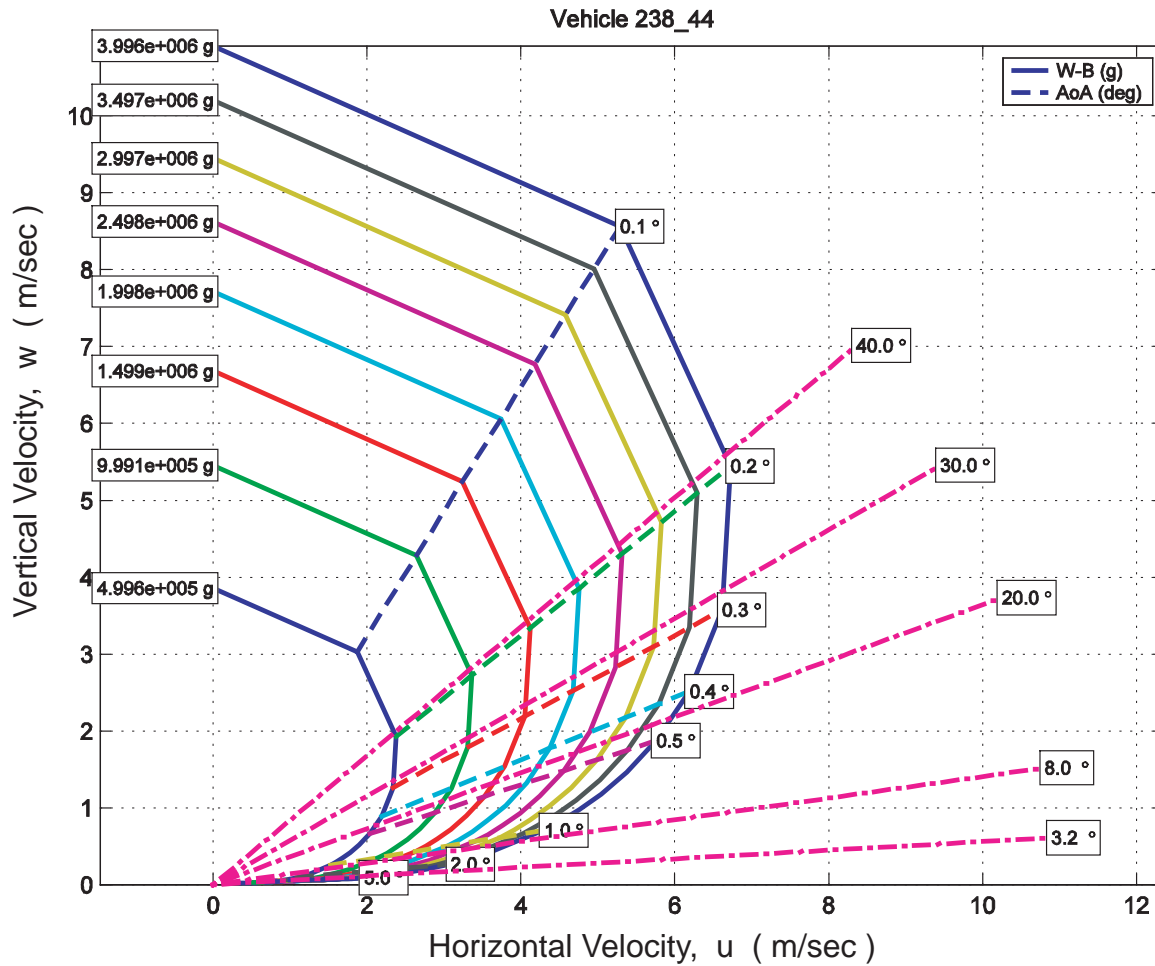
Figure 9.10. Glide Polar (upper), lift drag ratio and endurance ratio verses angle of attack (middle) and verses lift coeffiecent (bottom) for single payload flying wings. Root Cord = 0.60 m, Root Section Thickness = 0.17 m, Span = 2.75 m, Wing Area = 0.94 m2, and Volume = 42.47 liters.
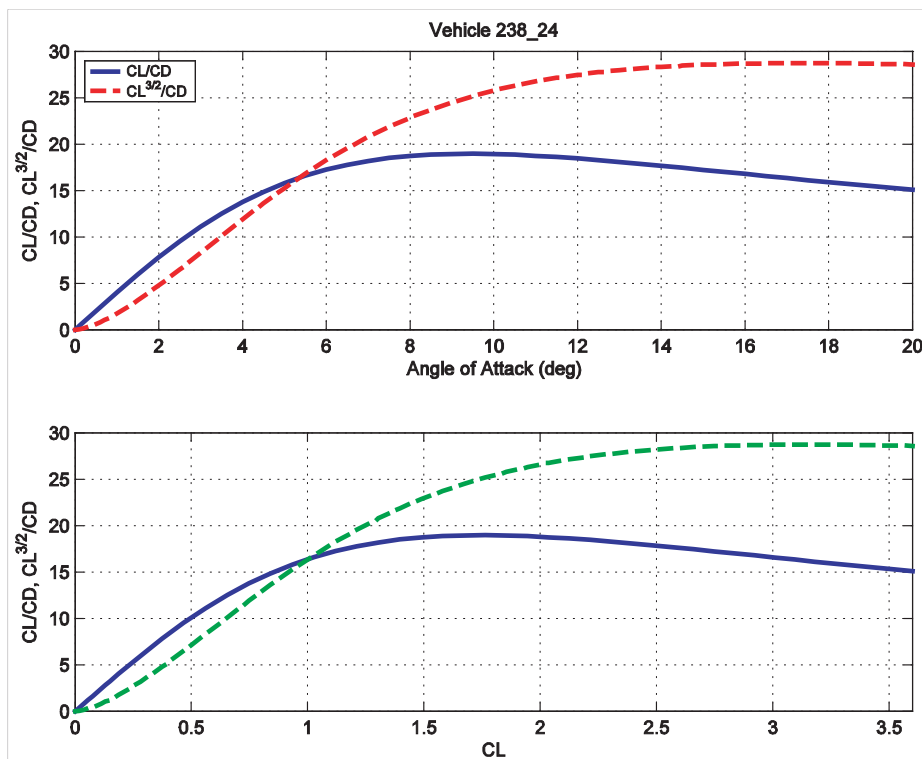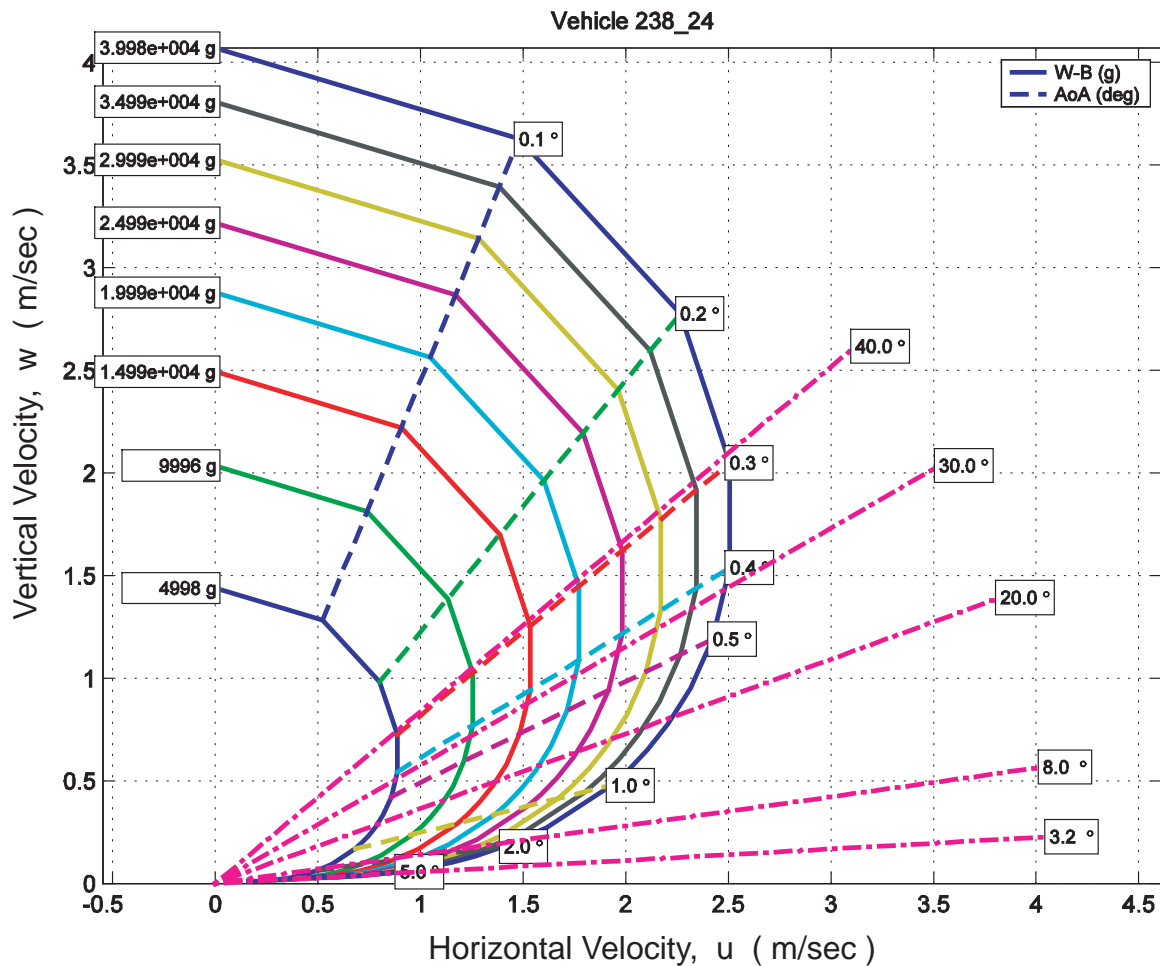
Figure 9.11. Glide Polar (upper), lift drag ratio and endurance ratio verses angle of attack (middle) and verses lift coeffiecent (bottom) for single payload flying wings. Root Cord = 1.0 m, Root Section Thickness = 0.29 m, Span = 4.58 m, Wing Area = 2.61 m2, and Volume = 172.7 liters.

Figure 9.12. Glide Polar (upper), lift drag ratio and endurance ratio verses angle of attack (middle) and verses lift coeffiecent (bottom) for single payload flying wings. Root Cord = 2.10 m, Root Section Thickness = 0.61 m, Span = 9.60 m, Wing Area = 11.52 m², and Volume = 1,566 liters.

Figure 9.13. Glide Polar (upper), lift drag ratio and endurance ratio verses angle of attack (middle) and verses lift coeffiecent (bottom) for single payload flying wings. Root Cord = 4.59 m, Root Section Thickness = 1.32 m, Span = 20.99 m, Wing Area = 55.14 m2, and Volume = 15,532 liters.

wing outside the cylindrical pressure hull shown in Figure 6.8. For more conventional non-pressure compensated batteries placed inside the pressure hull, lung capacity factors of $0.007 < n_b < 0.07$ are within present technology capabilities. In this range the maximum cross country speed capability of the largest heavy payload flying wings (eg, $V_0 = 622,408$ liters) is more like $u_{max} = 3.9$ m/sec, or about 57% of the high-speed performance shown by the purple glide polar line in Figure 9.13 for the densely-packed single payload wing. For lung capacity factors n_b typical of conventional buoyancy engines, the maximum along course speeds vary from as little as $u_{max} = 0.185$ m/sec at a loaded mass of $M = 100$ g for the 37 liter flying wing vehicle (Figure 9.9), to a $u_{max} = 2.7$ m/sec at a loaded mass of 10 kg for a 1,500 liter vehicle (Figure 9.12). In these plots the loaded mass, M, is varied by an order of magnitude with each value indicated in grams in the rectangular boxes along the $u = 0$ axis. A summary comparison of u_{max} versus loaded mass is found at the end of this section in Figure 9.15 for the flying wing versus other glider types evaluated. In all cases the maximum along course speed for the flying wing was obtained at a glide path angle of $\beta = -35°$, but the angle of attack varied from $\alpha = 0.4°$ for the smallest wings to a lower $\alpha = 0.3^0$ for the intermediate to large wings . Regardless of size the pitch angle is steeply nose-down in a descending glide (-34.6° to -34.7°).

For the heavy payload flying wings, cruise speeds are intermediate between best L/D speed and u_{max}, and use an angle of attack on the order of $\alpha = 0.5°$ along a glide path angle of $\beta = -20°$, giving a 19.5^0 nose-down pitch angle during a descending glide. This flight attitude was matched with depth unlimited roaming for payload hauls in the mid to upper end of the speed envelope. Typically large, bundled payload cruise speeds range from 0.25 m/sec for the 62 liter legacy scale glider at $M = 400$ g , to 2.2 m/sec for the 62,226 liter glider loaded to $M = 400$ kg; and ultimately 3.3 m/sec for the largest glider of this type at $V_0 = 622,408$ liters for $M = 4,000$ kg. Spreadsheet analysis gives the following interpolations of the energy consumption as measured by the net transport economy (NTE) for cruising at a glide angles of $\beta = -20°$ with the large payload flying wing:

```
Range = 3500 km , glide angle = 20 degrees
     Vol    Len  Net Buoy u      w    Range  Total_Pwr   NTE    Re         Cd
    Liter    m    Liter  cm/s   cm/s    km       MJ            Vol^1/3  Vol^2/3
     65.6   0.7    0.15  18.7    6.8   3500     16.3    3.16 6.7e+004   0.156
    163.4   1.0    1.50  47.9   17.4   3500     46.8    0.91 2.3e+005   0.129
   1365.0   2.0   15.00  82.3   30.0   3500    424.1    0.82 8.1e+005   0.107
  13409.3   4.4  150.00 127.7   46.5   3495   4205.2    0.82 2.7e+006   0.097
 133866.9   9.4 1500.00 189.2   68.9   3495  42030.4    0.82 8.6e+006   0.095
```

```
Range = 500 km , glide angle = 20 degrees
    Vol     Len   Net Buoy u        w    Range  Total_Pwr   NTE    Re        Cd
   Liter     m     Liter  cm/s    cm/s     km       MJ             Vol^1/3  Vol^2/3
    32.1    0.6    0.15   23.8     8.7     500      1.8      2.49 6.7e+004   0.156
    52.0    0.7    1.50   70.2    25.6     500      6.3      0.85 2.3e+005   0.129
   312.8    1.2   15.00  134.5    49.0     500     58.3      0.79 8.1e+005   0.107
  2978.3    2.6  150.00  210.9    76.8     500    579.8      0.79 2.7e+006   0.097
 29630.8    5.7 1500.00  312.8   113.9     500   5795.3      0.79 8.6e+006   0.095
```

If the glide path angle during cruise is reduced to β = - 8° by increasing the angle of attack to α =+ 2° then the cruise speed of the heavy payload flying wing slows down while the net transport economy improves (gets smaller):

```
Range = 3500 km , glide angle =  8 degrees
    Vol     Len   Net Buoy u        w    Range  Total_Pwr   NTE    Re        Cd
   Liter     m     Liter  cm/s    cm/s     km       MJ             Vol^1/3  Vol^2/3
    67.3    0.7    0.15   12.2     1.7    3501     17.0      3.30 4.2e+004   0.162
    89.3    0.8    1.50   36.6     5.1    3501     21.0      0.41 1.4e+005   0.150
   609.0    1.6   15.00   68.7     9.7    3501    161.2      0.31 4.9e+005   0.119
  5868.6    3.3  150.00  109.3    15.4    3501   1584.9      0.31 1.7e+006   0.103
 58485.5    7.1 1500.00  164.4    23.1    3501  15830.7      0.31 5.4e+006   0.099


Range = 500 km , glide angle = 8 degrees
    Vol     Len   Net Buoy u        w    Range  Total_Pwr   NTE    Re        Cd
   Liter     m     Liter  cm/s    cm/s     km       MJ             Vol^1/3  Vol^2/3
    32.3    0.6    0.15   15.6     2.2     498      1.9      2.58 4.2e+004   0.162
    43.9    0.6    1.50   46.4     6.5     498      2.8      0.38 1.4e+005   0.150
   211.8    1.1   15.00   97.6    13.7     498     22.5      0.31 4.9e+005   0.119
  1967.5    2.3  150.00  157.3    22.1     498    222.3      0.30 1.7e+006   0.103
 19513.6    4.9 1500.00  237.0    33.3     498   2220.9      0.30 5.4e+006   0.099
```

On the other hand, the small payload, flying wing gliders were given slower cruise speeds at a glide slope of β = −3.2° that approach (but do not reach) best L/D speed in depth limited environments. Limitations in the present control systems technology are ignored for the high angle of attack flight. The spreadsheet analysis was re-configured to accept an angle of attack α = 8° giving a β = −3.2° glide slope with a range of cruise speeds that vary from 0.07 m/sec for a 37 liter flying wing to 1.6 m/sec for a 15,500 liter glider. The net transport economy (NTE) of the single payload flying wings were interpolate in spreadsheet analysis from the modeled glide polars in Figures 9.9 through 9.13 and found for β = −3.2° to be:

```
Range = 3500 km , glide angle = 3.2 degrees
    Vol     Len   Net Buoy u        w    Range  Total_Pwr   NTE    Re        Cd
   Liter     m     Liter  cm/s    cm/s     km       MJ             Vol^1/3  Vol^2/3
    36.9    0.6    0.15    7.1     0.4    3500      3.7      4.99 2.0e+004   0.297
    42.3    0.6    1.50   21.6     1.2    3500      2.1      0.28 6.3e+004   0.289
   172.3    1.0   15.00   50.6     2.8    3500      9.4      0.13 2.4e+005   0.207
  1566.1    2.1  150.00   96.5     5.4    3500     89.0      0.12 9.4e+005   0.130
```

Vol	Len	Net Buoy	u	w	Range	Total_Pwr	NTE	Re	Cd
15532.1	4.6	1500.00	142.6	8.0	3500	887.2		0.12 3.0e+006	0.129

Range = 500 km , glide angle = 3.2 degrees

Vol Liter	Len m	Net Buoy Liter	u cm/s	w cm/s	Range km	Total_Pwr MJ	NTE	Re Vol^1/3	Cd Vol^2/3
36.6	0.6	0.15	7.3	0.4	501	3.6	4.85	2.0e+004	0.282
42.0	0.6	1.50	23.9	1.3	501	2.0	0.27	6.9e+004	0.237
172.3	1.0	15.00	56.0	3.1	501	9.3	0.13	2.6e+005	0.169
1566.1	2.1	150.00	97.9	5.5	501	89.0	0.12	9.5e+005	0.127
15532.1	4.6	1500.00	155.4	8.7	501	887.2	0.12	3.2e+006	0.109

Flight at minimum sinking rates would range from $w = 0.008$ m/sec for the 37 liter glider at $M = 100$ g , to $w = .1$ m/sec for the 15,500 liter glider at $M = 100$kg.

9.4 Pitch Stability, Winged-Bodies of Revolution versus Flying Wings:
Figure 9.14 compares the dependence of the pitching moment coefficient, C_M, on the lift coefficient C_L for the two variants of the winged-body of revolution and for the flying wing. Since the lift coefficient at lowest order is $C_L \sim K_L\alpha$, where $K_L = 2\pi$ $(1-2/Nr)$, the moment coefficient for all three basic configuration of vehicles is found to vary linearly with angle of attack, α, over all speed ranges up to u_{max} shown in Figure 9.15. Although C_M increases with increasing vehicle size the linear response of C_M to changes in C_L means that the pitch stability of these designs is well behaved within the operational speed regime of these calculations. There is no apparent departure from this linear behavior at high values of lift coefficient, as would be flown at best L/D speed. Therefore, the demands placed on the control system ought to be manageable, (see Section **11).**

9.5 Hybrid Glider: This class of vehicle is posed for applications requiring level flight for proper sensor or operations in very shallow water (eg harbors) with requirements of burst speed capability. The Hybrid glider is based on the Slocum Electric fitted with an aft mounted propeller to be used 10% of the mission on-station time. Because this vehicle is nearly identical in shape and dimensions to the winged body of revolution for single payloads, the glide polar data from Figures 9.1 through 9.3 are used for hydrodynamic input to the spreadsheet analysis of energetics and transport economy.
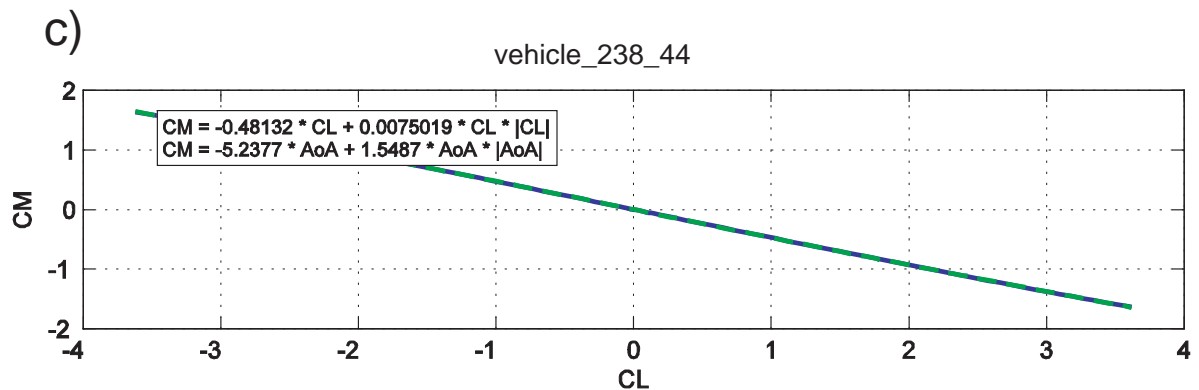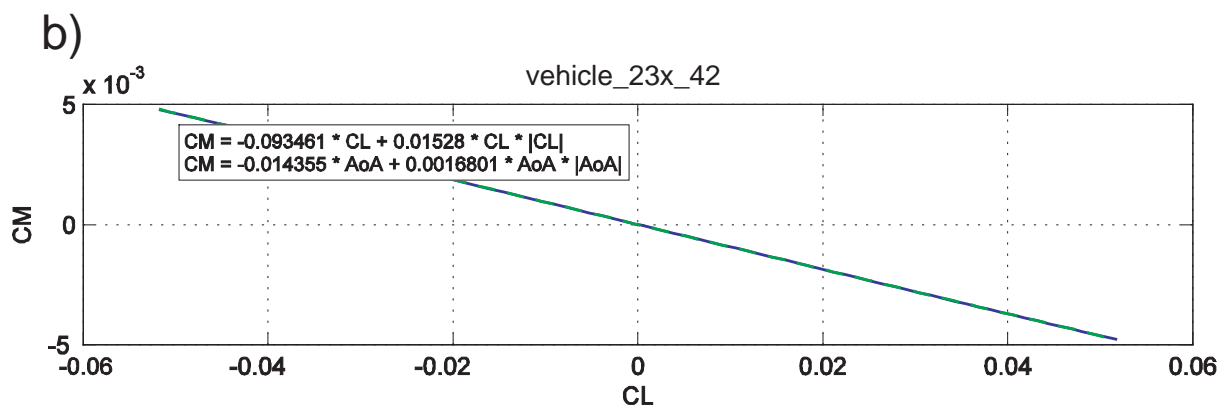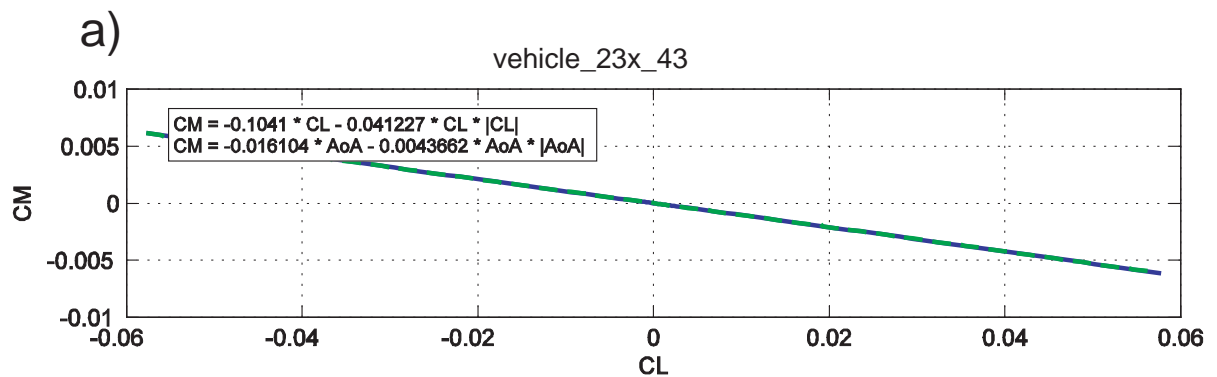
To determine the energy budget for the Slocum Hybrid, the following assumptions were made regarding ingress into a level flight mission area:

Range = 500 Km

Profile depth = 100 m

Dive angle = 33°

Glider constraints such as velocity, dive angle, payload and displacement are defined. Mission time and cycle number are then determined. The glider is then

Figure 9.14. Variation of moment coefficient, C_M vs lift coefficient, C_L for:
a) 2,000 liter winged-body-of-revolution for small (single) payloads;
b) 55,000 liter winged-body-of-revolution for heavy (mixed) payloads;
c) 15,000 liter flying wing for heavy payloads,
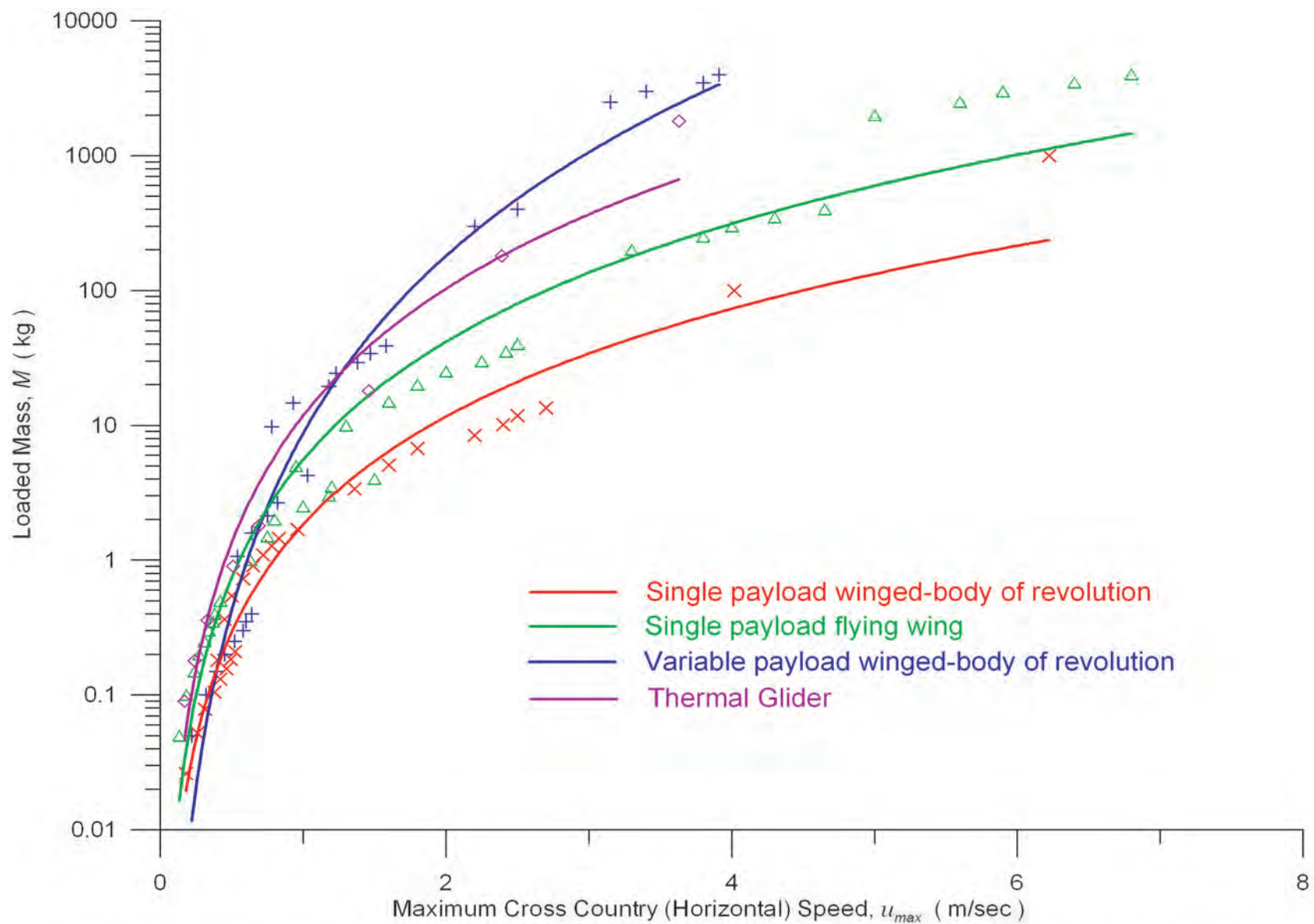
Figure 9.15. Maximum cross country (horizontal) speed for an underwater glider due to variation in the loaded mass ($M = B / g$) for winged-body of revolution carrying single (small) payloads (red); winged-body of revolution carrying bundled (large) payloads (blue); and the flying wing carrying single (small) payloads (green); thermal glider in winged-body-of-revolution configuration with single payload (purplr).

 divided into subsystems with known power consumption for a given cycle. The total power can then be determined based on average current used and voltage provided by the battery sources. Energy is then determined from the total power and the mission time.

Hull weight scales with volume. Pump size and power scale with buoyancy drive required. In addition, propeller size increases with required propeller thrust. The propeller is assumed on for 10% of the mission time with an efficiency of 70%. The required speed of the propeller is calculated as 3* glide velocity. The drive force of the glider is a function of the glide angle and is the axial component of the buoyancy desired. The thrust of the propeller is a function of the propeller diameter, the glider velocity and the propeller velocity. The propeller diameter is assumed equivalent to the hull diameter and scaled with volume maintaining a constant L/D ratio. Payload weight is fixed. The rest of the weight is assumed to be in the alkaline batteries and the propeller drive. Energy consumption is based on scaled hotel load, propeller load and additional pump load used to drive the buoyancy change. The propeller load is a function of thrust, propeller velocity and efficiency. Volume is calculated for the scaled buoyancy and the additional batteries needed for the given range. Velocity is then calculated based on the estimated volume and the Cd. Based on these assumptions and computational procedures, the net transport economy at cruise speed as a function of vehicle size is found to vary as a function of vehicle size:

Scale	Volume (Liters)	Net Buoyancy (Liters)	u prop (m/s)	u (m/s)	w (m/s)	Range (Km)	Total Power (Mj)	NTE	Re vol^(1/3)	Cd vol^(2/3)
0.5	37	.11	1.086	0.30	0.20	500	2.2	4.13	4.04E+04	0.062
1	38	.22	1.52	0.42	0.28	500	2.8	2.56	5.78E+04	0.062
2	41	.44	2.095	0.59	0.38	500	3.9	1.79	8.37E+04	0.062
5	50	1.1	3.11	0.87	0.56	500	7.4	1.36	1.42E+05	0.06
10	67	2.2	4.22	1.18	0.77	500	13.7	1.27	2.33E+05	0.059
100	421	22	8.62	2.41	1.57	500	150.8	1.39	1.61E+06	0.049
1000	5335	220	14.86	4.16	2.69	500	2.09E+03	1.94	1.51E+07	0.036
10000	75661	2200	23.64	6.61	4.29	500	3.01E+04	2.79	1.41E+08	0.032

9.6 Thermal Glider: This concept is posed for ultra long range depth unlimited roaming or for high endurance station keeping and is based on the original concept of Webb, et al, (2001). The concept is unique in that it gives the glider the ability of renewing its energy stores by harvesting environmental energy from the heat reservoir of the ocean. This results in minimal energy requirements for running life support systems with implications on vehicle lifetime and added power for sensor packages. Because th

The significance of harvesting the propulsion drive from the temperature differences of the cold deep water and the warmer surface water (available in 80% of the world's oceans) is that the vehicles propulsion is derived at no energy cost. The glider moves forward essentially for free. It then becomes conceivable to think of ranges of 30,000 to 40,000 km, circumnavigating the world.

Thermal propulsion depends on the volume change associated with the state change of a material with a melting/freezing point in the range of ocean temperatures resulting in a change in buoyancy. Heat is absorbed from the warm surface water and rejected to the cooler, deeper water during the vehicle's transit through the thermocline. This transition causes a change of state of an internal working fluid. The change of state of the fluid causes a volume change that provides an adequate change in buoyancy of a vehicle of constant mass to enable it to ascend and descend at a useful speed. This variable buoyancy, derived from environmental energy, is the sole source of glider propulsion power.

The heat pump uses a common state change between liquid and solid. The liquid contracts on freezing, then the expansion on melting exerts a large pressure that is well-matched to oceanic pressures. The heat exchange volume is inside tubes that run the vehicle's length and provide a large surface area for rapid heat flow. The four stages of the thermodynamic cycle are shown Figure 9.16 below.

Environmental energy is harvested by heat flowing into and out of the working fluid in chamber 1, which expands on freezing and contracts on melting.

The resulting work is transmitted around the system by the transfer fluid, typically mineral oil. Chamber 2 is an energy storage accumulator, with the transfer fluid pressurized by nitrogen at a pressure greater than the maximum external ocean pressure.
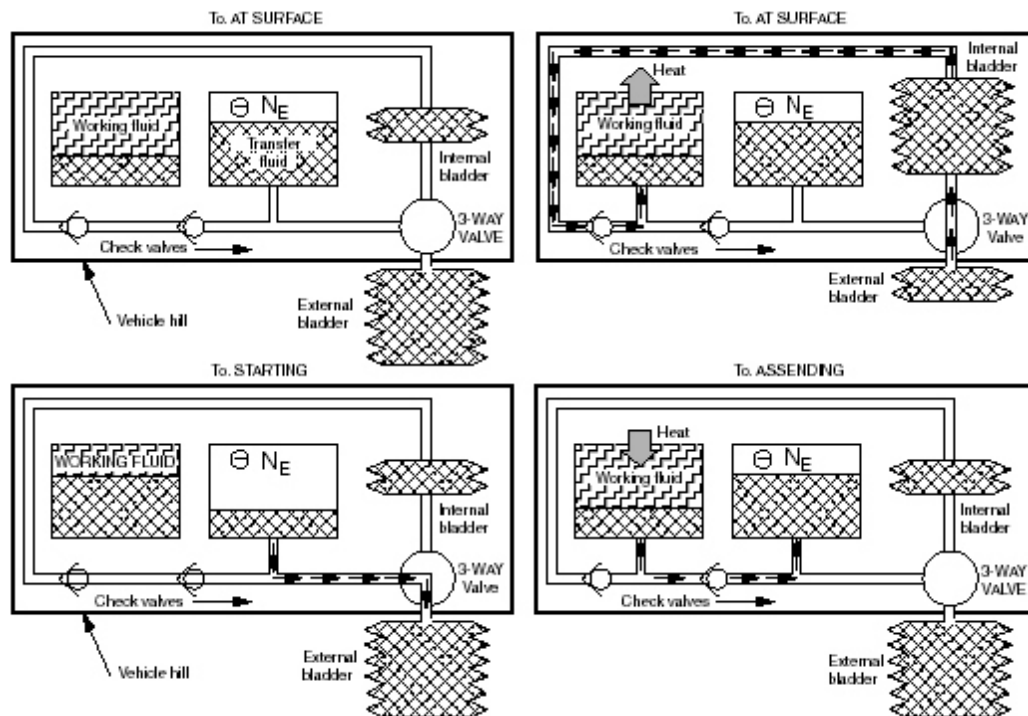
Figure 9.16 Thermodynamic cycle of the thermal glider heat pump (from Webb, et al, 2001)

- In the upper left panel of Figure 9.16 above, the vehicle is in stable thermal equilibrium in the warm surface water, N_2 compressed, external bladder inflated, and working fluid expanded.
- Descent begins by opening the three-way valve (Figure 9.16, upper right panel) venting the external bladder to the internal bladder. Maintaining the hull interior slightly below atmospheric pressure creates the pressure differential for this flow. As the vehicle reaches cold water, heat flows out of the working fluid, which freezes, contracts, and

draws in mineral oil from the internal reservoir.

- The beginning of ascent (Figure 9.16, lower left panel) results from opening the three-way valve, the pressurized oil in the accumulator moves to the external bladder and the vehicle changes from negative buoyancy to positive buoyancy.
- During ascent, (Figure 9.16, lower right panel), the vehicle ascends to warm waters, heat flows into the working fluid, which melts and expands, and oil flows to recharge the accumulator.

Because the thermal glider is nearly identical in shape and dimensions to the winged body of revolution for single payloads, the glide polar data from Figures 9.1 through 9.3 are used for hydrodynamic input to the spreadsheet analysis of energetics and transport economy. To make the transport economy analysis problem tractable the following assumptions were made regarding a long range depth unlimited roaming type of application:

Range = 35000 Km
Profile depth = 1300 m
Dive angle = 33°

Hull weight scales with volume. Thermal engines, oil required and compensator scale with buoyancy drive required. The drive force, (net buoyancy, B), is a function of the glide angle and is the axial component of the buoyancy desired. Payload weight is fixed. Energy consumption is based solely on hotel load. As the mission time decreases with increasing velocity, the total energy needed decreases. Volume is calculated for the scaled buoyancy, scaled thermal engines and scaled oil in bladders and compensator. Velocity is then calculated based on the estimated volume and the C_D. Energy is recalculated based on the new velocity and the volume is re-adjusted.

Scale	Volume	Net Buoyancy	u	w	Range	Total Power	NTE	Re	Cd
	(Liters)	(Liters)	(m/s)	(m/s)	(Km)	(Mj)		vol^(1/3)	vol^(2/3)
0.5	62	0.09	0.17	0.11	35000	18.86	0.61	3.2E+04	0.062
1	64	0.18	0.24	0.16	35000	13.44	0.22	4.6E+04	0.062
2	67	0.36	0.33	0.22	35000	9.65	0.08	6.6E+04	0.062
5	76	0.9	0.51	0.33	35000	6.36	0.02	1.1E+05	0.06
10	91	1.8	0.69	0.45	35000	4.67	7.5E-03	1.7E+05	0.059
100	358	18	1.46	0.95	35000	2.22	3.6E-04	8.8E+05	0.049
1000	3036	180	2.39	1.55	35000	1.35	2.2E-05	5.9E+06	0.036
10000	29809	1.80E+03	3.63	2.36	35000	0.89	1.4E-06	4.2E+07	0.032

Comparing the *NTE* figures above for some of the larger thermal glider size classes with Figure 6.1, it is apparent that the thermal glider is capable of transport economies unmatched by any natural or man-made flyer.

10. Optimal Scale Regimes and Vehicle Configurations

This section is concerned with identifying optimal scale regimes and vehicle configurations that are best suited for satisfying each functional category. To that end a rational design approach is posed for further refinement of vehicle scale and configuration once more specific information is known regarding payload and performance requirements within those functional classes. For the time being, the approach taken herein is to examine the transport economy and speed potential of the 5 basic glider types evaluated in Section 9, identify the scale regime that provides the best tradeoff between size, transport economy and speed, and then match glider types to functional categories on the basis of which set of optimal capabilities are best suited to that functional class.

10.1 Winged-Body-of Revolution for Single (small) Payloads: Figure 10.1 compares the net transport economy (*NTE*) of the single payload winged-body-of-revolution UW glider concept to that of the natural and man-made flyers shown in Figure 6.1. For reference the legacy gliders are shown as a purple triangle when ocean stratification effects are included in the *NTE* calculation, and as a yellow square when they are not. All of the *NTE* values in Figure 10.1 for the single payload winged-body-of-revolution account for ocean stratification at mid latitudes based on a density profile as represented in Figure 6.2. Net transport economy is shown for several different combinations of glide speed, range and diving depth, emphasizing that the achieved transport economy is highly influenced by how the glider is flown. The red curves and triangles represent *NTE* at cruise speeds resulting from $\beta = 20^0$ glide slopes flown between the surface and a 1000m depth over an along coarse range of 3500 km. The blue squares represent the same calculation but for a reduced range of 500 km. The purple line with X's represents *NTE* for the same 500 km glide using $\beta = 20^0$ but with the dolphin glide path confined to a depth limited regime between the surface and 100 m depths. The green line with circles in Figure 10.1 gives the *NTE* for slower more efficient glides flown closer to best L/D speed along a $\beta = 12^0$ glide slope between the surface and 1000 m depth. None of the *NTE* values in Figure 10.1 result from flying as slowly as best L/D speed because of limitations in the present technology control systems during high angle of attack flight, see Section 11.

The first most obvious result in Figure 10.1 is that, regardless of how the glider is flown, a significant improvement in transport efficiency (smaller *NTE*) occurs when the loaded mass exceeds the 100-300 gram regime of the legacy gliders. (The reader is reminded that *NTE* measures energy consumed per unit
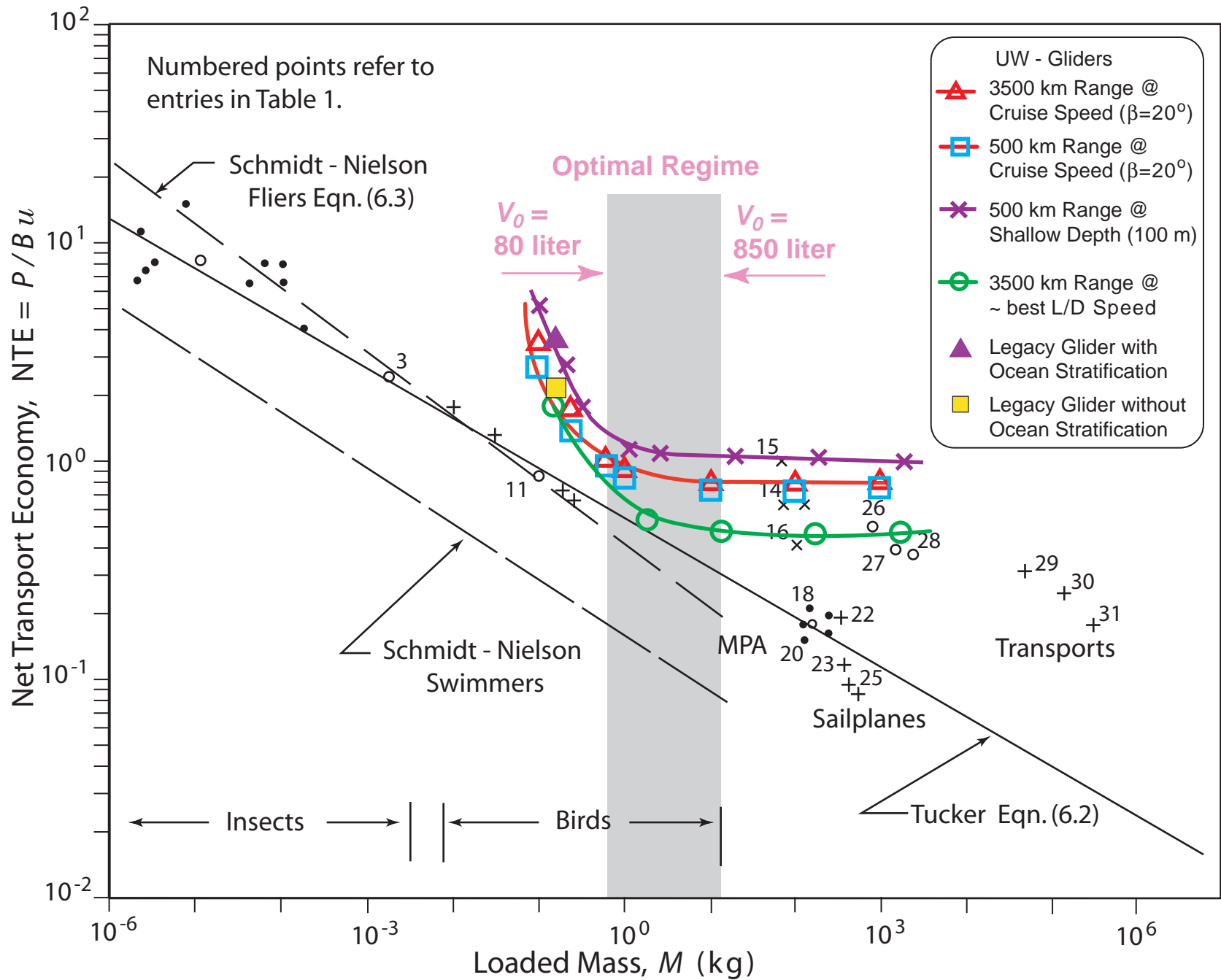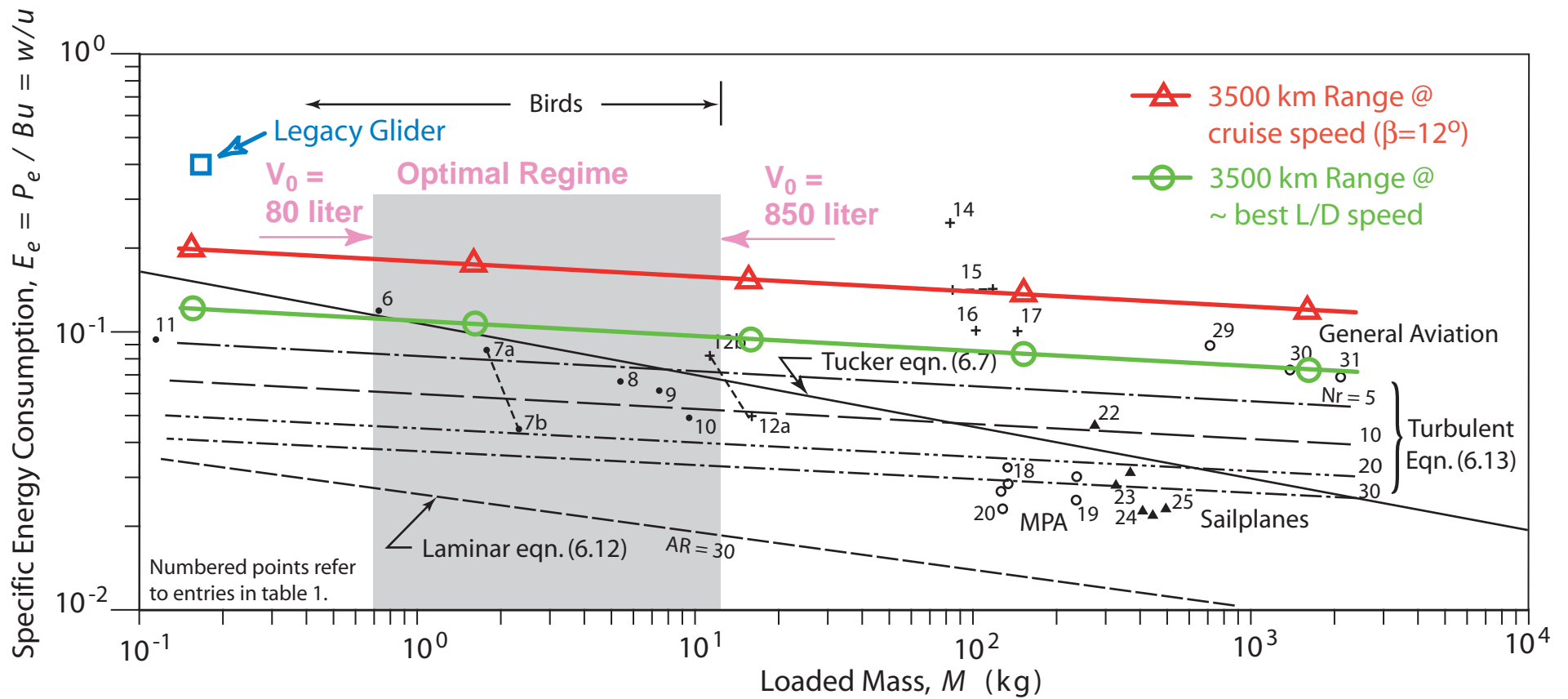
Figure 10.1. Net Transport Economy (NTE) for winged-body-of-revolution underwater glider concept with single payload operating at cruise speed (red) and near best L/D speed (green). Based on total energy (external + internal) consumption with ocean stratification.

immersed weight per meter traveled; hence smaller *NTE* represents more efficient transport). Because loaded mass is directly proportional to vehicle volume by the factor, n_b, this result implies that getting bigger than the legacy gliders gives better transport economy provided the buoyancy engine lung capacity exceeds the critical minimum $n_b \sim 0.37\%$ (see Equation 6.20). As discussed in Section 9.1, the lung capacity of the single payload variant is on the order of $n_b \sim 5\%$, well above this minimum. But the results in Figure 10.1 also indicate that transport efficiency does not improve indefinitely with increasing size. Transport economy improves rapidly with increasing size at the small end of the size spectrum, in part because the small vehicles travel more slowly and the longer duration of a 3500 km glide at these slow speeds leads to much greater energy consumption by the non-flight producing hotel loads. As the vehicle gets bigger and the glider's cross-country speed increases, these hotel loads become a smaller fraction of the total energy consumption. As the vehicle volume approaches $V_0 \sim 1,000$ liters, total energy consumption is dominated by the buoyancy engine pump (see Figure 4.3). Even the small versions of these high pressure pumps that propel the legacy scale gliders achieve a very impressive maximum efficiency 75% to 80% that does not improve significantly with further increases in size. Therefore, once the buoyancy pump dominates the energy budget at around $V_0 = 800 - 1,000$ liters, further increases in size do not improve the net transport economy. All improvements in transport economy that occur in the size regime between the legacy glider and a similar vehicle 20 times larger in volume are due to the hydrodynamic efficiency gains achieved when $n_b > 0.37\%$.

The other most notable improvement in transport economy is obtained by the way in which the glider is flown. Range does not appear to exert a significant effect on *NTE*, but the depth range in which the dolphin glide path is flown does have an effect over all size regimes. Comparing the red versus the purple line in Figure 10.1, it is apparent that energy consumption (*NTE*) increases 30% when the depth excursion of the glide profile is reduced from 1000m to 100m at glide slopes of $\beta = 20^0$. This is due to 2 factors: 1) the glider must penetrate the thermocline a greater number of times over a 3500 km glide profile when the depth excursion range is reduced , and 2) the buoyancy engine pump is less efficient at lower pressures (shallower depths). For Example, the Parker PGP PM5116 high pressure pump has an efficiency of only 23% at a depth of 100m, but increase to an efficiency of 75% at 1000m depth, (see VBD worksheet in Table 7.2). However, the most significant flight factor effecting transport economy is the choice of glide slope, which is simply another way of saying the choice made for cruise speed. Both the red and green lines in Figure 10.1 were the result of 3,500 km glides

using 1000m depth excursions; but the red line was flown at a glide slope of $\beta = 20^0$ while the green line was flown at a slower speed approaching best L/D speed using a glide slope of $\beta = 12^0$. The net transport economy at the slower cruise speed using $\beta = 12^0$ is 40 % less (better) than that obtained by cruising faster at $\beta = 20^0$. This translates directly into 40 % greater gliding range for an equivalent number of dive cycles or 40 % fewer number of dive cycles (and thus less surface exposure) for a given range. Moreover, in the range of loaded mass M ~ 10 kg (V_0 ~ 200 liters) the *NTE* values for the $\beta = 12^0$ glide slope approach those of Tucker's natural flyers (Equation 6.2) which are believed to represent the benchmark of transport efficiency achieved by millions of years of flight engineering by natural selection. But the single payload winged-body-of-revolution UW glider concept is capable of even better. Figures 9.1 –9.3 indicate the best L/D speed is flown at glide angles in the range of $\beta = 7.3^0$ to 8.3^0. Figure 10.2 compares just the component of *NTE* due to flight energy consumption (specific energy consumption, E_e) for 3500 km glides at the $\beta = 12^0$ glide slope (red) versus the best L/D glide slope $\beta = 7.3^0$ to 8.3^0 (green). We find that both are consistent with the slope of the turbulent solution for E_e (Equation 6.13), but that flight energy consumption is 39 % less for glides flown at best L/D speed than those obtained by cruising faster at $\beta = 12^0$. In fact, best L/D speed gives a specific energy consumption 64% less than cruising at $\beta = 20^0$; and that cruising at $\beta = 12^0$ gives E_e that is 41% less than cruising at $\beta = 20^0$, suggesting that nearly all of disparity between the red line and the green line in Figure 10.1 is due to the flight energy component of the net transport economy. If so then gliding the 200 liter small payload UW glider at best L/D speed should yield a *NTE* ~ 0.29, making it the equal of the largest most efficient soaring birds over land. Flying at best L/D speed would yield a 63 % greater gliding range than cruising at the higher speeds of a $\beta = 20^0$ or a similar reduction in numbers of dive cycles over a given range. However, the spreadsheet analysis was not able to make this calculation directly due to the lack of configuration in present control systems to fly at a nose opposite pitch angles relative to the glide slope during high angle of attack flight (see Section 11).

The difference between net transport economy in Figure 10.1 and specific energy consumption in Figure 10.2 gives a measure of the excess energy consumption due to hotel loads and buoyancy engine inefficiencies. Buoyancy engine inefficiency are due to the inefficiency of the pump itself and to the inability at present to recover the energy during the descending glide that was spent overcoming compressibility and penetrating the thermocline on the ascending glide. Inability of
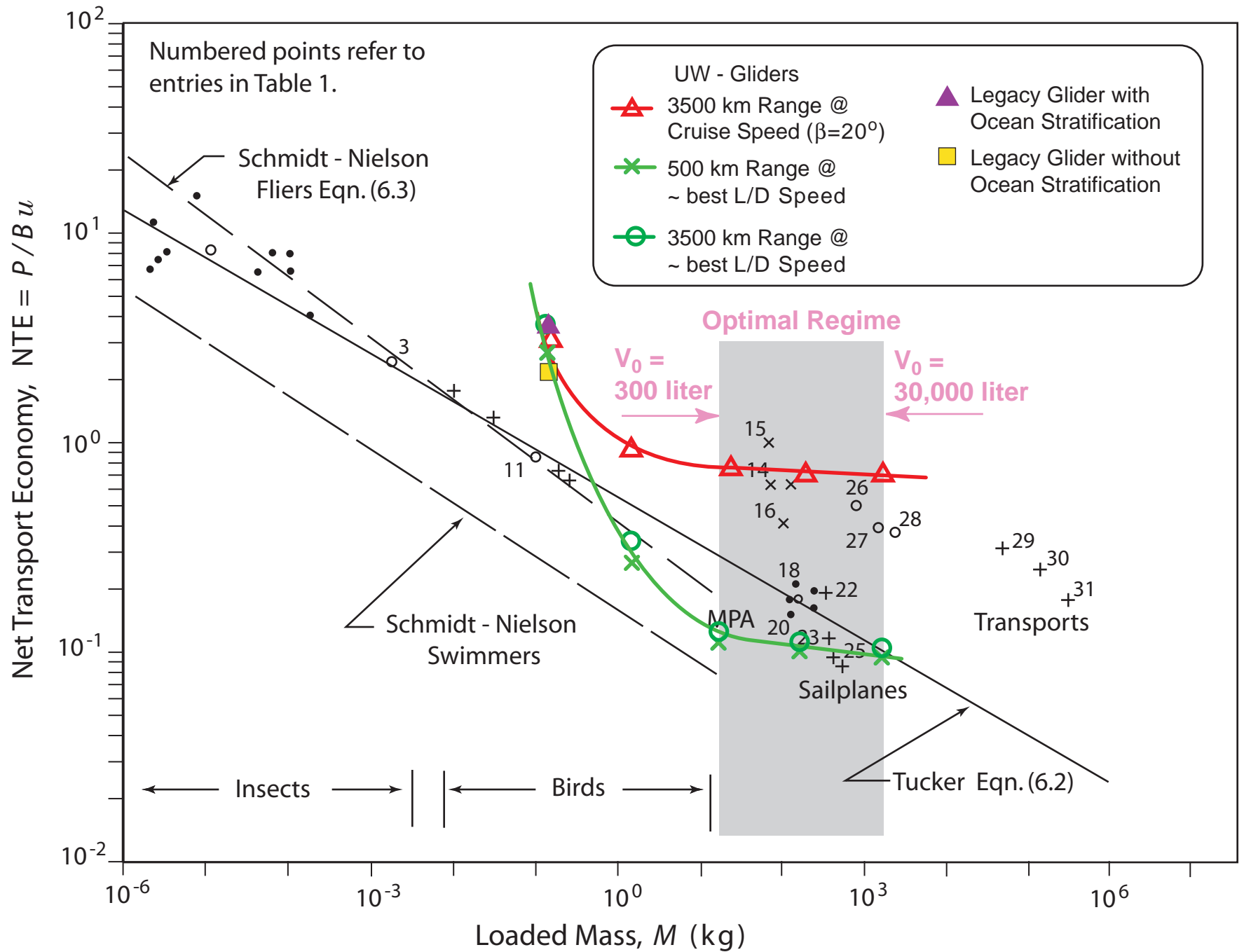
Figure 10.2. Specific Energy Consumption (E_e) for the winged-body-of-revolution underwater glider concept with single payload operating at cruise speed (red) and ~ best L/D speed (green). Based on external energy consumption without ocean stratification.

$$E_e \sim (A_t/A)^{4/7} \, (Nr)^{-2/7} \, (M)^{-1/7} \qquad \textit{pure laminar boundary layer}$$

$$E_e \sim (A_t/A)^{10/19} \, (Nr)^{-8/19} \, (M)^{-1/19} \qquad \textit{pure turbulent boundary layer}$$

Where: A_t = total wetted surface area
A = wing planform area
Nr = wing aspect ratio
M = loaded mass

present buoyancy engines to execute energy recover during the dolphin glide cycle was estimated in Section 6.1 to increase energy consumption by 30 % . At the small end of the size spectrum hotel loads and buoyancy engine inefficiencies account for 90 % of the total energy consumption. With buoyancy engine energy recovery, the figure for hotel consumption and buoyancy engine inefficiency could be reduced to 60% of total consumption. At the large end of the spectrum, hotel loads and buoyancy engine inefficiencies account for 55 % of the total energy consumption. Since hotel loads become a negligible fraction of the energy budget of a large glider, energy recovery technology would reduce excess consumption due to buoyancy engine inefficiency to only 25% of total energy consumption. If energy recovery was incorporated in the buoyancy engine then the theoretical best *NTE* of the optimal 200 liter single payload winged-body-of-revolution UW glider concept would be *NTE* ~ 0.2

The optimal size regime with respect to energetics is given by the locus of points that minimize the difference between net transport economy in Figure 10.1 and specific energy consumption E_e^* of the *optimal flyers* in Figure 10.2. We shall choose Tuckers Equation (6.7) as the rule to define *optimal flyers*, based on the premise that Nature is the ultimate engineering system and the fact that man has had great difficulty equally the efficiency of natural flyers. Calculations of (*NTE* $-E_e^*$) for a glide slope of $\beta = 12^0$ indicate that the optimal size regime of the winged-body-of-revolution configured for a single payload will have a vehicle volume of between $V_0 = 80$ liters and $V_0 = 850$ liters, with the unique minimum in (*NTE* $-E_e^*$) occurring at $V_0 = 200$ liters. It is most interesting that the lowest marginal rate of cost per unit vehicle volume, as estimated from AUV cost data in Figure 6.19, occurs in the range of V_0 ~ 200 - 300 liters. Therefore, this size of single payload winged body of revolution is not only flight efficient, but also likely to be cost efficient.

10.2 Flying Wing for Bundled and Single Payloads : Figure 10.3 compares the net transport economy of the flying wing UW glider concept to the envelope of natural and man-made flyers. The red curves and triangles represent *NTE* of the bundled payload variant at cruise speeds resulting from $\beta = 20^0$ glide slopes flown between the surface and a 1000m depth over an along coarse range of 3500 km. The green line with circles gives the *NTE* of the single payload variant flying slower more efficient 3500 km glides at cruise speeds approaching best L/D speed along a $\beta = 3.2^0$ glide slope between the surface and 1000 m depth. The green X's represent the same calculation but for a reduced range of 500 km. For the purpose of exploring the edge of the envelope, limitations in the present technology control systems are ignored for the high angle of attack flight at a

Figure 10.3. Net Transport Economy (NTE) for flying wing underwater glider concept with single payload operating at cruise speed (red) and near best L/D speed (green). Based on total energy (external + internal) consumption with ocean stratification.

$\beta = 3.2^0$ glide slope. For reference the legacy gliders are shown as a purple triangle when ocean stratification effects are included in the *NTE* calculation, and as a yellow square when they are not. All of the *NTE* values in Figure 10.3 for the single payload winged-body-of-revolution account for ocean stratification at mid latitudes based on a density profile as represented in Figure 6.2. The large payload flying wing at $\beta = 20^0$ in Figure 10.3 has a *NTE* scale relation (red) that is very similar to the small payload winged-body-of-revolution in Figure 10.1 also flying at $\beta = 20^0$. Achieving similar transport economy with a heavier payload is an example of the efficiency advantage of the flying wing derived from the small wetted area ratio, A_t /A. Even more remarkable is that this comparable transport economy is obtained by the heavy payload flying wing using a smaller buoyancy engine, nominally $n_b \sim 0.06\%$ versus $n_b \sim 5\%$ for the single payload winged-body-of-revolution. Both show the rapid improvement in NTE as loaded mass (and vehicle size) is initially raised above legacy glider standards due to the relative decline in hotel loads as the higher cruise speeds of larger vehicles reduce the mission time of a 3500km glide. Both also show a leveling off of NTE at some larger vehicle volume at which the buoyancy engine dominates the energy budget and the pump efficiency limits the achievable NTE. However for the flying wing, this limitation does not set in until larger vehicle volumes, about four times larger than for the single payload winged-body-of-revolution. At this limit, NTE ~ 0.79, while the specific energy consumption at $\beta = 20^0$ is $E_e \sim 0.36$. Hence the percentage of total energy consumption that is attributable to the flight energy of the large payload flying wing is $E_e / NTE \sim 54\%$, while the hotel loads and buoyancy engine inefficiencies account for $(NTE - E_e)/ NTE \sim 46\%$.
The transport advantage of the flying wing becomes especially apparent when the single payload configuration is flown closer to best L/D speed with a larger buoyancy engine, $n_b \sim 9.6\%$, as shown by the green line with circles for 3500 km range and X's for 500 km range. Again, there is very little range dependence of NTE shown over these distances. Flown at $\beta = 3.2^0$, the small payload flying wing is 85% more transport efficient than the large payload flying win cruising at $\beta = 20^0$. This translates directly into 85 % greater gliding range for an equivalent number of dive cycles or 85 % fewer number of dive cycles (and thus less surface exposure) for a given range. The small payload flying wing at $\beta = 3.2^0$ can equal to or exceed the transport efficiency of large birds and high performance man-made vehicles. UW-flying wings ranging in volume from $V_0 \sim 300 - 30,000$ liters are at or below the efficiency benchmark of both Schmidt-Nielsen Flyers (Equation 6.3)

and Tucker Flyers (6.2). The computations seem to support the expectation that reducing the leading order influence of the wetted area ratio A_t/A by copying the shape of natural flyers will achieve comparable transport economy. However this parity with natural flyers is achieved at loaded masses and size regimes that exceed natural flyers, allowing the underwater flying wing to exploit additional scale advantage beyond the structural limitations of birds. However, as the underwater flying wing gets larger, it gives up this advantage to pump efficiency limitations, ocean stratification, and compressibility. Thus there is an upper limit where bigger is not better.

To explore this limit, we investigate the specific energy consumption E_e of the single payload configuration of the flying wing. Figure 10.4 plots the specific energy consumption at best L/D speed in green based on the glide polars in Figures 9.9 –9.13. The result represents the theoretical minimum achievable consumption of flight energy in the absence of ocean stratification and is roughly equivalent to a turbulent wing solution in Equation 6.13 with an aspect ratio of 15-20, (even though the aspect ratio of the analytic surrogate from Figure 6.8 is only 8.5). The minimum E_e of the single payload flying wing (green line in Figure 10.4) remains below the E_e*of the optimal flyers from Tuckers Equation (6.7) until a loaded mass on the order of $M = 10^4$ kg. However, as the wing becomes more transport efficient, a smaller portion of the total energy consumption is due to flight energy, while a larger portion is due to buoyancy engine inefficiency that will not scale according to the green line in Figure 10.4. At a glide path angle of $\beta = 3.2^0$, $E_e \sim$ 0.056 indicating that only 46% of the NTE represented by the green line Figure 10.3 is flight energy. Therefore, the optimal size regime with respect to energetics is given by the locus of points that minimize the difference between net transport economy in Figure 10.3 and the specific energy consumption E_e*of the optimal flyers, even though $E_e < E_e$*. Calculations of (NTE $–E_e$*) for a glide slope of $\beta = 3.2^0$ indicate that the optimal size regime of the flying wing configured for a single payload will have a vehicle volume of between $V_0 = 300$ liters and $V_0 = 30,000$ liters, with the unique minimum in (NTE $–E_e$*) occurring at $V_0 = 1,050$ liters with $M = 100.6$ kg. At this size and wing loading the flying wing has a net transport of economy of NTE ~ 0.12 for glide slopes of $\beta = 3.2^0$. If buoyancy engine enhancements (hardware and software) could facilitate energy recovery from ocean stratification and compressibility effects, then net transport economy might be reduced to a theoretical minimum of NTE ~ 0.09, reducing hotel consumption and buoyancy engine inefficiency to 34% of total consumption, (NTE $–E_e$)/ E_e.
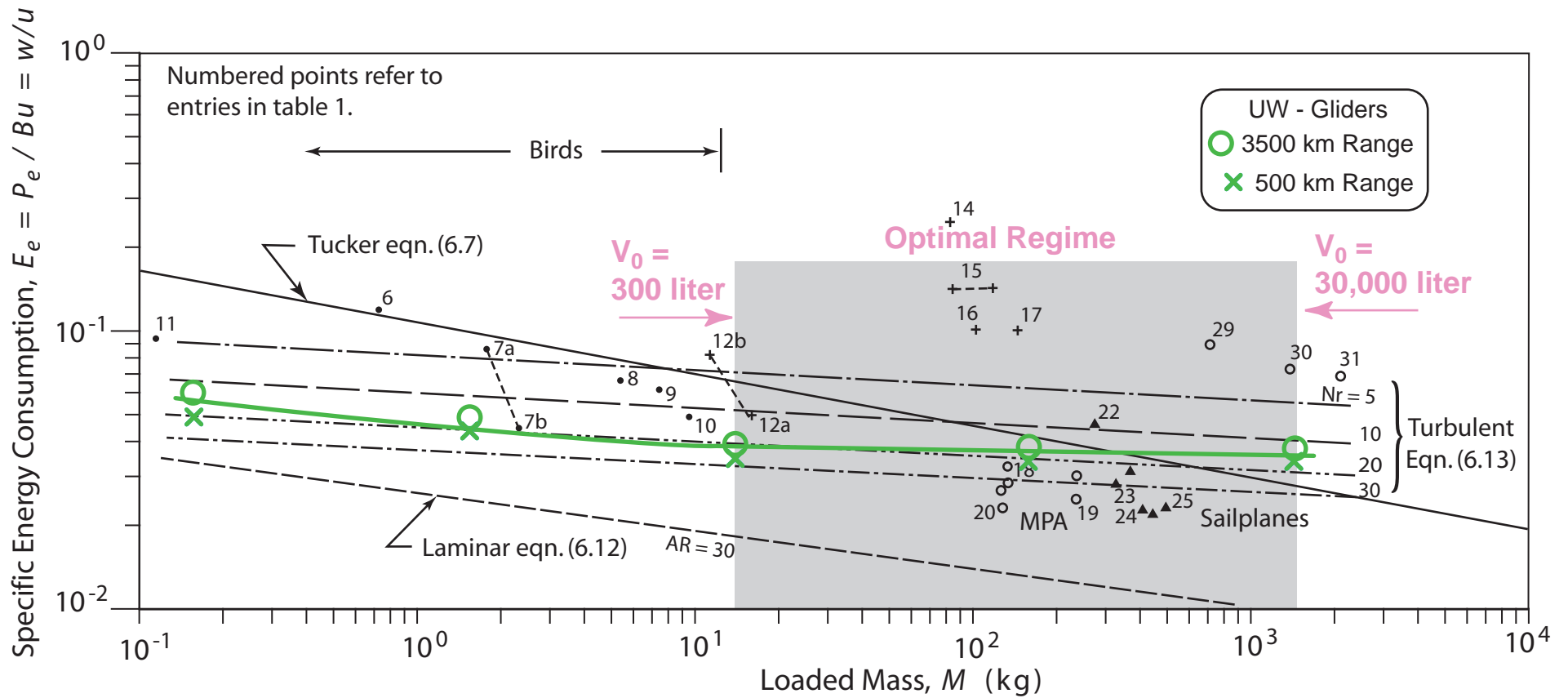
Figure 10.4. Specific Energy Consumption (E_e) for the flying wing underwater glider concept with single payload operating near best L/D speed. Based on external energy consumption without ocean stratification.

10.3 Winged-Body-of Revolution for Bundled (heavy) Payloads: Figures 10.5 through 10.12 present a set of continuous solutions for the vehicle flight profile and energetics as a function of depth excursion and buoyancy volume of the lung, $V_{buoyancy} = n_b V_0$, see Figure 4.3. These computations are based on a glide path angle of $\beta = 20^0$ and a range of buoyancy engine capacity of $0.3\% < n_b < 1.8\%$. Inspection of these figures shows: 1) Net transport economy (NTE) improves (gets smaller) as the depth excursion of the dolphin glide path increases; 2) The number of dive cycles for a given glide range decreases as NTE decreases; and 3) The glide range for a given number of dive cycles increases as NTE decreases. Also, the contours of NTE at small values of $V_{buoyancy}$ Figures 10.8, 10.10 an 10.12 are parallel to the depth axis in a cluster indicating rapid improvement (reduction) in NTE with increasing loaded mass once the buoyancy engine capacity exceeds the threshold, $n_b > n_b^* = .37\%$ from equation (6.20).

Reading Figures 10.8, 10.10 an 10.12 at a depth of 1000m yields Figure 10.13, comparing the net transport economy (NTE) of the bundled payload winged-body-of-revolution UW glider concept to that of the natural and man-made flyers shown in Figure 6.1. For reference the legacy gliders are shown as a purple triangle when ocean stratification effects are included in the NTE calculation, and as a yellow square when they are not. All of the NTE values in Figure 10.13 account for ocean stratification at mid latitudes based on a density profile as represented in Figure 6.2. The red triangles represent NTE at cruise speeds resulting from $\beta = 20^0$ glide slopes flown between the surface and a 1000m depth over an along coarse range of 3500 km. The red line is the Schmidt- Nielsen best fit line to natural flyers (Equation 6.3) offset for ocean stratification and the wetted area ratio of Seaglider ($A_t/A = 19$) $^{10/19}$ per Equation (6.13). The fit is rather good at the smaller end of the size spectrum as the loaded mass initially exceeds the 100-300 gram regime of the legacy gliders, showing that a significant improvement in transport efficiency (smaller NTE) occurs as loaded mass increases. Once the buoyancy pump dominates the energy budget at around $V_0 = 5,000$ liters, total energy consumption no longer scales by the Schmidt-Nielsen type relation and further increases in size do not improve the net transport economy. All improvements in transport economy that occur in the size regime between the legacy glider and a similar vehicle 100 times larger in volume are due to the hydrodynamic efficiency gains achieved when $n_b > 0.37\%$. For $V_0 > 5,000$ liters, the efficiency of the buoyancy pump limits the net transport economy at a $\beta = 20^0$ glide slope to NTE = 0.88. The specific energy consumption at this glide slope is $E_e \sim 0.36$. Hence 41 % of the total energy consumption is due to flight energy spent in overcoming drag, while 59% is due to the hotel loads of the heavy bundled
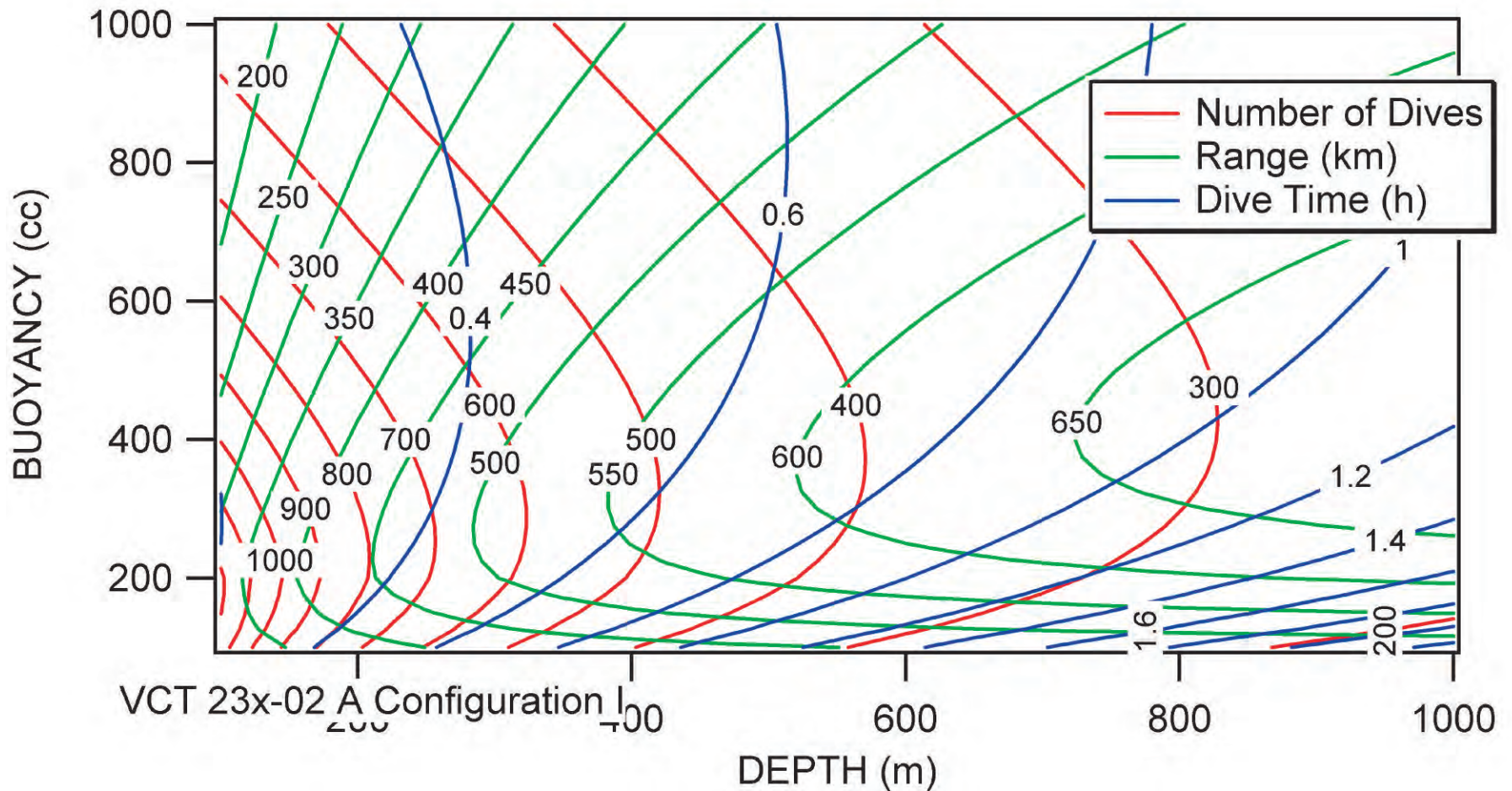
Figure 10.5. Flight Profile envelope for the bundled payload winged-body-of-revolution (The Bus). Iso-contours of number of dives (red), range (green), and dive time (blue) as a function of net buoyancy and depth. Glider Length = 1.83 m, Body Diameter = 0.27 m, Span = 1.09 m, Total Volume = 55.43 liters.
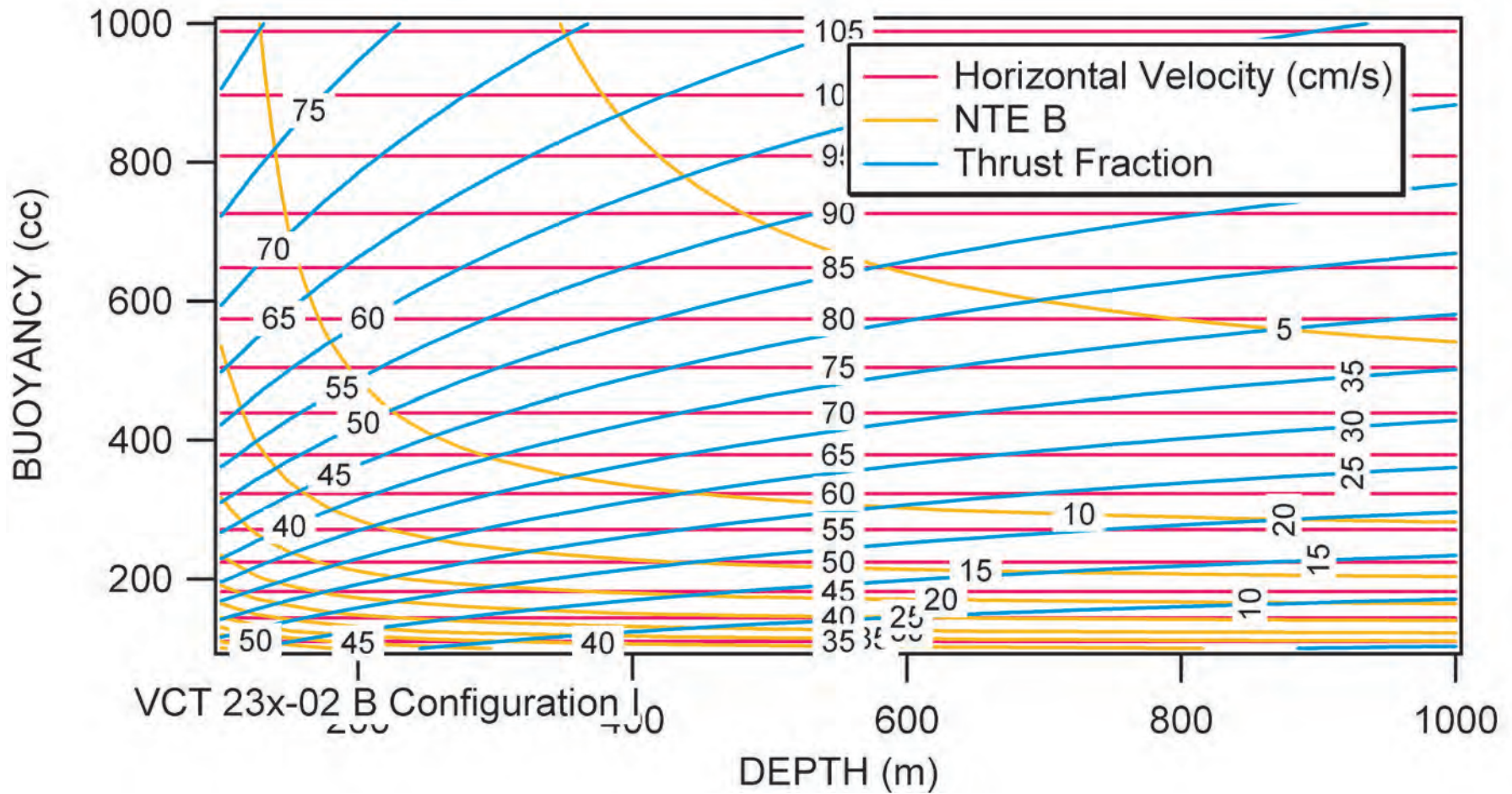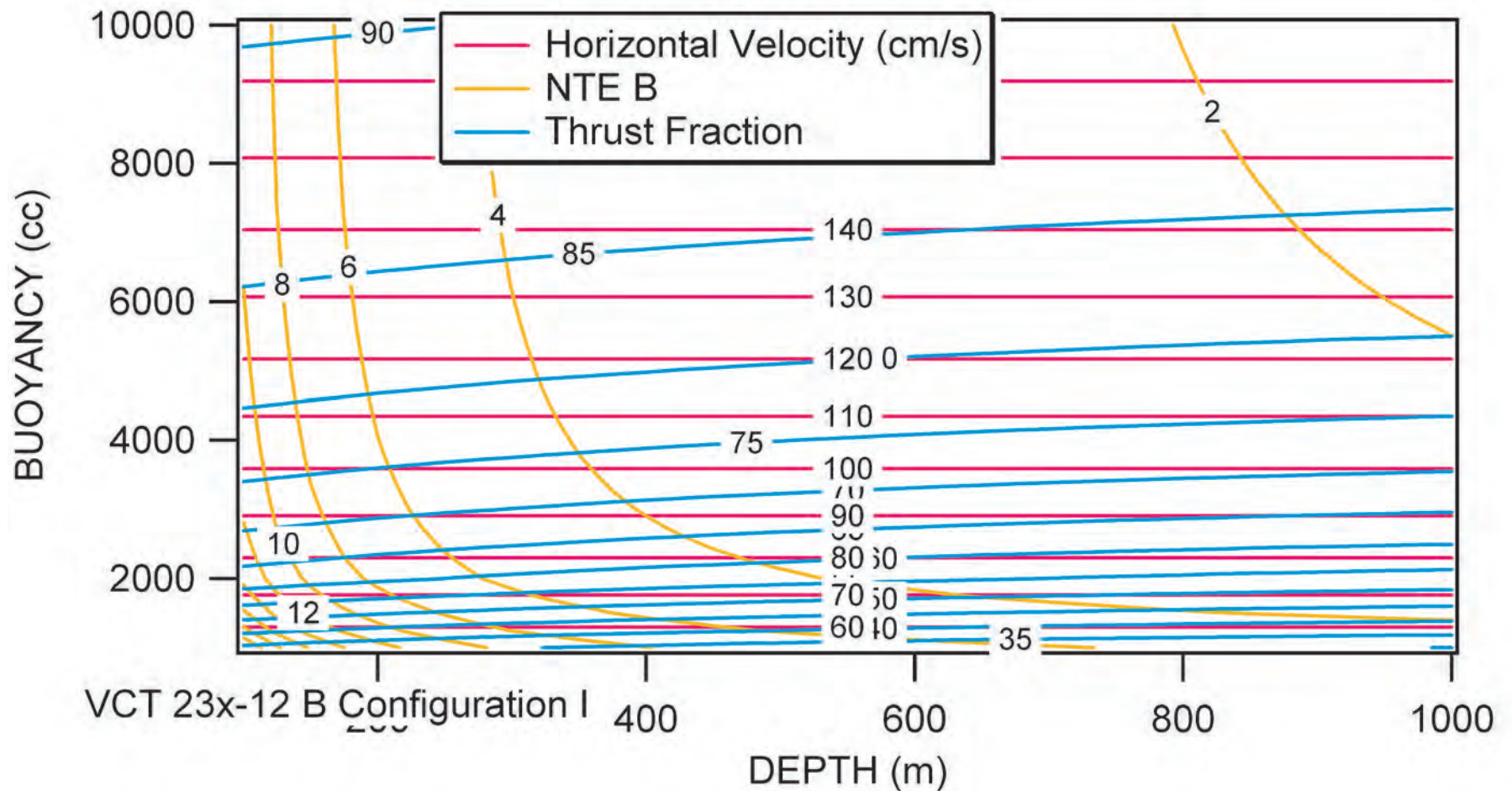
Figure 10.6. Flight profile energetics and cross country speed capabilities of a mixed payload winged-body-of-revolution (The Bus). Iso-contours of cross country speed, u (red), net transport economy (yellow), and percent of total energy consumed by buoyancy engine (blue) as a function of net buoyancy and depth. Glider Length = 1.83 m, Body Diameter = 0.27 m, Span = 1.09 m, Total Volume = 55.43 liters.
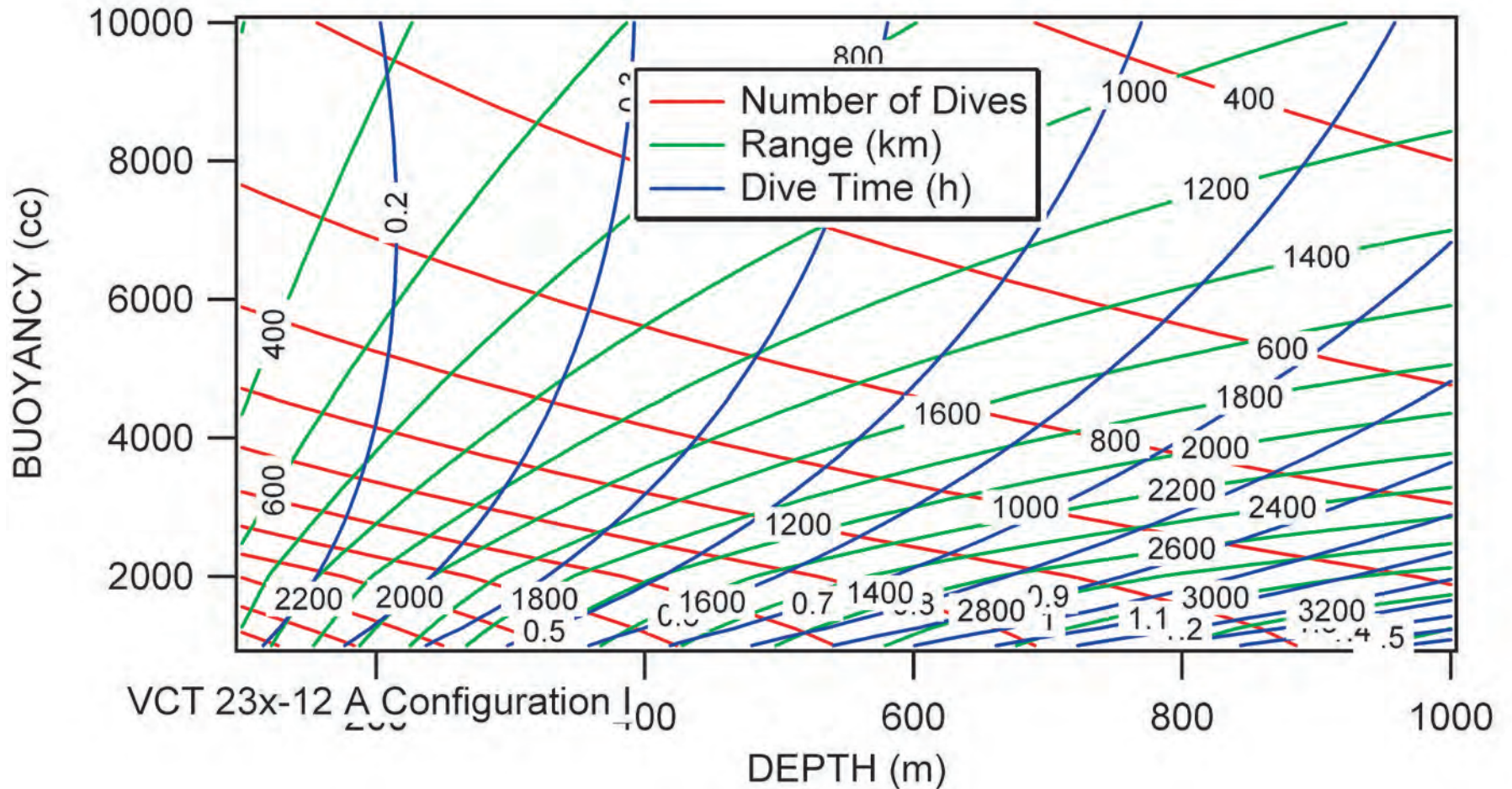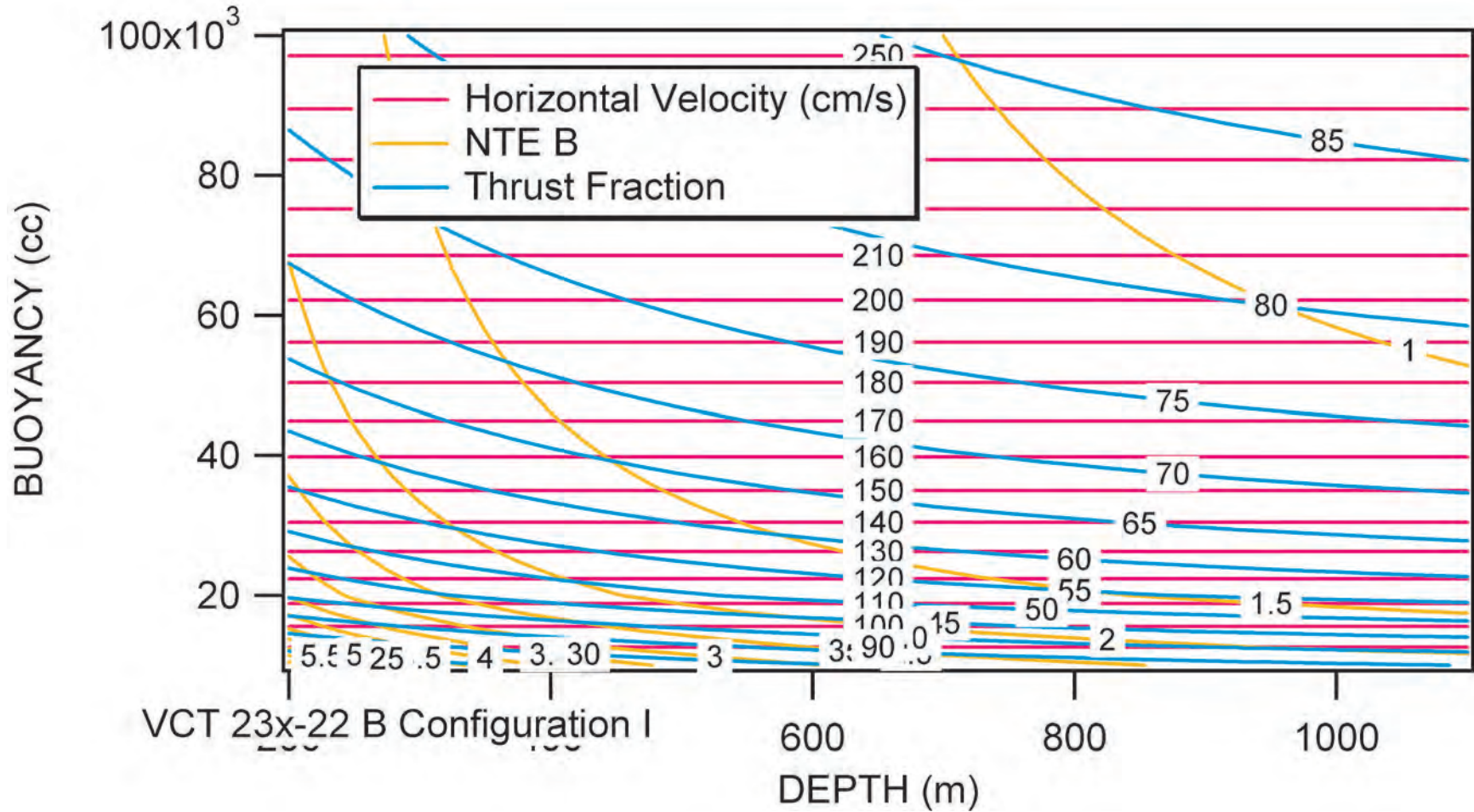
Figure 10.7. Flight Profile envelope for the bundled payload winged-body-of-revolution (The Bus). Iso-contours of number of dives (red), range (green), and dive time (blue) as a function of net buoyancy and depth. Glider Length = 3.94 m, Body Diameter = 0.57 m, Span = 2.35 m, Total Volume = 554.22 liters.

Figure 10.8. Flight profile energetics and cross country speed capabilities of a mixed payload winged-body-of-revolution (The Bus). Iso-contours of cross country speed, *u* (red), net transport economy (yellow), and percent of total energy consumed by buoyancy engine (blue) as a function of net buoyancy and depth. Glider Length = 3.94 m, Body Diameter = 0.57 m, Span = 2.35 m, Total Volume = 554.22 liters.

Figure 10.9. Flight Profile envelope for the bundled payload winged-body-of-revolution (The Bus). Iso-contours of number of dives (red), range (green), and dive time (blue) as a function of net buoyancy and depth. Glider Length = 8.49 m, Body Diameter = 1.24 m, Span = 5.07 m, Total Volume = 5542.9 liters.
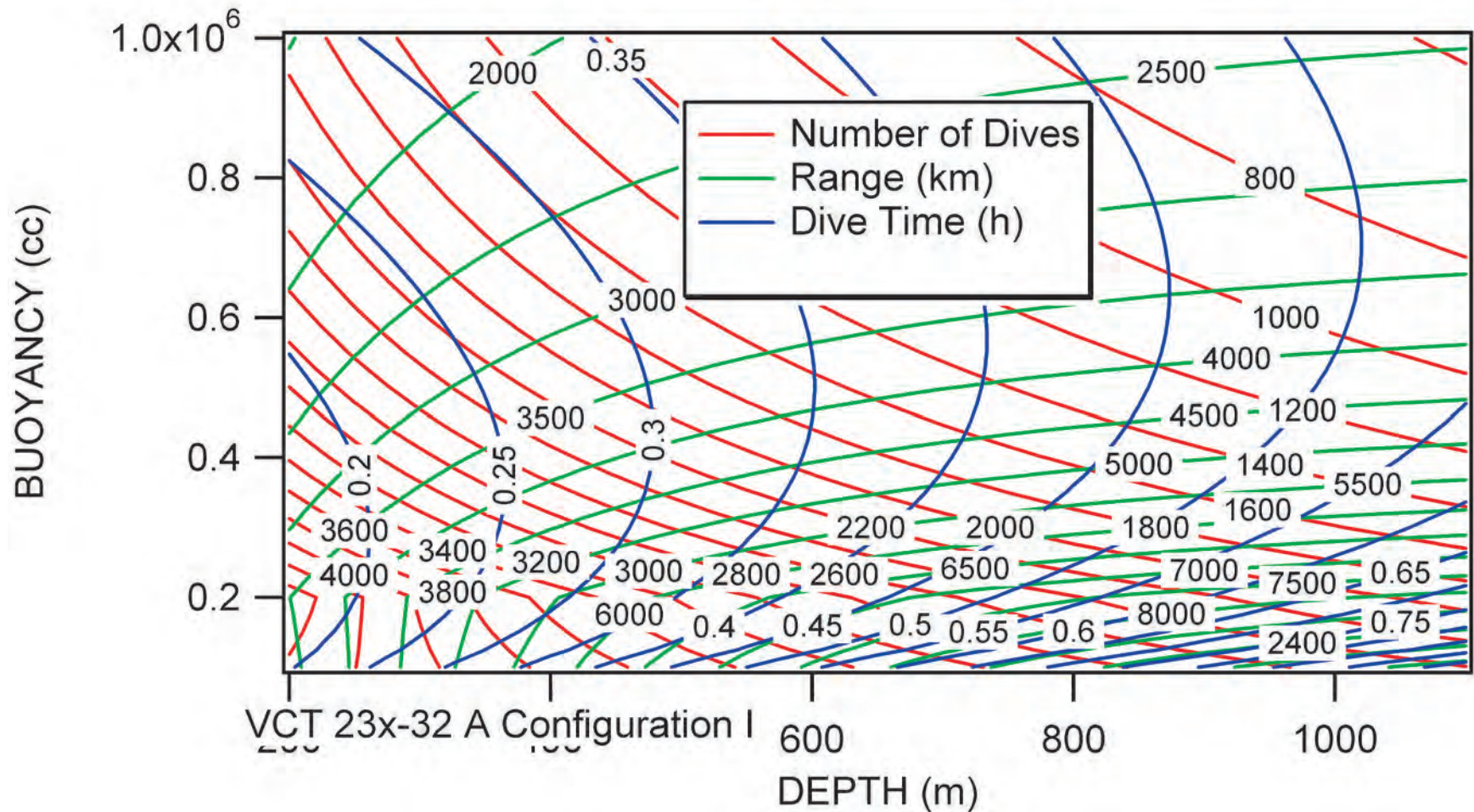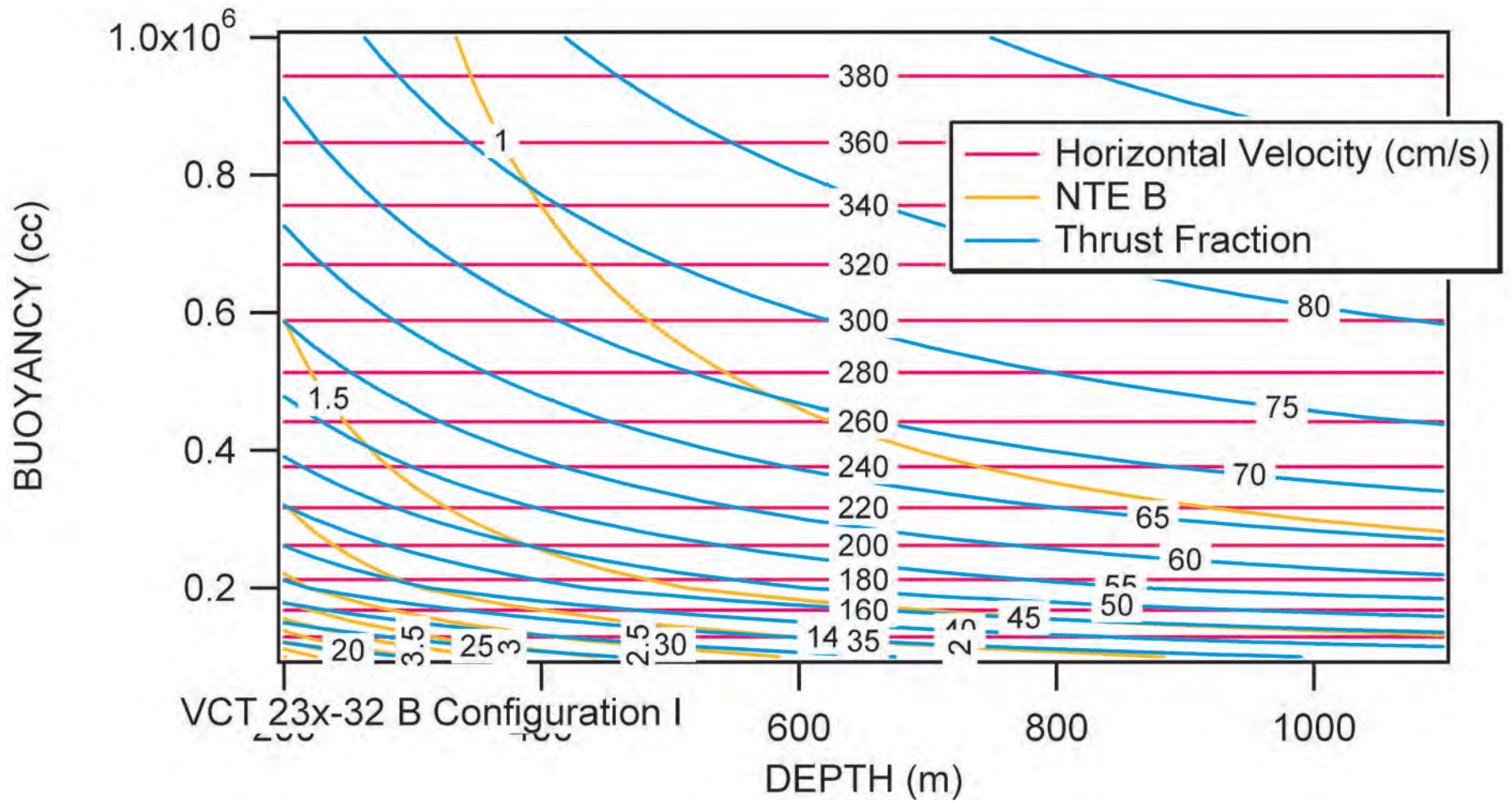
Figure 10.10. Flight profile energetics and cross country speed capabilities of a mixed payload winged-body-of-revolution (The Bus). Iso-contours of cross country speed, u (red), net transport economy (yellow), and percent of total energy consumed by buoyancy engine (blue) as a function of net buoyancy and depth. Glider Length = 8.49 m, Body Diameter = 1.24 m, Span = 5.07 m, Total Volume = 5542.9 liters.

Figure 10.11. Flight Profile envelope for the bundled payload winged-body-of-revolution (The Bus). Iso-contours of number of dives (red), range (green), and dive time (blue) as a function of net buoyancy and depth. Glider Length = 18.28 m, Body Diameter = 2.67 m, Span = 10.92 m, Total Volume = 55416.7 liters.

Figure 10.12. Flight profile energetics and cross country speed capabilities of a mixed payload winged-body-of-revolution (The Bus). Iso-contours of cross country speed, *u* (red), net transport economy (yellow), and percent of total energy consumed by buoyancy engine (blue) as a function of net buoyancy and depth. Glider Length = 18.28 m, Body Diameter = 2.67 m, Span = 10.92 m, Total Volume = 55416.7 liters.

 payloads and the inefficiencies of the buoyancy engine. If the buoyancy engine were equipped for energy recovery, then the theoretical lower limit on energy consumption would be NTE ~ 0.62, of which 58 % would be due to flight energy expenditure. The optimal size regime with respect to energetics is given by the locus of points that minimize the difference between net transport economy in Figure 10.13 and specific energy consumption E_e*of the optimal flyers in Figure 10.2 as defined by Tuckers Equation (6.7). Calculations of (NTE $-E_e$*) for a glide slope of $\beta = 20^0$ indicate that the optimal size regime of the winged-body-of-revolution configured for a heavy bundled payload will have a vehicle volume of between V_0 = 5000 liters and V_0 = 550,000 liters, with the unique minimum in (NTE $-E_e$*) occurring at about V_0 = 50,000 liters.

10.4 Hybrid Glider: Figure 10.14 compares the net transport economy (*NTE*) of the hybrid glider to that of the natural and man-made flyers shown in Figure 6.1. The hybrid glider consists of a single payload winged-body-of-revolution UW glider concept fitted with an aft mounted propeller. For reference the legacy gliders are shown as a purple triangle when ocean stratification effects are included in the *NTE* calculation, and as a yellow square when they are not. All of the *NTE* values in Figure 10.1 for the single payload winged-body-of-revolution account for ocean stratification at mid latitudes based on a density profile as represented in Figure 6.2. The red curves and triangles in Figure 10.14 represent *NTE* at cruise speeds resulting from $\beta = 33^0$ glide slopes flown between the surface and a 100 m depth over an along coarse range of 500 km. Net transport economy is based on a prop-on duty cycle comprising 10 % of the cruise duration, during which the hybrid is assumed to be in level flight. Therefore the average glide slope of the 500 km cruise and glide is $\beta_{ave} = 29.7^0$. The buoyancy engine lung capacity increases with increasing vehicle size, ranging from $n_b \sim 0.37\%$ for the smallest vehicle to $n_b \sim 0.4\%$ for the larger vehicles ($V_0 \sim$ 5,000 liters).

Figure 10.14 shows a well-defined minimum of NTE ~ 1.27 at a loaded mass of about M = 2.2 kg, corresponding to a vehicle volume of about V_0 = 70 liters. For smaller hybrids that fly at slower cruise speeds with smaller lung capacity, the 500 km mission durations are longer leading to larger hotel loads from the payload and correspondingly higher energy consumption (larger *NTE*). In spite of the larger buoyancy engines fitted to the larger hybrid gliders, The *NTE* significantly degrades with increasing size for vehicles large than $V_0 \sim$ 400 liters. This is attributed to the 10 % duty time of the propeller, whose energy consumption overwhelms the energy budget of the glider once $V_0 >$ 400 liters or so. The optimal size regime with respect to energetics is given by the locus of
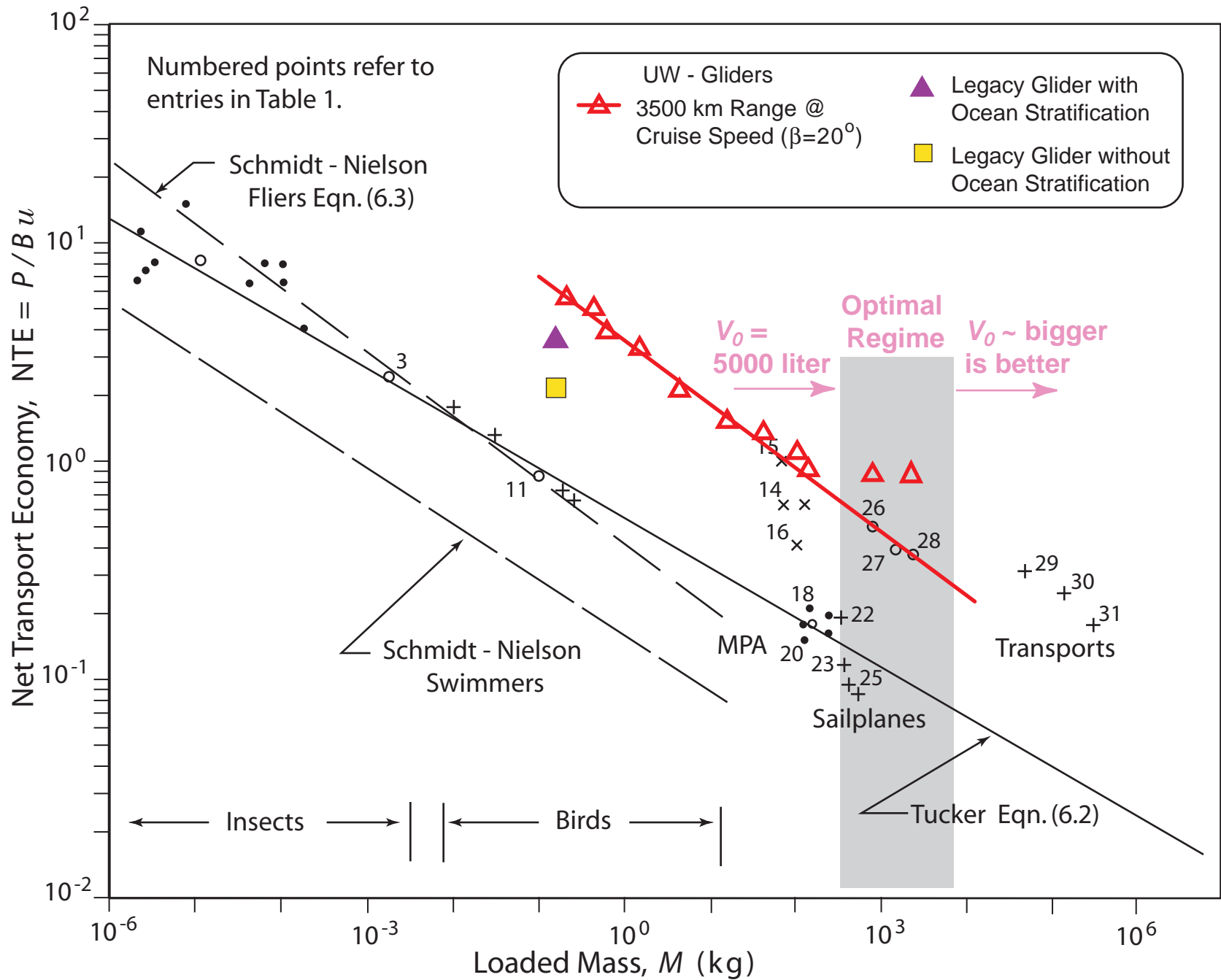
Figure 10.13. Net Transport Economy (NTE) for winged-body-of-revolution underwater glider concept with bundled (heavy) payload operating at cruise speed (red). Based on total energy (external + internal) consumption with ocean stratification.
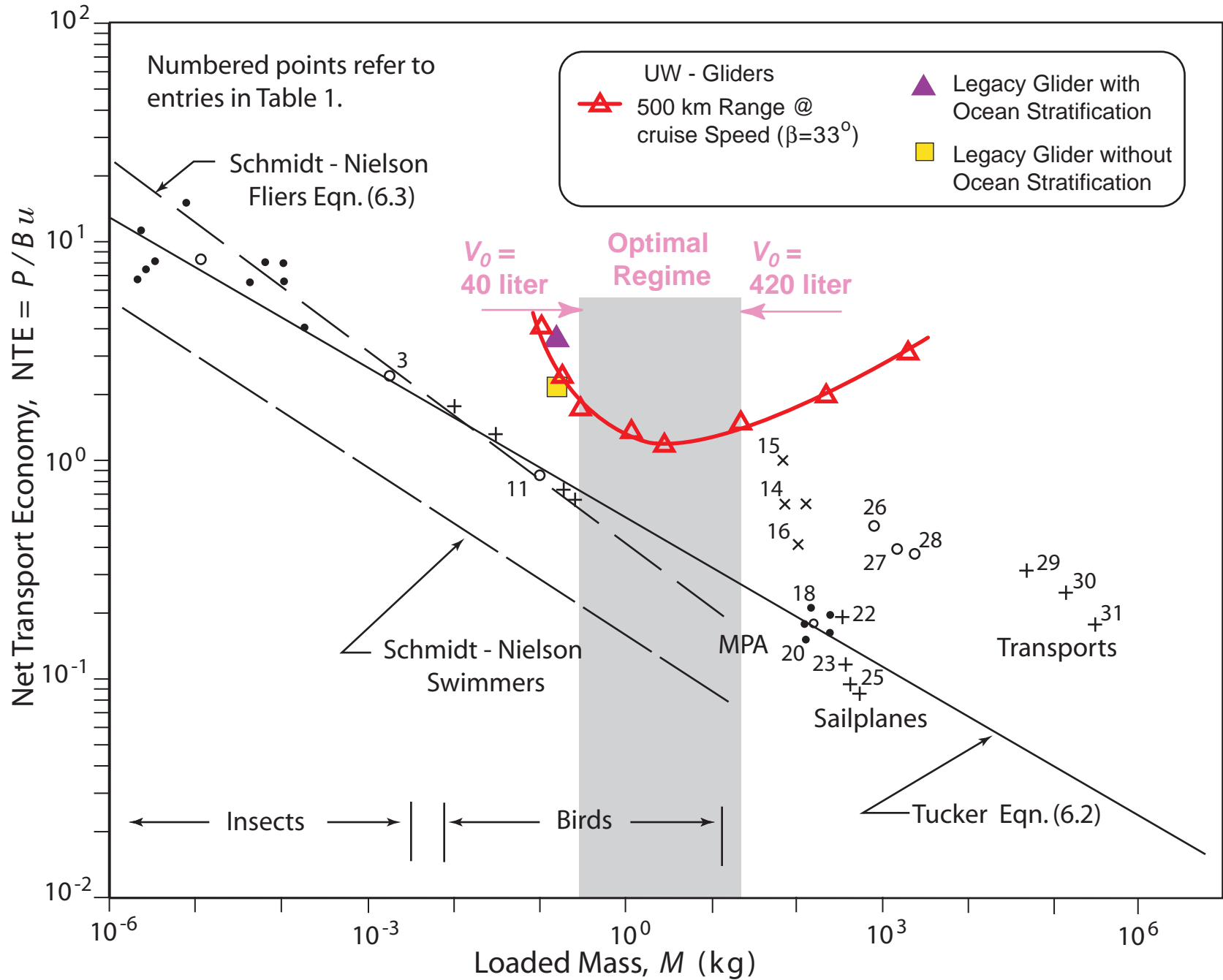
Figure 10.14. Net Transport Economy (NTE) for hybrid underwater glider concept with single payload operating at cruise speed (red). Based on total energy (external + internal) consumption with ocean stratification.

 points that minimize the difference between net transport economy in Figure 10.14 and specific energy consumption E_e* of the *optimal flyers* in Figure 10.2 as defined by Tuckers Equation (6.7). Calculations of ($NTE -E_e$*) for a glide slope of   β = 29.7^0 indicate that the optimal size regime of the hybrid glider configured for a single payload will have a vehicle volume of between V_0 = 40 liters and V_0 = 420 liters, with the unique minimum in ($NTE -E_e$*) occurring at V_0 = 67 to70 liters.

   Since the specific energy consumption at $β_{ave}$ = 29.7^0 is Ee ~ 0.57, then the energy consumed by hotel loads, buoyancy engine inefficiencies and propeller inefficiencies represent 55% of the total consumption at the 70 liter optimal size. If energy recovery technology could be incorporated into the buoyancy engine then those inefficiencies could be reduced to only 38% of total energy consumption.

   10.5 Thermal Glider: The net transport economy of the thermal glider described in Section 9.6 are plotted in Figure 10.15.The calculations are based on a glide slope of β = 33^0 and a 1,300 m depth excursion for a dolphin glide profile over a range of 35,000 km. The buoyancy engine capacity is configured for n_b = 6%, well above the threshold n_b*defined by equation (6.20). Thermal energy extraction is based on mid-latitude stratification as represented in Figure 6.2. For thermal gliders whose volume is V_0 > 70 liters, the *NTE* solution in Figure 10.15 out performs the *optimal flyers* as defined by Tuckers Equation (6.2). In fact the *NTE* of the thermal glider appears to improve indefinitely as the glider's loaded mass (size) increases. Hence the optimal size regime for the thermal glider from an energetics standpoint is any size V_0 > 70 liters , where bigger is better. Optimal size will instead be dictated by other factors such as cost constraints. Figure 6.19 indicates a rapid decline in the incremental cost at V_0 ~ 300 liters.

   Figure 10.15 suggests that the thermal glider approaches a state of perpetual motion with increasing size. For example NTE ~ 10^{-6} for V_0 ~ 30,000 liters, wherein 99.9999% of total energy consumption is hotel loads. The larger thermal gliders are able to drive the buoyancy engine almost entirely from the thermal energy that is recovered. There is no precedent for this among the natural and man made flyers. High performance sailplanes carry water ballast for high speed performance, but they only have capability to reduce the gravity forces (net buoyancy) acting on them by jettisoning ballast, not reverse the sign of those gravity forces the way the thermal glider can. It might be argued that the sailplane harvests energy from land thermals, but is not given credit for that in the accounting of the NTE in Figures 6.1 and 10.15. However, the sailplane does not harvest that energy directly to alter the gravity forces acting on it, rather it harvests the kinetic energy of the updrafts produced by thermal energy. Moreover, thermals
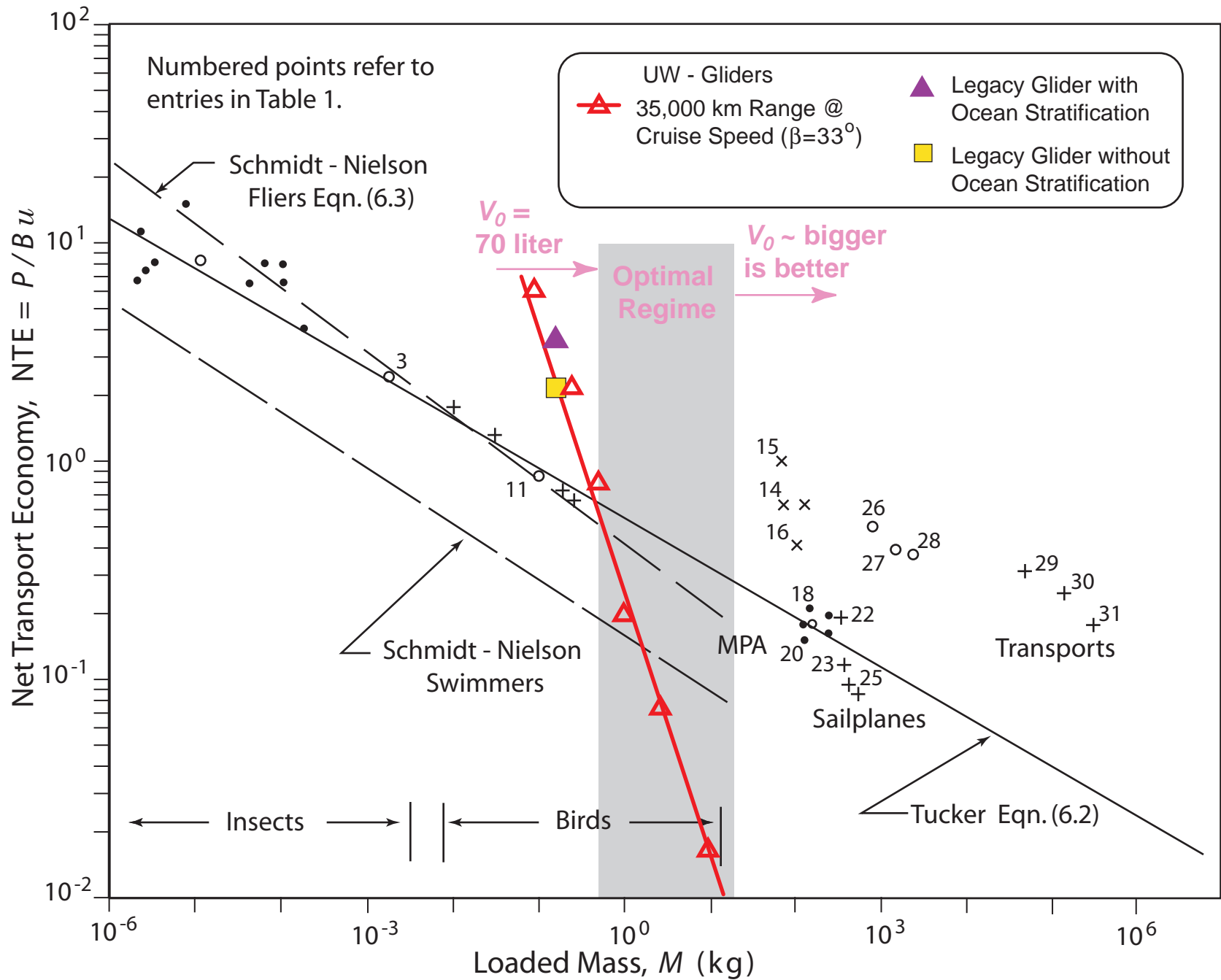
Figure 10.15. Net Transport Economy (NTE) for thermal underwater glider concept with single payload operating at cruise speed (red). Based on total energy (external + internal) consumption with ocean stratification.

over land are not continuous, but rather are discrete columns of warm fluid and are widely dispersed at distances proportional to the thermal height with down drafts in between the thermals that usurp the sailplane's energy. The sailplane must expend considerable energy and time to find thermals and to avoid the intervening downdrafts. Ocean stratification is ubiquitous and can be relied upon to intercept the thermal gliders dolphin glide path during each dive cycle. Hence a steep glide slope is better because it gives more dive cycles per distance traveled in which to harvest energy. Hence the ocean media with it's thermal energy may be considered as a reservoir component of the thermal glider system; and hence it is appropriate to credit that energy to the thermal glider transport system in the *NTE* calculation.

10.6 Comparison of Maximum Cross-Country Speed Capability: Figure 9.15 compares the maximum speed capability of the 4 basic pure glider concepts for the variants considered for vehicle shape and payload capacity. The hybrid glider was omitted from this comparison, although results in Section 9.5 indicate that the prop-on mode of the hybrid (which accounts for 10% of the duty time) ranges from $u_{max} = 1.1$ m/sec for $V_0 = 37$ liters, to $u_{max} = 23.6$ for $V_0 = 75,661$ liters. Therefore, the burst speed capability of the hybrid is quite considerable. In the gliding mode, values of cruise speed tabulated in Section 9.5 indicate that the cross-country speed capability of the hybrid is comparable to the single payload winged-body-of-revolution.

For the pure glider concepts, Figure 9.15 indicates that all the vehicle types become faster as the loaded mass (and hence size) gets bigger, but that the single payload winged-body-of-revolution gives the greatest high-speed performance for any given choice of loaded mass. The variable payload version of the winged-body-of-revolution (*The Bus*) has excessive surface area associated with its large payload capacity body and is consequently the lowest performing vehicle in terms of speed capability. Even though the thermal glider is a single payload winged-body-of-revolution, it has additional body surface area for its heat exchanger, and therefore has a speed capability only slightly better than *The Bus*. The flying wing is intermediate between these cases and achieves exceptionally high speeds for large vehicles (with wing spans between 32 and 68 m). The predominate factor in these high-speed performance comparisons is the percentage of vehicle volume dedicated to the buoyancy engine, (n_b). The two highest performing vehicle types employ the largest amount buoyancy engine lung capacity per unit volume of vehicle, consistent with the expectations of Equation (6.26). The single payload winged-body-of-revolution is configured for $n_b \sim 5\%$ while most of the flying wings in Figure 9.15 use a buoyancy engine lung capacity on the order of $n_b \sim 7\%$.

Because of the large percentage of vehicle volume dedicated to payload space, the variable payload version of the winged-body-of-revolution (*The Bus*) operates at about $1/10^{th}$ the lung capacity, $0.2\% < n_b < 0.7\%$. The net transport economy and specific energy consumption advantage that the flying wing derives from its low wetted area ratio (A_t/A) does not translate into a high speed advantage over the single payload winged-body-of-revolution when both are configured for equivalent n_b. The reasons for this are three: 1) both operate at low angles of attack and at the same low L/D = 1.4 when flying at u_{max}; 2) although the wetted area ratio (A_t/A) of the flying wing is low, the wing area A is large and hence the flying wing's profile drag at low angles of attack is greater; and 3) at low angles of attack and low L/D the single payload winged-body-of-revolution profile drag coefficient (C_{D0}) is low because its large body surface area is co-axial with the flow and surfers little or no cross-flow drag.

The comparative results of Figure 9.15 reveal three basic design rules for maximizing cross-country speed capability of an underwater glider:

1) Design as large a glider as practical within constraints of cost and operational considerations
2) Dedicate the largest percentage of vehicle volume to the buoyancy engine

    lung capacity that is practical within constraints of payload volume
3) Employ a winged-body of revolution configuration with minimized wetted area profiles and minimized profile drag coefficient (C_{D0}) specific to the operational Reynolds number regime

10.7 Rational Approach to Selecting Optimal Size and Configuration (excerpts from Graver, et al, 2003):

The main components of an underwater glider include the external hull, wings and tail, ballast system, computer, payload, control actuators, and an energy source (batteries). Design of an autonomous underwater glider must take several mission requirements into account, including range, mission duration, required speed and payload. Using a design tool such as the University of Washington's glider data spreadsheet gives an initial estimate for glider volume. The glider wings and ballast tanks can then be sized accordingly. The desired wing size and ballast size will depend on the required glide speed. Once initial vehicle sizing is complete, a series of design tradeoff studies and iterations can be performed to give a final design.

10.7.1 Lift and Drag Lift and drag are determined by the geometry of the underwater glider. Wetted surface area ratio (A_t/A) and wing area A are important

factors in the glider lift/drag Ratio. In general, the internal volume of a glider will be determined by mission and payload requirements. It then remains to choose a suitable hydrodynamic design for that volume and mission. The three legacy gliders each have a streamlined axis-symmetric body and small flat plate wings. In this configuration the wings provide most of the lift on the vehicle and the body is the main source of drag. Increasing the wing aspect ratio and using an airfoil section instead of a flat plate would improve the efficiency (reduce the drag) of the wings. When operated at zero angle of attack, the streamlined bodies are reasonably close to the lowest drag configuration for a given volume. Figure 10.16 shows the electric Slocum glider in a typical configuration. Drag on the glider is a function of the glider geometry, speed through the water, angle of attack and sideslip angle. Drag can be divided into profile and induced drag. Profile drag
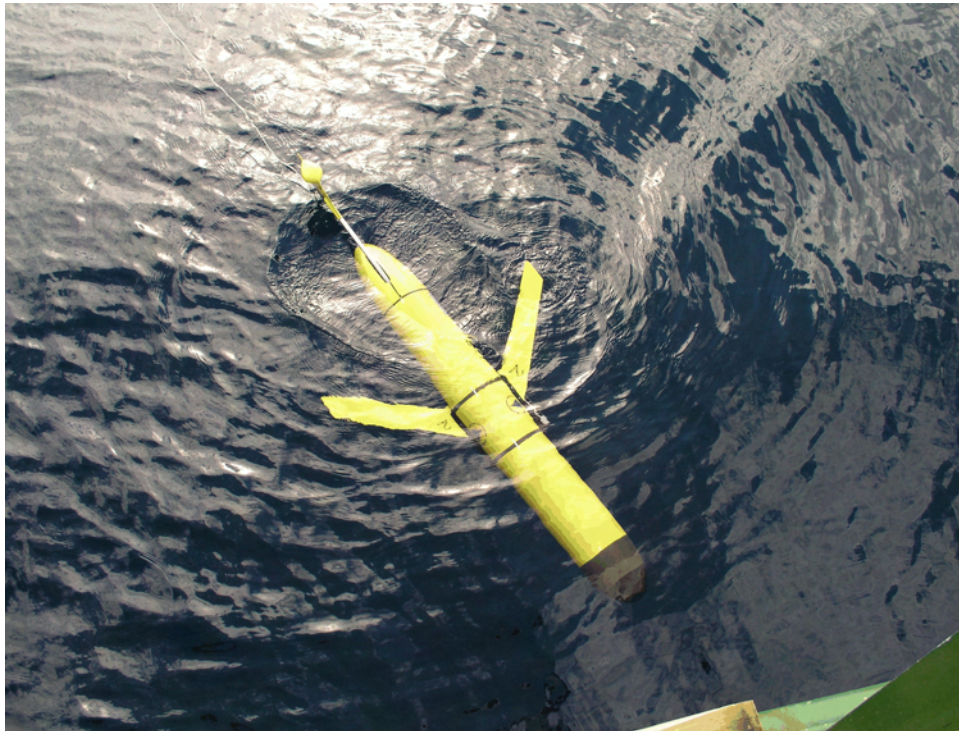
Figure 10.16: Slocum glider.

consists of skin friction and pressure drag on the vehicle. Induced drag is drag associated with the glider's production of lift. Proper design of the glider's body and wings can minimize profile drag through the use of streamlined shapes and minimize induced drag using efficient wing shapes. These methods are well developed from aircraft and marine vehicle design and are readily applicable to design of underwater gliders.

Because the existing legacy gliders are designed to glide up and down in the same manner, their bodies and wings are top-to-bottom symmetrical. This limits their hydrodynamic performance and maximum lift/drag ratio. Cambered wing sections, for example, are asymmetric but provide better lift/drag performance than symmetrical wing sections. Designs using moving flaps or wings with adjustable camber or other geometry may give better lift/drag performance than the legacy gliders.

10.7.2 Choice of Glide Paths Figure 10.17 shows the glide speed along the glide path and horizontal speed of a legacy type glider similar to the Slocum. A range of possible glide angles for a downward glide is shown. Note that the shallowest glide paths do not take stall or separation effects into account.

When choosing a glide path angle for designing a glider, two glide path angles are of special interest: the shallowest possible glide path angle and the glide path angle giving maximum horizontal speed. The shallowest glide path angle is limited by the glider's maximum lift/drag ratio and gives the greatest horizontal distance for each glide up and down. The fastest possible glide path is limited by the glider's drag profile and the size of its ballast system. Selection of an optimum glide path angle involves trading horizontal speed for distance per glide, and will depend on the relative mission costs such as pumping energy, hotel load and travel time. The choice of a steady glide path for glider operations requires tradeoffs between speed of travel and lower pumping work. The shallowest glide path angle will give the maximum horizontal travel for a given number of dives, but will give a relatively slow glide. Because it is steeper, the fastest possible glide angle will give less horizontal distance for a given number of dives to a given depth.
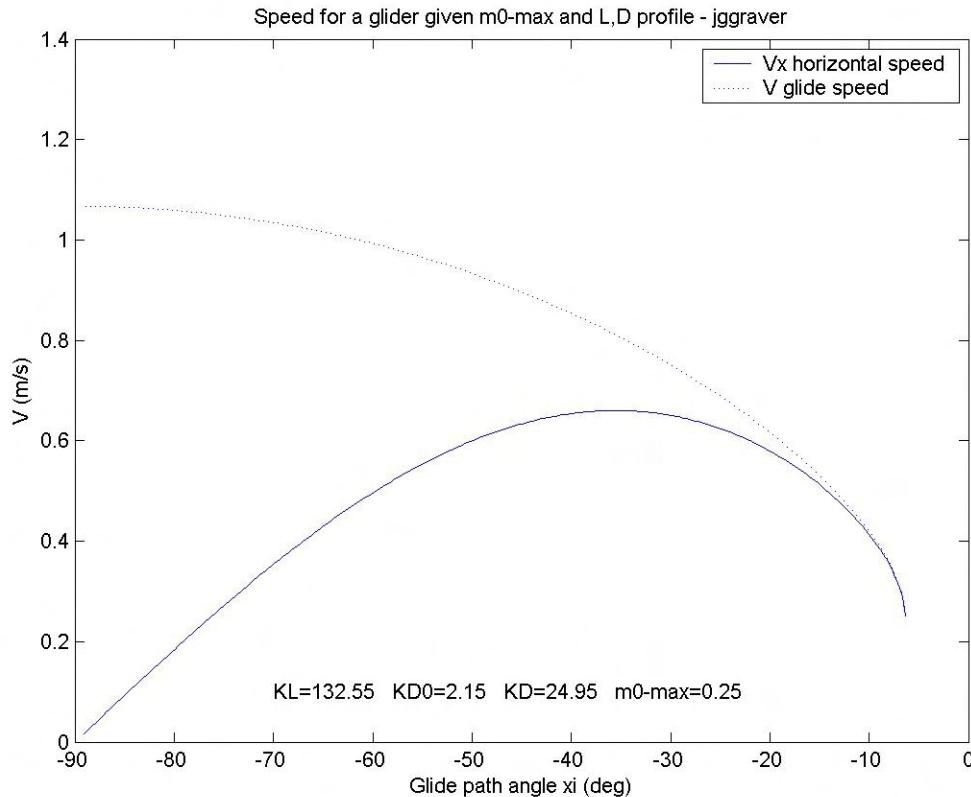
Figure 10.17: Legacy type glider speed vs. glide path angle.

Power consumption is a chief concern in gliders and other AUV's. Some energy costs will scale with the number of glides, including pumping work and the work involved with moving the sliding mass and controls when inflecting between dives. Other energy costs will scale with time, such as energy used by the glider hotel load. Gliding faster will in general require pumping more ballast, which results in more pumping work. Depending on the glider's mission, the tradeoffs between speed and energy conservation will give a desired operational glide path angle. If hotel loads and time based costs dominate the cost of travel, the fastest glide possible is desirable. If pumping work dominates the costs of travel and speed is not an important factor, gliding at shallower glide angles with smaller ballast and lower speeds are desirable. This gives an example of some of the optimization and tradeoffs involved in design and choice of glides. The spreadsheet method used as part of this ONR study and developed at the University of Washington gives a more detailed optimization for a given glider design.

10.7.3 Glider Design vs. Glide Path: The analysis of the maximum glide

speed and minimum glide path angles suggest that different designs may be best suited for fastest or shallowest glide paths. If the shallowest possible glide path is desired, a design with high lift/drag ratio is required. This requires large, efficient wings with high aspect ratio. In general the wetted area ratio, (A_t/A), is an indicator of maximum lift/drag ratio. Lower wetted area ratios tend to give more efficient gliders with higher lift/drag ratios. Traveling at shallower glide paths involves traveling below the maximum speed of a given glider, as shown in the speed analysis. If the fastest horizontal velocity is required for the design, then a steeper glide is necessary. Design for speed requires a glider with minimum possible drag and wings just large enough to provide the required lift/drag ratio. Minimizing drag on the vehicle plays a greater role in fast gliding than the lift/drag ratio. The fastest glide angle possible is around thirty-five degrees, which requires a lift/drag ratio of only 1.4. The legacy gliders fall within this design criterion.

10.7.4 Preliminary Sizing and Design: Comparison of glider designs requires some method for sizing gliders for a given mission. Mission requirements such as payload, speed, and range can be used to calculate the volume required. The largest internal systems such as batteries, buoyancy engine and payload space can all be estimated from the mission requirements, giving a first estimate of the glider's volume. A first cut design can use a legacy-type glider layout, with a streamlined body with wings. The body can be designed to minimize the drag for a given volume. It is then possible to determine optimum speed and glide path requirements and size the ballast system. Glide path selection will determine operational lift/drag ratio, which will drive the wing design. Wing aspect ratio will probably be limited by construction requirements. In aircraft the wing structural weight limits the possible span, but this is not as significant an issue in gliders because the wing loads and stresses are much smaller so the wing structures are lighter. Instead, the wings can be sized for optimum hydrodynamics. Increasing wing aspect ratio reduces the induced drag of a wing. Increasing wing area reduces wing loading and induced drag, but as the wing becomes larger this effect is overcome by the increased skin friction drag. The critical point between these two drag effects determines the optimum wing size, as illustrated by Figure 10.18.
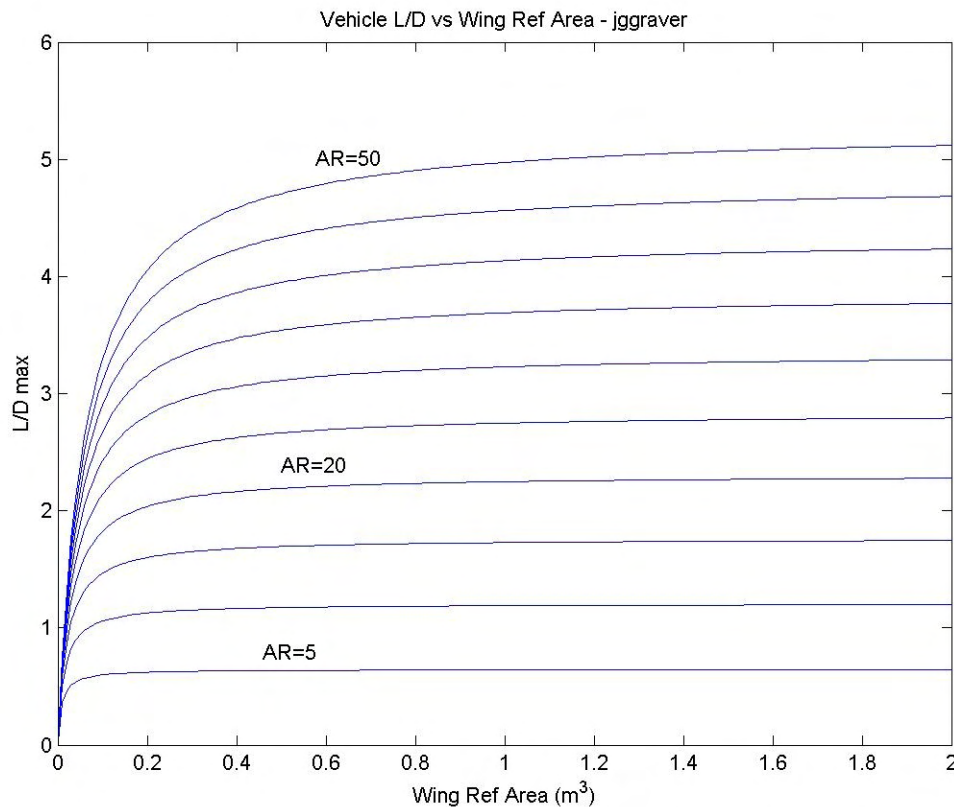
Figure 10.18: Lift/drag ratio vs wing area *A* for Slocum type legacy glider at fixed angle of attack.

Once a base design is made using a conventional glider layout, it is possible to perform trade studies, including the use of movable flaps and surfaces on the wings, reconfigurable wings, and blended wing/body or flying wing designs. Three types of designs are of special interest:

1. The top/bottom symmetrical legacy glider design used in Slocum, Spray and Seaglider.

2. A legacy type design with streamlined body and wings incorporating moving wings or flaps or other reconfigurable surfaces. Also possible is a glider optimized for one angle of attack which rolls over 180 degrees when switching between upwards and downwards glides.

3. A flying wing design that minimizes the glider's wetted area ratio (A_t/A) and

lift/drag ratio, L/D.

Figure 10.18 shows an example of maximum lift/drag ratio for a legacy type glider with wings of a variable aspect ratio (AR = 5 to 50). In the legacy design, the wings provide the majority of the lift, while the body provides a significant fraction of the drag. To compare a legacy glider design with a flying wing design, we compare vehicles of the two types with the same useful internal volume. The legacy design, with its cylindrical hull, gives a high internal volume for its wetted surface area. The hull shape is also suited to carrying the internal components. Fitting the payload and components in a flying wing may be more difficult given its geometry. Define the packing factor as the fraction of the total vehicle displaced volume that can be used to hold internal components such as payload, computers, batteries and the like. The packing factor plays an important role in the performance of the flying wing design when compared to a legacy-type design.

The different performance envelopes of these designs suggest that different designs are suited to different glider functional categories. This analysis indicates that operational glide path and speed will drive the choice between a legacy type glider and flying wing design and can be summarized as follows:

1. A flying wing design has higher profile (minimum) drag than the equivalent legacy glider. This is caused by the larger wetted surface area of the flying wing design, which results in more skin friction drag. Profile drag on the flying wing may be 50 to 100 percent higher than the legacy design, depending on wing packing factor. This means that a legacy glider would be faster at steeper glide path angles where not much lift is required.

2. The flying wing design has much higher maximum lift/drag ratio than the legacy design. The flying wing has a maximum lift/drag between 25 and 30, while the symmetrical legacy design has maximum lift/drag around five even with high aspect ratio wings.

3. A flying wing design has lower drag at higher lift/drag ratios and shallower glide path angles than the legacy design. This means that a flying wing gliding with a shallow glide path angle would be faster than a legacy glider with the same ballast capacity gliding at the same glide path angle. These tradeoffs between flying wing and legacy glider designs suggest that they are suited to different applications. The legacy glider performs better at higher glide path angles, which are important for high glide

speeds. The flying wing offers better performance at shallower glide path angles, which may allow more efficient flight when hotel power loads on the glide are low and pumping work dominated glider power use. Note that a vehicle design using a legacy-type layout and incorporating cambered airfoils and moving flaps and hydrodynamic surfaces could offer performance in between the legacy and flying wing designs or possible even better. This is a subject of continuing work.

10.8 Matching Glider Scale and Configuration to Functional Classes: Proceeding from the rational approach outlined in Section 10.7, we will now match the glider types evaluate in Sections 9 and 10 with the *functional classes* outlined in Section 5. These matches are intended to be generic, and no attempt has been made to be mission specific. Table 10.1 summarizes these matches and provides information on dimensions, vehicle volume, loaded mass, speed and range, net transport economies, and cost estimates made from Claytons Law (6.43). The net transport economies listed are based on cruise speeds and not the theoretical most efficient transport obtained by precise flying at best L/D speed. Similarly, energy recovery in the buoyancy engine has also not been considered in the net transport economy tabulations. The table is intended to present what is possible by direct expansion in scale of off the shelf technology. For each glider type the full range of scale that has been evaluated is tabulated. The optimal scale regimes within each of these ranges has been identified in Sections 10.1-10.5 and are indicated approximately by the magenta colored bands in Table 10.1.

The bundled payload configuration of the winged-body-of-revolution has been matched with the functional classes of depth unlimited roaming and payload delivery. The match is based on considerations of payload capacity and cruise performance. Cruise performance requires operating at relatively steep glide path angles $(\beta = 20^o)$ and consequently, unlimited depth excursions are best suited for accommodating a given range in the fewest possible number of dive cycles. The number of dive cycles is a consideration because of the vulnerability of the glider to detection when near the surface. In addition, the unlimited depth regime provides the most efficient buoyancy pump operation. Because of the large payload capacity requirement has resulted in a relatively large wetted area ratio (A_t/A) this glider is intrinsically less efficient from a hydrodynamic standpoint and requires a deep operating depth to make up for that inefficiency by way of high buoyancy pump efficiency.

The single payload variant of the winged-body-of-revolution was matched with the functional classes of depth limited roaming and station keeping. The minimal wetted area ratio (A_t/A) of this legacy type design gives it greater

transport efficiency and allows it to fly at high speed with flatter glide slopes (β = 12°). The high speed and flat glide slope of this glider type make it well suited to depth limited coastal environments where strong currents may prevail. Similarly, high speed capability is often essential to maintain station and flat glide slopes permit station keeping with minimal depth excursion.

The bundled payload variant of the flying wing was matched with depth unlimited roaming and payload delivery because its optimal operating regime occurs for large glider volumes. This glider type has impressive cruise speed capability in the large size regime while maintaining good transport economy comparable to a single payload legacy type vehicle. Because the high speed capability of these large wings is only realized for steep glide slopes $(\beta = 20^o)$ they are best suited for a depth unlimited environment in order to minimize near surface exposure time.

The small payload variant of the flying wing has been matched with depth limited roaming and payload delivery because of its exceptionally flat glide slope, excellent transport economy, and adequate cruise speed capability in spite of the flat glide path angles $(\beta = 3.2^o)$. Furthermore, the optimal regime for these wings occurs in the large size end of the scale regime, thereby providing high payload capacity. The cruise speed capability of the large single payload wings is 2-3 knots, providing penetration capability in shallow coastal environments with strong currents. The transport economy of these vehicles is the best of any of the gliders studied and consequently the highest cost effectiveness.

The hybrid glider has been matched with the functional classes for level flight and depth limited roaming because of its ability to use its propeller when constant depth maintenance is required for proper sensor operation or for penetration into extremely shallow waters (harbors). This vehicle is essentially a conventional AUV with self-delivery capability to the operational area when flown with the propeller shut down.   It also has exceptional burst speed capability (4-40 knots) for use in evasive action in shallow water. However, the optimal scale regime for best transport economy of this vehicle makes it best suited for single payloads of small size. The cost effectiveness of this glider type also favors relatively small vehicles.

The thermal glider is matched to the functional classes of depth unlimited roaming and station keeping primarily because it must be flown at steep glide slopes (β = 33°) in order to be effective in harvesting thermal energy from ocean temperature gradient fields. However, it has excellent cruise speed capability making it well suited to station keeping in strong currents when maintenance of limited depth regimes is not required. Exceptionally long range capability of these

vehicles (35,000 km) give them trans basin capability in the worlds major oceans and thereby open the possibility of long range reconnaissance with indefinite on-station capability.

Table 10.1. Summary of findings -page 1.

Glider Type	Length Ft	Wing Span Ft	Volume Cu Ft	Loaded Mass (Net Buoyancy) Grams	Cruise Speed Kts	Best L/D Speed Kts	Maximum (Best) *L/D	**Net Transport Economy
Winged-Body-of-Revolution (Depth Unlimited Roaming, Payload Delivery)								
23W-02	6.0	3.6	2.0	150	0.95	0.41	6.9	4.49
23W-12	12.9	7.7	19.6	1,500	1.5	0.76	7.1	1.30
23W-22 Range = 3500 km	27.9	16.6	195.7	15,000	2.3	1.22	7.8	1.04
23W-32 (bundled payloads)	60.0	35.8	1957.0	150,000	3.6	1.58	8.5	0.88
23W-SS	129	77.1	19,569	3,975,000	7.3	3.7	9.2	0.88
Winged-Body-of-Revolution (Depth Unlimited Roaming, Station Keeping)								
23S-03	4.8	2.90	1.1	100	0.62	0.42	6.3	2.22
23S-13	5.1	3.04	1.3	500	1.3	0.62	6.4	0.54
23S-23 Range = 3500 km	5.4	3.24	1.5	1,000	1.7	0.80	6.8	0.47
23S-33 (single payload)	9.2	5.5	7.7	10,000	3.2	1.51	7.1	0.47
23S-43	19.4	11.6	71.5	100,000	4.85	2.32	7.7	0.47
23S-SS	42.7	25.5	698.0	1,000,000	9.75	4.6	7.8	0.79
Flying Wing (Depth Unlimited Roaming, Payload Delivery)								
238-02	2.3	10.5	2.2	400	0.49	0.16	18.1	2.49
238-12	5.0	22.6	22	4,000	1.46	0.44	19.5	0.85
238-22 Range = 3500 km	10.7	48.7	220	40,000	2.78	1.12	23.0	0.79
238-32 (bundled payloads)	22.9	104.9	2198	400,000	4.35	2.03	24.8	0.79
238-42	49.5	226.1	21,980	4,000,000	6.47	3.09	27.0	0.79
Flying Wing (Depth Limited Roaming, Payload Delivery)								
238-04	2.0	9.0	1.3	150	0.14	0.13	17.8	4.85
238-14	2.0	9.0	1.5	1,500	0.46	0.40	18.0	0.27
238-24 Range = 3500 km	3.3	15.0	6.1	15,000	1.09	0.99	19.1	0.13
238-34 (single payload)	6.9	31.5	55.3	150,000	1.91	1.84	22.8	0.12
238-44	15.1	68.9	548.5	1,500,000	3.02	2.91	23.5	0.12

Table 10.1. Summary of findings -page 2.

Glider Type	Length Ft	Wing Span Ft	Volume Cu Ft	Loaded Mass (Net Buoyancy) Grams	Cruise Speed Kts	Best L/D Speed Kts	Maximum (Best) *L/D	** Net Transport Economy
Hybrid Glider (Level Flight, Depth limited Roaming)					prop on/ glide			
WRC-H05	5.7	3.2	1.31	110	2.1 / 0.6	0.41	4.4	4.13
WRC-H1	5.9	3.3	1.34	220	2.9 / 0.8	0.76	4.4	2.56
WRC-H2 Range = 500 km	6.1	3.4	1.45	440	4.1 / 1.1	1.22	4.4	1.79
WRC-H5 (single payloads)	6.5	3.6	1.77	1,100	6.0 / 1.7	1.58	4.5	1.36
WRC-H11	7.1	4.0	2.37	2,200	8.2 / 2.3	0.80	4.8	1.26
WRC-H12	13.2	7.4	14.9	22,000	16.7 / 4.7	1.51	5.0	1.39
WRC-H13	30.7	17.2	188.4	220,000	28.9 / 8.1	2.32	5.5	1.94
WRC-H14	74.2	41.5	2,672	2,220,000	43.9 / 12.8	4.6	5.9	2.79
Thermal Glider (Depth Unlimited Roaming, Station Keeping)								
WRC-T05	5.7	3.2	1.1	90	0.33	0.16	5.5	0.61
WRC-T1	5.9	3.3	1.8	180	0.47	0.44	5.5	0.22
WRC-T2 Range = 35,000 km	6.0	3.3	11.1	360	0.64	1.12	5.6	0.08
WRC-T5 (single payloads)	6.2	3.5	105.8	900	0.99	2.03	5.8	0.02
WRC-T11	6.6	3.7	1.5	1,800	1.34	0.40	6.0	0.0075
WRC-T12	10.4	5.8	6.1	18,000	2.84	0.99	6.4	0.0004
WRC-T13	21.2	11.9	55.3	180,000	4.65	1.84	6.9	0.00002
WRC-T14	45.5	25.4	548.5	1,800,000	7.05	2.91	7.5	0.000001

* L/D is the lift to drag ratio and is a measure of glide efficiency, where bigger values represent more efficient gliding. The inverse of L/D gives the glide slope.

** Net transport economy is the energy expended per immersed weight per distance traveled. It is a measure of energy consumption, and smaller values represent more efficient transport.

Optimal Scale Regime

11. Flight Strategies and Vehicle Control Requirements

Having defined vehicle characteristics and capabilities in Sections 9 and 10, here we explore flight strategies and control system requirements to insure that vehicle characteristics and capabilities are exploited to the fullest extent possible. It was learned in Sections 6, 9 and 10 that performance is as much dependent on how the glider is flown as it is on intrinsic vehicle capability. For example, it was found that net transport economy of legacy gliders could be improved by 75% if they were flown slower at best L/D speed. This would require control systems capable of steering the glider at a pitch angles opposite to the glide path angle, (pitch angle nose-up in a descending glide and pitch nose-down in an ascending glide); which is a flight configuration unfamiliar to the present generation legacy control systems. However, the steeper glide angles of the legacy gliders were selected for the specific function of gathering ocean sounding profiles and control system evolved around the requirements of that function.

Speed of travel is an important consideration in many possible glider applications. In the oceanographic sensing application of the three legacy gliders, high speed is not required. High-speed travel could be especially important for applications in areas with high currents and in littoral areas. The Slocum glider is designed for shallower gliding than the Spray and Seaglider designs and is capable of slightly higher glide speeds. Even so, all three gliders are relatively slow, capable of maximum horizontal speeds on the order of 0.4 m/s (0.8 knots). The effects of currents on gliders traveling at low speeds can be significant. Although many aspects of flight strategies will be dictated by the needs and limitations of the payload, there are certain rules for how to most efficiently operate a glider in a moving ocean. These rules are referred to as "speed to fly" and feasibility for implementation of these rules (given sensor and navigation capabilities of underwater gliders) will be explored in this section. In addition, the feasibility of certain flocking or collective/coordinated operations or adaptive sampling schemes for underwater gliders will also be considered

11.1 Speed-to fly in a Moving Ocean: In Section 6.2 relations were developed for glide speeds that achieve the minimum glide slope and best transport economy (Equations 6.21 – 6.23) and also for speeds that maximize cross-country transit (Equation 6.25) or minimize the descent/ascent rate through the water column (Equation 6.27). These derivations apply to a quiescent ocean and all of the modeling and transport analysis in Sections 9 and 10 are based on the assumption of no ambient ocean water mass movement. A rather lengthy set of derivations in

Reichmann (1978) show that optimal vehicle characteristics are not altered by motion in the flying media, but that the optimal speeds at which best vehicle characteristics are realized will change. A simple graphical presentation of the low speed portion of the glide polar will illustrate this point. Figure 11.1 shows the glide polar for a descending glide in still water (black curve and coordinate system) with the vertical velocity component w shown downward. The flattest possible glide slope corresponding to $(L/D)_{max}$ occurs at the point of tangency for the black line projected from the origin of the stationary coordinate system, also drawn in black. This point of tangency is the best L/D speed U' in a stationary ocean, as given by Equation 6.23). However, if the glider is flying against an opposing steady current, $-v$, then the coordinate system will be shifted along the axis of the horizontal velocity, u , by an increment $+v$ in order to maintain a stationary reference with respect to the seabed. The glide polar is referenced to the moving fluid, but the glide slope is measured with respect to the stationary seabed. Hence the flattest glide slope over the seabed is given by the by blue tangent line in the motion compensated coordinate system (also in blue). Even though the cross-country speed is now $u - v$, the point of tangency to the glide polar occurs at a faster speed relative to the fluid. The opposing current reduces the maximum L/D and steepens the glide slope over the seabed, but the speed relative to the moving water at which this maximum L/D is achieved is increased. The opposite occurs for a following current shown by the red shifted coordinate system and red tangent line in Figure 11.1. As a consequence, speed to fly for $(L/D)_{max}$ and best transport economy will increase when flying against a current and will decrease when flying with the current.

To give perspective on how much speed to fly can change for an under water glider, Figure 11.2 gives the same type of graphical presentation using the glide polar of the 31 liter single payload variant of the winged-body of revolution shown in Figure 9.1 for a loaded mass of $M = 205$ grams. In a still ocean, speed to fly for $(L/D)_{max} \sim 7$ is $U' = 23$ cm/sec. If the UW glider flies against a 20 cm/sec opposing current then speed to fly increases to 34 cm/sec while $(L/D)_{max}$ is decreased to only 1.8. For a following current of v = 20 cm/sec then speed to fly approaches $u_{wmin} = 20$ cm/sec (Equation 6.27) while $(L/D)_{max}$ increases to 11. Consequently ocean currents can greatly enhance or degrade glide efficiency. Failure to respond to those currents with appropriate adjustments to speed to fly can result in failure to exploit performance improvement offered up by Nature free of charge or can make even worse already catastrophic losses of performance.

The simple graphical representation of speed to fly adjustments to ocean currents in Figures 11.1 and 11.2 are not adequate or correct when flying along a
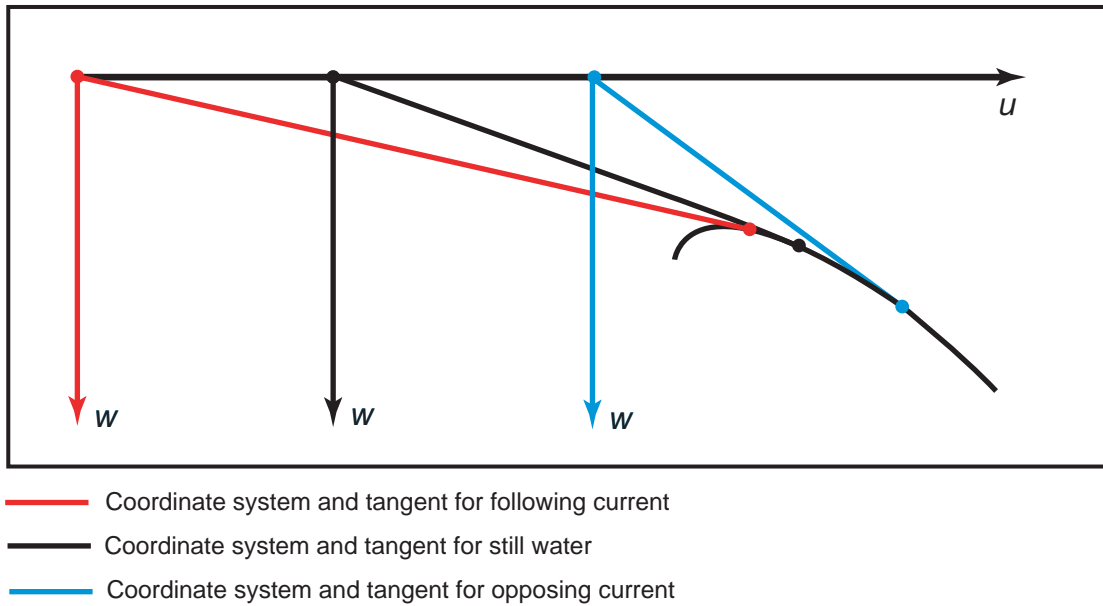
Figure 11.1. Speed to fly during decending glides (-B) for still water (black tangent), opposing current (blue tangent), and following current (red tangent). [after Reichmann, 1978] For clarity, only the portion of the glide polar below u_{max} has been plotted from Figure 6.10 and is inverted for decending glides (-w) .
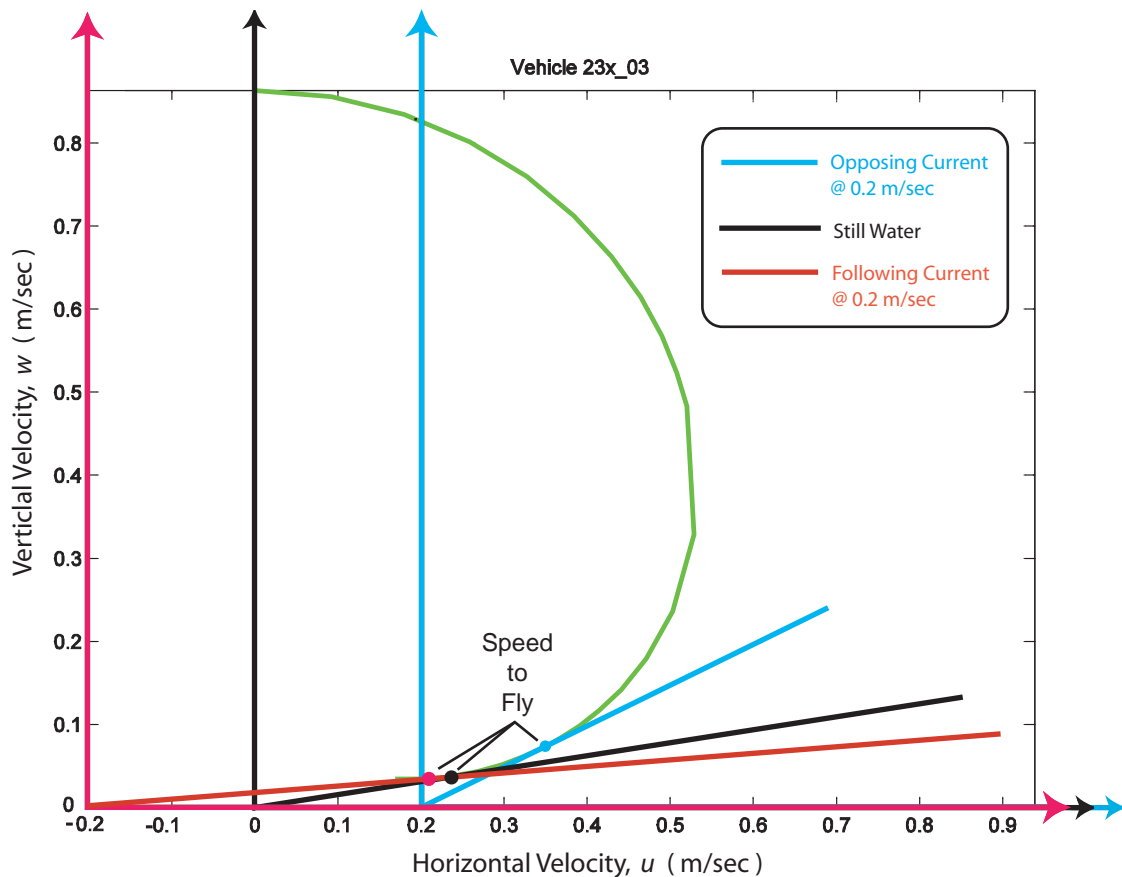
Figure 11.2. Speed to fly for still water (black tangent), opposing current (blue tangent), and following current (red tangent). Glide Polar (green) for 31 liter winged-body-of-revolution with a loaded mass of B = 209 g, per Figure 9.1.
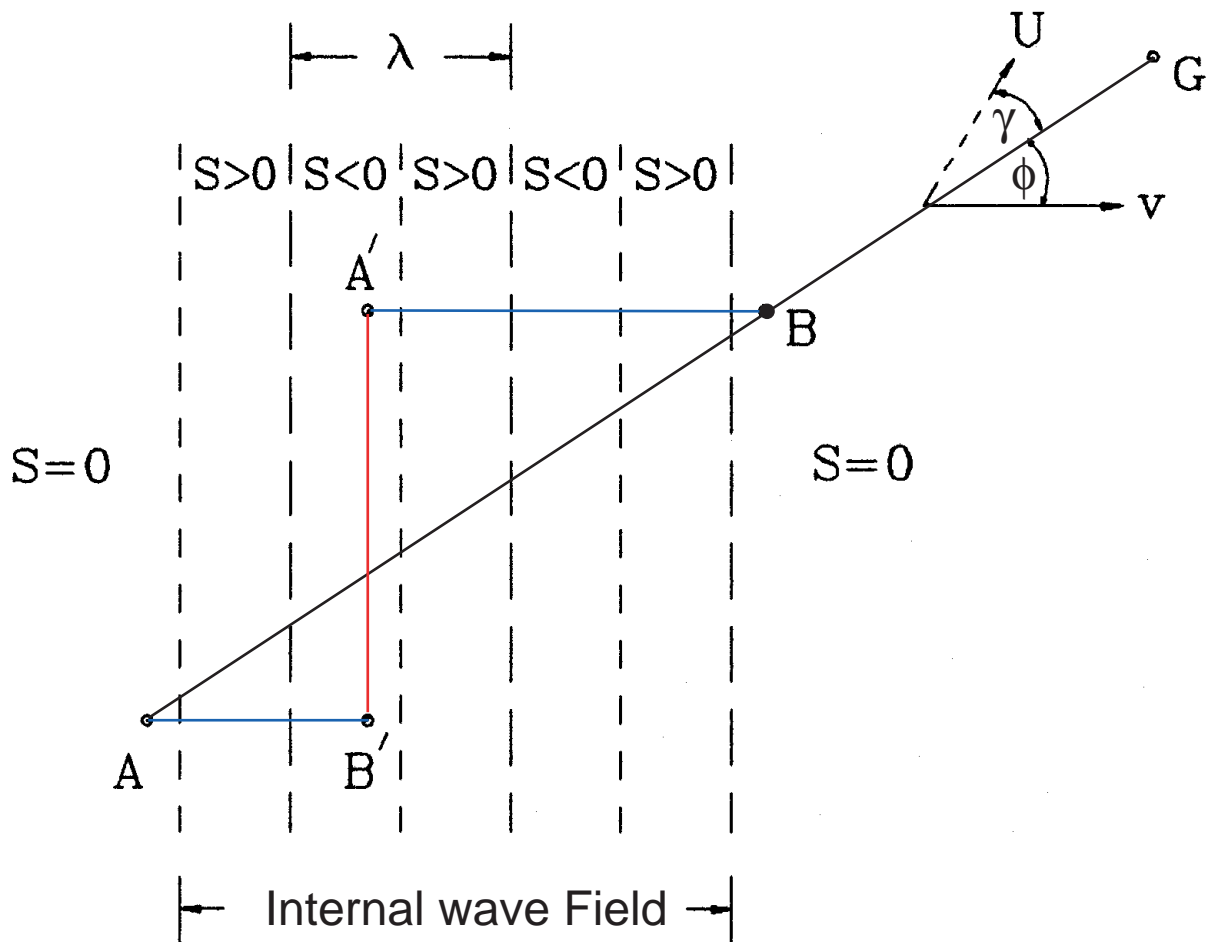
Figure 11.3. Schematic of constant course strategies with internal waves. [after Jenkins and Wasyl, 1991]

coarse heading that is oblique to the current. Let us consider the general case shown in Figure 11.3, where an arbitrary coarse heading is chosen between points A and B, flown at an angle of obliquity, ϕ , relative to the current, v. To maintain the coarse heading along AB, the glide velocity U will have to be flown at some countering crab angle, γ, opposed to the angle of obliquity of the current. Let us further suppose that the UW glider encounters an internal wave field while along coarse line AB in which the vertical velocity of the water column is $-S$ (rising) on the front side of wave crests and S (sinking) on the backside. The general speed to fly solution to this problem is due to Jenkins and Wasyl, (1991), who found the following analytic form for weak cross currents:

$$U' = \left[+ \sqrt{\frac{d_o^2}{4} + \frac{f_3^3}{27}} \right]^{1/3} + \left[-\frac{d_o}{2} - \sqrt{\frac{d_o^2}{4} + \frac{f_3^3}{27}} \right]^{1/3}$$
$$- 2v_o \cos\gamma$$

where

$$d_o = (1/27)(2p_0^3 - 9p_0q_0 + 27r_0)$$
$$f_3 = (1/3)(3q_0 - p_0^2)$$
$$p_0 = 2v_0\cos\gamma$$
$$q_0 = [-(f_3 + S + 2f_2v_0^2\sin^2\gamma - v_0b\ \cos\gamma)/f_2]$$
$$r_0 = (v_0^2b\ \sin^2\gamma/f_2)$$
$$v_0 = v << \sqrt{U_0^2/\sin^2\gamma}$$

(11.1)

In Figure 11.4, the speed to fly solution in (11.1) was applied to the 4.58 m span flying wing for single payloads (from Figure 9.11) for currents varying over a speed range of $v = +/- 90$ cm/sec, acting obliquely to the coarse line over a range of directions $\phi = +/- 90^0$. For simplicity, vertical water mass movements were neglected in this calculation. Speed to fly for maximum L/D and best transport economy is found to vary from a maximum of U' ~ 110 cm /sec for a $v = -60$ cm/sec current directly opposing the coarse line ($\phi = 0^0$), to a minimum of
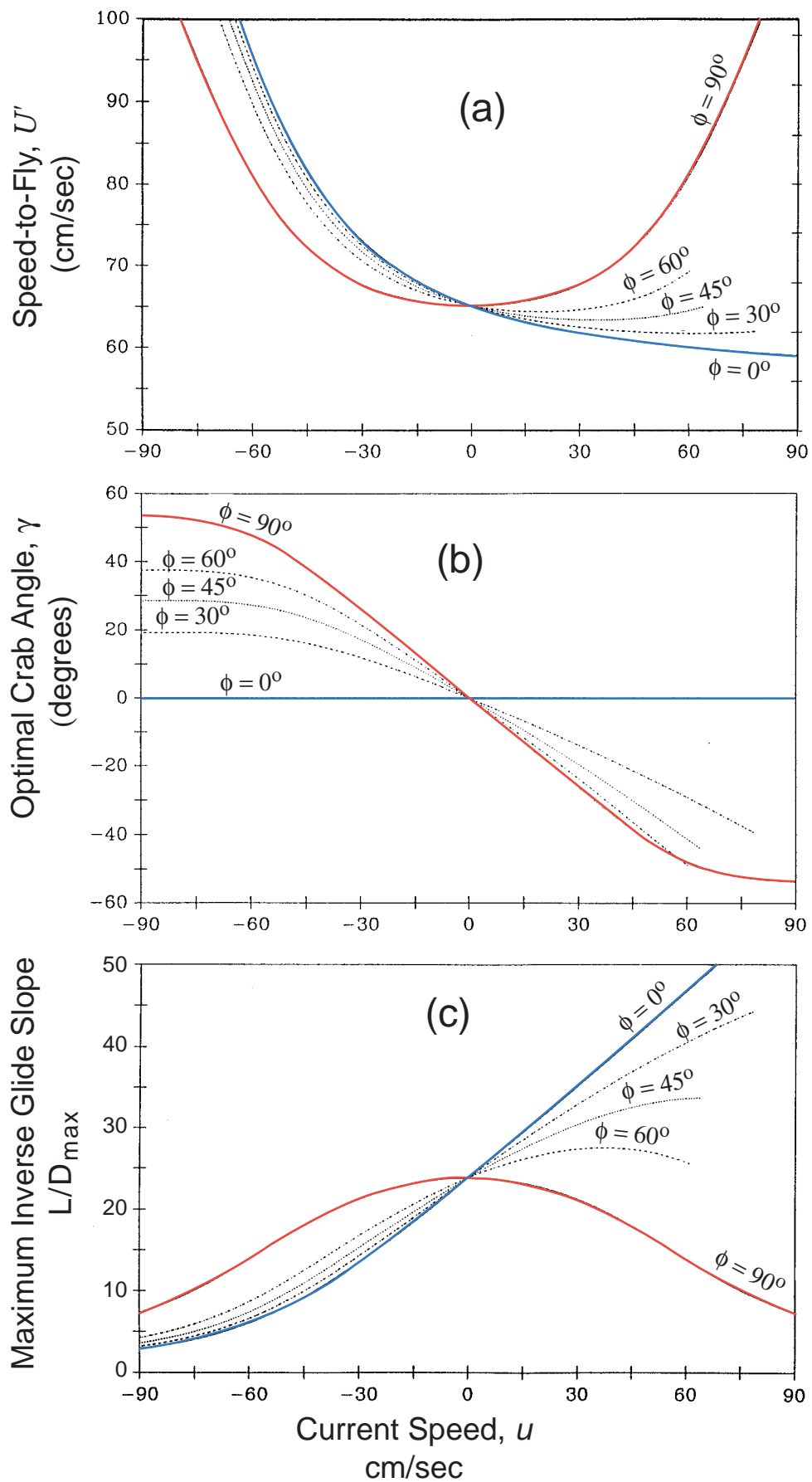
Figure 11.4. Effect of current speed and direction on: a) speed-to-fly; b) optimal crab angle; and c) inverse glide slope L/D$_{max}$ for a 173 liter, 4.85 m span flying wing. [after Jenkins and Wasyl, 1991]

U' ~ 58 cm /sec for a directly following current at v = +60 cm/sec. Achieved $(L/D)_{max}$ (inverse glide slope) ranged from a minimum of 5 when gliding against the 60 cm/sec current to a maximum of 77 when gliding with the current. For currents flowing normal to the course line, speed to fly increases in direct proportion to the current speed, reaching a maximum of U' ~ 90 cm /sec for a v = +60 cm/sec direct cross current. The optimal crab angle in these 60 cm/sec direct cross currents is about $\gamma = 50^0$. The maximum inverse glide slope $(L/D)_{max}$ degrades as the cross current strength increases, declining to only 8 for a, v = +60 cm/sec current when the flying wing would ordinarily do $(L/D)_{max}$ = 17.8 in a quiet ocean. For moderately oblique following or opposing currents the speed to fly is approximately the same as for a directly following or opposing current, with all the cross current compensation being performed with crab angle adjustments.

If the speed to fly problem now admits to vertical water mass movements, then the strategic factor of the coarse heading chose enters into the optimization process. It can be shown from Equation 11.1 that an orthogonal set of coarse headings across an internal wave field (AB' to B'A' to A'B) will out perform a direct course line (AB) taking obliquely through the waves. This strategy requires the ability to sense the vertical water mass movement and to at least be able to discriminate between regions of upwelling (S <0) as opposed to regions of downwelling (S>0). The strategy involves traversing cross current in a region of upwelling (B'A') to maximize L/D by minimizing *w*, and then proceeding directly down current through regions with downwelling (A'B) to minimize time spent in sinking water mass. To sense whether the water mass is rising or sinking while the glider is continuously rising or sinking itself under glide polar effects, the UW glider must be fitted with a total energy variometer. Figure 11.5 shows 4 different total energy variometer concepts in use in soaring today that might be potentially adapted to underwater gliders. All involve the use of a capacity reservoir which maintain either a reference pressure or reference volume. In the underwater application the capacity reservoir will require a captured air bubble to allow flow in and out of the instrument in response to speed and depth changes. The capacity reservoir will also require a temperature sensor to perform temperature compensation of the captured air bubble. There are two basic types of variometers, 1) those which measure volume changes in the capacity reservoir (Figure 11.5 a & b); and 2) those which measure mass exchanges from flow in and out of the capacity reservoir (Figure 11.5 a & b). The volume change measuring devises in panels a &b of Figure 11.5 are unaffected by density variations in the flight media and are therefore the most likely to prove successful when used in ocean stratification.

Equation (11.1) and Figures 11.4 and 11.5 make the point that a great deal of
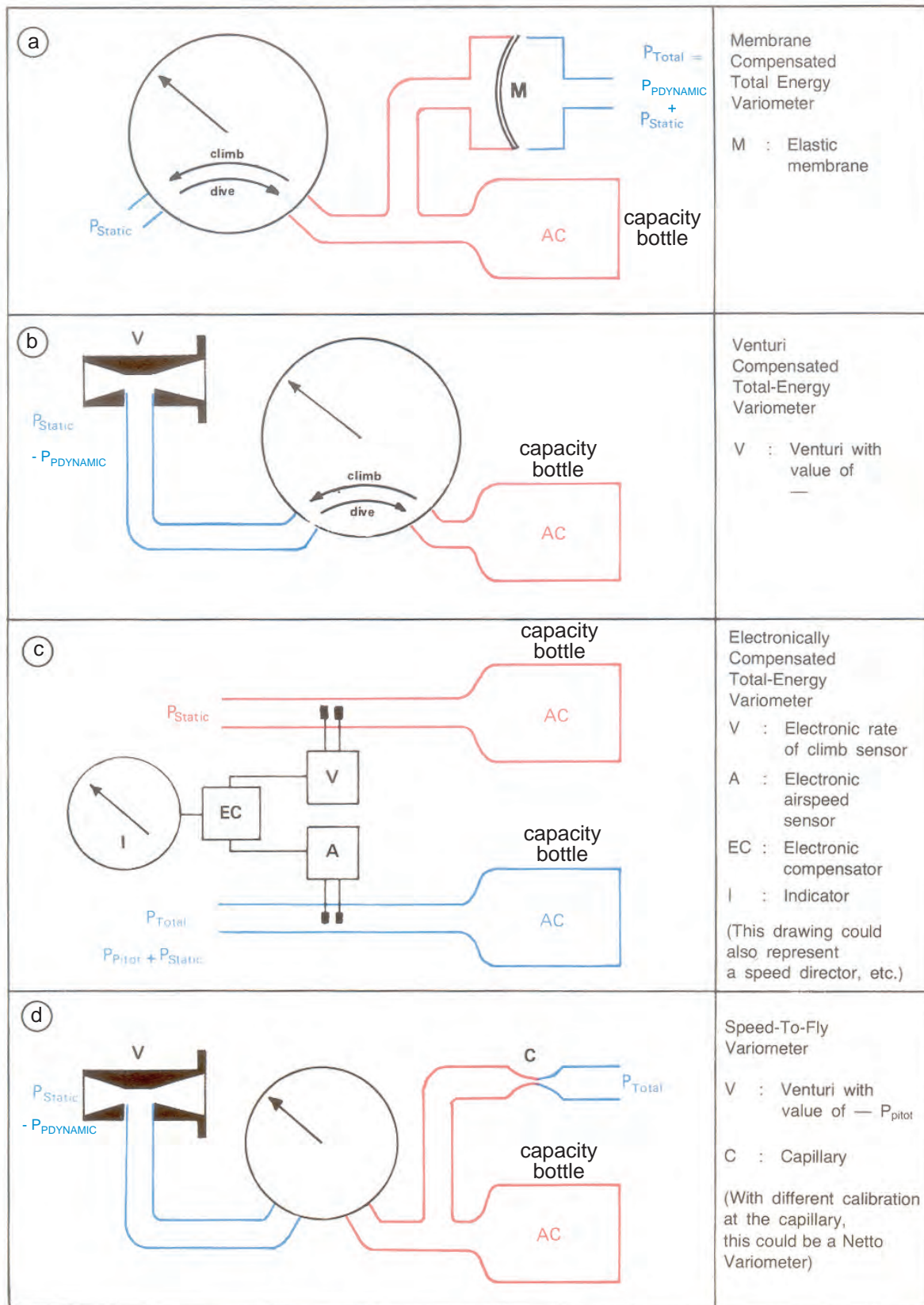
Figure 11.5. Total energy variometer concepts for implementing speed-to-fly strategies for underwater gliders a) Membrane compensated total energy variometer; b) Venturi compensated total energy variometer; c) Electronically compensated total energy variometer; d) speed-to-fly variometer.

articulation is required in the glide speed , glide angle and glider coarse heading in order to successfully implement speed to fly strategies and get the most out of an optimized glider design. To do so will require incorporation of flight and navigation instrumentation into the control system, utilizing feedback from variometer and inertial navigation systems. But there also more primitive issues to be resolved.

11.2 Glider Dynamics Model (after Graver, et al, 2003): A dynamic glider model describes a glider with arbitrary body and wing shapes, Fig. 11.6. The equations of motion in three dimensions are derived using Newton's laws. The relationship between vehicle momenta and velocities is derived from computation of the vehicle total Kinetic Energy. This includes the Kinetic Energy of an ideal fluid derived from a potential flow model using Kirchhoff's equations, with the added mass terms. Added
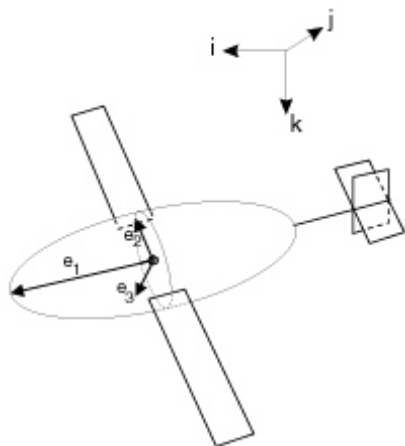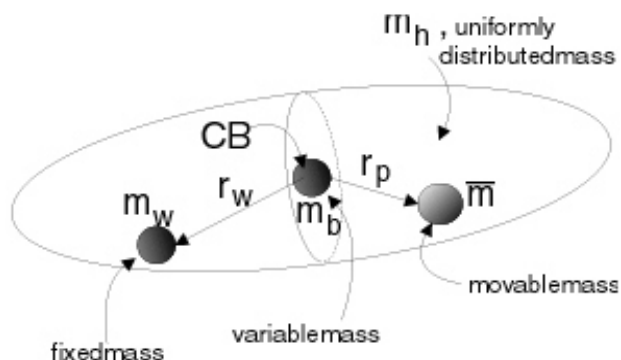

Figure 11.6: General underwater glider.

Figure. 11.7: The internal masses as they represented in glider model.

mass is a significant factor in glider dynamics, since gliders and water have similar densities. The model further includes hydrodynamic forces such as lift, drag and moment. The Model can be adapted to model a specific glider and more complicated geometries. Work is underway to adapt the model to the dynamics of the Slocum vehicle and compare the model prediction with experimental data from flight tests.

Figure 11.7 shows the mass distribution used to model a general glider configuration, including variable mass buoyancy system and moving internal mass. The mass distribution and other properties of the model can be adjusted to match a specific glider. In the glider model, control is applied to two point masses inside

the vehicle: we control the mass of a point with fixed position and the forces on a mass with variable position. The model describes the nonlinear coupling between the vehicle and the shifting and changing mass. This system of shifting internal masses is used in all three legacy gliders. In the case of the Slocum, modeling is also done on the control effect of the rudder. A model-based approach may also prove useful in determining optimal glider motions.The glider dynamic model is derived in [Graver,et al 2001], where we examine steady glides, controllability and observability in the vertical plane. Other uses include design analysis and parametric studies, for example: computing bandwidth, control authority estimates and size vs. speed calculations, comparing different control actuators such as ailerons, flaps, rudders and internal moving masses, and analysis of control and navigation methods (Figure 11.8)
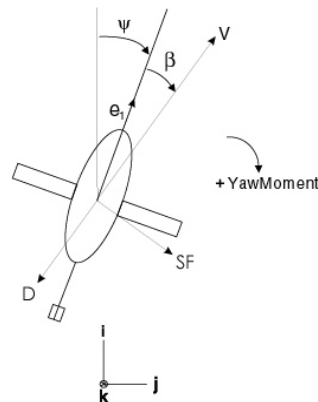

Figure 11.8: Glider angles and hydrodynamic forces in lateral plane, viewed from above.

11.3 Choice of Equilibria: Solving for the steady glides in the glider dynamic equations reveals a number of interesting properties of the gliding equilibria. First, it is possible to independently choose the glide path angle and the speed of the glide. The minimum (i.e. shallowest) glide path angle is fixed by the glider geometry and maximum Lift/Drag ratio. The steepest possible glide is straight down (or up). The maximum glide speed is determined by the glider drag properties and the glider's maximum net buoyancy. The choice of glide path fixes what lift/drag the glider must use. Depending on the glider lift/drag polar this will fix an angle of attack for that glide path angle and lift/drag ratio. The glide speed along the glide path is then determined by the net buoyant force acting along the glide path. Changing the amount of ballast pumped in and out of the glider controls the net buoyancy. Once the speed

and glide path angle are chosen, the equilibrium equations can be solved to give the internal sliding mass position necessary to balance the hydrodynamic moments on the vehicle at that flight condition. Solving the equilibrium equations for the sliding mass positions gives a line of possible mass positions along the direction of gravity, see Figure 11.9. Because the torque due to the sliding mass depends only on the horizontal distance between the sliding mass and the glider's center of buoyancy, moving the sliding mass vertically will not change the torque produced. It will, however, change the glider stability, with lower mass positions generally producing a more stable glide. In the existing gliders the sliding mass is constrained to travel along the glider long axis, so one position of the sliding mass will result in one pitch angle. See [4] for more detail.
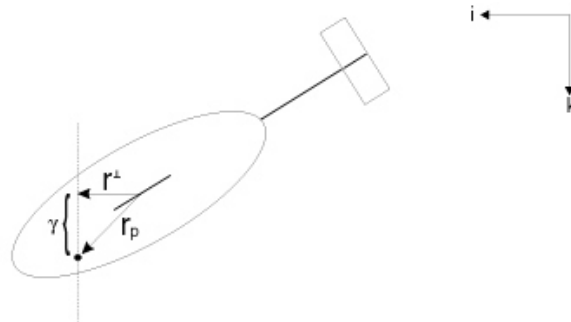

Figure 11.9: Possible sliding mass locations for a given equilibrium.

11.4 Control Systems: (from Bachmayer, et al, 2003, and Jones, 2003)

Steering and attitude techniques being used are internal weight shift, controlled external planes, and realizing symbiotic simultaneously adjusted pitch with buoyancy drive. All of the early gliders accomplished steering through a radial mass shifter (usually some subset of the batteries) to roll the vehicle to induce a turn. Depending on wing placement, the flow acts on different surfaces resulting in steering control. If the wings are placed far aft on the glider, then in descent the glider's port wing is dropped so that lift on the wing drives the stern to port, overcoming lift off the tail fin (vertical stabilizer), and realizes a turn to starboard. In ascent, the opposite is true, the starboard wing is dropped to turn to starboard. Hydrodynamic lift on the side-slipping hull produces the centripetal force to curve the course. If the wings are placed closer to the middle of the glider the lift force is realized on the tail fin of the glider. In descent, to turn to starboard the starboard wing is dropped and the lift force on the tail fin results in a starboard side turn of

the glider and the opposite for the ascent. An advantage of the internal mass shift steering is that there are no external moving parts. The turning radius is on average 25 meters and having to change roll at each inflection causes some counter steering force. This is typically not an issue where there is a great water depth and inflections are infrequent, and turning quickly is of no great advantage.

In shallow water, however, where the glider is inflecting frequently and it is important to recover heading after surface communication a tail fin control surface as a rudder gives the benefit of no counter steering during inflections, a turning radius reduced to 7 meters, and the capability to remain level in flight. Level flight is important to some optical sensors and to the altimeter used for bottom avoidance and bathymetry measurements.

Glider pitch is achieved also by using a mass shifter. This mass can be either the same mass used for steering change or a mechanism of two separate masses for pitch and roll. Some gliders are designed so that the major pitch change is symbiotically achieved by the already necessary buoyancy drive change for inflections thus maximizing on energy conservation. A pitch vernier adjust, the mass shifter, is still necessary for fine-tuning yet the movement (energy) needed is greatly reduced.

Simplicity of operation, extreme endurance and stealth are some of the principal advantages of autonomous underwater gliders. These advantages come at the expense of a minimalist approach in the sense of actuation and permissible power consumption. Also by nature the gliders are highly dependent on their operational environment, notably currents and density gradients. A control system that is able to cope with this challenging dynamic environment and the actuation and sensing constraints has to be robust with respect to environmental uncertainties and at the same time it has to be optimal in the sense of power consumption and accuracy.

11.4.1. Current Controller Design: Currently most of the operational gliders have implemented a simple proportional controller for heading and pitch control. A combination of controller dead-band, variable controller update time and actuator rate limitations in conjunction with the proportional controller is implemented to achieve the goals of energy efficiency and controller accuracy. The choice of the various modules of this controller as well as the associated parameters is based on experience and field-tests by the designers and operators of the gliders. Figure 11.10 shows the general control structure as it is implemented in
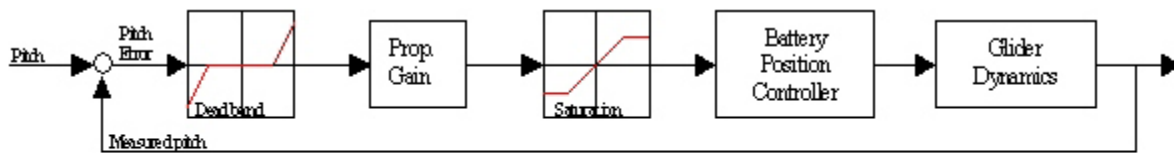
Figure11.1 0: Schematic for typical controller. Pitch controller shown as an example

most of today's gliders, the schematic does not show the variable update time of the controller design. The controller update-time can be a function of the history of the pitch- or heading-error.

In order to show the potential for improvements of the overall glider behavior and, correspondingly, the potential for an increase in the operational envelope, we show some results of recent experiments that have been performed with the Slocum gliders.

The Slocum gliders are actively controlled in pitch, depth and heading. Roll is not controlled on the electric version of the glider. The objective of the experiments was to improve the glider's response in its pitching behavior using the existing controller structure, Fig.0. In addition to the controller structure described above, the glider software uses a look-up function of the linearized, steady-state relationship between pitch angle and battery position in order to determine the expected battery position for a given pitch angle.

The data shown in Figures 11.11, 11.12 and 11.13 was collected this spring during a cruise on the Canadian Forces Auxiliary Vessel Quest in collaboration with SPAWAR System Center, San Diego and DRDC Atlantic, Halifax, Canada. Each of the experiments was composed of a set of double yo maneuvers with each yo consisting of one up and one down leg at a desired pitch angle of ±25°. The gliders were flying in a straight line collecting data at a 2 second sampling interval. All data presented was collected using the same glider. Figure 1 shows a comparison of measured and commanded state trajectories for some of the glider's internal and external states, such as battery position, total ballast pumped, pitch angle and depth as a function of time in seconds.
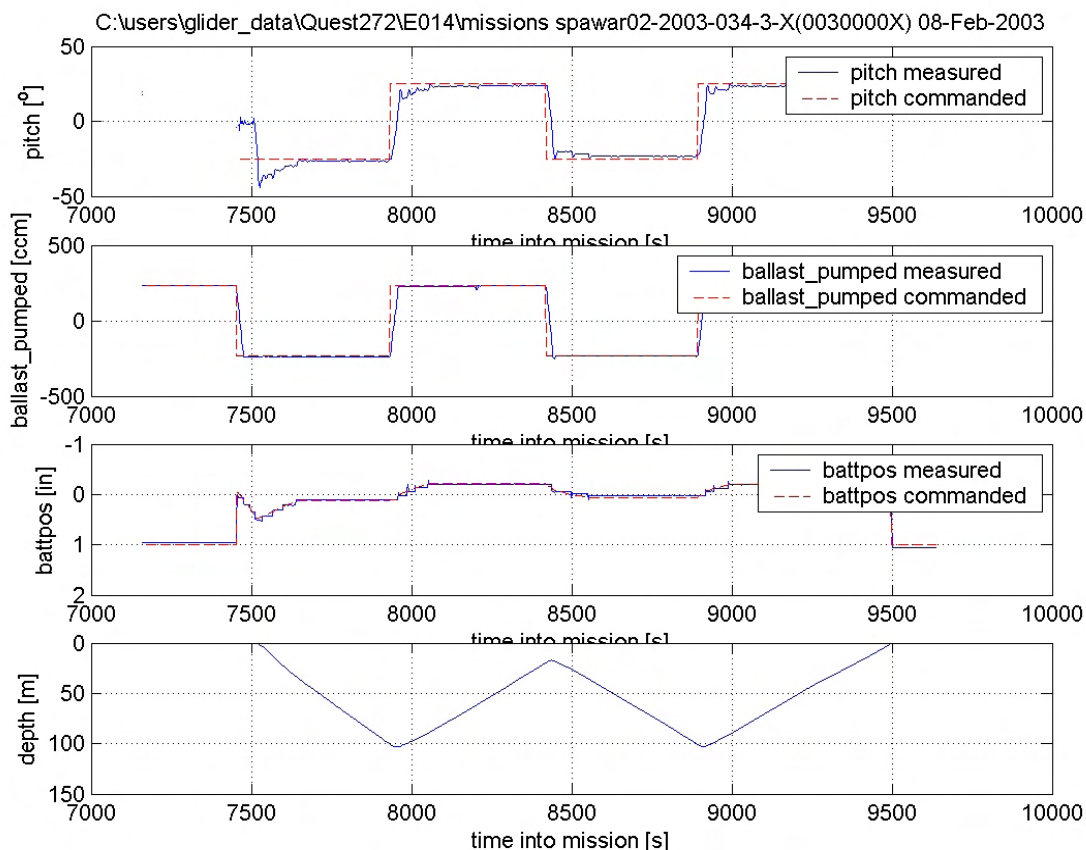
Figure 11.11: Double yo mission with a 25˚ pitch angle and the initial controller setting.

The glider's pitch response is over-damped and the glider takes a significant amount of time and therefore depth to reach the desired pitch angle. By the time the glider reaches its desired pitch it already has descended from the surface to a depth of approximately 40m. This causes significant limitations for shallow water operations. The slow rate of convergence is caused by the incremental changes of the battery position servo.

Based on the slow response of the actuator, the step size limit of the actuator was increased from 0.02in to 0.5in. Figure 2 shows the results of this change of parameters for the same type of glides.

The dramatic increase in actuator authority resulted in a much faster response of the vehicle. It also showed the controller gain to be too high, a fact that was previously hidden by the rate limit of the actuator. The considerable oscillations around the desired pitch angle are a direct result of the high gain.
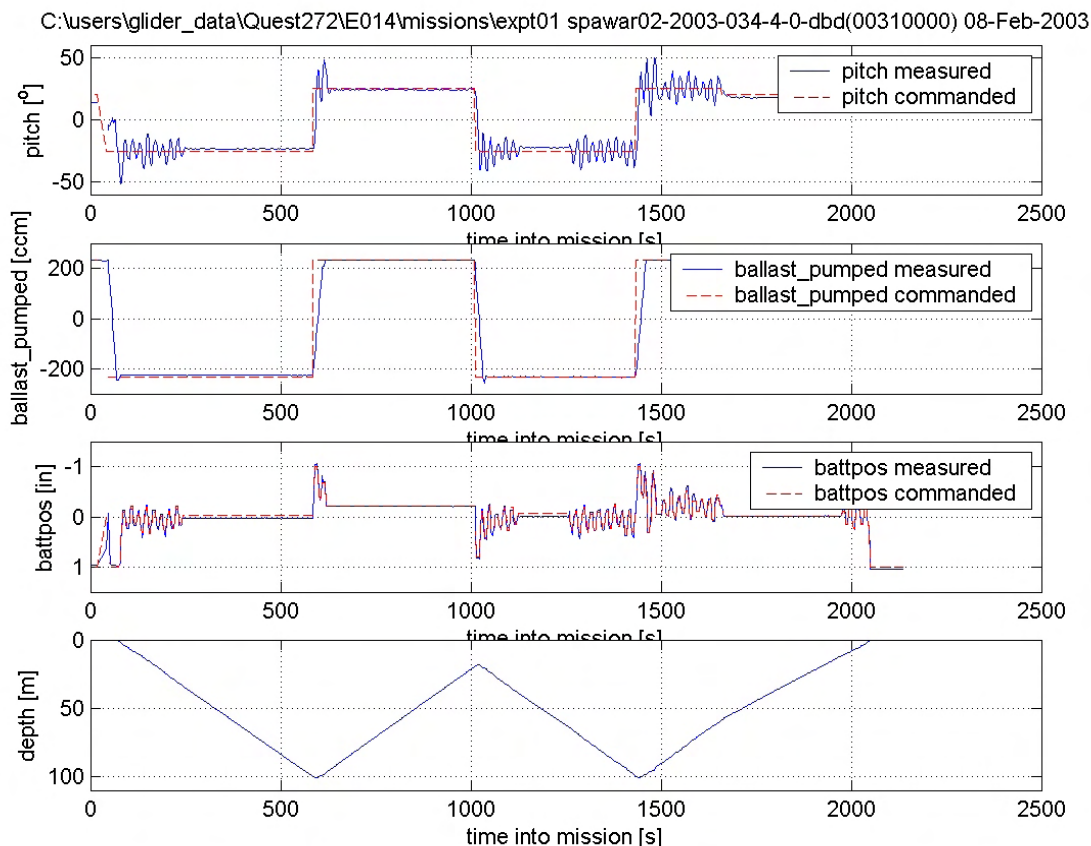
Figure11.12: Double yo mission with a 25˚ pitch angle and the step size limit increased from 0.02" to 0.5"

In a next step the controller gain was changed to -0.5 from -2.86. Figure 11.13 shows the final results from the change in the controller parameters. The change in gain showed no significant overshoot with an improved response time. As a result of these improvements the glider can reach its desired pitch angle in less than 10m of water depth. This example shows how even a modestly better understanding of the dynamics and controls of the glider can significantly enlarge the operational envelope of the gliders.

11.4.2. Future Developments: The above example clearly demonstrates the potential for improvements in the current controller design even within the current control structure. However a more systematic approach is needed in order to design controllers that fulfill the requirements of robustness and energy-efficiency, which are essential to the glider. Future developments in glider control will be able to

benefit from current developments in nonlinear model-based control [4], robust and optimal control. For glider missions involving a change in mass or buoyancy distribution, recent developments in adaptive control might prove to be a good starting point for future research.

While the above mentioned improvements in controller design can benefit a broad range of glider operations, some more specific glider operations, such as glider operations in the littoral regions pose special challenges to the control system. These more dynamic environments warrant a closer, integrated look at glider design, dynamics and control as well as fouling resistant embedded sensing and actuation.

Further, because of their endurance and versatility, gliders are expected to perform well when used cooperatively in a fleet, e.g., as a mobile, re-configurable sensor network. Continued effort on coordination and cooperative control laws for glider fleets are needed to make this a reality [5,6]. These strategies can build on the low-level glider control developments to make the cooperative fleet motion efficient and robust. The ability to network the gliders, e.g., by means of acoustic modems, should be supported in this context.

11.5 Remote Control of Multiple Vehicles: Long-range and satellite remote sensing systems are being realized in the ocean measurement field. These systems are being used to quantify currents, sea surface height, temperature, and optical properties of the water enabling modeling and prediction of ocean state variables. A similar nested grid of subsurface observations is required to maximize the impact of the more extensive surface remote sensing observations. The remotely sensed data needs to be ground-truthed and correlated to a third dimensional data component to be fully utilized. Gliders are of long endurance yet of low to moderate speed. In order to make conclusive temporal and spatial resolution measurements it will require a fleet of gliders coordinated in an intelligent adaptive network. Command/Control centers are being constructed
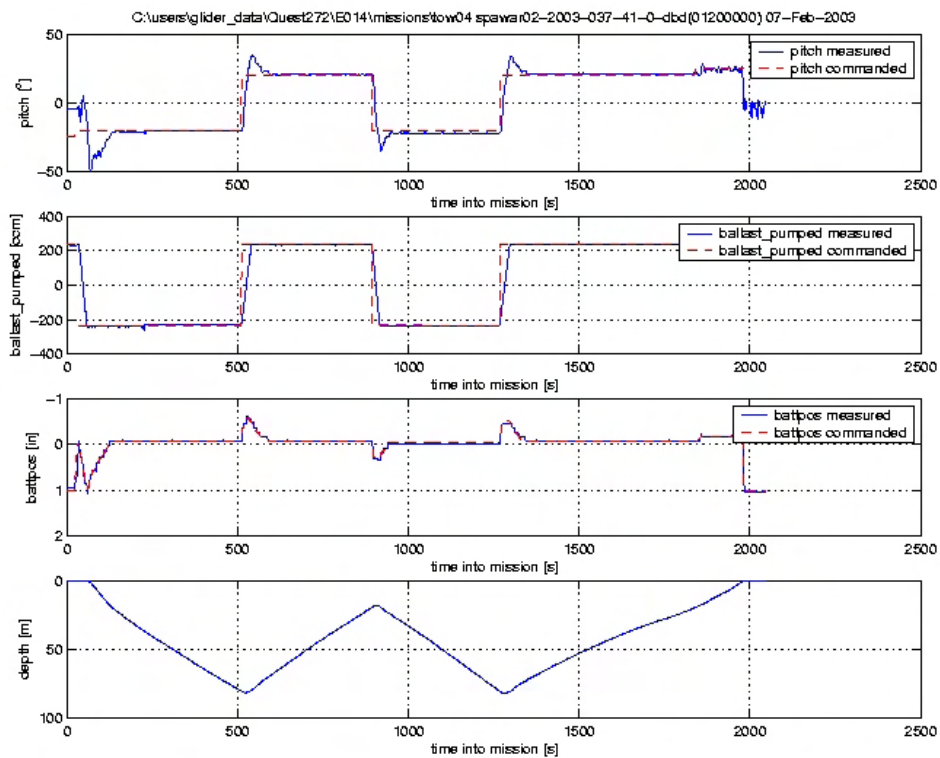
Figure 11.13. Double yo mission with a 25˚ pitch angle, increased step size limit and a controller gain of kp = -0.5 instead of -2.87.

capable of managing/flying multiple gliders from a single remotely accessible center. Gliders initiate the communication link, data istransferred, and if applicable - new mission parameters are downloaded. The center is a FEB (Front End Box) capable of storing and disseminating the data. Products are then created either on the communications machine or on another machine after the ftp process. These products include reformatting for ingestion into models, engineering data, charts, data pictorials, etc. A key concept is that the center is capable of storing new mission parameters for the gliders allowing the fleet to be automated to a level of an adaptive array. The intelligent portion of the center driven by a Bayesian network is tasked with target goals, understands the dynamics of the AUVs in its control, and arranges resources accordingly. For example a satellite image product needing ground-truthing or providing target feature identification triggers a re-routing of a fleet of gliders. This automated update of a glider waypoint set is

determined using other inputs such as surface current data (CODAR) information and a knowledge of glider functionality to best facilitate the need. In other words, a number of inputs are used as influences to drive the target need. This will be a large ongoing effort to best utilize this new breed of tools.

11.6: Operational Handling: The legacy gliders are all of the nominal 50 kg displacements, allowing for one or two person deployments from small vessels such as a RHIB. Scaling to larger gliders also scales the handling requirements and ship size relative to some of today's larger AUV systems as a model. Care must be taken to not damage sensors, break wings, and tail structures. Yet these are relatively easy constraints to design around and with the exception of long wings present AUV systems are similar. One advantage of the gliders is their long deployment duration, thus minimizing deployment/recovery as compared to propeller driven AUVs.

Re-powering today involves opening the vehicle and replacing either Alkaline or Lithium primary battery packs. Attention to weight must be exercised to ensure proper ballasting trim, but other than that the pre-made packs are relatively easy to slide into place. Lithium primary batteries have a greater energy density allowing for a longer endurance in the field although at a greater purchase cost and with higher shipping DOT restrictions. Presently, Lithium batteries must be shipped separately from the instrument to the site based on DOT regulations and then re-installed. Alkaline batteries are much more readily shippable pre-installed in the vehicle and are considered non-hazardous on military vessels and commercial and military aircraft. For the littoral zone gliders one important future advance that will make sense both economically and for ease of operator use will be the investigation into packaging in secondary (rechargeable) batteries. Lithium Ion batteries are a candidate with only slightly less energy density than Alkalines, and will allow for topping up the energy prior to deployment. Also, for consideration is fuel cell technology which has been making advances in availability.

Environmental survivability is of major concern. Gliders by their economical energy nature do not have a great deal of drive force, therefore things such as fouling, high currents, and trawlers will be problematic. Certain mission behaviors such as flying backwards to shed weed could be implemented. Intelligent considerations in mission planning could take advantage of currents to aid in travel and repositioning to work back against lesser currents. Fishing and trawling will be an issue. Discussion from the Discus shaped vehicle with bottoming capability to hydrophones and avoidance intelligence to low cost

expendability are all on the table. Bottom trawl resistance is a relatively easy test to conduct with a number of dummy glider shapes and different trawl equipment. Intelligent avoidance is much more difficult as there are bottom trawls, mid-water trawls, etc. and difficulty in discerning the approach of the vessel. The threat may be recognizable as a trawler approaching but the correct action may be a gamble – better to bottom, flee from the bottom, surface? One strong argument is to make these instruments inexpensive and thereby somewhat expendable – accept a loss of 20% or so. It is fully expected that this will be an important area of future study.

11.7 Special Control Issues of Hybrid Vehicles: Combining the long endurance qualities of a Glider with the short burst higher speed capabilities of a propeller drive may fit well into specific missions creating the concept of a Hybrid Glider. While gliders are capable of control in the x-y plane, the addition of z or depth position for things like docking do not suit a glider well. Also, some of the environmental problems as discussed above could be solved with an available increase in speed. Sent in at ~ 1 knot from over the horizon and loitering for weeks in a denied access area and then with perhaps 10% of the mission energy being available for 3 knot maneuvering has been identified as a Navy desire.

The control requirements for a propeller driven AUV are already incorporated into a glider. Guidance system, steering, data collection, etc. with the additional bonus of buoyancy control, reducing the amount of energy needed for a typically positively buoyant AUV having to drive itself under the water. Adding a thruster in the aft wet section of a glider would be fairly straightforward. Considerations are the increased weight of the thrust mechanism, drag associated with the propeller in the water flow while gliding, and available energy for thrust operation. Adding payload takes away from energy that could have been carried; a thruster not only removes weight energy capability but also presumes to consume quite a bit of it while operating. This of course must be accounted for in mission planning and may significantly cut into the very thing gliders are good at - endurance. Therefore it will be important to make sure that event the thruster is energy efficient that usually requires slow spin large propellers. This leads directly to the drag consideration of carrying a propeller on a gliding vehicle. Efforts to feather the prop or perhaps fold it into a streamlined shape while gliding will have to be examined. Of potential note is to utilize Nekton foil thrusters as surrogate wings that would only be actuated in need of higher propulsion.

11.8 Advanced Control Software Concepts (by L. Fogel , Natural Selections): To be fully effective, the UW Glider must follow pre-assigned instructions and, in addition, properly respond to unforeseen circumstance due to natural causes or human activity. The UW Glider may have to maneuver to avoid disclosure of its existence and/or various threats. For example, it would be particularly useful for the UW Glider to sense and evade an oncoming trawler net. Proper planning is essential. *In addition, real-time, intelligently interactive, re-planning is crucial to mission success.*

This intelligently interactive capability must be purpose-driven. Therefore, the first step is to define the mission in concise terms so that any encountered situation has a corresponding overall degree of success. This can be accomplished by using the Valuated State Space™ Approach. Here, the various parameters of concern are weighted in relative importance and made measurable in terms of a series of class intervals that correspond with those differences that make a difference in degree of achievement. Each of these defined class intervals is attributed a value so that the overall worth of any situation is the aggregate of these values, taking into account the degree of criticality of the parameters. The worth of any prospective move (tactic) is then the difference between the overall worth of the anticipated and current situations.

There are an enormous number of possible moves at any given time. The task is therefore to search this immense domain in a highly efficient manner in order to arrive at a useful move in real-time. Here, evolutionary computation can be used to discover increasingly appropriate behaviors in fast-time. This stochastic search procedure is remarkably efficient, for example, within the context of the traveling salesman problem, a least-distance path visiting 100 randomly placed cities can be found in a matter of seconds on an ordinary laptop computer. This requires examining only some 10^7 of the 10^{156} possible paths.

Evolutionary computation has be used for detecting unknown signals in noise, the prediction of non-stationary time series, modeling an unknown transducer / plant, and for the control of that plant, even when the plant is an enemy that resists being controlled (multi-player gaming).

The Valuated State Space™ Approach coupled with evolutionary computation has been demonstrated in automated tank warfare and the control of unmanned aeronautical vehicles. It can provide a UW Glider with the required real-time, intelligently interactive re-planning capability.

CONCLUSIONS:

The goals of this study are to determine how to advance from present capabilities of underwater glider (and hybrid motorglider) technology to what could be possible within the next few years; and to identify critical research issues that must be resolved to make such advancements possible. These goals were pursued by merging archival flight data with numerical model results and system spreadsheet analysis to extrapolate from the present state-of-the–art in underwater (UW) gliders to potential future technology levels. Using existing underwater gliders (legacy gliders) as calibration, this merger approach was applied to six basic glider types that were conceived to satisfy the requirements of five functional classes. Functional classes were posed based on an evaluation of the attributes and limitations of underwater gliders in the context of a broad range of potential Navy needs in the littoral and deep-water regimes. Those functional classes included:

Depth- Unlimited Roaming
Depth-Limited Roaming
Virtual Station Keeping
Payload Delivery
Level-Flight Hybrids

The glider types were composites of two basic payload packages (single and bundled), two classes of vehicle shape (body-of-revolution with wings and a flying wing), and three alternative propulsion systems (buoyancy lung, lung with propeller and lung with heat exchanger). Proceeding from the weight, space and power requirements of the payload packages, the analysis worked backward through a series of numerical modeling and spreadsheet computations to map out the viable performance envelope of each glider type. Scaling rules for speed and transport economy were then applied to these performance envelopes to identify the optimal regime of each glider type and to facilitate matching glider type with functional class. Table 10.1 provides a summary of the matching of glider types with functional class and the expected dimensions and performance capabilities resulting from those matches. The shaded magenta bands in this table indicate the optimal scale regime for each glider type.

Beneath the surface of Table 10.1, a number of interesting findings were made that shed light on critical research issues. Many of these findings come from close examination of the existing technology.

1) The achieved performance of the UW glider is as much dependent on the intrinsic vehicle characteristics as it is on how it is flown.

2) Presently, legacy gliders operate in a scale regime equivalent to that of bats and small birds.

3) The present legacy glider performance does not match the transport economy of its bird and bat counterparts because of the way it is flown, insufficient loading of the wing, excessive wetted surface area and inefficiencies of the buoyancy engine.

4) Legacy gliders are not flown in the most transport efficient manner. They are flown at steep glide angles in order to profile ocean water masses. If they were flown at the flattest glide slopes within present capability (L/D_{max}), their transport economy would improve three fold. To do so would require the controller to trim the glider for nose high attitudes during descending glides and nose low attitudes during ascending glides. Present control systems lack sophistication and supporting flight instrumentation necessary for maintaining such stable high angle of attack flight attitudes.

5) The present glider shapes are analogous to gliding blimps, and have too much wetted surface area for the wing loading at which the gliders are flying. Two remedial approaches were studied: increasing the wing loading by increasing the capacity of the buoyancy engine; and reducing the wetted surface area. Numerous sets of computations based on higher ratios of net buoyancy volume to total vehicle volume found that it is possible to make underwater gliders perform very close to the transport economy of natural flyers when operating in the present scale regime of birds. In larger scale regimes, these computations found that underwater gliders can equal or better the transport economy of some of the most efficient man-made flyers. Numerical modeling was also performed to seek more efficient shapes having less wetted area per unit area of wing, such as flying wings and blended wing-body configurations, wherein nearly all of the wetted area is efficient lift generating area. These new shapes were found to have superior range and speed capability for less energy consumption than more conventional bodies of revolution fitted with wings, (see Table 10.1). The remaining alternative for reducing the wetted surface area would be to reduce the volume requirements of the glider body by placing the batteries outside the pressure hull in some free flooding compartment. This concept was not pursued due to uncertainties in the status of pressure compensated battery technology.

6) The buoyancy engines that propel the legacy gliders do not recover the energy on descent that was expended on ascent in order to overcome ocean stratification and hull compressibility. By throwing away that energy, the buoyancy engine is consuming about 30% more than the flight energy required.

7) Flying the UW glider to deeper depths is intrinsically more efficient. Energy consumption increases 30% when the depth excursion of the glide profile is reduced from 1000m to 100m . This is due to 2 factors: 1) the glider must penetrate the thermocline a greater number of times over any given gliding distance when the depth excursion is reduced , and 2) the buoyancy engine pump is less efficient at lower pressures (shallower depths). For Example, the Parker PGP PM5116 high pressure pump has an efficiency of only 23% at a depth of 100m, but increase to an efficiency of 75% at 1000m depth.

8) A certain minimum ratio of net buoyancy volume to total vehicle volume was found ($n_b = V_{buoyancy}/ V_0 \sim 0.4\%$), beyond which, bigger gliders always achieve better transport economy. This improvement is accompanied by higher speed capability, see Table 10.1.

9) Maximum along coarse speed in still water is always obtained at a 35 degree glide angle, regardless of vehicle shape or other hydrodynamic properties. Winged bodies of revolution with maximum buoyancy engine capacity (n_b) are the optimal combination for maximum speed.

10) For a given n_b, flying wings of equivalent vehicle volume are slower then winged bodies of revolution, but have superior range and transport economy and require fewer dive cycles (and less near surface exposure time) for a given distance traveled, (see Table 10.1)

11) A procedure was defined for sizing and shaping gliders for mission specific functions, although our analysis remains generic in the context of broad functional classes.

12) Communications systems are presently the weak link of the UW glider technology. Near surface exposure time for the purpose of 2-way communications must be minimized. There are a number of attractive communications solutions for the UW-glider missions, including: local geosynchronous phone solutions; high bandwidth satellite solutions; radio frequency solutions in the line of sight (LOS) (UHF/VHF band) to aircraft or UAVs or over the horizon (OTH) (HF groundwave) to ship, shore, gateway node or buoy relay; and UAV data links such as Tactical Common Data Link (TCDL)

Long Term Recommendations:
1) Develop more sophisticated control systems with supporting flight data instrumentation and software for achieving stable high angle of attack flight and for implementation of speed to fly or avoidance/evasion strategies.

2) Improve the buoyancy engines for energy recovery during descending glides. Explore options for increasing buoyancy engine capacity and utilizing latest developments in high pressure, high efficiency pumps.

3) Develop and implement pressure compensated battery technology (particularly for the bigger gliders) that will allow the battery package to be placed outside the pressure hull while remaining compatible with safety requirements.

4) Develop vehicle shapes optimized for well posed mission requirements. Exploit computational methodologies that solve for minimum wetted surface area within constraints of volume and position requirements of internal components.

5) Develop optimized wing technologies for bi-directional angle of attack flight. Explore options for articulated wing incidence angle and for variable geometry.

6) Continue development of the thermal glider. Evaluate the potential for extracting and utilizing alternative geophysical energy sources, eg. dynamic soaring in vertical velocity gradients, wave soaring in internal waves, extraction of energy from surface waves via Katzmyr effect, et al.

7) Develop low cost pressure hulls with compressibility that matches seawater. Explore options for maximizing the packing of components and subsystems both inside and outside the pressure hull.

8) Develop an optimal communications solutions for the UW-glider missions from among the list of potential candidates listed above.

Near Term Recommendations:

Develop an Advance Concepts Demonstrator Featuring:
- · At Least 4-Fold Scale (Volume) Increase over Legacy
- · Configure for ASW Sentry Payload Package
- · New Geometry
    - Flying Wing
    - Legacy Type with Articulated Wing Incidence
    - Apply Surface Area Minimization Codes
- · Code for Maximization of Internal Systems Packing
- · Maximize Buoyancy Engine Capacity Within Packing
- · Off-the Shelf Systems for Glide Cycle Energy Recovery?
- · High Pressure Pumps Specific to Patrol Depths
- · Incorporate Inertial Navigation System with Horizon
- · Control Codes Interactive with Navigation/Flight Data
- · TCDL Communication System from Existing AUV

13) Bibliography

Abbott, J. H. and v. Doenhoff , A. E., <u>Theory of Wing Sections</u>, Dover, N. Y., 1959.

Althaus , D., <u>Stuttgarter Profilkatalog I</u>, Institut fur Aerodynamik und Gasdynamik der Universitat Stuttgart, 1972.

Althaus, D. and Eppler, R., "Airfoils With a New Hinge for Ailerons and Flaps". NASA CR-2315, Nov. 1973.

Bachmayer, R. and N. E. Leonard. "Vehicle Networks for Gradient Descent in a Sampled Environment." *Proc. 41st* <u>IEEE Conference on Decision and Control</u>, 2002.

Bachmayer, R., Graver, J. G., and Leonard, N. E., "Glider Controllers - Current Design and Future Prospects", Technical Report submitted to the ONR Committee for Underwater Glider Systems Study, Princeton University, April 2003, 5 pp.

Berry, J., "Communications Options for Autonomous Gliders", Johns Hopkins University, April 2003, 8 pp.

Barlee, J.,"Flying for Business and Pleasure". <u>Soaring</u>, Nov.-Dec. 1956, pp. 10-16.

Bikle, P., "Polars of Eight 1971". <u>Soaring</u>, June 1971.

Blick, E. F., "Bird Aerodynamics". <u>Shell Av. News</u>, No 402, 1971, pp. 2-7 and <u>Soaring</u>, June 1972.

Bolsunovsky. A.L, et al., "Flying Wing – Problems and Decisions". <u>Aircraft Design</u>, Vol. 4, 2001, pp 193-219.

Bramwell, C. D. and Whitfield, G. R., "Biomechanics of *Pteranodon*" <u>Phil. Trans. R. Soc. London B</u>, Vol. 267, 1974, pp. 503-581.

Chauvin, R., <u>The World of Insects</u>, N. Y. World U. Lib. (McGraw-Hill), 1967.

Clayton, J., "Progress Report - Under Water Glider System Study", Technical Report submitted to the ONR Committee for Underwater Glider Systems Study, Webb Research Corporation, April 2003, 10 pp.

Clayton, J., "Progress Report on Cost Scaling - Under Water Glider System Study", Technical Report submitted to the ONR Committee for Underwater Glider Systems Study, Webb Research Corporation, April 2003, 2 pp.

Clayton, J., "Progress Report on Glider Scaling Regime - Under Water Glider System Study", Technical Report submitted to the ONR Committee for Underwater Glider Systems Study, Webb Research Corporation, April 2003, 4 pp.

Clayton, J., "Progress Report on Energy Budget - Under Water Glider System Study", Technical Report submitted to the ONR Committee for Underwater Glider Systems Study, Webb Research Corporation, April 2003, 6 pp.

Clem, T. and Carroll, P., "Non-Acoustic Sensors and Glider Applications", Technical Report submitted to the ONR Committee for Underwater Glider Systems Study, Naval Coastal Systems Station, April 2003, 22pp.

Cleveland, F. A., "Size Effects in Conventional Aircraft Design", J. Aircraft, Vol. 7, No. 6, Nov.-Dec. 1970, pp. 483-511.

Cone, C. D. Jr., "The Aerodynamics of Flapping Birdflight" Virginia Inst. of Marine Sci, Spec. Sci. Rpt. No. 52, 1968.

_____, "Thermal Soaring of Birds". Amer. Scientist, Vol. 50, No. 1, March 1962, pp. 180-209.

_____, "The Soaring Flight of Birds". Sci. Amer., April 1962, pp. 130-40.

Cornish, J. J., III and Wells, W. G., "Boundary Layer Control Applications to Man-Powered Flight". Can. Aero. Space J., Feb. 1963, pp. 55-61.

Dryden, H. L., "Review of Published Data on the Effect of Roughness on Transition, from Laminar to Turbulent Flow". J. Aero. Sci., Vol. 20, 1953, pp. 477-482.

Eaton, G. F., "Osteology of Pteranodon". <u>Mem. Connecticut Acad.</u> Sci., Vol. 2, 1910, pp. 1-38.

Eppler, R., "Laminarprofile fur Segelflugzeuge", <u>z. f . Flugwiss</u> 3, 1955, pp. 346-353.

Eppler, R.: Laminar-Profile fur Segelflugzeuge". OSTIV Pub. II.

Eppler, R., "Direkte Berechnung von Trag Flugelprofilen aus der Druckverteilung <u>Ing.-Arch.</u>, Vol. 25, 1957, pp. 32-57.

_____, "Uber die Entwicklung Moderner-Tragflugelprofile". <u>D. Ingenieur</u>, Vol. 77, 1965, pp. 117-122.

_____, Laminarprofile fur Reynolds-Zahlen grosser als $4\text{-}10^6$," <u>Ing.-Arch.</u>, Vol. 38, 1969, pp. 232-40.

Eriksen, C. C., et al., "Seaglider: A Long-Range Autonomous Underwater Vehicle for Oceanographic Research". <u>IEEE Journal of Oceanic Engineering</u>, Vol. 26, No. 4, October 2001, pp 424-436.

Fiorelli, E, et al., "Adaptive Sampling Using Feedback Control of an Autonomous Underwater Glider Fleet."

Gabrielli, G. and von Karman, Th., "What Price Speed?". <u>Mech. Eng.</u>, Oct. 1950, pp. 775-81.

Galvao, F., "Some Thoughts on Nature and Sailplane Design". <u>Aero-Revue,</u> Nov. pp. 609-10; Dec. 1973; Jan. 1974, p. 41.

Gentry, A. E., "The Aerodynamics of Sail Interaction". Proc. 3rd AIAA Symposium on the AER / hydronautics of sailing, Western Periodicals Co., 13000 Raymer St., North Hollywood, CA 91605.

Graver, J. G., Bachmayer, R., and Leonard, N. E., "ONR Underwater Glider Systems Study Glider Design Notes", Technical Report submitted to the ONR Committee for Underwater Glider Systems Study, Princeton University, April 2003, 11 pp.

Graver, J. G., Bachmayer, R., and Leonard, N. E., "ONR Underwater Glider Systems Study Glider Design Notes Part 2", Technical Report submitted to the ONR Committee for Underwater Glider Systems Study, Princeton University, April 2003, 5 pp.

Hartmann, F. A., "Locomotor Mechanisms of Birds". Smithsonian Misc. Coll., Vol. 143, No. 1, 1961.

Hendricks, F.: "Extraction of Flow Energy by Gliding in a Wind of Uniform Vertical Shear". Notes, UCLA Short Course on Mechanics of Natural Flight, April 30-May 4, 1973.

Hertel, H., Structure-Form Movement, NY. Reinhold, 1963.

Humphreys, D. E., et al., "Validation of the Hydrodynamics & Maneuvering Model for the University of Washington – APL Sea Glider". VCT Technical Report #69, Vehicle Control Technologies, Inc., Reston VA, March 2003, 38 pp.

Humphreys, D. E., et al., "Validation of the Hydrodynamics & Maneuvering Model for the Webb Research Corporation Slocum Glider". VCT Technical Report #70, Vehicle Control Technologies, Inc., Reston VA, March 2003, 26 pp.

Humphreys, D. E., et al., "Validation of the Hydrodynamics & Maneuvering Model for the Scipps Institution of Oceanography Spray Glider". VCT Technical Report #71, Vehicle Control Technologies, Inc., Reston VA, March 2003, 27 pp.

Jacobs, E. N., Ward, K. E. and Pinkerton, R. M., "The Characteristics of 78 Related Airfoil Sections from Tests in the Variable Density Wind Tunnel", NACA TR 460, 1933.

Jacobs, E. N. and Sherman, A., "Airfoil Section Characteristics as Affected by Variations of the Reynolds Number". NACA TR 586, 1937.

Jameson, Wm., The Wanderin Albatross, N. Y. Morrow, 1959.

Jenkins, S. A., et al., "Glide Optimization for Cross Country Wave Flights". Technical Soaring, Volume 16, Number 1, January 1992, pp 3-16.

Jenkins, S. A., and Wasyl, J., "Optimization of Glides for Constant Wind Fields and Course Headings". Journal of Aircraft, Volume 27, Number 7, July 1990, pp. 632-638.

von Karman, Th., Aerodynamics, Ithaca. Cornell U. Press, 1954.

Lasiewski, R. C. and Dawson, W R., "A re-examination of the Relation Between Standard Metabolic Rate and Body Weight in Birds". Condor, Vol. 69, 1967, pp. 13-23.

Laurson, H. von and Zacher, H., "Flugmessungen mit 52 Segelflug zeugen". Aero-Revue, Oct. 1973, Dec. 1973.

Lawson, D. A., "Pterosaur from the Latest Cretaceous of West Texas: Discovery of the Largest Flying Creture [*Quetzal coatlus northropii*] Science, Vol. 188, 16 March 1975 pp. 947-48.

Leonard, N.E. and J. Graver. Model-Based Feedback Control of Autonomous Underwater Gliders. IEEE Journal of Oceanic Engineering, **26**:4, 2001, 633-645.

Liebeck, R. H. and Ormsbee, A, I., "Optimization of Airfoils, for Maximum Lift". Jour. of. Aircraft, Vol. 7, No. 5, Sept-Oct. 1970, pp. 409-415.

Liebeck, R. H., and Smyth, D. N., "A Simple Model for the Theoretical Study of Slat-Airfoil Combinations". AIAA Paper 72-221, 1972.

Liebeck, R. H., "A Class of Airfoils Designed for High Lift in Incompressible Flow". AIAA Paper No. 73-86, Jan. 1973; J. Aircraft, Vol. 10, Oct. 1973, pp. 610-17.

Lippisch, A. M. "The Seed that Became a Tree". Soaring, March-April 1953, PP. 3-11.

Loftin, L. K. Jr. and Smith, H. A., "Aerodynamic Characteristics of 15 NACA Airfoil Sections at Seven Reynolds Numbers from 0.7 x 10^6 to 9.0 x 10^6" NACA TN 1945, 1949.

McMasters, J. H., "An Introduction to Geometric Programming and Its Application to Sailplane Design". NASA CR-2315, Nov. 1973.

McMasters, J. H., "An Analytic Survey of Low Speed Flying Devices – Natural and Man-Made". Technical Soaring, Volume 3, Number 4, Fall 1974, pp 17-42.

McMasters, J. H., "The Optimization of Kremer Competition Man-Powered Aircraft". AIAA Paper No. 74-1026, Sept. 1974.

McMasters, J. H., "Some Opportunities for Progress in Ultralight Aeronautics". AIAA Paper No. 74-1034, Sept. 1974.

McMasters, J. H., et al., "Two Airfoil Sections Designed for Low Reynolds Number", Technical Soaring, Volume 6, Number 4, May 1981, pp 2-24.

McMasters, J. H., The Optimization of Low-Speed Flying Devices Natural and Man-Made. (In preparation).

Moitie, R. and Ensieta, N. S., "Guidance and Control of an Autonomous Underwater Glider". Proceedings of the 12th International Symposium of Unmanned Untethered Submersible Technology, AUSI, August 2001, Derham, New Hampshire. 14 pp.

Nash-Webber, J. L., "Motorless Flight Research", 1972 NASA CR-2315, Nov. 1973.

Osborne, M. F. M.: "Aerodynamics of Flapping Flight with Application to Insects". J. Biol., Vol, 28, 1951, pp. 221-45.

Oversmith, R.H. and Leadon, R.E. "Concept Whisper". General Dynamics/Convair, GD/C-62-206A, Nov 1962 (CONFIDENTIAL).

Parrot, G. C., "Aerodynamics of Gliding Flight of a Black Vulture, *Coragyps atraus*. J. Biol. Vol. 53, 1970, pp. 363-74.

Pennycuick, C. J., "Gliding Flight of the Fulmar Petrel". J. Exp. Biol., Vol. 37, 1960, pp. 330-38.

_____ "A Wind-Tunnel Study of Gliding Flight in the Pigeon *Columba Livia*". <u>J. Exp. Biol.</u>, Vol. 49, 1968, pp. 509-26.

_____ "Gliding Flight of the White-Backed Vulture *Gyps Africanus*". <u>J. Exp. Biol.</u>, Vol. 55, 1971, pp. 13-3d.

_____ "Control of Gliding Angle in Ruppel's Griffon Vulture *Gyps Ruppellii*"., <u>J. Exp. Biol.</u>,Vol. 55, 1971, pp. 39-46.

_____ "Gliding Flight of the Dog-Faced Bat *Rousettus Aegyptiacus* Observed in a Wind Tunnel". <u>J. Exp Biol.</u>, Vol. 55, 1971, pp. 833-45.

_____ "Structural Limitations on the Power Output of the Pigeon's Flight Muscles". <u>J. Exp. Biol</u>., Vol. 45, 1966, pp. 489-98.

_____ "The Strength of the Pigeon's Wing Bones in Relation to Their Function". <u>J. Exp. Biol.</u>, Vol. 46, 1967, pp. 219-33.

_____ , "The Mechanics of Bird Migration". Ibis, Vol. III, 1969, pp. 525-56.

_____, <u>Animal Flight</u>, London., Arnold, 1972.

_____, "Mechanics of Flight", in <u>Avian Biology</u>. J. R. King and D. S. Farmer (ed.), NY. Academic Press, 1972.

_____, "Soaring Behavior and Performance of Some East African Birds, Observed from a Motorglider". <u>Ibis</u>, Vol. 114, 1972, pp. 178-218.

_____, "The Soaring Flight of Vultures". <u>Sci. Amer.</u>, Dec. 1973, pp. 102-109.

Tucker, V. A. "Respiratory Exchange and Evaporative Water Loss in the Flying Budgerigar". <u>J. Biol.</u>, Vol 48, 1968, pp. 66-87.

_____, "Energetic Cost of Locomotion in Animals". <u>Comp. Biochem. Physiol.</u>, Vol. 34, 1970, pp. 841-6.

_____, "Metabolism During Flight in the Laughing Gull, *Laurus artrivilla*". <u>Am. J. Physiol.,</u> Vol. 222, 1972, pp. 237-45.

_____, "Bird Metabolism During Flight: Evaluation of a Theory". J. Exp. Biol., Vol. 58, 1973, pp. 689-709.

_____,"The Energetics of Bird Flight". Sci. Amer., 1971.

_____, and Parrot, G. G., "Aerodynamics of Gliding Flight in a Falcon and Other Birds". J. Exp. Biol., Vol. 53.

Pick, G. S. and Lien, D. A., "The Development of a Two-Dimensional, High Endurance Airfoil with given Thickness Distribution and Reynolds Number". NASA CR-2315, Nov. 1973.

Pinkerton, R. M. and Greenberg, H., "Aerodynamic Characteristics of a Large Number of Airfoils Tested in the Variable Density Wind Tunnel". NACA TR-628, 1938.

Pringle, J. W. S., Insect Flight, Cambridge. Cambridge U. Press, 1957.

Publication I-XII, Organization Scientifique et Technique Internationale du Vol-a-Voile (OSTIV). Available from SSA, P. 0. Box 66071, Los Angeles, CA 90066.
Rains, C. P., "Analytical Investigation of the Performance Characteristics of Cyclic Glide Undersea Vehicles". General Dynamics Corp., Electric Boat Division, Marine Technology Center, San Diego, CA C419-69-006 Feb 1968.

Raspet, A., "Biophysics of Bird Flight", Soaring, Aug. 1960, pp. 12-20.

Reichmann, H., Cross-Country Soaring, Thomson Publications, Motorbuch Verlag, Stuttgart, Germany, 1978.

Riegels, F. W., Aerofoil Sections; Butterworth. London. 1961.

Roman, D., et al., "Aerodynamics of High-Subsonic Blended-Wing-Body Configurations". 41st Aerospace Sciences Meeting and Exhibit, American Institute of Aeronautics and Astronautics, January 2003, Reno, Nevada. 9 pp.

Schmidt-Nielsen, K., How Animals Work, Cambridge. Cambridge U. Press, 1972.

Schmitz, F. W., <u>Aerodynamik des Flugmodells</u>, Duisburg: Carl Lange, 1960. <u>Trans:</u> N70-39001, Nov. 1967, Nat. Tech. Info. Service, Springfield, Va.

Shenstone, B. S.,"Unconventional Flight". <u>J. R. Aero. Soc.</u>, Vol. 72, Aug. 1968, pp. 655-60.

Sherman, J., "Notes on Pumping Requirements for a Glider, as a Function of the Density Profile and Hull Compressibility", Technical Report submitted to the ONR Committee for Underwater Glider Systems Study, Scripps Institution of Oceanography, January 2003, 3 pp.

Sherman, J., "Pressure Case Design Displacement as a Function of Depth", Technical Report submitted to the ONR Committee for Underwater Glider Systems Study, Scripps Institution of Oceanography, March 2003, 6 pp.

Sherman, J., et al., "The Autonomous Underwater Glider *Spray*". <u>IEEE Journal of Oceanic Engineering</u>, Vol. 26, No. 4, October 2001, pp 437-446.

Sherman, J. and R. E. Davis. The Autonomous Underwater Glider Spray. <u>IEEE Journal of Oceanic Engineering</u>, **26**:4, 2001, 437-446.

Sherwin, K., <u>Man-Powered Flight</u>, Model and Allied Pub., Herts., 1971.

Smith, A. M. 0., "Aerodynamics of High-Lift Airfoil Systems". AGARD CP 102, 1972.

Speidel, L., "Messungen an zwei Laminarprofilen fur Segelflugzeuge". <u>Z. f. Flugwiss,</u> 3, 1955, pp. 353-359.

Stratford, B. S., "The Prediction of Separation of the Turbulent Boundary Layer". <u>J. Fluid. Mech.</u>, Vol. 5, Jan. 1959, pp. 1-16.

Stevens, W. A., Goradia, S. H. and Braden, J. A., "Mathematical Model for Two-Dimensional Multi-Component Airfoils in Viscous Flow". NASA CR-1843, 1971.

<u>Technical Soaring</u>, B. Paiewonsky, ed., 9309 Burning Tree Road, Bethesda, MD 20034.

Tennekes, H., <u>The Simple Science of Flight</u>, The MIT Press, Massachusetts Institution of Technology, Cambridge, MA, 1997.

Thom, A. and Swart, P., "The Forces on an Airfoil at Very Low Speeds". <u>J. Roy. Aero.</u> <u>Soc.</u>, Vol. 44, 1940, p 61-70.

Ulanov, A. V., "Optimization Criteria and Hierarchy of Mathematical Models of an Underwater Gliding Vehicle". Unpublished Technical Paper, Saint-Petersburg Marine Technical University, Saint-Petersburg, Russia.

Ulanov, A. V., "Finding Rational Parameters of a Control System for a Vesoplan". Unpublished Technical Paper, Saint-Petersburg Marine Technical University, Saint-Petersburg, Russia.

Vaughn, T. A., "Flight Patterns and Aerodynamics". Biol of Bats, Vol. 1, Wm. Wimsatt, ed., N.Y., Academic Press, 1970.

Vogel, S., "Flight in Drosophila - I. Flight Performance of Tethered Fliers". <u>J. Exp. Biol.</u>, 1966, pp. 567-78.

Webb, D. C. and Simonetti, P.J., "A Simplified Approach to the Prediction and Optimization of Performance of Underwater Glider". <u>Procedings of the 10th International Symposium on Unmanned Untehered Submersible Technology</u>, 1996, pp. 60-69.

Webb, D. C., et al., "SLOCUM: An Underwater Glider Propelled by Environmental Energy". <u>IEEE Journal of Oceanic Engineering</u>, Vol. 26, No. 4, October 2001, pp 447-452.

Weis-Fogh, "The Flight of Locusts". <u>Sci. Amer.</u>, March 1956, pp. 116-24.

Welty, C., "Birds as Flying Machines". <u>Sci. Amer.</u>, March 1955, pp. 88.

Welty, J. C., <u>The Life of Birds,</u> Philadelphia: W. B. Saunders, 1962.

Wilkinson D. H., "A Numerical Solution of the Analysis and Design Problems for the Flow Past One or More Airfoils or Cascades". British R and M, No. 3545, 1968.

Whitfield, G. and Bramwell, C.: "Paleoengineering: Birth of a New Science". New Scien., 23 Dec. 1971, pp. 202-5.

Wortmann, F. X., "Ein Beitrag zum Entwurf von Laminarprofilen fur Segelflugzeuge and Hubschrauber". Z. f. Flugwiss, 3, 1955, pp. 333-345.

_____, "Experimentelle Untersuchungen an neuen Laminar-Profilen fur Segelflugeuge und Hubschrauber". Z. f. Flugwiss, 5, 1957, 228-243.

_____, "Progress in the Design of Low-Drag Airfoils". Boundary Layer and Flow Control G. V. Lachman, ed., London, 1061, pp. 748-770.

Wortmann, F. X., and Schwoerer, K., "Einfluss der Profilpolaren auf die Flugleistungen von Segelflugzeugen", Aero-Revue, Sept. 1963. Summarized in Soaring, Jan. 1964, pp. 6-7.

Wortmann, F. X., "Some Laminar Profiles for Sailplanes". Aero-Revue, Nov. 1963. Reprinted Soaring, Jan. 1964, pp. 14-18, and OSTIV Pub. VII.

_____, "Zur Optimierung von Klappenprofilen". Aero-Revue, Vol. 44, 1969, pp. .99-92. Reprinted OSTIV Pub. IX and Soaring , May, 1970, pp. 23-27.

_____, "Drag Reduction in Sailplanes". Soaring , June and July 1966, and OSTIV Pub. VIII.

_____, "Airfoils for the Variable Geometry Concept". Aero-Revue, May 1971, pp. 249-251.

Wortmann, F. X.: "Symmetrical Airfoils Optimized for Small Flap Deflection". OSTIV Congress 1972, Vrsac, Yugoslavia.

_____, "The Sailplane" Aero-Revue . June 1971.

_____, "Design of Airfoils with High-Lift at Low and Medium Subsonic Mach Numbers". AGARD CP 102, 1972.

_____, "A Critical Review of the Physical Aspects of Airfoil Design at Low Mach Numbers". MIT Symposium, Oct. 1972.

_____, "Airfoils with High Lift-Drag Ratio at a Reynolds Number of About One-Million". NASA CR 2315, Nov. 1973.

"Aerodynamic Characteristics of Airfoils". I, NACA TR 93; II, TR 124; 111, TR 182; IV, TR 224; V, TR 286. (See Riegels, Ref. 19 before using these data). Ref MIT Symposium (1974).